

**FRENCH ABSORPTION SPECTROSCOPY BEAMLINES IN
MATERIAL AND ENVIRONMENTAL SCIENCES**

**REPORT TO SAC'S
BM30 & BM16
REVIEW PANEL**

MAY 2021



Table of contents

1. INTRODUCTION	3
2. ORGANISATION AND STAFF	- 6 -
2.1. FRENCH CRGs ORGANISATION	- 6 -
2.2. FAME & FAME-UHD STAFF	- 7 -
3. BEAMTIME STATISTICS.....	- 11 -
4. TECHNICAL SPECIFICITIES OF THE BEAMLINES	- 17 -
4.1. GENERAL FEATURES	- 17 -
4.1.a. <i>optical elements</i>	- 17 -
4.1.b. <i>detection systems</i>	- 19 -
4.1.c. <i>control-command</i>	- 23 -
4.2. SAMPLE ENVIRONMENTS	- 24 -
4.2.a. <i>Liquid helium cryostats</i>	- 26 -
4.2.b. <i>HP/HT setup</i>	- 28 -
4.2.c. <i>XAS characterization of catalysts under operando conditions</i>	- 31 -
5. EXPERTISE AND INTERACTIVITY BETWEEN OUR TEAM AND THE USERS	- 34 -
5.1. FAME+ AND ASTER'X	- 34 -
5.2. SSHADE.....	- 35 -
5.3. FRENCH CRG WORKSHOP IN 2019.....	- 36 -
5.4. EXTERNAL COLLABORATIVE WORKS	- 37 -
5.4.a. <i>Scientific collaborations with users on other synchrotrons</i>	- 37 -
5.4.b. <i>Instrumentation collaborations</i>	- 37 -
6. PERSPECTIVES: THE MAGNIFIX PROJECT	- 39 -
6.1. GENERAL CONTEXT	- 39 -
6.2. WHICH SCIENCE IN PERSPECTIVE?.....	- 39 -
6.3. NEW EXPERIMENTAL SETUP: USE OF THE ENHANCED COHERENCE OF THE BEAM	- 43 -
6.4. IMPACT ON THE BEAMLINES: NEW EQUIPMENTS.....	- 46 -
<i>Optical elements</i>	- 46 -
<i>New Detectors</i>	- 47 -
<i>Experimental devices</i>	- 47 -
<i>Infrastructure</i>	- 48 -
<i>Data analysis</i>	- 48 -
6.5. ACTUAL AND FUTURE TECHNICS FAME & FAME-UHD	- 48 -
7. SCIENTIFIC RESULTS	- 49 -
GEOCHEMISTRY AND ENVIRONMENTAL SCIENCES.....	- 51 -
<i>Fate of metallic contaminants in soil-plant systems</i>	- 51 -
<i>Fate of silver nanoparticles in agricultural soils amended with sewage sludge</i>	- 53 -
<i>Impact of a Model Soil Microorganism and of Its Secretome on the Fate of Silver Nanoparticles</i>	- 55 -
<i>High-Energy Resolution Fluorescence Detected X-Ray Absorption Spectroscopy: A Powerful New Structural Tool in Environmental Biogeochemistry Sciences</i>	- 58 -
<i>Evidence that soil properties and organic coating drive the phytoavailability of CeO₂ nanoparticles</i>	- 60 -

Table of contents

<i>Multi-scale X-ray computed tomography to detect and localize metal-based nanomaterials in lung tissues of in vivo exposed mice</i>	- 61 -
HYDROTHERMAL FLUIDS	- 63 -
<i>Hydrothermal controls on the genesis of rare earth elements deposits</i>	- 65 -
<i>Effect of sulfur on the aqueous and gaseous transport of Cu in porphyry and epithermal systems</i>	- 68 -
<i>Sulfur-bearing complexes of zinc and cadmium in hydrothermal fluids</i>	- 70 -
<i>An arsenic-driven mineral pump for gold in hydrothermal systems</i>	- 73 -
<i>Resolving the enigma of gold deposit formation using XAS</i>	- 75 -
BIOCHEMISTRY	- 77 -
<i>Sub-ppm level high energy resolution fluorescence detected X-ray absorption spectroscopy of selenium in articular cartilage</i>	- 78 -
<i>Investigation of silver(I) coordination in copper(I) biological binding sites</i>	- 80 -
<i>How prions are generated by a copper switch</i>	- 82 -
<i>Mercury trithiolate binding (HgS₃) to a de novo designed cyclic decapeptide with three preoriented cysteine side chains</i>	- 85 -
<i>XAS measurements of Cu-ProlAPP complexes at physiological micromolar concentrations</i>	- 86 -
CATALYSIS & MATERIAL ENERGY	- 88 -
<i>Platinum nanoparticles living on the edge</i>	- 89 -
<i>Tracking the evolution of Pt single site on CeO₂ by HERFD-XANES</i>	- 92 -
<i>Operando XAS observation of Mo transforming to its active phase for converting methane to aromatics</i> ..	- 95 -
<i>In-operando elucidation of bimetallic CoNi nanoparticles during high-temperature CH₄/CO₂ reaction</i>	- 98 -
<i>Establishing efficient cobalt-based catalytic sites for oxygen evolution on a Ta₃N₅ photocatalyst</i>	- 100 -
<i>Catalyst structure identified in an operating PEM fuel cell</i>	- 102 -
<i>Unravelling redox processes of Li₇MnN₄ upon electrochemical Li extraction–insertion using operando XAS</i> .	- 104 -
<i>An innovative method to study volatile fission products speciation in nuclear fuels under severe accident conditions</i>	- 105 -
<i>Operando X-ray Absorption Spectroscopy and Emission Kβ_{1,3} study of the manganese redox activity in high-capacity Li₄Mn₂O₅ cathode</i>	- 106 -
MATERIAL SCIENCE	- 108 -
<i>In situ characterization of cerium oxydation in YAG:Ce nanocrystals</i>	- 110 -
<i>Magnetic switchability in new molecular materials</i>	- 112 -
<i>Strain engineering of photo-induced phase transformations in Prussian blue analogue heterostructures</i> .	- 114 -
8. SCIENTIFIC PRODUCTION 2015-2021	- 107 -
ARTICLES.....	- 109 -
HIGHLIGHTS.....	- 124 -
PHD THESIS AND FRENCH HABILITATIONS À DIRIGER LES RECHERCHES	- 125 -
9. LIST OF SELECTED PUBLICATIONS	- 129 -

The French Absorption spectroscopy beamlines in Material and Environmental Sciences

May 2021

Report to SAC's BM30-BM16 Review Panel

1. Introduction

History

In conjunction with the construction of the ESRF in 1991, the first third-generation European synchrotron, CNRS, CEA and the regional authorities, eager to take advantage of this new very large research facilities, promoted the construction of two national beamlines. By the time the first photons were delivered by the ESRF in 1992, the French collaborative research group [F-CRG](#) was created, which included the beamline [IF](#) (BM32) for the study of surfaces and interface with an experimental hutch dedicated to X-ray absorption Spectroscopy (XAS) and the [D2AM](#) (BM02) beamline for anomalous diffraction/diffusion for materials science. Based on their success and their impact on the national scientific community, a third line dedicated to bio-crystallography was commissioned in 1999 and originated the [FIP](#) beamline. This was followed in 2002 by the construction of the fourth beamline with moving the spectrometer from the IF beamline to the second port of BM30 shared with FIP, namely [FAME](#), dedicated mainly to XAS in environmental and geosciences. Based on the success of FAME (which can be quantified by its oversubscription ratio), a couple of years later, in 2017, the last and fifth CRG beamline dedicated to XAS on ultra-diluted elements, the [FAME-UHD](#) beamline, was opened to users. This beamline was partly funded by an [EQUIPEX](#) project and supplemented by the funding provided by our advisory council (CEA and CNRS). Following the upgrade of the machine and the impossibility to keep FIP and FAME on the same port, the FIP beamline was moved to the BM07 port, leaving the whole infrastructure to the FAME beamline since 2019.

Scientific case

FAME and FAME-UHD are the French Absorption spectroscopy beamlines for Material and Environmental Sciences at the ESRF, two of the five French Collaborating Research Group beamlines, dedicated to X-ray Absorption Spectroscopy (XAS) for FAME and High Energy Resolution for FAME-UHD (HERFD-XAS). The aim of these two beamlines is to cover a wide

Introduction

variety of common applications of XAS in materials science, biophysics, chemistry and mainly in environmental and geochemical sciences. Since 2002 we have concentrated our effort on the *in situ* and *operando* studies of diluted elements and small samples.

One of the particularities of XAS measurements in the field of environmental sciences is that the probed element (for instance a pollutant) often exists in highly diluted form in a surrounding medium. To optimize the XAS analysis at the FAME beamline we aim at providing the highest possible photon flux on the sample together with an efficient fluorescence detection. The detection limit for XAS measurements is estimated to be ~50ppm with the 30 elements SSD detector. To improve the sensibility in detection, in accordance with the recommendations of the last beamline review panel (2014), we have implemented a 14-crystal analyzer spectrometer on the new beamline FAME-UHD (opened in 2017). This spectrometer decreases drastically the concentration detection limit by a factor 10, down to ppm or lower, and thus allows the investigation of multi-element natural samples with enhanced precision. This spectrometer is now quite user-friendly and has extended the range of application of XAS towards molecular environmental science (High Energy Resolved Fluorescence Detected X-ray spectroscopy - HERFD-XAS - and X-ray Emission spectroscopy - XES -). Thanks to this new low detection limit linked to a sub-millimetric beam-size and the new facilities given by the spectrometer, the scientific community has expanded in particular to catalysis and Earth sciences.

In addition, the experimental setup of FAME and FAME-UHD and our different sample environments are very well-adapted to *in situ* and *operando* measurements. This point is particularly suitable for high pressure - high temperature measurements in Earth science, in catalysis (*operando* analysis, as a function of temperature, gas pressure...), electrochemistry... With these two very complementary beamlines, one with high throughput possibilities and a detection limit close to 50 ppm (FAME), the other for high resolution studies and a detection limit close to 0.5 ppm (FAME-UHD), managed by the same operating team, the French CRGs have now a complete and homogeneous X-ray Spectroscopy platform.

The technical and instrumentation development made on FAME and FAME-UHD are illustrated by the scientific contributions highlighted in this report in geochemistry, Earth and material Sciences, catalysis and biology. The high level of the scientific activity on both beamlines is confirmed *i)* by a large number of publications (around 30 per year) and *ii)* by a strong attractiveness of the beamline (average oversubscription rate around 4 for the ESRF beamtime allocation panels).

Students and users trainings

The two beamline are also actively involved in training activities (European HERCULES course, teaching practicals for graduate students of the University of Grenoble) and FAME+, a dedicated CNRS users training annual school we organize since 2004. Another fundamental contribution of FAME to training activities is the successful defence between 2015 and 2021 of around 60 *PhD* theses and French HDRs based on experiments carried out on the beamline. We are also intensively participating to the [SSHADe database](#), filling a lack in this domain and anticipating machine learning used and data policy requirements.

Applications of the main recommendations of the last BLRP in 2014.

We will detailed in the report all the points, but we would like to summarize them here. The principal recommendations were as follows:

Introduction

Summary of recommendations.

The panel:

- Strongly recommends the upgrade of the fluorescence detector system on FAME.
- Supports the crystal analyser development at FAME-UHD
- Recommends the hiring of a new engineer for the two beamlines
- Supports the combined XAS-Raman spectrometer development
- Recommends the establishment of a dedicated port for FAME in the framework of the ESRF phase II upgrade
- Highlights the excellent in-house research in hydrothermal fluids and encourages the staff to further extend their own research in this direction

Item 1: FAME fluorescence detector

Due to the deterioration of the thirty-element fluorescence detector dating from 1993, in 2016 we purchased a second-hand 13-element detector (dating from 2013) with lower performance from the Swiss synchrotron. We were lucky, as the 30-element detector did not restart when we restarted in 2020 after the upgrade.

However, following the success of our funding application Equipex MAGNIFIX, one of the first operations to be started will be the call for tenders for a new detector and a new high-performance electronic, for a commissioning and aperture to users End-2022.

Item 2: Spectrometer:

The new 14-crystal spectrometer is now operational at BM16.

Item 3: Manpower

We obtained the recruitment of Mauro Rovezzi in 2017 as a research engineer and have just obtained a new research engineer position, with expertise in chemistry. However, we are still in need of a mechanical technician position.

Item 4: Simultaneous measurement of XAS and RAMAN

Given the different optical characteristics of X-ray and visible light on the windows and on the sample container, we have decided to build a new autoclave allowing both types of measurements and have also created a new Raman station at the Néel Institute dedicated to Raman measurements using this new autoclave.

Thus, users coming to perform an experiment on one of the beamlines can perform Raman measurements on the same experimental system under the same conditions at the Néel Institute.

Item 5: Single port

Due to the new configuration of the machine after the EBS, the double beamlines could not coexist and so the FAME beamline stayed on the BM30 port and the FIP beamline moved to the BM07 port.

Item 6: Inhouse hydrothermal fluid research

Our specific research on hydrothermal fluids has been greatly expanded and enhanced since the last BLRP, as shown for example by the various publications in this field and the various

Introduction

collaborations we have established. In particular, our expertise has enabled us to obtain dedicated funding on this topic via the PLANEX equipex. It was used to build new autoclaves and their automatic regulation extending the pressure and temperature range and especially to equip each beamline as well as a Raman station and an X-ray absorption station on a micro source at Néel Institute with its own equipment.

Development of the collaborations

In accordance with the conclusions and recommendations given by the last beamline review panel, the staff has continued to establish a wide-ranging network of collaborations, both national and international (KAUST Saudi Arabia, GET Toulouse, ISTO Orléans, LAL Orsay...).

i) Strong collaborations are developed within our in-house research activity on hydrothermal fluids through a French National Research Agency (ANR) funding ([RADICALS project](#)), and the Equipex [PLANEX](#) with ISTO Orléans.

ii) The beamline activity in catalysis associated with the development of the new high-resolution spectroscopy is carried out through our strong collaboration with King Abdullah University of Science and Technology (KAUST) for now nearly 7 years in the field of heterogeneous catalysis

Projects and perspectives

In-house research activity on hydrothermal fluids

Still in accordance with the conclusions of the last beamline review panel, in a first step, our team has implemented a new dedicated Raman spectrometer and X-ray absorption installation for in-house research activity on hydrothermal fluids at the Neel Institute. In a second step we developed *i)* new high pressure/high temperature (HP-HT) vessels dedicated to both visible (Raman) and X-ray (XAS, XES, SAXS...) analysis, *ii)* fixed corresponding pressure and temperature regulations systems on the beamlines as well as *iii)* a transportable regulation system to be able to perform such kind of experiments everywhere (ESRF, SOLEIL,...).

The new HP-HT autoclave was developed in the framework of the Equipex project Planex. Planex aims at developing an (HP-HT) experimental and analytical platform allowing to perform *1) in situ* chemical, structural and isotopic analysis on fluids (molten silicates and salts, hydrous fluids) and gases, and *2)* the simulation of fluid transfer processes in geomaterials or their synthetic equivalents. Our team has been integrated in this consortium for our strong expertise in the development of HP and HT experiments, including the study of the behavior of fluids as a function of temperature and pressure using X-ray absorption spectroscopy, Raman scattering... We now have, since several years, a renowned expertise in the study of hydrothermal fluids and supercritical fluids using small angle X-ray scattering, Inelastic X-ray Raman spectroscopy, Raman spectroscopy and X-ray absorption Spectroscopy analysis.

FAME and FAME-UHD with the ESRF upgrade

All the optical and experimental elements were properly aligned during the EBS shutdown. FAME-UHD was the first CRG equipped with the new source in March 2020, FAME in June. In July we performed in-house research experiments with external users, in order to be able to perform official users' experiments in Autumn 2020, and to benefit from the extremely stable new source.

Introduction

However, FAME with its obsolete optics and detection systems needs to be refurbished to take full advantage of the quality in emittance and brilliance of the new source. This will be realized soon thanks to the funding of the [MAGNIFIX](#) project. The conventional XAS station will be completed by the creation of a μ beam station, allowing the possibility to perform nanoscale spectral measurements.

FAME-UHD, with its state-of-the-art optics, will also benefit from MAGNIFIX funding to complete its portfolio of analyser crystals to cover all element emission lines in the 4-20 KeV energy range.

Staff requirement

Since the last report, the staff has slightly increased, but it is now in charge of the operation of two beamlines. Our main requests concern then the evolution of the beamlines staff. Even if one of our goal is to automatize the beamlines as much as possible, our team has to manage FAME and FAME-UHD with only four permanent "local contact" positions (three Beam Line Operating Manager (BLOM) and one full time scientist) and the support of only two technicians. A new position of BLOM specialized in chemistry has just been attributed in 2021 and a young researcher in chemistry specialised in Ptychography has been recruited at the Néel Institute in 2019. But to maintain, develop and reinforce the scientific and technical activities of the beamlines portfolio, further permanent positions is needed. Firstly, to boost a research activity in geosciences at the highest level around these beamlines, the assignment to the Néel Institute of a young researcher in Earth Science is required. Secondly, to fully operate both beamlines, a mechanical technician is required.

Analysis of statistics

The FAME beamline is still one of the most popular on the international programme committees with a corresponding scientific output even with the opening of FAME-UHD.

For FAME-UHD, its start-up, combined with the continued installation of the new 14-crystal spectrometer, has been very successful and has a rapidly growing demand rate.

A rather negative point is the low number of applications via the French committees, which is general for all French CRGs (IF, D2AM, FIP, FAME, FAME-UHD). In total, we have more French applications via the ESRF committees than *via* the French committees, whereas the time distributed is only one third via ESRF and two thirds via SOLEIL. Our analysis, supported by discussions with French users, is that for the experiments via the CRG-SOLEIL French committees, there is no user support for the CRG users (they have to pay all the missions costs), in contrary to SOLEIL users. It seems important to find a solution to this inequality of treatment.

The report

After a presentation of the two beamlines, their organisations, some statistic of use, technical specificities and perspectives, selected scientific topics representative of results obtained at FAME and FAME-UHD in recent years will be brought to the attention of the committee, in geochemistry & environmental sciences, hydrothermal fluids, biochemistry, catalysis and material for energy, materials science. A selection of significant papers are reprinted in the appendix, they are representative of the various scientific topics in which the beamlines is clearly involved: hydrothermal fluids (*e.g.* Pokrovski et al. 2015), geochemistry (*e.g.* Prada et al. 2016), biochemistry (*e.g.* Bissardon et al. 2019), catalysis (*e.g.* Maurer et al. 2020) and material science (*e.g.* Dantelle et al. 2018).

2. Organisation and Staff

2.1. French CRGs Organisation

The five French CRGs are jointly managed by the CNRS and the CEA to enhance the access of French researchers to the European Synchrotron. This consortium is organized through a council (or steering committee) gathering the directors, or their representatives, from the four involved CNRS institutes (Physics, Chemistry, Environmental and Universe Science and Biology) and from the CEA (Large Research Infrastructures of the Fundamental Research Department). It is also annually evaluated by a Scientific Advisory Committee. This organisation is summarized on **Figure 1**. The beamlines operation, annual reporting, financial and human resources needs are coordinated by a local “structure d’exploitation” animated by the directors of the two main laboratories involved (CNRS - Institut Néel, CEA – IRIG) and the beamline responsables. All the staff (researchers, technicians and engineers) involved on the five beamlines are also staff of Grenoble laboratories, offering opportunity to develop strong technical and scientific collaborations with these support labs.

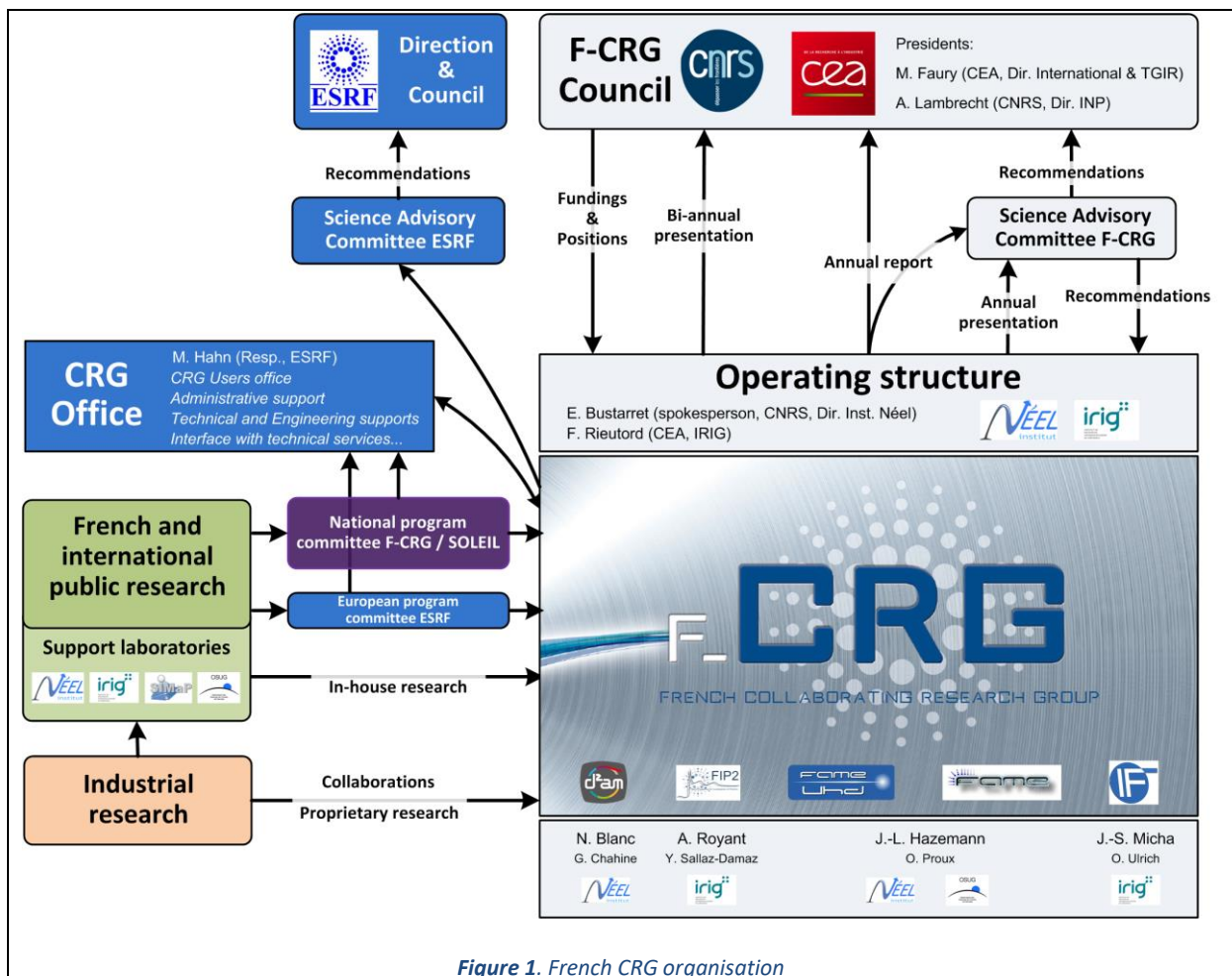


Figure 1. French CRG organisation

2.2. FAME & FAME-UHD staff

Both FAME and FAME-UHD beamlines are managed by a common staff of 7 CNRS permanent employees and 2 post-doctoral scientists. The recommendation of the previous BLRP (2014) concerning the staff evolution for the operation of two beamlines was the “addition of at least one more engineer”. This point was solved in 2017 with the recruitment of Mauro Rovezzi with the opening of FAME-UHD as an "Ingénieur de Recherche CNRS" (new position), a position similar an ESRF BeamLine Operating Manager, like Isabelle Kieffer and Olivier Proux.

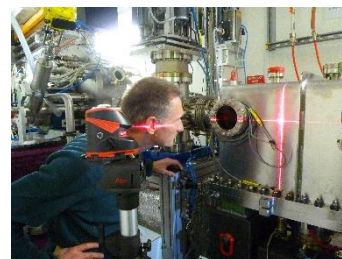
	Organism	Position	Time on Beamline	Professional degree	from	to
Hazemann J.-L.	CNRS ¹	Senior scientist, Beamline responsible	50%	Geophysics	beginning	*
Testemale D.	CNRS ¹	Junior scientist	50%	Physics	03/2007	*
Da Silva J.C.	CNRS ¹	Junior scientist	20%	Physics	10/2019	*
Maurin I.	CNRS ¹	Junior scientist	10%	Physics	01/2020	*
Aguilar Tapia A.	CNRS ¹	Post-doc. Fellow	50%	Chemistry	11/2016	10/2020
	KAUST ²	Post-doc. Fellow	50%	Chemistry	01/2021	08/2021
Bazarkina E.	CNRS ¹	Post-doc. Fellow	50%	Geophysics	11/2016	03/2021 [#]
Proux O.	CNRS ³	Research engineer, technical responsible	100%	Physics	beginning	*
Kieffer I.	CNRS ³	Research engineer	100%	Physics	12/2011	*
Rovezzi M.	CNRS ³	Research engineer	100%	Physics	01/2017	*
Del Net W.	CNRS ³	Technical engineer	100%	Electronic	08/2006	04/2020 [§]
Min S.	CNRS ³	Technical engineer	100%	Electronic	10/2020	*
Lahera E.	CNRS ³	Technical engineer	100%	Engineering	beginning	*
Prat A.	CNRS ¹	Mechanical engineer	20%	Physics	beginning	*
Ulrich O.	CEA ⁴	Control-command engineer	10%	Electronic and computing	beginning	*

Table 1. Beamline actual staff for the 2015-2021 period. **1** : Institut Néel, Grenoble, CNRS; **2** : King Abdullah University of Science and Technology - Catalysis Center **3** : Observatoire des Sciences de l'Univers de Grenoble, CNRS-UGA Grenoble; **4** : CEA Grenoble - INAC/SP2M/ Nanostructure et Rayonnement Synchrotron *: permanent position. #: now at CRG-ROBL/BM20. §: now at Laboratoire de Physique Subatomique et de Cosmologie, CNRS-UGA-Grenoble INP, Grenoble

Organisation and Staff

Jean-Louis Hazemann

Beamline responsible for all scientific and technical aspects. Scientific interests include the study of aqueous solutions in sub- or supercritical conditions. This research area leads him to develop high pressure / high temperature instrumentation for *in situ* characterisations by X-ray Absorption Spectroscopy, Small Angle X-ray Scattering... Assists users to perform their experiments.



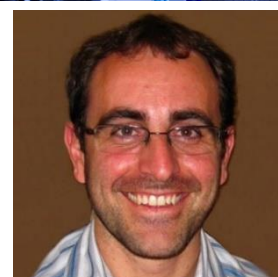
Denis Testemale

Permanent scientist at the Néel Institute. Scientific interests include the study of aqueous solutions in sub- and supercritical conditions, transport of metals in hydrothermal fluids. Denis also works on the development of HP/HT instrumentation and assists users in their experimental runs.



Julio Cesar Da Silva

Permanent scientist at the Néel Institute since October 2019. Julio has a strong experience with 3D X-ray nanoimaging and numerical analysis. He will develop the ptychography end-station on BM30, in the frame of the MAGNIFIX EquipEx.



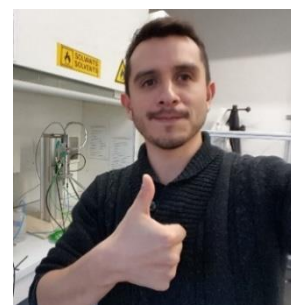
Isabelle Maurin

Permanent scientist, that recently moved to Néel Institute, after a one-year sabbatical at the FAME and FAME-UHD beamlines in 2020. Isabelle has an expertise in solid-state chemistry, frequently using large-scale facilities (XRD, XAS, SAXS) to monitor the growth mode of nanomaterials or understand relationships between structure/microstructure and properties. She has a marked interest for the development of *in situ* studies of photo-induced phase transformations in molecular solids and hybrid architectures.



Antonio Aguilar-Tapia

After a PhD in Material science and engineering (end in 2016) from Universidad Nacional Autónoma de México, Antonio has acquired a strong theoretical basis and practical skills in the characterization of materials by XAS, first in a 1-year postdoctoral position at KAUST in Saudi Arabia, then on FAME group. Antonio works on the design, preparation and realization of experiments involving catalytic studies under *operando* conditions.



Elena Bazarkina

After a PhD (end in 2009) on hydrothermal fluids at GET (Toulouse) and IGEM RAS (Moscow), Elena obtained a scientist position in IGEM RAS on geochemistry, and started to develop strong collaborations with other labs, GeoRessources (Nancy, from 2012 to 2016) then FAME group (2017-2021). Elena works

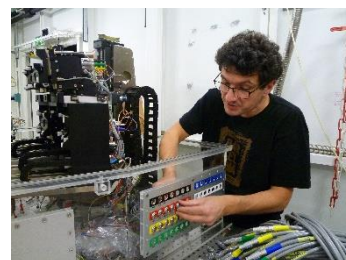


Organisation and Staff

on preparation and realization of experiments involving hydrothermal fluids studies under *in situ* conditions

Olivier Proux

Beamline Operation Manager (CNRS "Research Engineer"), assists J.-L. Hazemann in the beamline management, upgrade and development. Engineering interests include the development of crystal analyser spectrometer projects. Assists users in performing their experiments.



Isabelle Kieffer

Beamline Operation Manager (CNRS "Research Engineer"), assists J.-L. Hazemann in the beamline management, upgrade and development. Engineering interests include the development of the control-command systems. Assists users in performing their experiments.



Mauro Rovezzi

Beamline Operation Manager (CNRS "Research Engineer"), assists J.-L. Hazemann in the beamline management, upgrade and development. Engineering interests include the development of the detection systems. Assists users in performing their experiments.



Sophie Min

Technical engineer. Responsible of all the software and hardware instrumentations on the beamline.



Eric Lahera

Technical engineer. Designs, draws and constructs mechanical apparatus (1st and 2nd crystals supports of the monochromator, Si diodes, crystal analyser spectrometer, high pressure / high temperature vessel...).



Alain Prat

CNRS "Research Engineer". Designs and draws optical and experimental devices (monochromator axis, high pressure / high temperature vessel and derivate catalysis cell...).



Olivier Ulrich

Beamline Operation Manager (CEA "Research Engineer"). Responsible of all the software and hardware instrumentation on BM32 (CRG-IF) beamline. High level technical assistance for software and hardware instrumentation issues.



Other supports

The beamlines benefit also from external supports:

- Eric Dettona coordinates, for all the CRG beamlines, the interactions with ESRF technical services, among other things (0.07 FTE per beamline),
- Noël Levet is in charge of the alignment interventions (optical elements, experimental devices...), for all the CRG beamlines (0.07 FTE per beamline),
- ESRF beamline software support (~1day/month and per beamline, *i.e.* ~0.05 FTE per beamline),
- French CRG control-command software development (for BLISS development, common position for the 5 F-CRG beamlines, *i.e.* 0.2 FTE per beamline),
- Design and mechanical workshop of the Néel Institute, the [SERAS](#) (a rough estimation of the time spent by the SERAS is 3 FTE for the 5 F-CRG per year, *i.e.* 0.6 FTE per beamline)

These supports give an equivalent of ~1 FTE per beamline on technical aspects.



	Per beamline	Per beamline (including external support)	Other non-French CRG	Public beamlines	Public beamlines (including pools)
Local-contact & instrumentation	2.65	2.65	4.5	4	6.8
Technical support	1.15	2.15	1.5	1.5	2.8

Table 2. Recapitulation of the staff FTE (Full-Time Equivalent) for FAME and FAME-UHD, compared to other non-French CRG and a typical public ESRF beamline. The consolidated staff was estimated by including external supports for FAME and FAME-UHD, from the 2020 ESRF highlights for public beamlines, by dividing the staff involved (table p. 190 beamlines, instruments and experiments line) by the number of beamlines (34.85).

3. Beamtime statistics

Like all the other CRG beamlines, beamline access follows these rules:

- ESRF program review committees allocate $\frac{1}{3}$ of the shifts, ~ 140 shifts/year (“public beamtime”),
- French program review committees allocate $\frac{2}{3}$ of the shifts, ~ 280 shifts/year (“private beamtime”). This number of shifts can be adjusted after discussion with the committees depending on the technical developments on the beamlines (for example the anticipated closure of FAME end-2018 in order to allow FIP beamline to move from BM30 to BM07 front-end) or to take into account staff necessities,
- The remaining shifts are dedicated to in-house research, training sessions and technical developments.

The beamtime repartitions realized on both beamlines are shown as a function of the kind of beamtime (public, private, IHR..., on Figure 1), the origin of the users from an institute point of view (*i.e.* from a scientific thematic point of view, on Figure 5) and from a geographic point of view (Figure 6). The requested beamtime on both beamlines are shown as a function of the ESRF program committees (*i.e.* from a scientific thematic point of view, on Figure 4) and as a function of the available beamtime (Figure 2). Comparison of the FAME and FAME-UHD overbooking ratio with those of the other beamlines is shown on Figure 3.

Historically only French researchers could access the $\frac{2}{3}$ private part, but since we joined the SOLEIL review committee in 2011 to form a common F-CRG / SOLEIL program committees (in order to have a unique access point for the French beamtime access), this rule no longer applies. Compared to the public beamtime, the main difference lies in the non-reimbursement of the users' travel and accommodation expenses for the experiment. Consequently, even if most of the non-French laboratories researchers apply through the public beamtime, some of them also applied via the private one (mainly our collaborators). Second consequence, even if still a large majority of French laboratories researchers apply through the private beamtime, a non-negligible fraction of them only apply via the public one. This might be one of the reasons which explain the smaller overbooking ratio on private beamtime compared to public one (Figure 2).

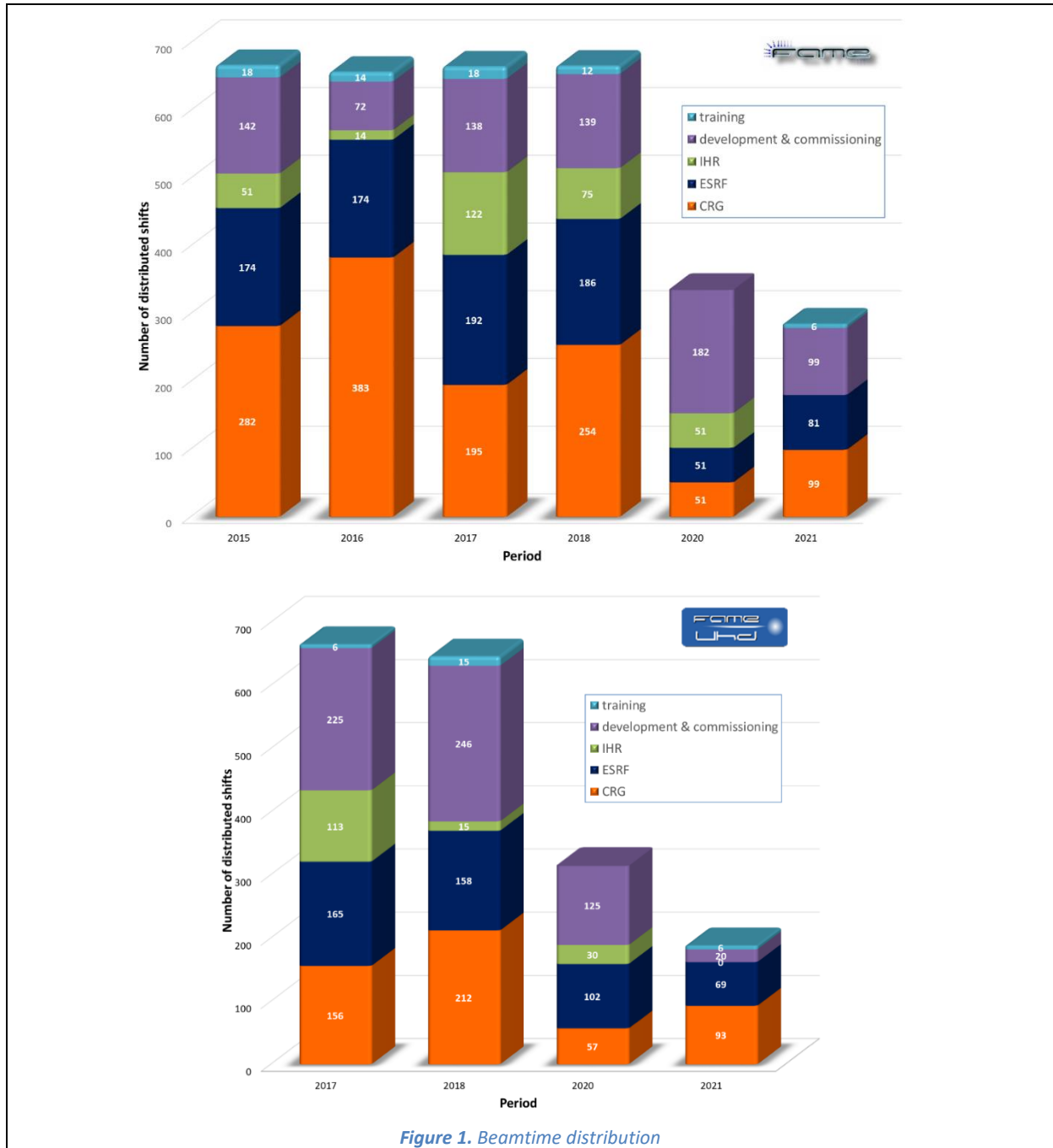
The commissioning shifts are distributed to test and develop new instruments. During the review period, the commissioning time on FAME-UHD was at a quite high level in 2017-2018 (Figure 1 bottom) since we just opened the beamline to regular users but still have developments and optimizations to perform. On FAME (Figure 1 top) the commissioning time at the same period was mainly dedicated to software and electronic tests (2015-2017) then to the beamline preparation for the upgrade (last month of 2018 beamtime). On both beamlines the commissioning time in 2020 and 2021 was mainly dedicated to the optical optimization after the EBS-upgrade, and to new control-command tests (BLISS, on FAME).

The in-house-research (IHR) beamtime is distributed among the beamline staff to develop our own scientific projects (mainly with our PhD student or postdocs, M. Irar¹, A. Aguilar-Tapia and E. Bazarkina on this period).

¹ Irar M., “Spectroscopie d'absorption des rayons X appliquée à l'étude des fluides hydrothermaux”, *Thèse de doctorat de l'Univ. Grenoble Alpes, Grenoble* (2017) <http://www.theses.fr/2017GREAY060>

Beamtime statistics

Finally, the number of shifts dedicated to training sessions is around 15 per year (except in 2020 and 2021, for COVID reasons). This training activity is of great importance for all of us, and for our users' community. A part of this report will be dedicated to it.



Overbooking ratio. FAME remains one of the highest requested beamline at the ESRF (Figure 3) while FAME-UHD presents an increasing overbooking ratio since its aperture to users, to reach a value slightly higher to the mean value.

Beamtime statistics

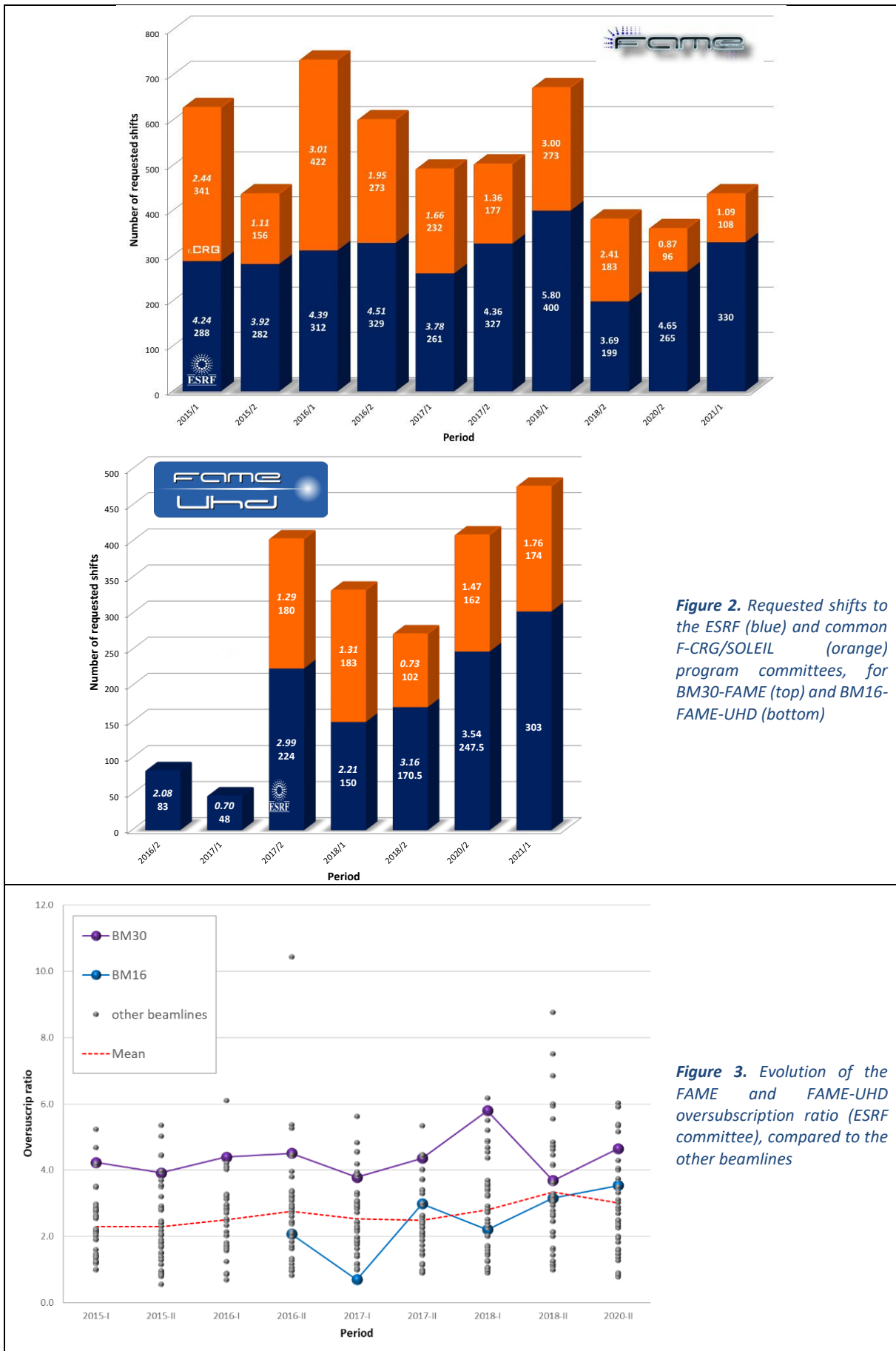
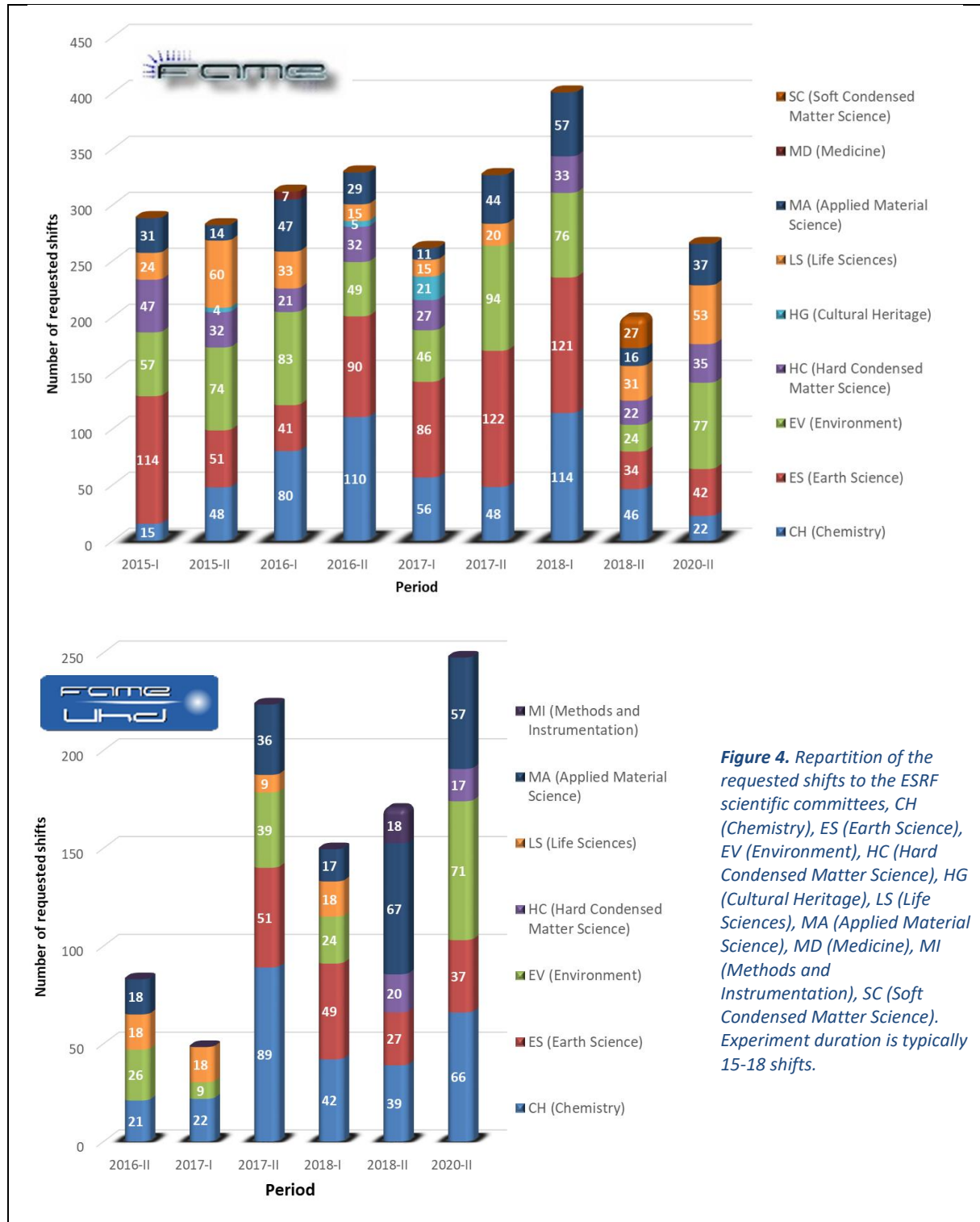


Figure 2. Requested shifts to the ESRF (blue) and common F-CRG/SOLEIL (orange) program committees, for BM30-FAME (top) and BM16-FAME-UHD (bottom)

Figure 3. Evolution of the FAME and FAME-UHD oversubscription ratio (ESRF committee), compared to the other beamlines

Beamtime statistics

Beamtime requests are mainly done on chemistry and Earth and environmental sciences program committees (Figure 4). Consequently, the users are mainly issued from the corresponding French laboratories, mainly from CNRS-INC and INSU respectively, both on FAME and FAME-UHD (Figure 5).



Beamtime statistics

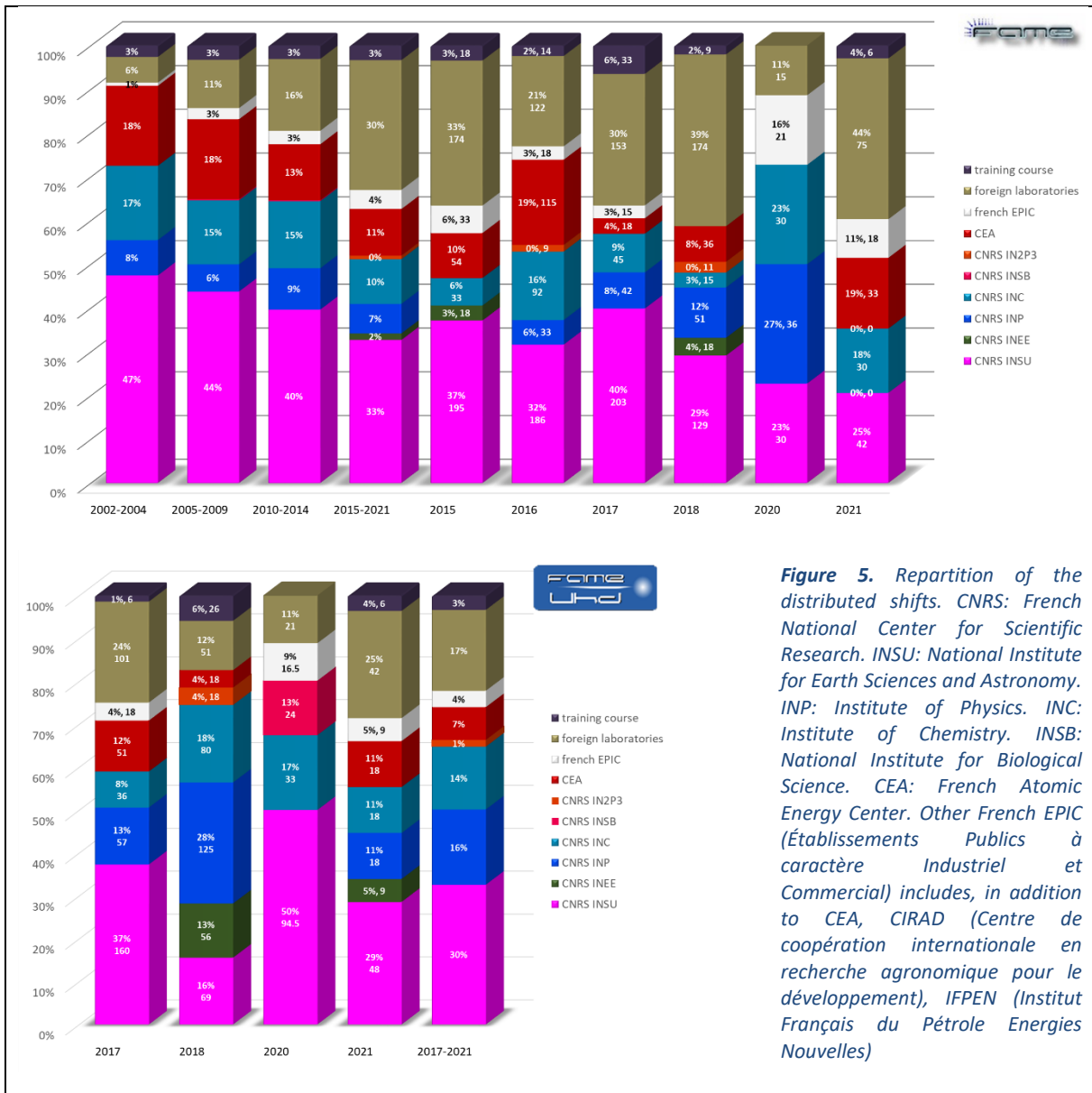
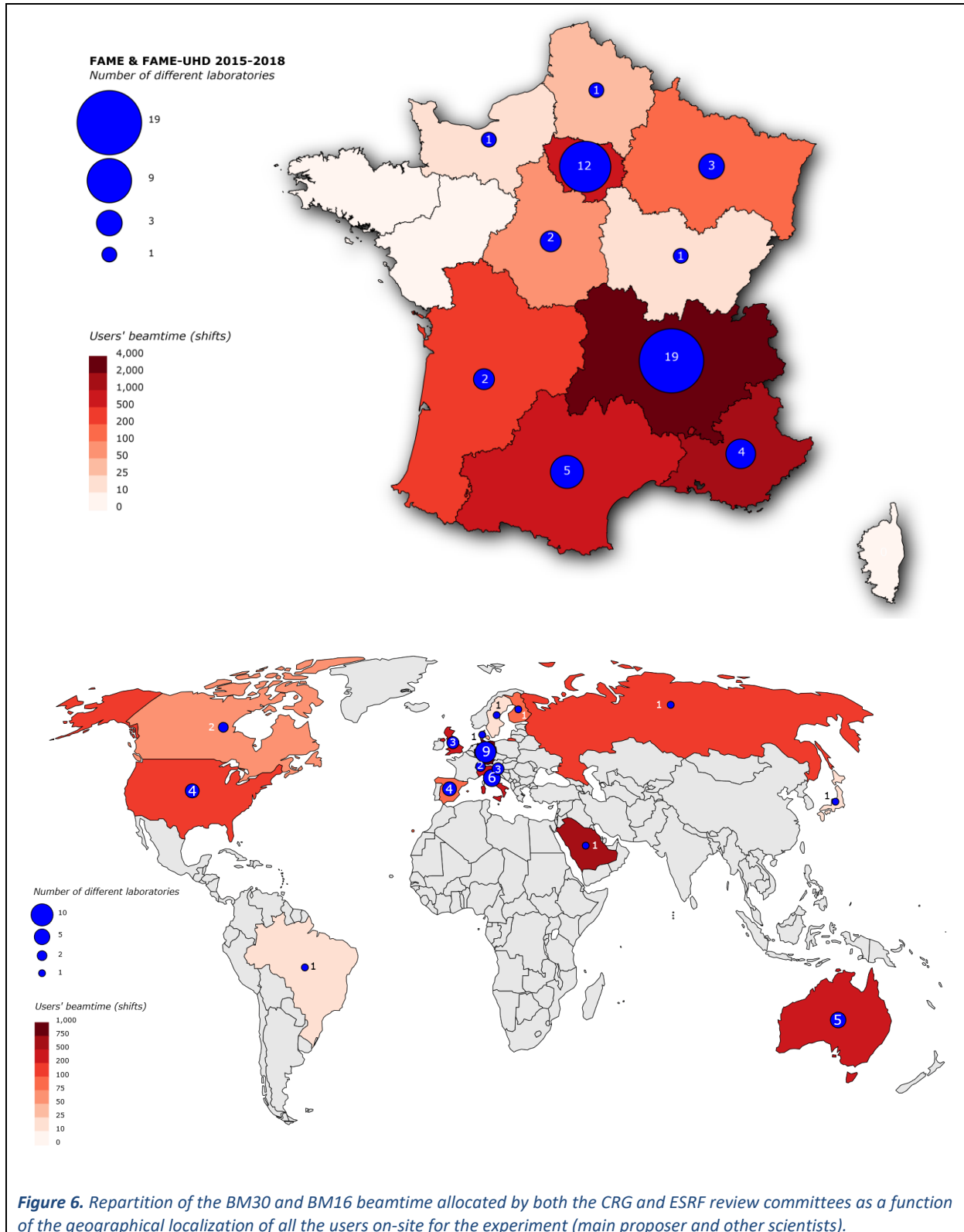


Figure 5. Repartition of the distributed shifts. CNRS: French National Center for Scientific Research. INSU: National Institute for Earth Sciences and Astronomy. INP: Institute of Physics. INC: Institute of Chemistry. INSB: National Institute for Biological Science. CEA: French Atomic Energy Center. Other French EPIC (Établissements Publics à caractère Industriel et Commercial) includes, in addition to CEA, CIRAD (Centre de coopération internationale en recherche agronomique pour le développement), IFPEN (Institut Français du Pétrole Energies Nouvelles)

Beamtime statistics

FAME and FAME-UHD beamlines are national and international beamlines. From a geographical point of view (Figure 6), 30% (FAME) and 17% (FAME-UHD) of the users are from non-French laboratories, mainly from Germany (9 labs), Italy (6 labs) for European countries, from Australia (5 labs) and USA for non-European ones (Figure 6). In France, users are mainly coming from Auvergne-Rhône-Alpes (19 labs), Paris and suburb (12 labs) and south of France (9 labs in total).



4. Technical specificities of the beamlines

4.1. General features

4.1.a. optical elements

BM16 and BM30 beamlines have been built in the same spirit, fulfilling the same requirements:

- prioritizing the energy resolution,
- optimizing the beamline stability,
- maximizing the photon flux.

Those requirements led us to the scheme shown in Figure 1 (bottom).

Both beamlines have:

- a first mirror for harmonic rejection and vertical collimation. It is a bendable Rh-coated silicon mirror cooled by water,
- a Si[220] 2-crystal monochromator. First crystal is liquid-nitrogen cooled. Second crystal not cooled is bendable to insure the horizontal focusing, with a dynamic angular adjustment to optimize the angle between both crystals, both system allowing to maximize the flux on the sample,
- a second mirror for harmonic rejection and vertical focusing. It is also a bendable Rh-coated silicon mirror, but not cooled,
- several pairs of vertical or horizontal slits to define the beam between each optical element,
- a shutter protected by an absorber at the end of each optics hutch.

The main differences between the two beamlines are due to geometrical constraints. Firstly, although the ideal positioning of the elements implies short lever arms to improve stability and therefore placing all the optical elements as close as possible to the source, this was not possible on BM30, due to the initial presence of the FIP beamline (until the EBS upgrade). Secondly, to maximize the flux, it was chosen to integrate the maximum of the horizontal divergence delivered by the bending magnet. Nevertheless, it was not possible to accept more than 2.1 mrad on BM30, again due to the presence of FIP vessels. In contrast, BM16 accepted up to 4 mrad. This difference has disappeared since the EBS, with a Short Bending Magnet which delivers only 2 mrad.

The other differences derive from improvements implemented on BM16, either from the experience acquired on BM30, or from technical advances by the manufacturers. In particular, the cooling system of the first mirror has been entirely redesigned to improve the management of the heat load on the center of the optical surface. The quality of the mirrors themselves has also been improved for BM16 (built in 2015-2016) compared to BM30 (2000-2001), with, for example a slope error of $<0.6\mu\text{rad}$ (M1) and $<0.5\mu\text{rad}$ (M2) for BM16 compared to $2.4\mu\text{rad}$ (M1) and $3.0\mu\text{rad}$ (M2) for BM30.

The layout of both beamlines are presented in Figure 1 (up and middle).

To complete the optical scheme, one can mention that, since the monochromator is not fixed exit, the sample and detection set-up have to follow the beam during a scan in energy. Both beamlines are equipped with a table that moves when the photon energy changes. BM16 benefits from an hexapod-based table which is able to support 500 kg and to move vertically with a resolution of $0.1\mu\text{m}$ while BM30 benefits from a more conventional table which is able to support the same weight but to move with a resolution of around $2\mu\text{m}$.

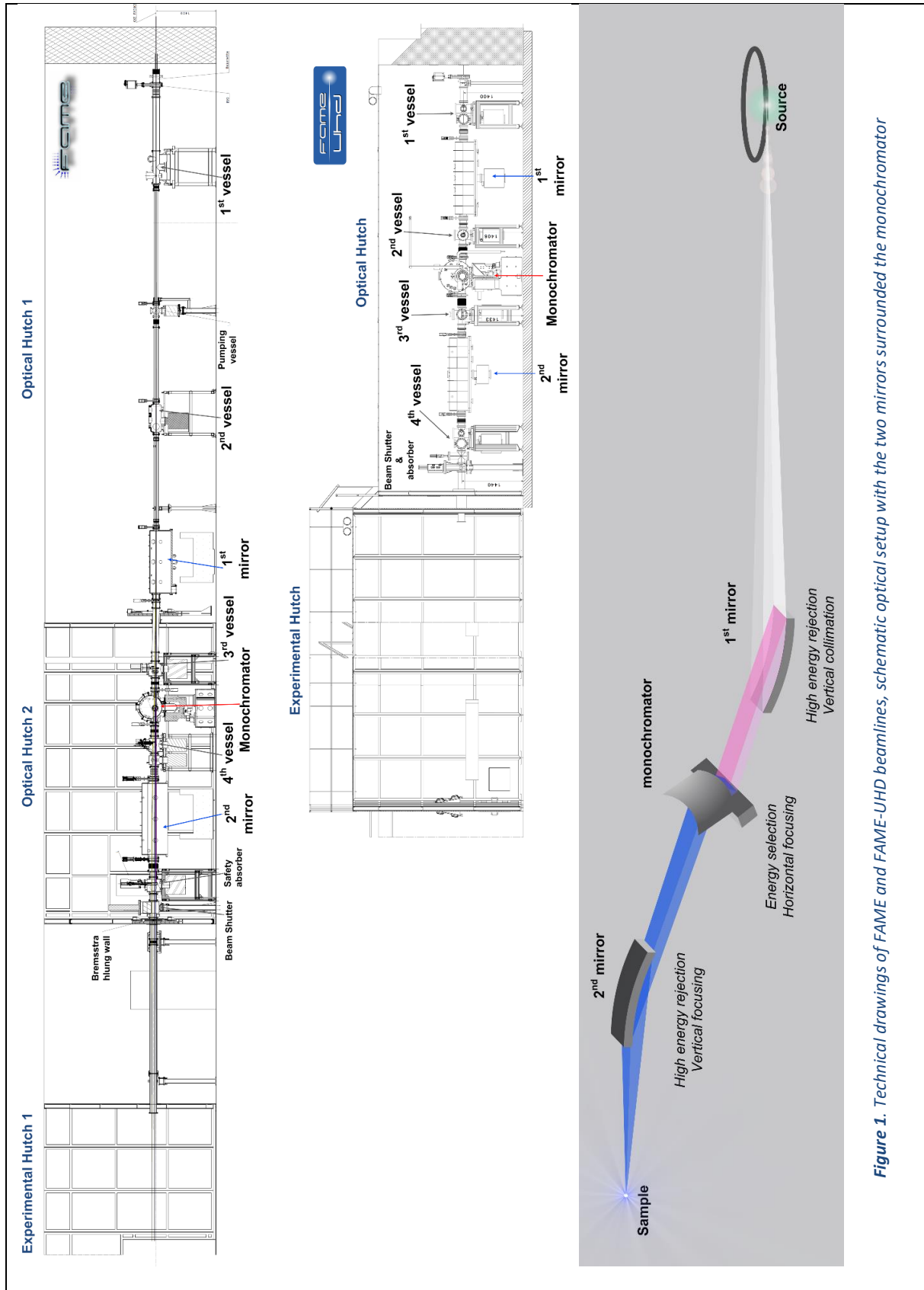
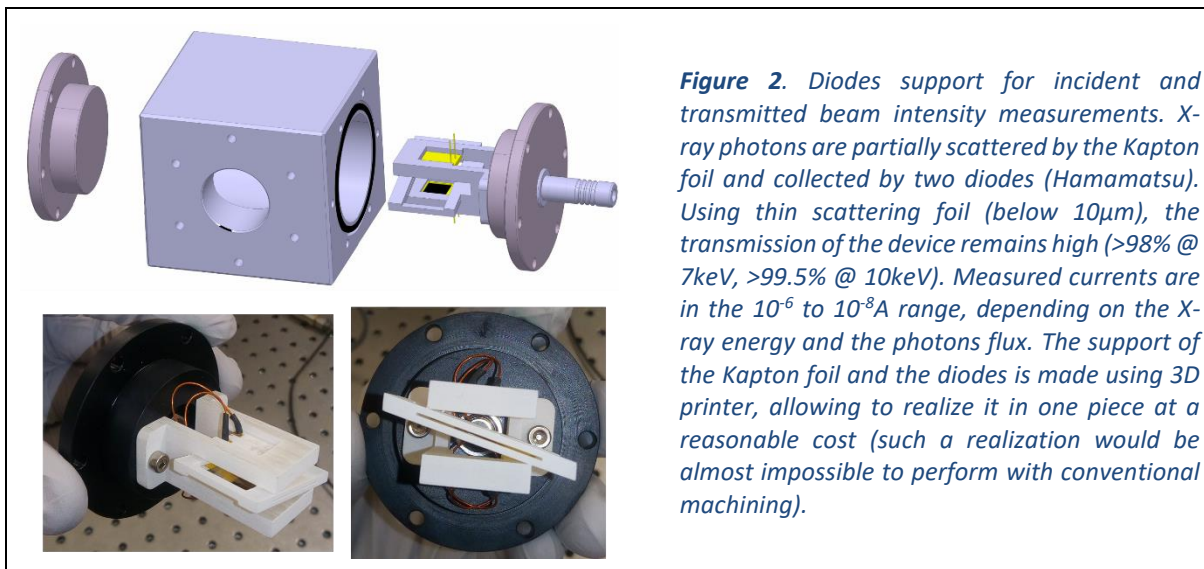


Figure 1. Technical drawings of FAME and FAME-UHD beamlines, schematic optical setup with the two mirrors surrounded the monochromator

4.1.b. detection systems

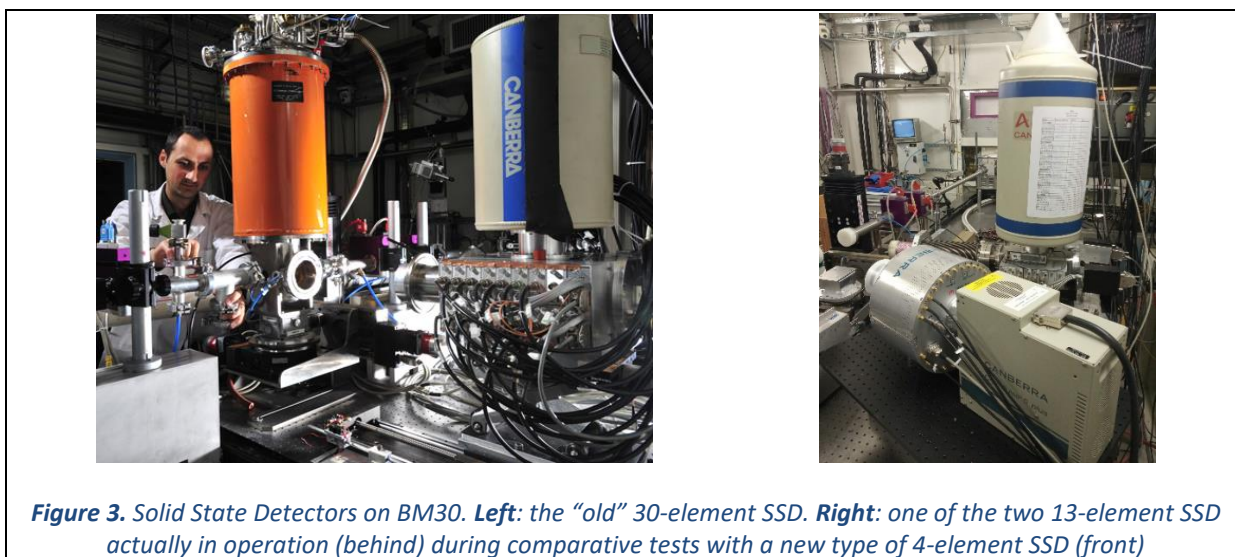
Incident and transmitted beams measured using diodes  

Incident and transmitted beam intensities (I_0 , I_1 , I_2) are measured with an homemade setup shown on Figure 2. A classical setup is used (Figure 2). It consists in measuring the current given by two silicon diodes collecting the scattered X-ray beam provided by a kapton foil placed on the beam at 45°.



Fluorescence measurement with Solid-State Detector 

On BM30, a germanium Solid-State Detectors (SSD) is used to measure fluorescence photons with an energy bandwidth in the 200-300eV range. To increase the collecting area, the SSDs are composed of several elements. Most of the experiments shown on this report have been performed using a 30-element SSD. This unique detector combines germanium array detector technology with fast processing electronics (Figure 3, left). The detector assembles 6 germanium crystals with 5 detectors per crystal, into an extremely small area (40x40 mm²). For a shaping time of 0.5 μ s, it allows EXAFS data collection at count rates of 30 kcts/s (without deadtime correction) per channel with an energy resolution of \sim 250 eV. This detector, built in collaboration with Canberra in 1993-1996, is now over, since September 2020.



Technical specificities

We are now using either our “discrete” 13-element germanium SDD, bought to the Swiss Light Source several years ago as a spare, or its equivalent borrowed to the ESRF detector pool. This transitory situation will continue until we acquire a new one. We already performed tests on a Canberra-Mirion 4-element prototype (Figure 3, right), to define which kind of detector will be the more suitable for us.

Fluorescence measurement with Crystal Analyzer Spectrometer

BM16 beamline allows high resolution fluorescence detection using a 14-crystal Crystal Analyzer Spectrometer (CAS). This CAS is the fruit of the developments performed on BM30 since 2004 which allowed to prove that such a detection system can be more than useful on a bending magnet beamline,¹ and well-adapted to ultra-high dilution XAS measurements. Following the 1-crystal CAS prototype design and due to its performances², a 5-crystal CAS (0.5m radius of curvature, later adapted to 1m) was built³ and opened to regular users in 2010-2011. These technical works and scientific uses were at the basis of the French EquipEx project which leads to FAME-UHD construction. At the beginning in 2017, BM16 was equipped with the 5-crystal CAS (1m configuration). In 2018 the current 14-crystal CAS was installed.

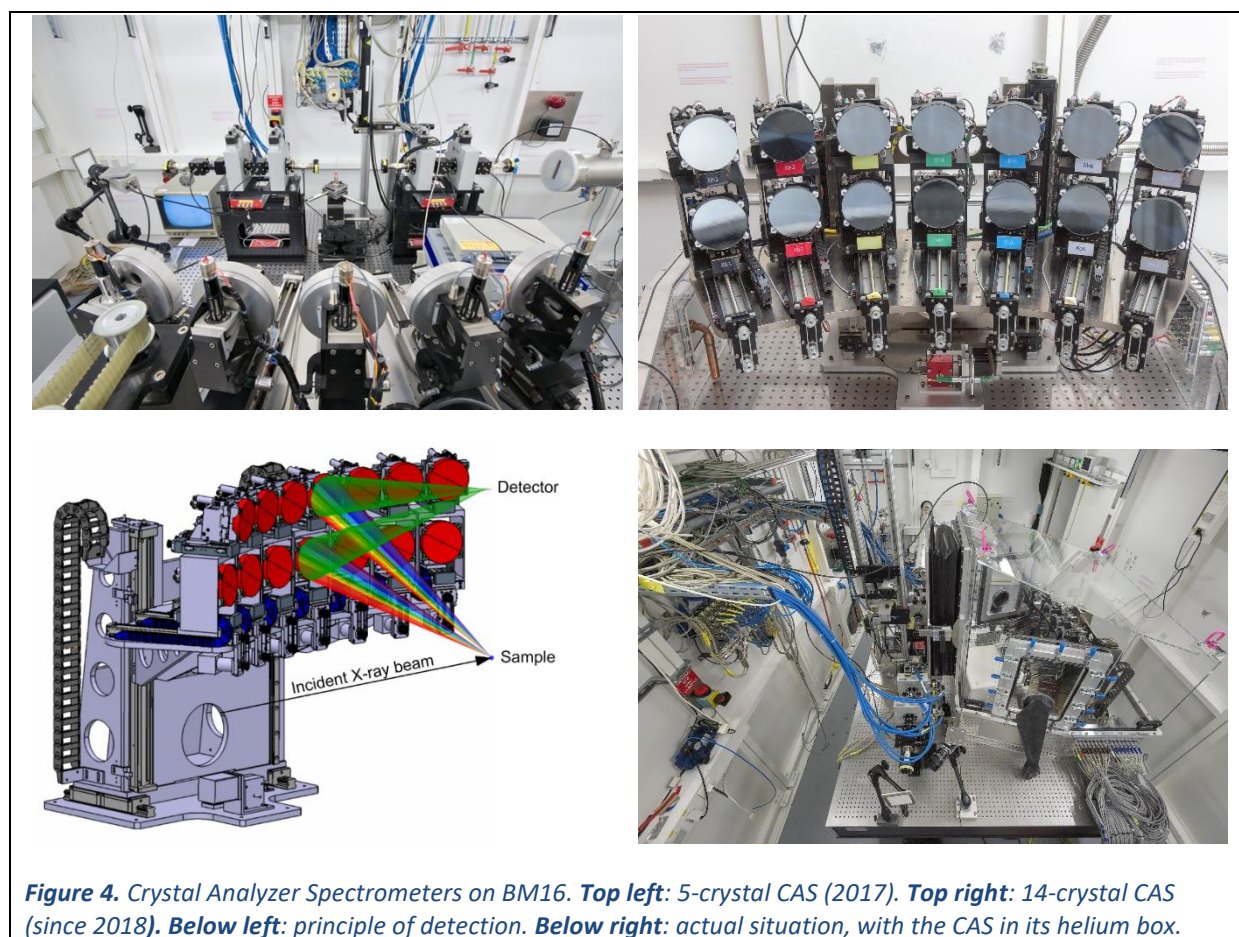


Figure 4. Crystal Analyzer Spectrometers on BM16. **Top left:** 5-crystal CAS (2017). **Top right:** 14-crystal CAS (since 2018). **Below left:** principle of detection. **Below right:** actual situation, with the CAS in its helium box.

The principle of energy selection is based on diffraction properties of the analyzer. Each crystal is aligned in order to fulfill Bragg's condition with respect to the energy of the photons to select. Moreover, using bent crystals allow to focus the diffracted photons

¹ Hazemann et al., *J. Synchrotron Radiat.* **16** (2009) 283-292 <http://dx.doi.org/10.1107/S0909049508043768>

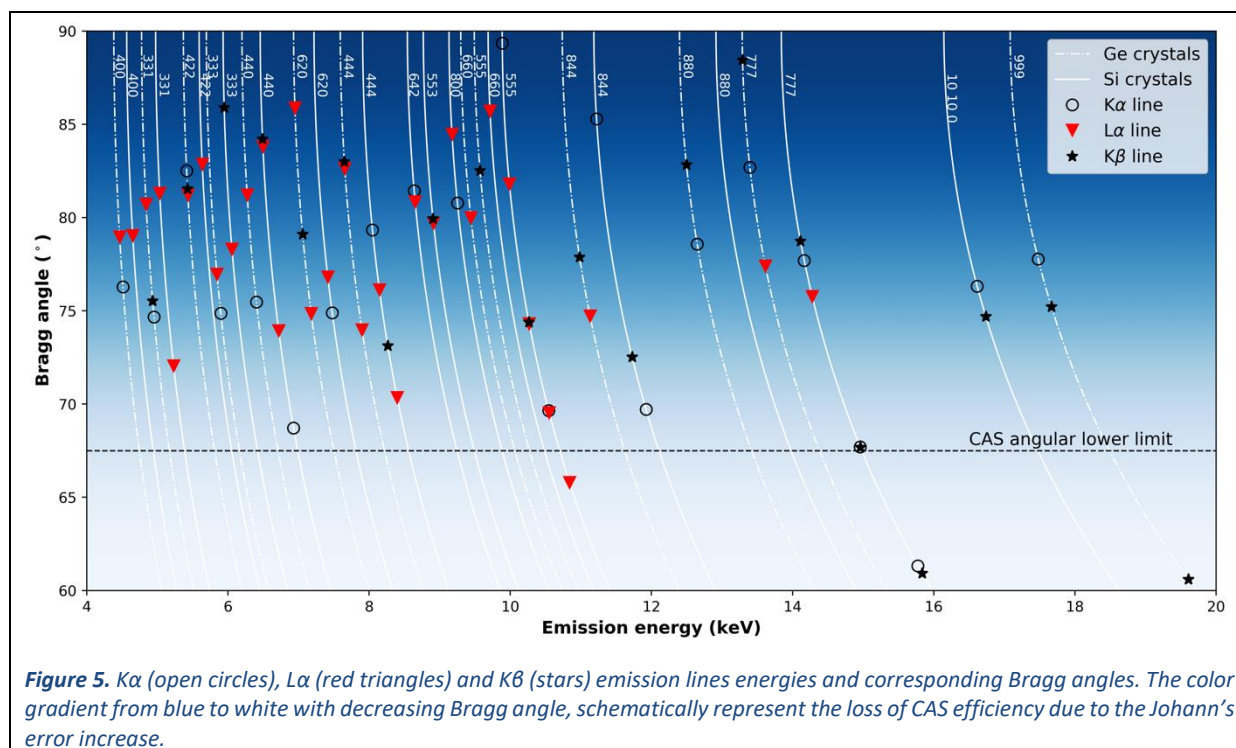
² e.g. Rodolakis et al., *Phys. Rev. Lett.* **104** (2010) 047401 <http://dx.doi.org/10.1103/PhysRevLett.104.047401>

³ Llorens et al., *Review of Scientific Instruments* **83** (2012) 063104 <http://dx.doi.org/10.1063/1.4728414>

Technical specificities

on a detector to count them. In Johann's geometry such focusing properties are optimum in the crystal vertical direction, less in the horizontal one, while the diffracting properties are optimum in the horizontal direction, less in the vertical one. Such a compromise allows to use the same spherically bent crystals on a large angular range.

The spectrometer can be equipped with up to 14 spherically bent crystals in a Rowland geometry. Crystals have a 1m radius of curvature, with a Bragg angle ranging from nearly 89° up to 67.5° , allowing to probe most of the emission lines of interest in a configuration where the Johann's error can be considered as negligible (Figure 5), with an energy bandwidth in the eV range. The entire spectrometer is located in a helium Plexiglas box to limit the absorption of the fluorescence signal on the sample - crystals - detector path ($\sim 2\text{m}$ length). Photons diffracted by the crystals are focused on either a Silicon Drift Detector (Ketek, energy resolution: $\sim 150\text{-}250\text{ eV}$; diameter: 8mm) or a 2D hybrid pixel detector (ImXPAD S70; active area: $15 \times 70\text{mm}^2$). By using an energy resolved detector one can at this level discriminate again, with a medium energy bandwidth. This second discrimination allows to decrease the background signal close to zero, a fundamental point when the signal of interest is low (case of the ultra-diluted element). By using a 2D detector, the alignment of the spectrometer is easier and the detection area is larger.



Detection limit

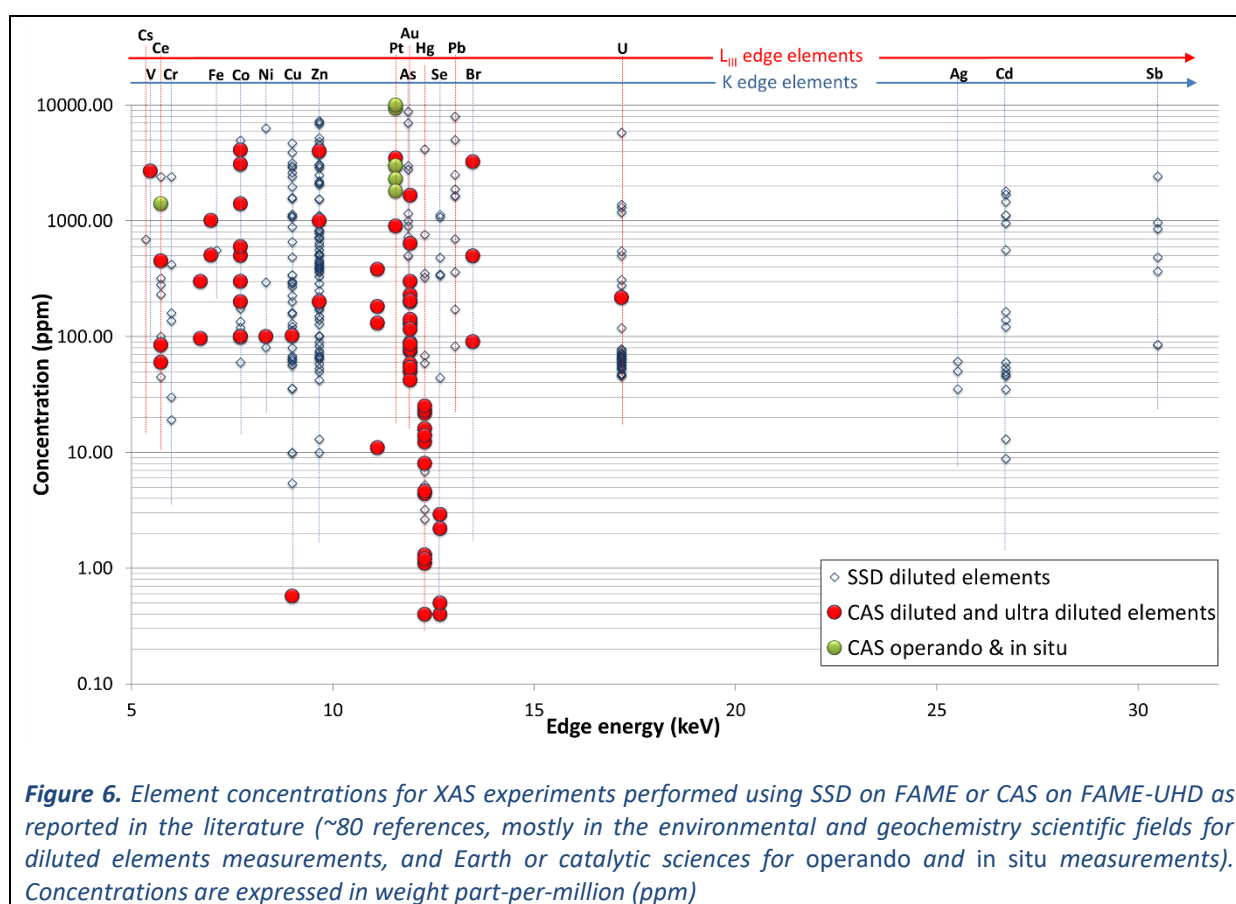
A figure of merit to illustrate the possibilities offered by both beamlines is the detection limit. We gathered on Figure 6 the concentration of elements probed by XAS on FAME and FAME-UHD. Using a SSD, the lowest concentrations are around 10-100ppm to measured EXAFS signals on FAME, while XANES measurements at concentrations as low as 0.5ppm have been performed with CAS on FAME-UHD.

Technical specificities

Using SSD detector can be also problematic in some particular cases, even if the element of interest is not highly diluted but in a matrix containing elements presenting fluorescence lines superimposed with the interesting ones. In these cases CAS constitutes an efficient solution. This was the case for the study of Ge diluted in Sphalerite (ZnS)⁴, or more recently of Au diluted in arsenopyrite^{5,6}.

Reversingly, using CAS for concentrated elements studies or for high energy experiments is not the best options.

Working with the same team operating the two beamlines allows to dispatch the users' experiments on the optimum way, depending on the optimum detection system.



⁴ Bonnet et al., "Characterization of germanium speciation in sphalerite (ZnS) by X-ray absorption spectroscopy", *Minerals* **7** (2017) 79 <http://dx.doi.org/10.3390/min7050079>

⁵ Pokrovski et al., "The nature and partitioning of invisible gold in the pyrite-fluid system", *Ore Geology Reviews* **109** (2019) 545-563 <https://doi.org/10.1016/j.oregeorev.2019.04.024>

⁶ Filimonova et al., "The state of Au and As in pyrite studied by X-ray absorption spectroscopy of natural minerals and synthetic phases" *Ore Geology Reviews* **121** (2020) 103475 <https://doi.org/10.1016/j.oregeorev.2020.103475>

4.1.c. control-command

The ESRF is implementing a new beamline control system, BLISS, that aims at replacing SPEC. In this context, we are developing all the specific parts necessary to carry out experiments on both BM16 and BM30. Most of the elements can now be controlled through BLISS on both beamlines. Nevertheless, due to all the work necessary to restart the beamlines after the upgrade, it was not possible to dedicate beamtime to migrate experiments to BLISS at the restart. Moreover, controlling the detector via BLISS on BM30 highly depends on the acquisition of a new electronic system. On the other hand, we are still working on synchronization issues, and continuous scan, which will offer new possibilities to the users: performing continuous scans enables faster experiments but it also provides more stability in the measurements. Preliminary results obtained during tests on BM30 are really promising (see Figure 7).

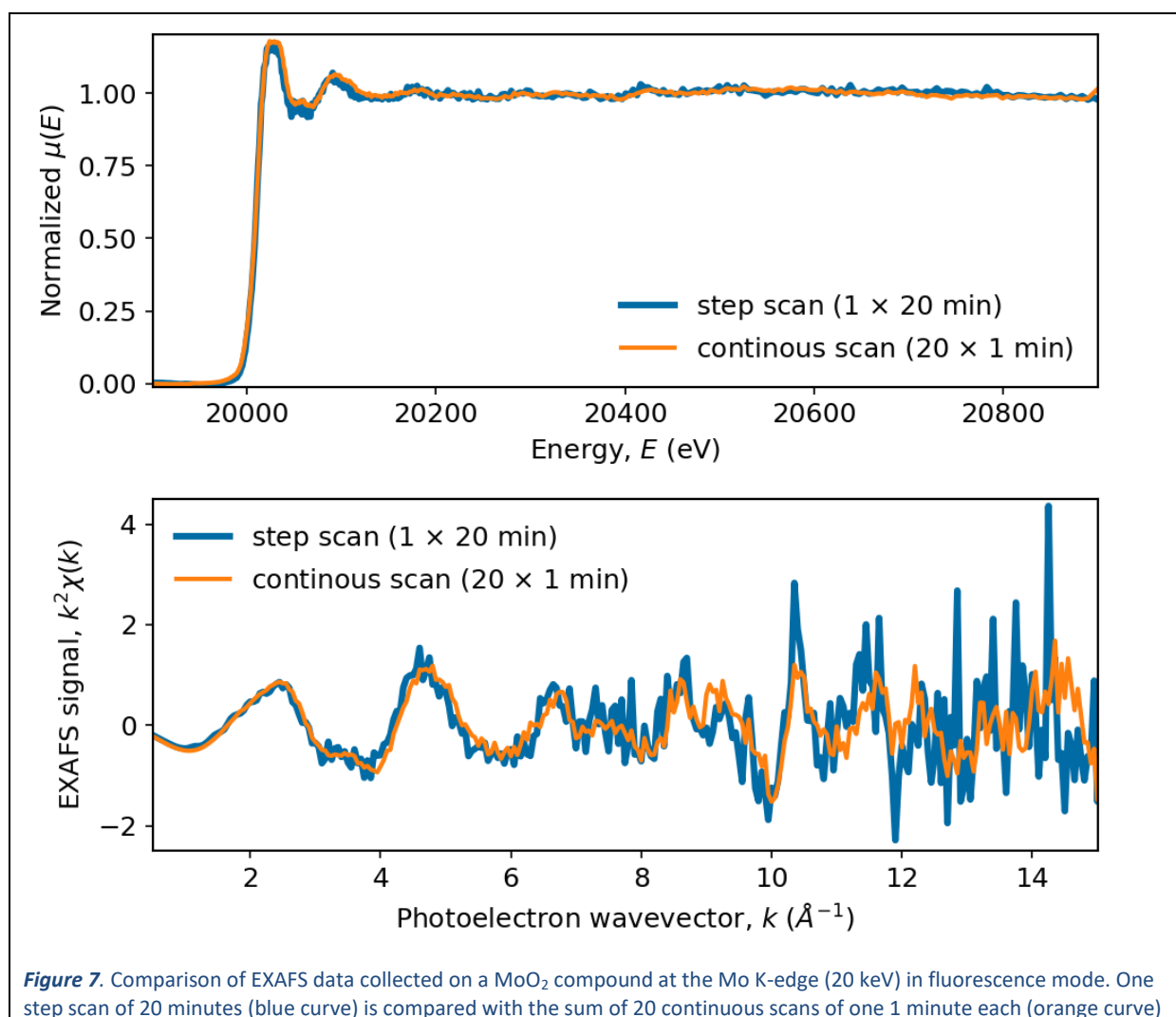


Figure 7. Comparison of EXAFS data collected on a MoO_2 compound at the Mo K-edge (20 keV) in fluorescence mode. One step scan of 20 minutes (blue curve) is compared with the sum of 20 continuous scans of one 1 minute each (orange curve)

4.2. Sample environments

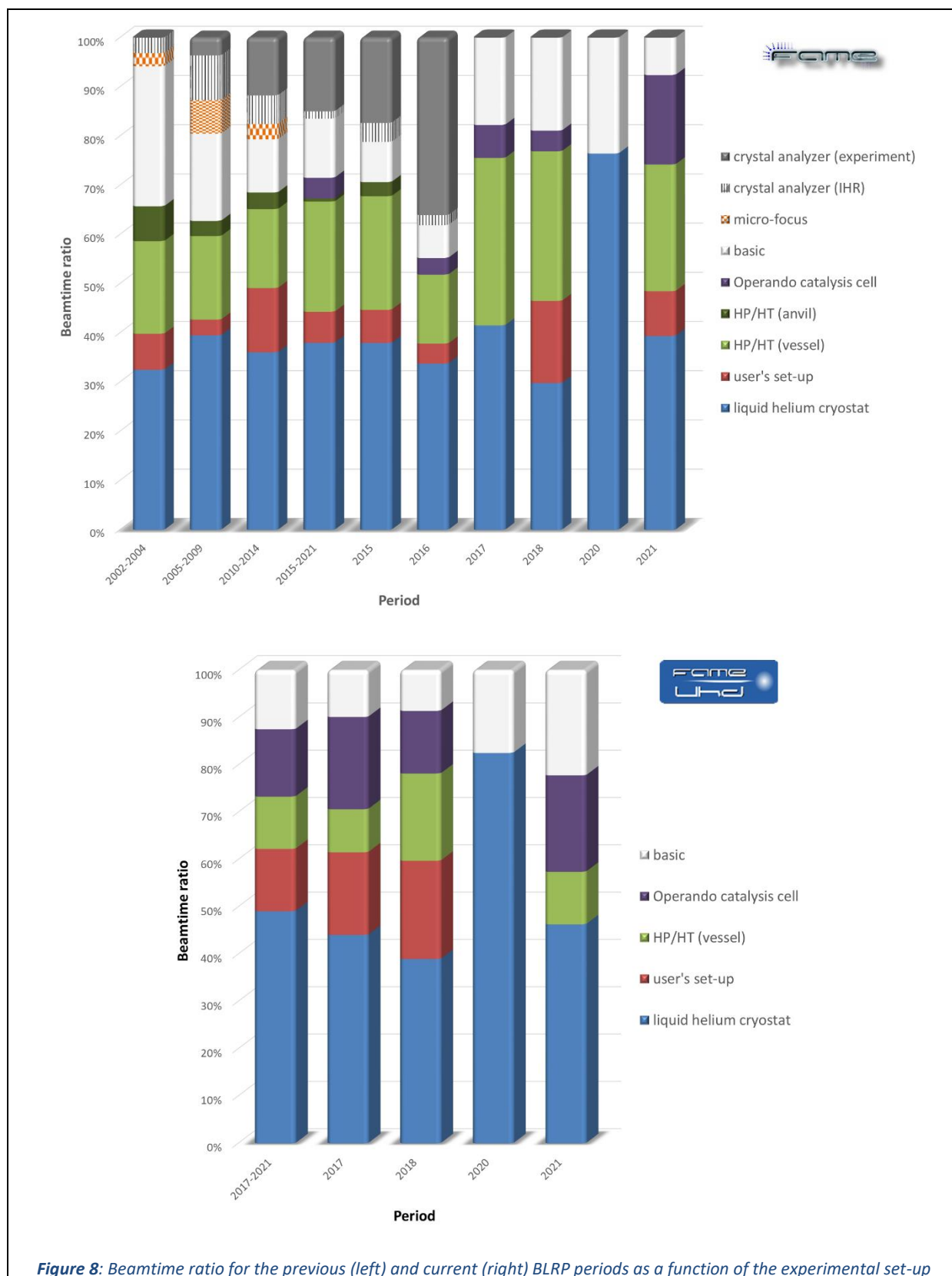


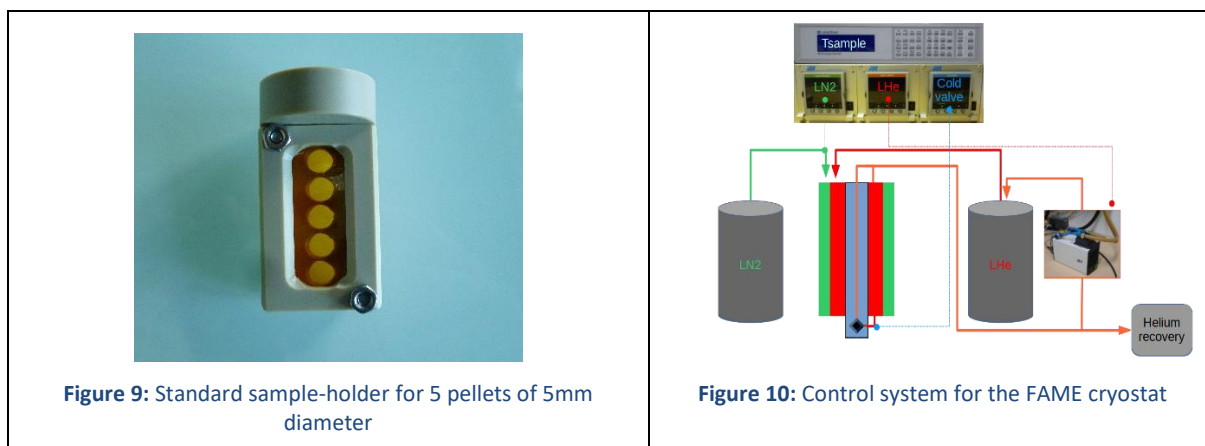
Figure 8: Beamtime ratio for the previous (left) and current (right) BLRP periods as a function of the experimental set-up

4.2.a. Liquid helium cryostats

Most of the experiments conducted on the beamlines make use of liquid helium (LHe) cryostats. Especially those in the field of environmental science and biology. The main purpose is to reduce radiation damage, keeping the sample in a “safe”/stable state for a measuring time between 30 minutes and 1 hour, that is, the typical acquisition time of a spectrum, before moving to a fresh spot. Both cryostats available at FAME and FAME-UHD are LHe flow-type cryostats, that is, the sample holder is kept in the LHe vapours (second exchanger’s chamber). The advantages of this type of cryostat with respect to a “cold-finger” type are: 1) uniform temperature on the sample and close to the exchanger’s temperature. 2) fast sample holder exchange, in the order of few minutes, as the cryostat is always kept at low temperature while the samples are extracted or inserted.

The “Orange” cryostat at FAME

The LHe cryostat at FAME is an ILL (Institut Laue Langevin) “orange” cryostat (Figure 3 left). It is in operation since 1994, and was fully refurbished in 2010. It can operate from 300 K down to 4 K. The rotation and the vertical translation of the sample-holder are motorized and up to five pellets of 5 mm \varnothing can be inserted simultaneously (Figure 9).



A control system is integrated with the beamline control software (Figure 10). Not only it permits controlling and monitoring the temperature of the sample, but also performing the refill of the cryogenic tanks of the cryostat from the LN2 and LHe reservoirs. This has the advantage that the users will not deal with performing cryogenic tasks during the whole experiment (apart those required to change the sample).

Despite many years of loyal operation at the beamline, the “orange” LHe cryostat is a massive instrument and will be replaced by the “mini” LHe cryostat available at FAME-UHD.

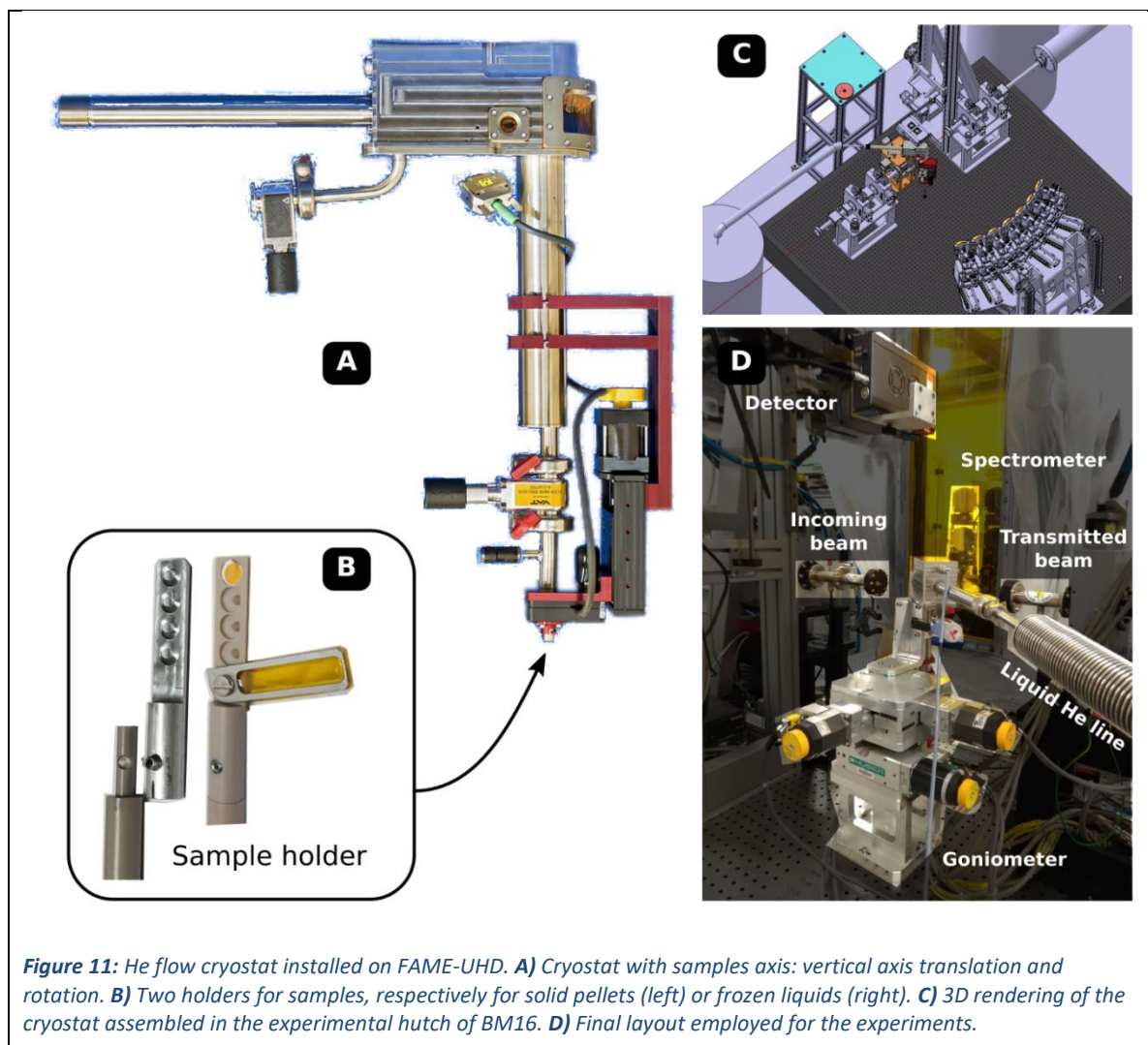
The mini “Ricardo” cryostat at FAME-UHD

The LHe flow cryostat at FAME-UHD was designed by Ricardo Steinmann and manufactured by the company “AS – special devices”. It is in users’ operation since 2018. The temperature operation range is 300-4 K, with a minimum He consumption at around 10 K. When running at this temperature and with a sample exchange twice a day, the cryostat consumption is approximately one full dewar (10 kg of LHe) per experiment (usually 18 shifts). The cryostat, samples holder and assembly on the beamline are shown in Figure 11.

The sample holder is mounted on an insulating rod made out of PEEK (polyethylene ether ketone) and of 8 mm diameter. Three apertures are present on the cryostat, two small ones permitting the direct X-ray beam to reach the sample and pass through it, and a bigger one

Technical specificities

permitting the emitted fluorescence to reach the fourteen crystal analyzers of the spectrometer in the whole scanning angular range. Furthermore, the large window may be used as an entrance window for photo-excitation experiments with a laser. The apertures are sealed with Kapton windows of 50 μm thickness. The sample's rod can move inside the cryostat via two motorized axes: a translation along the vertical direction and a rotation around it. This allows to align up to four pellets of 5 mm diameter and to adjust the incidence angle around 45° . The secondary heat exchanger is connected to the primary one inside a vacuum chamber that is kept under static vacuum via an absorption pump.



The whole cryostat is mounted on a three-axis goniometer (X, Y, and Z) to align it with the X-ray beam. The space constraints introduced by the presence of the spectrometer and in particular the detector arm moving along the vertical axis and reaching the top of the cryostat for Bragg angles close to 90° , force the sample extraction from the bottom. This operation is simple, as the whole goniometer is mounted on a rail, permitting to move the cryostat out of the experimental table. A typical user usage of the cryostat over five days of experiment is shown in Figure 12. The cryostat is cooled down to approximately 10 K at the beginning of the experiment, after a degassing procedure of the absorption pump that permits running the cryostat in a static vacuum for the whole experiment. Changing the sample holder takes less than 10 minutes and within 30 minutes the temperature is back to the working one (10 K).

Technical specificities

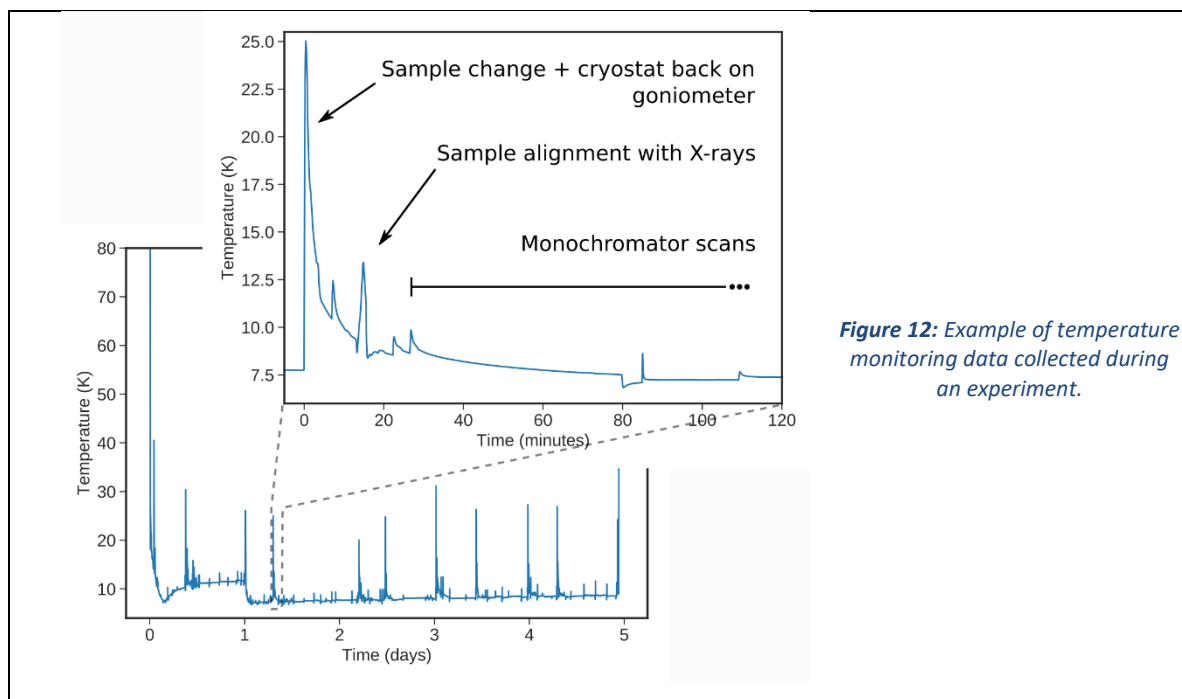


Figure 12: Example of temperature monitoring data collected during an experiment.

4.2.b. HP/HT setup

Since the start of the FAME beamline operation the autoclave devices have been staple items of our pool of sample environments. Indeed, hydrothermal fluids studies constitute one of the main topics of in-house research at the FAME and FAME-UHD beamlines, and they drive the constant development and improvement of such HP/HT tools for our users. The development is done in collaboration with the technological support group [X'Press](#) of the Néel Institute, which has a very strong expertise in HP technology. The result consists in an experimental equipment unique on international synchrotrons which offers the possibility of in situ XAS measurements, essential to obtain solubility and speciation data, in very challenging hydrothermal conditions (see scientific examples in this report). It is a premium tool for studies of metal transport by geological fluids.

The main issues addressed on the FAME beamlines during the period 2015-2020 are :

- The development of a new version of our autoclaves. Over the period 2012-2020 we've been involved in the [PLANEX](#) EquipEx (« Experimental planet: simulation and in-situ analyses under extreme conditions ») and we were in charge of upgrading our equipment with better geometry and thermal behaviour : the P/T range available is now [1-2000 bar] and [5-1100°C]. Several units are now fully operational at FAME and FAME-UHD (XAS), but also in laboratories at the Néel Institute and ISTO (Orléans).
- The integration of the equipment on the FAME-UHD beamline. The large angular aperture of the HP beryllium windows are a real asset and allows the use of 6 crystals : this geometry, combined with the low absorption of the materials used, provides high quality data from in situ hydrothermal experiments, even at low X-ray energies and low concentrations. Figure 13 shows a technical drawing and a real-life picture of the autoclave in operation at FAME-UHD.

Technical specificities

- The less visible but necessary technical development and maintenance to make our equipment even more reliable and user-friendly. An example is the optimization of machining protocols for the internal cells to improve the tube-piston seal and to reach a wall thickness of 150 μm (both glassy carbon and sapphire): the latter has a very positive impact on the data quality by limiting the elastic scattering.
- The set-up of autoclaves dedicated to the catalysis research (see related part in this document). This equipment is derived from our autoclave design and adapted to the specific needs of catalysis studies.

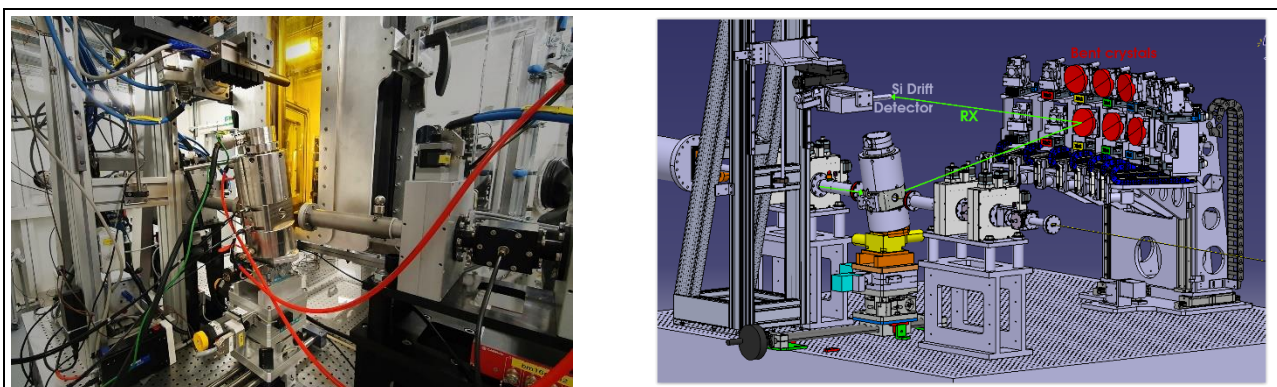


Figure 13. *Left* : picture of the new PLANEX autoclave installed on the FAME-UHD spectrometer. *Right*: technical representation with the same elements as in the picture ; the 6 crystals in red are fully used thanks to the unique design of the HP windows.

Our equipment has reached a solid national and international reputation due to its uniqueness and the quality of the data that it gives access to. Its high technicality, user friendliness and reliability are great assets to attract users, reinforced by our teaching actions about the autoclaves (during the annual FAME+/ASTER'X workshops, or the recent ESRF workshop about synchrotron HP techniques).

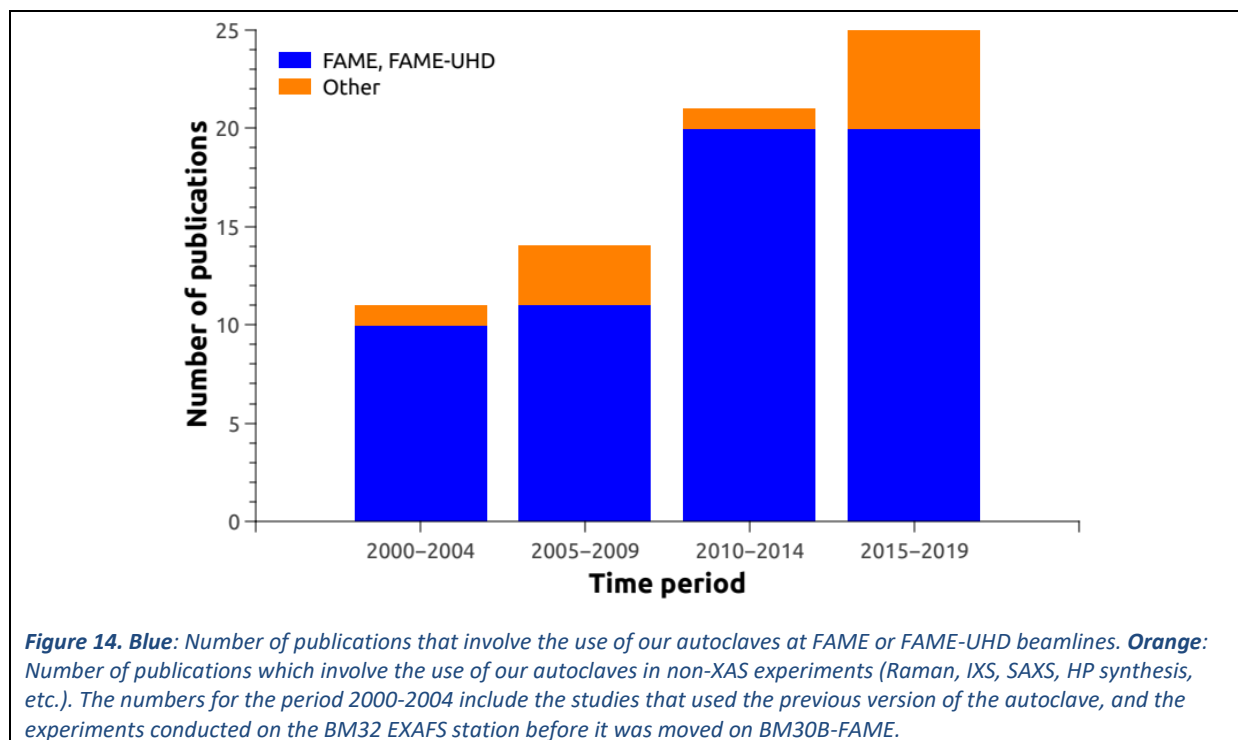


Figure 14. *Blue*: Number of publications that involve the use of our autoclaves at FAME or FAME-UHD beamlines. *Orange*: Number of publications which involve the use of our autoclaves in non-XAS experiments (Raman, IXS, SAXS, HP synthesis, etc.). The numbers for the period 2000-2004 include the studies that used the previous version of the autoclave, and the experiments conducted on the BM32 EXAFS station before it was moved on BM30B-FAME.

Technical specificities

Figure 14 shows the number of publications involving the use of our autoclaves in the period 2000-2019: that's a total of 71 publications. A complement to this statistical analysis is to consider our 2005 technological publication⁷ that describes our autoclave equipment: it has been cited 75 times since 2005. Indeed, in the period 2002-2019 where FAME was fully operational, ~100 experiments (~6 days each) using the autoclaves were conducted on our beamlines. A strong indicator of the quality of our equipment is also the trust placed in us by regular users who come back to our beamline for hydrothermal research, and our capacity to attract new autoclave users.

Finally, an associated research activity is conducted by J.L. Hazemann and D. Testemale at the Néel Institute where the same autoclave equipment is installed on a Raman spectrometer and a laboratory X-ray micro-source (Figure 15). Hence, two configurations of the autoclaves coexist:

- [1] one (beryllium HP windows and glassy carbon internal cells) dedicated to X-rays studies such as X-ray absorption spectroscopy at FAMEs beamlines and density measurements at the Néel Institute on a laboratory X-ray source ;
- [2] a second one (both HP windows and internal cells made of sapphire) dedicated to measurements with visible light such as Raman spectrometry, visual observation, light scattering, etc. Since 2015, in the framework of the PLANEX project (see above) a new Acton spectrometer was installed at the Néel Institute, along with a new optical line for an improved data quality. The topics investigated are the supercritical solvents (H₂O-CO₂ supercritical mixtures) and organic species in hydrothermal conditions.

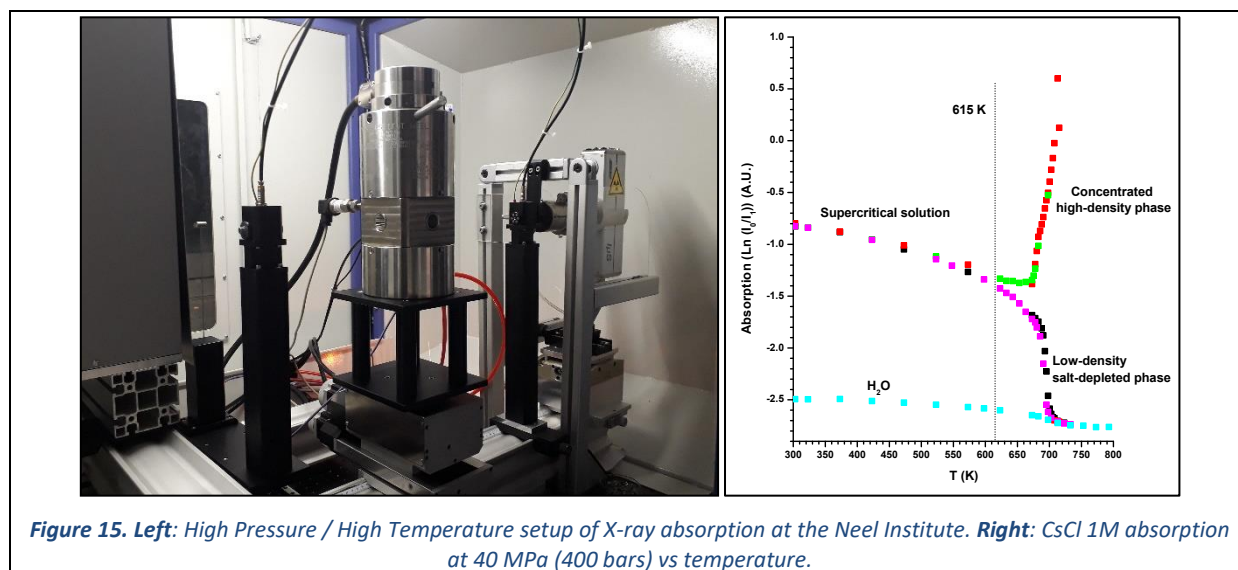
One of the new features is the availability of X-ray absorption measurements in the laboratory. Indeed, the setup can operate with X-ray absorption in autoclaves (0.2 GPa, 1400 K). If many setups coupling DAC or PE press with laboratory X-ray sources already exist, X-ray absorption in autoclave is not so common (Figure 15, left). The instrument uses an Incoatec high-energy X-ray source (Ag K α _{1,2} radiation: $\lambda = 0.56 \text{ \AA}$, $E = 22 \text{ keV}$), with high brilliance and a focused beam of $160 \mu\text{m}^2$ at 575 mm from the source. The scan of the high-pressure device is carried out by vertical and horizontal motorized sample-holders. Low-noise detection is performed by home-made detectors for alignment and X-ray absorption measurements. The system is controlled by a Labview software. Our very first X-ray absorption data in autoclave are highlighted here.

In the field of hydrothermal geological fluids research, the role of supercritical water for the solvation of species is a key issue. As an example, X-ray absorption measurements of a model salt solution of cesium chloride 1 M are presented using our new design of autoclave (Figure 15, right). The CsCl solution (0.1 - 0.3 cm³ volume) was contained inside a glassy carbon tube (5 mm internal diameter) and helium-pressurized by two glassy carbon pistons. By following the transmitted-over-initial intensity ratio (Beer-Lambert law), the absorption of the fluid is characterized during the heating under pressure (40 MPa or 400 bars). Below 600 K, the absorption is slowly decreasing with temperature, in good agreement with the density decrease of the supercritical fluid. Suddenly, at 615 K, the demixing takes place between a low-density salt-depleted phase and a concentrated high-density one. Thanks to the performances of the instrument, we were able to follow very properly the absorption evolution of both phases. These new data show that the structural change of water in the vicinity of its critical

⁷ Testemale D., Argoud R., Geaymond O. and Hazemann J.-L. (2005) High pressure/high temperature cell for x-ray absorption and scattering techniques. *Review of Scientific Instruments* **76**, 043905 <https://doi.org/10.1063/1.1884188>

Technical specificities

density (0.32 g/cm³) is directly correlated with the appearance of phase separation in the fluid. This result was suspected by previous synchrotron measurements, but the need for finely scrutinizing the origin of the phase separation could not be clearly exhibited due to limited beamtime.



Following these original results, the further development of an X-ray fluorescence measurement will ultimately enable to select and quantify the element partition-coefficient during the phase separation. This knowledge is of great importance in the understanding of hydrothermal fluid ore deposits.

This new HP-HT laboratory platform will then become an essential instrument to point out relevant parameter values and thus so to clearly target further synchrotron experiments.

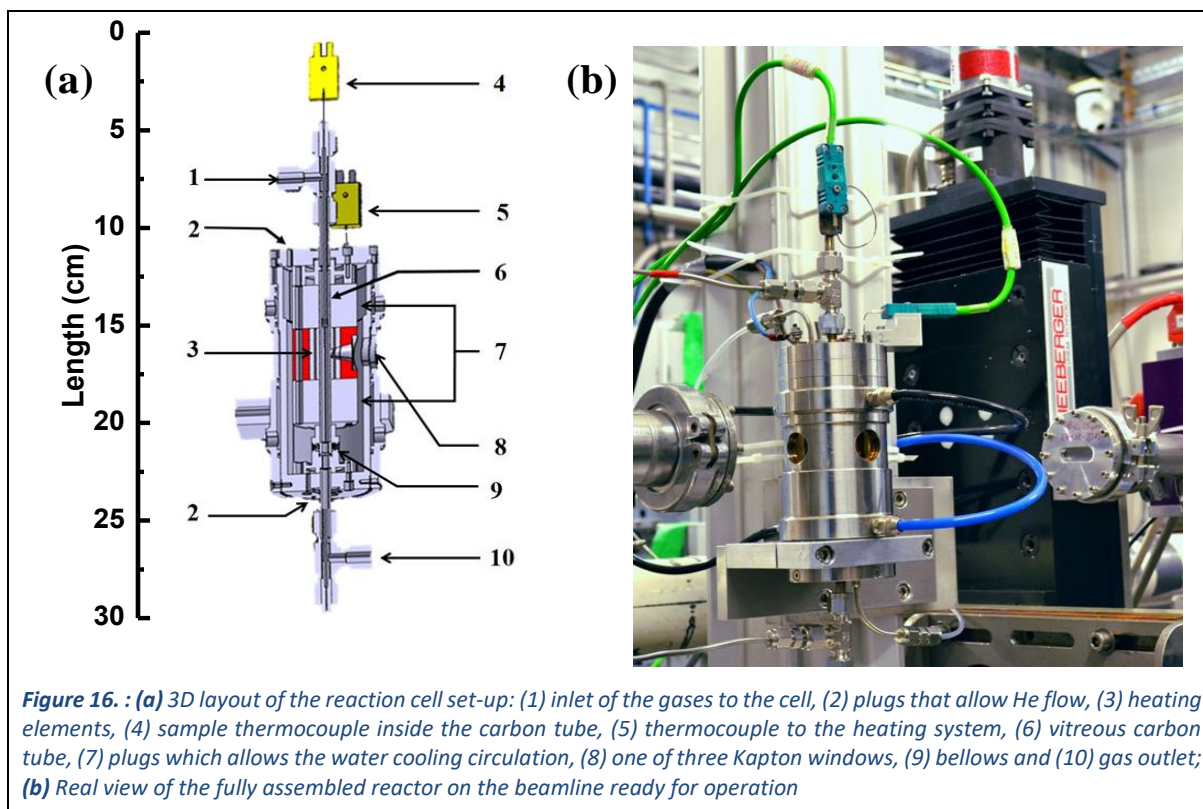
4.2.c. XAS characterization of catalysts under operando conditions

High temperature system

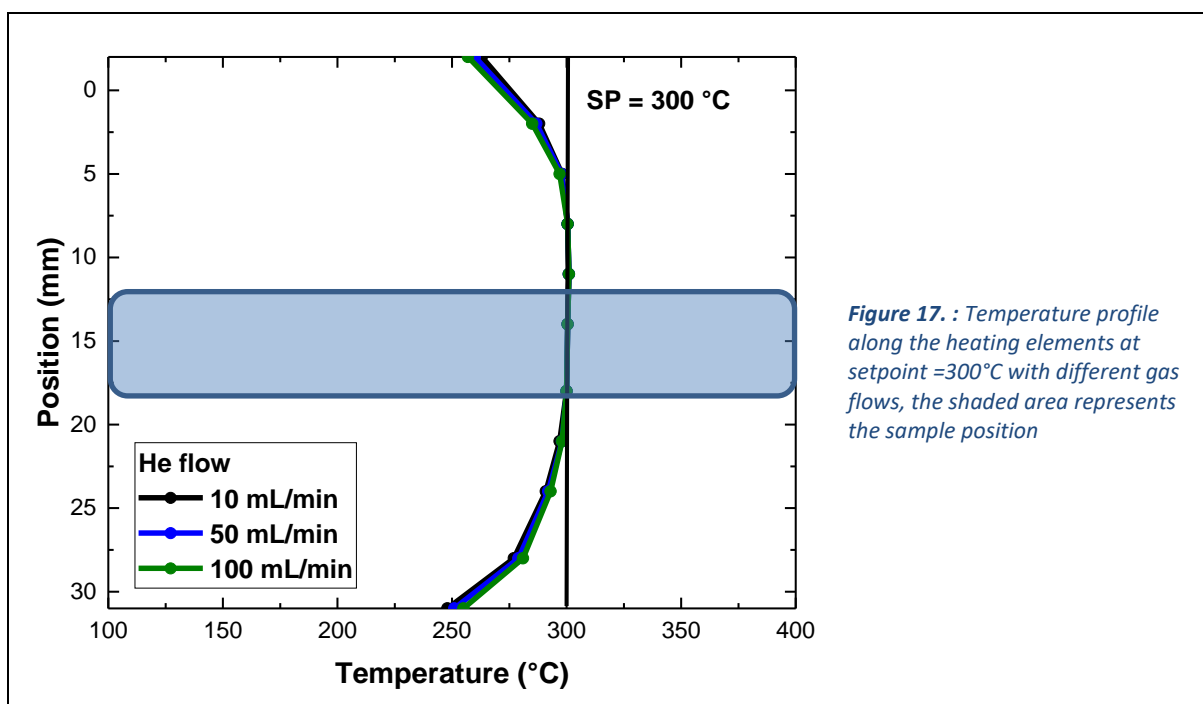
Heterogeneous catalysts commonly exhibit a variety of different surface sites which are difficult to identify, even if such identification is critical for the design and development of improved catalytic materials. Ideally, characterization of a catalyst involves the measurement of its properties during the catalytic reaction, *i.e.* *operando* conditions. Currently, X-ray absorption spectroscopy is one of the most widely used techniques for analysis of catalysts due to the high penetration depth of X-rays, enabling adequate analysis of the electronic and structural properties even in complex environmental conditions.

A dedicated cell for *operando* XAS characterization was designed to perform dynamic reaction as a plug-flow reactor using powder samples, which requires gas flow and thermal treatment in order to reproduce the high-temperature real conditions in a conventional dynamic microreactor (Figure 16a). The glassy carbon tube is located in the middle of the heating elements, and the design uses a thermocouple to control the temperature of the oven and a second thermocouple is located close to the sample. The assembled reaction cell on the beamline ready for operation is shown on Figure 16b, with one of the two transmission windows as well as the fluorescence window. The body of the cell was built using stainless steel. The design of the cell allows operation from room temperature up to 1000 °C.⁸

⁸ Aguilar-Tapia A. *et al.* *Review of Scientific Instruments* **89**, 035109 (2018)



The design of the heating elements ensures a homogeneous and stable temperature. Figure 17 shows a temperature profile along the oven using various flows of He and using a temperature set point of 300 °C. The shaded area represents the sample position. It can be observed that the gas is quickly heated and the temperature remains constant independent of the gas flow.



Technical specificities

Further modifications of the cell lead to the construction of a new reaction cell. The main goal was to increase the solid angle of the fluorescence window from 22 to 70° in the horizontal axis and make the most of the FAME-UHD 14 crystals analyzer spectrometer (Figure 18). This aperture will allow the fluorescence signal to light the 14 crystals.

The dedicated system for the study of catalyst under real conditions includes a completely automated gas distribution system. It is used to deliver a mixture of gases through the reaction cell and the venting. Each gas line is controlled by one or two mass flow controller calibrated for each gas. The main features of this set-up are:

- a complete remote control of the gas distribution using a PC,
- a pressure valve protects the vitreous carbon tube from an unusual increase of pressure which could break the reactor,
- a 4-way valve allows to switch between a by-pass and the line to the reaction cell,
- a 6-way valve allows the study of catalysts by pulsing a known and controlled amount of a specific gas⁹.

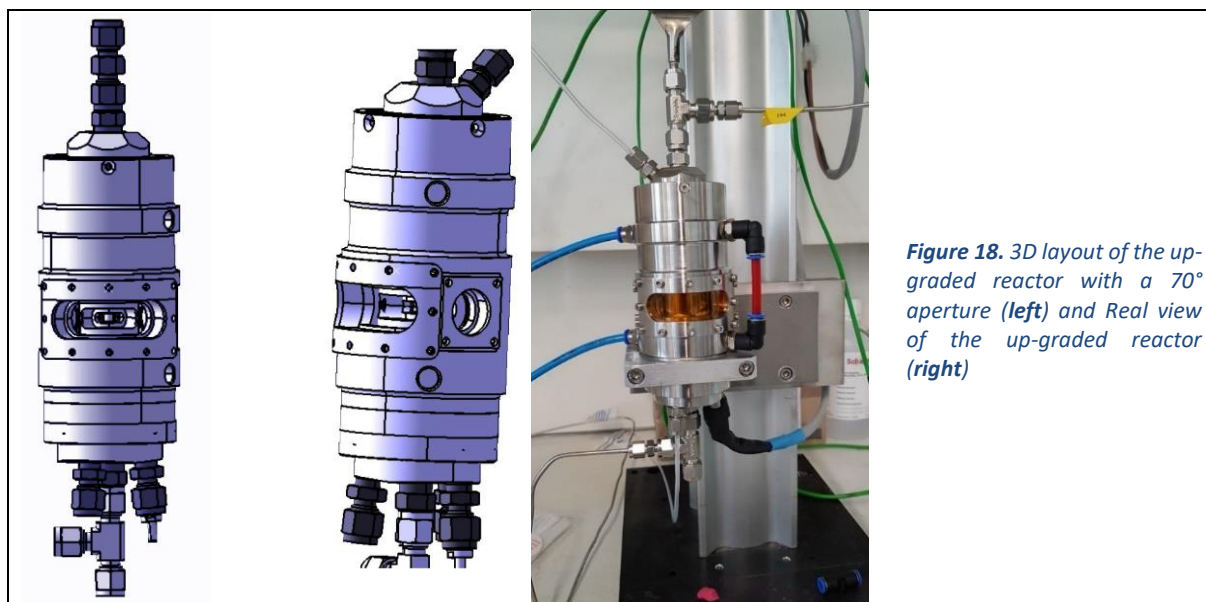


Figure 18. 3D layout of the up-graded reactor with a 70° aperture (left) and Real view of the up-graded reactor (right)

High pressure-high temperature system (1000 bar, 1000°C)

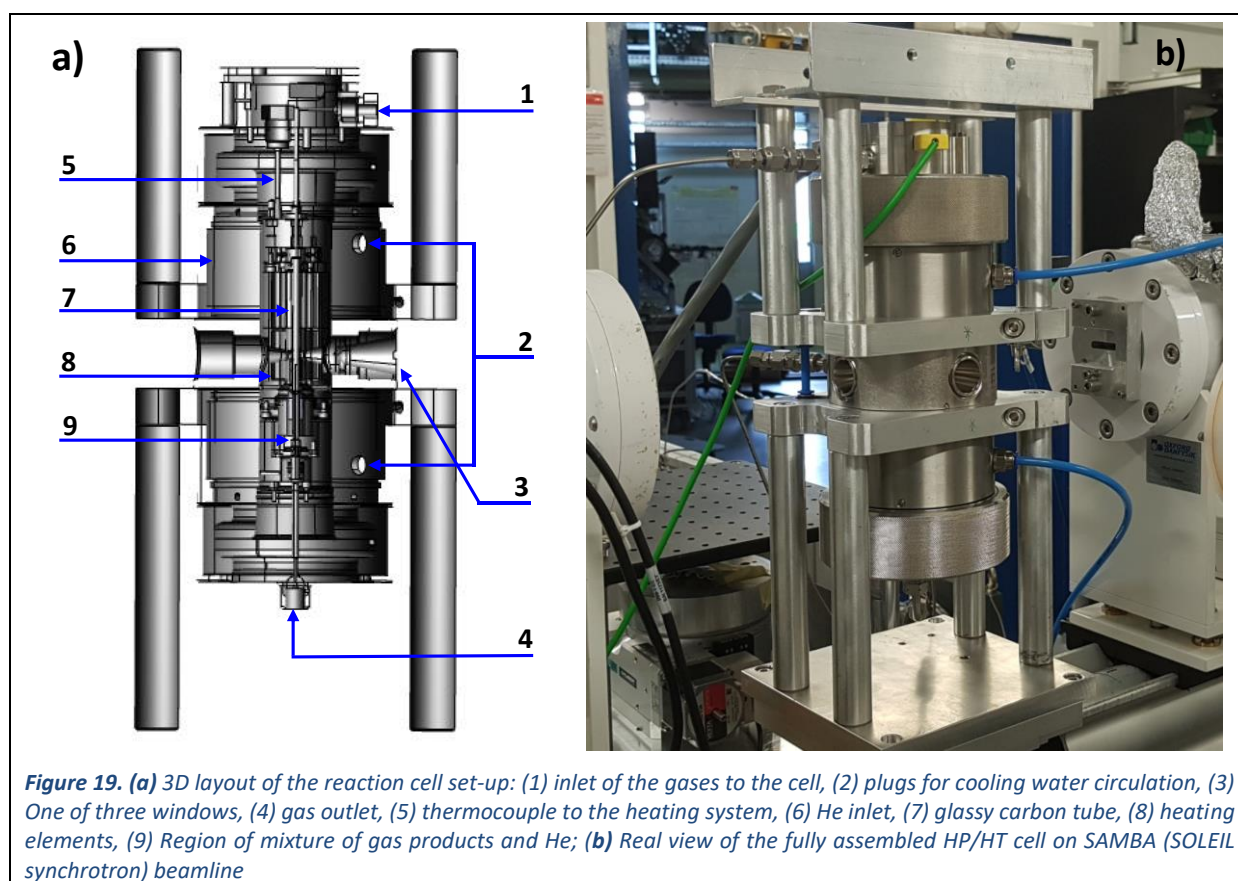
Recently, a new XAS reaction cell was designed to perform dynamic reaction using powder samples, which requires a gas flow a thermal treatment and a pressure control in order to reproduce the high-pressure real conditions in a conventional dynamic microreactor. Figure 1a shows a 3D layout of the components of the cell. The glassy carbon tube is located in the middle of the heating elements, and the design uses a thermocouple to control the temperature of the oven. Figure 19b shows a photograph of the assembled reaction cell on the beamline ready for operation; the image shows one of the two transmission windows as well as the fluorescence window. The body of the cell was built using stainless steel.

⁹ See the highlight in the scientific results section, “Operando XAS observation of Mo transforming to its active phase for converting methane to aromatics”

Technical specificities

Increasing the pressure is possible flowing the reaction mixture (1 in Figure 19a) through the glassy carbon reactor and the helium through the body of the cell (6 in Figure 19a) at the same time to equilibrate the internal pressure. The mixture of the products of the reaction and the He happens just before the exit of the cell (9 in Figure 19a). Delivery of the gases to the reaction cell is made by a fully remote-controlled high-pressure gas distribution system. The pressure regulation is made at the exit of the reaction cell using a pressure regulator and the required pressure set point can be modified manually by a control software depending on the requirement of the reaction conditions

In each reaction system, the gas composition from the reactor is monitored on-line by an EcoCat-P portable mass spectrometer system from ESS that can be operated remotely. The system is equipped with two identical capillary inlets for the on-line analysis of the reactor outlet and a bypass line. The response time of the inlet is 150 ms. The system also allows quantitative analysis and has the capability to monitor up to 64 species in real time. In addition, the mass spectrometer also identifies unknown compounds and offers detection levels down to ppb levels.



5. Expertise and Interactivity between our Team and the users

5.1. FAME+ and ASTER'X

A synchrotron radiation facility is an instrument that federates at the same place and with similar scientific problems, different communities which are interdependent in their experimental needs. It is however necessary to create and to maintain continuously *i)* emulations around the beamline, *ii)* interactions with the users. We organized or participated to several punctual or recurrent operations since 2002 and the beginning of FAME operation. We detail hereafter the most relevant.

Training courses for students

Each year, about 5 days are allocated for teaching practicals on the beamline for scientists and for University graduate students. For the 2015-2021 period we participated to several specific courses

- each year, the HERCULES course with 2 days of practicals on FAME and on both beamlines since 2018 and 2 days of tutorials at the Neel Institute,
- since 2011 and each year, 1 day of practicals for the PhD school of the Grenoble Institute of Technology (Grenoble INP),
- in 2018, practicals for Master students of the Grenoble-Alpes Univ. ("Ressources", resp. L. Truche)

FAME+: a course dedicated to our users

Considering the technical complexity of synchrotron radiation experiments and the difficulty to obtain beamtime *via* the various program committees, few new teams having scientific problems adapted to these instruments use the beamlines. We decided in 2004 to organize an annual training for users (actual or potential): FAME+ (Formation en Absorption X pour la Maîtrise de l'Expérience et le Pilotage d'une Ligne Utilisant un Synchrotron). This training is organized with the help of the CNRS permanent training team and very well recognized. The main goals of this training are to explain

- the technical aspects of the experiment and the various analysis possibilities,
- the optical adjustments of the beamline.

The training is conceived with lectures, practicals on the beamline and tutorials on computer. To summarize, the training clarifying the FAME operations have several interests:

- to open the beamline to the whole communities,
- to make more autonomous the current or future users, from a technical point of view,
- to increase the safety on the beamline,
- to give to the users a critical glance on all the important points which allow the realization of an experiment under optimal conditions,
- to give to the users the up-to-date tools to analyse their data,
- to train the users to the beamline evolutions.

Concerning the last point, we trained the users to the scientific interest, to the experimental points to take care about... of the Crystal Analyzer Spectrometer measurements, well before their use on FAME, simultaneously with the first tests. When the spectrometer installed on FAME and then on FAME-UHD opened to regular users, they were ready.

This project was initially reserved for the Earth sciences community but it has been quite soon opened to the other scientific communities. Since 2004 and to the last session in 2018, 192

trainees (mainly PhD students) issued from 73 laboratories followed this course.

The next step: ASTER'X

In order to continue our training mission, we decided to change the FAME+ training sessions, by incorporating new techniques (X-ray imaging for example) but keeping the strengths of the school *i.e.*

- much more practicals and tutorials than lectures,
- a large part of the school dedicated to technical aspects, in order for the users not to consider the beamlines as a “black box”.

We conceived then the ASTER'X CNRS Thematic School (Analyses par Spectroscopies, Tomographie et Emission de Rayons X), with colleagues already involved in FAME+ (from Grenoble and Montpellier) and new ones (from CEREGE, Aix-en-Provence). ASTER'X will offer to 20 PhD students, postdoctoral or scientists a complete one-week training on X-ray absorption, X-ray emission and X-ray imaging (tomography and ptychography). The school will provide lectures on the theoretical, optical and instrumentation aspects, tutorials for data analysis and practicals on the FAME and FAME-UHD beamlines. It will allow to discover, to better understand, well-known technics but also quite emerging ones (such as ptychography). The school was funded by the CNRS in 2020, re-scheduled in May 2021 and it will finally take place in September 2021. Complementary funds were obtained in 2021 from ReGEF¹, Institut Néel, Université Grenoble Alpes and Grenoble-INP, LabEx OSUG@2020... More information can be found in the dedicated webpages.²

5.2. Sshade

Building a database that gathers the reference spectra acquired on our beamlines has been in our plans for many years. But several difficulties, among which manpower to create a powerful and detailed infrastructure, had slowed down our wills up to now.

First, the ESRF has integrated the PaNOSC data policy framework, which aims at developing the use of the FAIR (Findable, Accessible, Interoperable, Reusable) principles in 7 European neutron and photon facilities. The guidelines have been written in 2015 and the data policy is being implemented since the end of 2020. From now on, all the data acquired at the ESRF will be automatically stored with their metadata for 10 years and made accessible after a 3-year embargo. All the data are concerned, whatever they appear excellent, good, noisy, or containing errors. For the moment, no specific frame has been developed for the description of the samples, which make the data public but barely usable. The ESRF data policy have been implemented on both BM16 and BM30.

In parallel, in 2014, we decided to join the SSHADE Europlanet 2020-RI programme, which falls within the same FAIR approach, with a complementary aim of describing the samples for selected data.

The SSHADE database infrastructure³ hosts spectral data from many different types of materials: minerals, meteorites, organic matters, ..., as well as calculated spectra, covering the whole electromagnetic spectra from gamma rays to radio wavelengths. Its searching / viewing / downloading interface is open to users since February 2018. The SSHADE consortium currently gathers 21 laboratories from 11 different countries.

¹ <https://www.regef.fr/>

² <http://f-crg.fr/ecole-thematique-cnrs-asterx-2021/>

³ <http://www.sshade.eu>

In this context, the ESRF FAME and FAME-UHD beamlines have created the SSHADE/FAME database. Two main goals motivated this initiative:

- filling the lack of XAS databases. Indeed, few databases exist in the domain and they generally provide too few details in the sample descriptions, so that it is difficult to reuse the spectra for data analysis. This leads the users to carry out the same measurements several times, generating a global waste of beam time.
- anticipating the current political trend which requires that the scientific community make all the data available; but also ensuring that the data is effectively accessible, reusable, indexed and containing enough details to build a repository that could be used by individuals for related scientific works, as well as, in the future, by simulation codes (e.g. based on artificial intelligence).

Being part of SSHADE, the SSHADE/FAME database is a long-lasting solution (it has been labeled by the CNRS/INSU as a National Observation Service). It is based on an elaborate data model which enables a very precise description of all the components of a dataset (from the sample to the measurement) and an efficient search strategy. Moreover, by attributing a DOI (Digital Object Identifier) to each data set, it offers the possibility to make the spectra available in a robust way and accordingly to the current and future publication recommendations. Our work consisted in helping to modify the SSHADE data model to integrate XAS data, and building the software tools to input FAME data in the database. The SSHADE/FAME database already contains more than 400 XAS spectra (and more than 2900 spectra in the global SSHADE database).

The data ingestion is based on users volunteering. Data are ingested by the FAME staff at the end of each experiment and made available online only when a publication has been accepted, or on explicit demand of the users.

The search tool is quite elaborate and offers the possibility to find spectra either by absorption edge, by sample, by species in the sample... Data can be downloaded with a registration on the site. Projects aiming at using the database for data mining are in discussion.

5.3. French CRG workshop in 2019

The French CRG “prospective days” workshop took place at the ESRF on 9th-11th December 2019⁴. More than 110 participants attended the workshop, despite the travel restrictions, featuring 4 keynote speakers, 13 oral contributors, gathering beamlines scientific and technical staff along with X-ray users and a broad panel of representative investigators in various scientific fields covered by the five French CRG beamlines at ESRF: D2AM, FAME, FAME-UHD, FIP2 and IF respectively on port BM02, BM30, BM16, BM07 and BM32. The scientific presentations and the four round tables allowed to discuss with the users communities of the current and future capabilities of these beamlines in the frame of the ESRF - EBS project and to identify new instrumentations, new X-ray techniques and data handling that should be implemented in a close future.

These days were really useful to precise our MAGNIFIX project which was written in the following months (January-June 2020), to have a project as close as possible to the users' needs.

⁴ <http://f-crg.fr/workshop-2019/>



Figure 1. French-CRG workshop

5.4. External collaborative works

The scientists involved on the beamlines have of course external collaborations, and their descriptions are far from the scope of this report. We will here show how we recently use our expertise on FAME and FAME-UHD beamlines to develop external collaborations.

5.4.a. Scientific collaborations with users on other synchrotrons

Within the context of the ESRF shutdown during 18 months, we accompanied regular FAME and FAME-UHD users on other synchrotrons, with the objectives to maintain the collaborations, to pursue works in progress, but also to perform some technological watch. This was the case for example with a team from CEREGE (Aix-en-Provence) at SSRL (main proposer: Le Bars Maureen) for XAS measurements on environmental samples, with collaborators from Néel Institute (Grenoble) and CRISMAT (Caen) for experiment on battery (main proposer: Diaz-Lopez Maria) at SOLEIL and DIAMOND⁵. In the framework of the strong collaboration we have with KAUST, we participated at a two weeks experiment at SOLEIL, bringing also in Paris all the *operando* devices developed on our beamlines.⁶

5.4.b. Instrumentation collaborations

ThomX Compact Light Source

Since 2012 we are involved in the ThomX project⁷, a compact light source in construction at the Laboratoire de l'Accélérateur Linéaire in Orsay (France). This Compton-inverse source will deliver an X-ray fan with energy ranging from 10 to 90keV. Our role is to develop the X-ray line (PI: Marie Jacquet, LAL), with the technical support of the Service Etudes et Réalisation d'Appareillages Scientifiques (SERAS, Néel Institute) and scientific ones by colleagues from ID17 at ESRF. The source and the beamline are installed at the old LURE-DCI synchrotron place (Figure 2) First photons are expected on the X-ray line at the end of 2021, but we already

⁵ Diaz-Lopez *et al.*, "Reversible densification in nano-Li₂MnO₃ cation disordered rock-salt Li-ion battery cathodes", *J. Mater. Chem. A* **8** (2020) 10998-11010 <https://doi.org/10.1039/D0TA03372C>

⁶ De *et al.*, "Stable Cr-MFI Catalysts for the Nonoxidative Dehydrogenation of Ethane: Catalytic Performance and Nature of the Active Sites", *ACS Catalysis* **11** (2021) 3988-3995 <https://dx.doi.org/10.1021/acscatal.0c05170>

⁷ <https://thomx.lal.in2p3.fr/>

validate several components on FAME.⁸

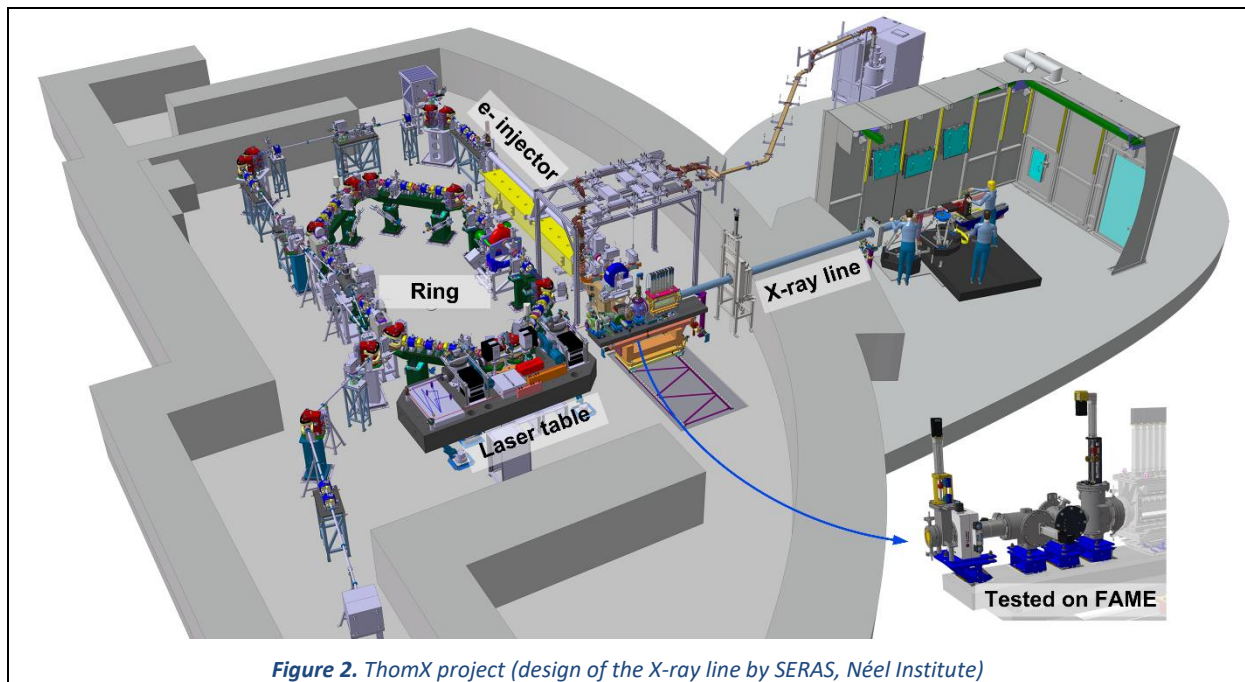


Figure 2. ThomX project (design of the X-ray line by SERAS, Néel Institute)

Crystal Analyzer Spectrometers

Within the EcoX project, financed by the French national research agency (ANR), Mauro Rovezzi has worked in collaboration with the ID26 beamline staff (ESRF) from 2017 until 2019 to help with the installation and the commissioning of a tender X-ray spectrometer (“TEXS” project).⁹ Moreover, during July 2019 Mauro Rovezzi was invited for three weeks at the Advanced Photon Source (APS) at the ID13 beamline (GSECARS) to work in collaboration with Matt Newville in mounting a test spectrometer for combining the micro-focusing capabilities of the beamline with high energy resolution spectroscopy.

Data Policy on CRG beamlines at ESRF

Since the restart of the ESRF, all the beamlines, including CRGs, should follow the Data Policy. This engagement has been signed by the ESRF and 5 other institutes in the frame of PaNOSC. It aims at making available to everyone all the data acquired in these institutes after a 3-year embargo. The implementation of the routines that are able to store and make available all the data with their metadata implies several changes:

- reorganization of the schemes of data collection to respect the FAIR principles (findability, accessibility, interoperability, and reusability);
- resizing of the data storage system, taking into account the huge volume of data that is being produced with the new 2D detectors and the fact that the data should be available for at least ten years;
- standardization of the metadata;
- inclusion of all the different needs, depending on the scientific communities.

In this context, Isabelle Kieffer is representing the CRG beamlines in the data management workgroup that has been set up to gather computing staff and beamline representatives.

⁸ Dupraz et al., “The ThomX ICS source”, *Physics Open* 5 (2020) 100051 <https://doi.org/10.1016/j.physo.2020.100051>

⁹ Rovezzi et al., “TEXS: in-vacuum tender X-ray emission spectro-meter with 11 Johansson crystal analyzers” *Journal of Synchrotron Radiation* 27 (2020) 813–826 <https://doi.org/10.1107/S160057752000243X>

6. Perspectives: the MAGNIFIX project

6.1. General context

Today, at the beginning of operation of the ESRF's Extremely Brilliant Source Upgrade ([EBS](#)), there are two spectroscopy French CRG beamlines, FAME and FAME-UHD, covering practically all research domains involving the use of synchrotron radiation. This newly upgraded synchrotron source offers a beam with exceptional properties, inducing new opportunities to envisage ambitious and promising scientific projects on these beamlines.

If the FAME-UHD beamline is almost at the state-of-the-art, it is not the case for FAME which construction started more than 20 years ago. The majority of its elements is obsolete. Considering the characteristics of the source, a redesign project of this beamline is under progress. Indeed, if the old bending magnets could not be competitive with insertion device beamlines in terms of beam size and flux, this is no more the case today. Therefore, in addition to the upgrade of the beamline, we plan to create a new experimental station dedicated to 2D & 3D imaging and μ XAS, associated with spectral Ptychography imaging to take full advantage of the beam coherence.

After several iterations with our scientific council, French CRG beamlines proposed a new project, abbreviated as MAGNIFIX, to upgrade their internationally renowned instruments to take full advantage of the exceptional qualities of ESRF-EBS new source and offer cutting-edge synchrotron-based characterization technology to the scientific community. In addition to the integration of state-of-the-art instrumentation, this ambitious project also integrates optimized data acquisition, data processing, and data analysis tools as well as a data policy for data storage in agreement with the European regulations. [This MAGNIFIX project](#) aims to completely exploit the properties of the new source and to provide unprecedented scientific opportunities. It has just been accepted and funded under the EquipEx+ PIA3.

6.2. Which science in perspective?

The innovative spectroscopy F-CRG project is supported by scientific consultation with the national community and the F-CRG Scientific Advisory Board. These new orientations and new scientific challenges are also the result of a [F-CRG Workshop](#) involving both the scientific users from different national laboratories and the expertise of the scientific advisory board. This workshop took place over 3 days and provided an opportunity to consolidate the project.

Within the five French beamlines, FAME and FAME-UHD can be distinguished by their analysis methods. These two beamlines are the X-ray absorption spectroscopy beamlines of the F-CRG portfolio, while the others are small-angle scattering or diffraction or beamlines.

Therefore, some technological locks will be lifted and new challenges will be taken up in different scientific fields, such as for this **spectroscopy F-CRG platform**, and as summarized schematically on Figure 1.

In environmental and earth sciences:

Molecular Speciation, Transfer and remediation of Contaminants

Earth and environmental scientists are making an intensive use of synchrotron facilities to improve knowledge on geological materials, from the core to the mantle (*i.e.* under extreme pressure and temperature conditions), on minerals, on soils (natural or polluted), as well as on materials resulting from the interaction between inorganic and organic compounds within soils and sediments (the so-called environmental biogeochemistry). The project will enable a technological breakthrough toward **detection limits of a few hundred ppb for trace elements**

or molecules, as well as integrated **spatial resolution with the spectral ptychography station** at the scale of biological, mineral or anthropogenic (e.g. nano-plastics) nano-constituents, a major worldwide challenge to the earth science community.

A better understanding of the mechanisms controlling metal homeostasis in plants and of key processes for metal uptake, hyperaccumulation, detoxification... are needed for a better risk evaluation and optimization of phytoremediation techniques¹. At the same time, new kinds of experiments emerged worldwide, and the F-CRG were pioneers on this subject, being able to take into account the pollutants not only in their ionic state, but also when they were present as nanoparticles². The MAGNIFIX project will allow pollutant studies under conditions as close as possible to the predictable concentration of these elements in the ecosystem, which can be as low as a few hundreds of ppb.

Strategic element resources

The project will provide an opportunity for geochemists and mineralogists to exploit the interest of **high energy resolution fluorescence detected XAS** on FAME-UHD to overcome the intrinsic limitation of conventional XAS measurement and to obtain data with an improved spectral resolution³. The ability of studying surfaces or interfaces is one of the strengths of the F-CRG: it can be exploited to study the chemical reactions occurring at the water-minerals interaction. The upgraded spectroscopy F-CRG beamlines will also provide a more precise understanding of the mechanisms of surface layer formation during the dissolution of minerals, and their consequences for mineral reactivity, the kinetic of the process, the thickness of the layer.

The knowledge of the key characteristics of ore deposits⁴ of economically important metals such as Au, Mo, Re and Pt group elements, their source, concentration and distribution in the economically important deposits from magmatic, hydrothermal and metamorphic settings, are the core parameters in geo-resources, offering new opportunities for their prospection. The study of geothermal fluids is of great importance to understand the processes controlling the mobility of the elements in the Earth's crust. FAME and FAME-UHD are currently worldwide leaders on this research topic⁵, as they articulate scientific expertise, dedicated instrumentation and state-of-the-art data analysis. This status will be accentuated by the experimental developments of the upgrade project, which will directly benefit this scientific field, thanks in particular to increased spatial resolution and chemical sensitivity.

These new challenges are perfectly in line with the new prospects developed by [CNRS-INSU](#).

In material sciences toward a green energy:

Catalysis

Heterogeneous catalysis is a key technology because it enables faster, large-scale production and the selective formation of chemicals. In this field, there is nowadays a growing interest for new processes based on non-fossil carbon sources. The synthesis of future fuels and chemicals will proceed via innovative concepts regarding the design of catalysts, while the

¹ Sarret et al., "Use of Synchrotron-Based Techniques to Elucidate Metal Uptake and Metabolism in Plants", *Advances in Agronomy*, **119** (2013) 1-82 <http://dx.doi.org/10.1016/B978-0-12-407247-3.00001-9>

² Rose et al., "Physical-chemical properties of nanoparticles in relation with toxicity", *Encyclopedia of Nanotechnology*, B. Bhushan editor, Springer **16** (2012) 2075-2085 http://dx.doi.org/10.1007/978-90-481-9751-4_334

³ Layet et al., "Evidence that soil properties and organic coating drive the phytoavailability of cerium oxide nanoparticles", *Environmental Science & Technology* **51** (2017) 9756-9764 <http://dx.doi.org/10.1021/acs.est.7b02397>

⁴ Brugger et al., "A review of the coordination chemistry of hydrothermal systems, or do coordination changes make ore deposits?", *Chemical Geology* **447** (2016) 219-253 <http://dx.doi.org/10.1016/j.chemgeo.2016.10.021>

⁵ Bjorn P.von der Heyden, "Shedding light on ore deposits: A review of synchrotron X-ray radiation use in ore geology research", *Ore Geology Reviews* **117** (2020) 103328 <https://doi.org/10.1016/j.oregeorev.2020.103328>

fundamentals of the associated reactions must be understood at the molecular level to further enable more performant catalysts. Last but not least, the real technical catalysts are complex multicomponent bodies, ranging from dozens of micrometers to several centimeters, consisting of active phases, supports and numerous additives in shaped forms suitable for their commercial application.

With the EBS upgrade and the refurbishing of the Spectroscopy F-CRG platform, the sum of technological improvements will benefit directly to the *operando* studies of catalyst with notably *i*) a smaller beam size (improved lateral resolution), *ii*) a higher brightness and an enhanced beam position stability (improved signal to noise), and *iii*) faster acquisition times (improved time resolution) which is an essential feature to resolve fast kinetics and reduce data via multivariate curve resolution.

Despite their tremendous relevance, our understanding of the complexity of such multicomponent systems and the consequences for their structure-texture-function relationships is still poor. This is mainly due to limitations of characterization techniques. The ability of visualizing complex structures with high sensitivity and nanometer spatial resolution is pivotal to improve the engineering of these materials. Thanks to the implementation of the ptychography imaging station, this multi-scale characterization of technical catalysts will suddenly become feasible and a comprehensive study of their active catalytic site will come within reach, with the additional spectral- or XANES-ptychographic imaging development, as planned by contributors to the present project.

Batteries

Several attractive technologies for energy storage are already available, such as Li-ion batteries or fuel cells. Scientists and industrials are still improving existing systems or imagining new ones, which require precise descriptions and understanding of both each individual components and complete operational device. *In situ* and *operando* synchrotron tools are perfectly suitable to address these fundamental and applied questions, and F-CRG are strongly involved on this purpose using a multiscale approach, on new Li-ion batteries from local orders⁶, as well as on fuel cells⁷. With MAGNIFIX, time-resolved measurements will allow to characterize anode, cathode and electrolyte during fast charge and discharge cycles. High resolution X-ray imaging will allow to observe defects (micro-cracks for example), chemical inhomogeneities (concentration and strain mapping using using XANES-Ptychography⁸).

Complex materials

Similarly, what makes accelerated material design particularly challenging for metallic alloys and carbon-based composites, especially those that need to sustain mechanical loads, is that their properties are not directly controlled by their composition (about 10 elements in today's industrial alloys) but instead by a specific multi-scale microstructure that develops through complex processing. At the nanoscale, the distribution of phases in terms of volume fraction, size, shape and chemistry, depends both on composition and processing parameters through the kinetics of solid-state phase transformations. This can be easily measured by spectral ptychography increasing spatial resolution, which would allow the characterization of graded

⁶ Diaz-Lopez et al., "Li₂O:Li-Mn-O disordered rock-salt nanocomposites as cathode prelithiation additives for high-energy density Li-ion batteries", *Advanced Energy Materials* **10** (2020) 1902788 <http://dx.doi.org/10.1002/aenm.201902788>

⁷ Siebel et al., "Identification of catalyst structure during hydrogenoxidation reaction in an operating PEM fuel cell", *ACS Catalysis* **6** (2016) 7326–7334 <http://dx.doi.org/10.1021/acscatal.6b02157>

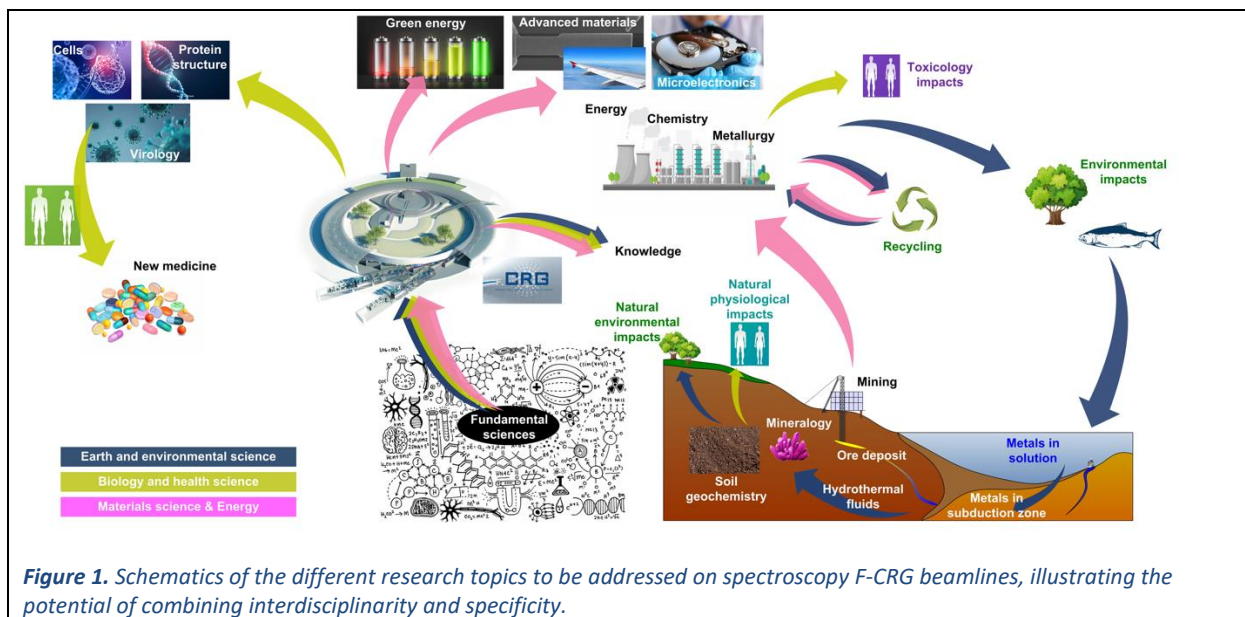
⁸ Yu et al., "Three-dimensional localization of nanoscale battery reactions using soft X-ray tomography", *Nature Communications* **9** (2018) 921 <https://doi.org/10.1038/s41467-018-03401-x>

composition alloys and thus a more efficient exploration of metallurgy processes. More generally, taking advantage of the extended penetration depth of “hard” X-rays, the study of “real” (but complex) materials, where disordered and ordered phases coexist, as well as nanoparticles, (from industrial waste to be recycled to cultural heritage and historical materials) will become possible using high-resolution spectral imaging.

In life sciences:

Contamination of soil and water by traces of heavy metals and toxic chemical compounds resulting from human activities has become a major environmental hazard to animal and human health. Remediation of polluted environments using physico-chemical technologies is often cost prohibitive, and a way to convert toxic organic compounds into harmless products is the use of the enzymes and storage proteins of microorganisms or plants. The spectroscopy F-CRG platform is uniquely equipped to tackle these questions in life sciences where X-ray spectroscopic methods will determine the subtle details of metal environment. Moreover, metalloenzymes will be studied either in very dilute samples or even in their native cellular environment. Ultimately, the development of ptychography coupled to X-ray fluorescence spectroscopy will allow users to map the localization of metalloenzyme complexes at the surface, but also of metalloenzymes in sub-cellular compartments.

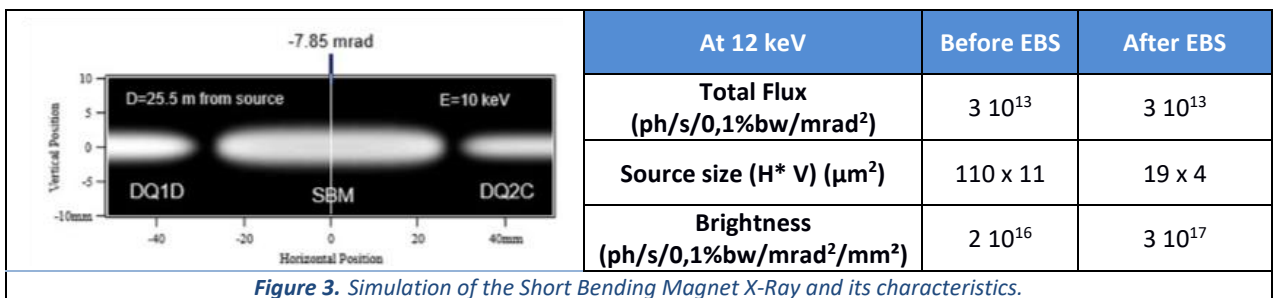
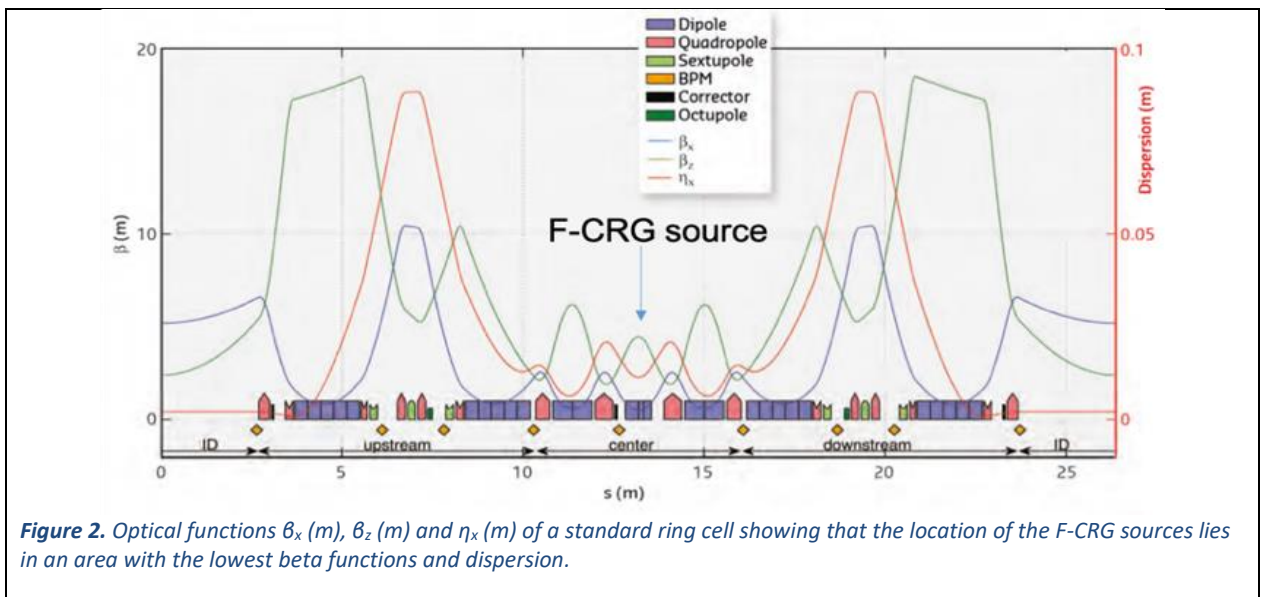
The spectroscopy platform is also a unique facility to scrutinize the traces of life, whether in meteorites or reproducing hydrothermal conditions. Although experiments have already been carried out previously (study of the activity of barophilic and thermophilic bacteria, meteorites, serpentinization, etc.), the new possibilities offered by the platform, in particular the instrumental development of a high-pressure, high-temperature chemical reactor coupled with advanced X-ray spectroscopy, which can be traced back to the speciation of light elements (C, N, O), will make it possible to recreate the conditions of hydrothermal sources and to monitor in situ the elementary brick formations of life. The main objective of this ambitious research area is thus inspired by Miller's famous experiment, the fundamental undertaking that gave birth to prebiotic chemistry, with momentous consequences in the understanding of the origins of life and its location.



6.3. New experimental setup: use of the enhanced coherence of the beam

Perspectives

The upgraded synchrotron source, which constitutes the fourth generation, offers an electron beam with exceptional properties, such as a unprecedented vertical and a horizontal emittance of 110 pm and 5 pm, respectively. The characteristics of this new source ([EBS Parameters](#)) opens new opportunities to envisage ambitious and promising scientific projects in F-CRG beamlines. In particular, the “Short Bending Magnet” selected by spectroscopy FAME and FAME-UHD and their localization in the ring geometry, provides the cleanest beam on the sample and give them the best emittance and the best stability (Figure 2). Consequently, the performance of these two beamlines will be boosted and we will see their brightness increased by a factor of 2 and a coherent flux fifty times higher than the existing one. Indeed, many experiments driven on spectroscopy F-CRGs require a clean sharp beam with no spurious signal.



The objectives of the new instrumentations are:

- 1) to preserve the characteristics of the new source down to the sample: size, coherence, brightness and stability, by an appropriate state-of-the-art optics;
- 2) to exploit all the signals by an efficient detection: energy selective, fast and at a high rate in accordance with the photon gain on the sample;
- 3) to optimize the online acquisition (no dead-time) and processing mode (advanced data analysis and artificial intelligence if necessary) in order to increase the overall beam time efficiency.

Moreover, the proposed project will also provide a new experimental station dedicated to:

- 4) X-ray spectroscopy imaging heterogeneous samples with a resolution around mm for XAS spectroscopy and with an ultra-high spatial resolution a round 20nm for spectral

Ptychography. A micro-station will be installed on a dedicated hutch. Beside the regular use of this new imaging technique, which fully exploit the X-ray beam coherence properties, its combination with our expertise in X-ray Absorption Spectroscopy (XANES-Ptychography) will provide the French community with a world-class instrument giving simultaneously high resolution 2D or 3D information on heterogeneous samples, and the spatial distribution of a target chemical element combined with chemical and structural information about this particular element.

Table 1 lists the target properties and estimated values of the key measurement's parameters, as well as the required instrumentation which would not only improve but radically change the relevance and impact of the existing instruments.

Target Improvement	Target specifications	Required instrumentation
10 times faster	< 10 ms	continuous scan fast detectors
10 times smaller	<1 μ m monochromatic	micro positioning /optical elements
10 times more flux	Flux 10 ¹⁰ - 10 ¹² photons/s	optical elements /high efficiency detectors
10 times less noise	Signal/noise >1000	Crystal analyzers

Table 1. Technical targets and associated requirements

Coherent X-rays are becoming powerful tools for imaging complex, heterogeneous structures with spatial resolution below focused synchrotron beam sizes. Many beamlines designed and optimized for exploiting coherent X-rays are mainly based on insertion devices as photon sources. Combining the source size with long source-sample distance increases the coherence length and defines the size of fully coherent beams.

With the increase in brightness of the X-ray beams delivered by bending magnet beamlines and the stability of the source, positioning the F-CRG in the landscape of coherent X-ray studies has become suddenly highly relevant

This project is structured both on the spectroscopy expertise of the FAME team and on the recruitment in 2019 at the Néel Institute of a young researcher J.C. Da Silva. He is indeed an expert in this technique from both an experimental and analytical point of view and has just obtained young researcher funding (ANR) involving a post-doctoral student and a PhD student. Thus, thanks to the financing of the MAGNIFIX project and the staff enhancement, we'll be able to develop the use of coherence and the implementation of a ptychography station on the FAME experimental end station and more particularly the spectral ptychography.

X-ray ptychography is a coherent X-ray imaging technique capable of providing highly detailed images of a sample's complex-valued transmittance.⁹ Thanks to oversampled scanning techniques recording both the phase and the amplitude, one of the main benefits of ptychography is that spatial resolution is not limited by the imaging optics nor by the beam size, but rather by the highest scattering vector for which speckles can be detected.¹⁰

Spectral-ptychography combines the X-ray spectroscopy and ptychographic imaging methods. The imaging experiment is repeated at different energies over a range of ± 50 eV from the

⁹ e.g da Silva J. C. and Menzel A., "Elementary signals in ptychographie", *Optics Express* **23** (2015) 33812-33821 <https://doi.org/10.1364/OE.23.033812>

¹⁰ J.M.Rodenburg, "Ptychography and Related Diffractive Imaging Methods", *Advances in Imaging and Electron Physics* **150** (2008) 87-184 [https://doi.org/10.1016/S1076-5670\(07\)00003-1](https://doi.org/10.1016/S1076-5670(07)00003-1)

absorption edge to estimate elemental speciation, such as oxidation state and site geometry evolution.

The first tests conducted in 2018 before the ESRF source shutdown clearly confirmed the potential of the new source for exploiting coherence. These experiments showed the possibility of detecting well-resolved coherent fringes from a structured tungsten pattern in transmission geometry (Figure 4). Moreover, the ESRF EBS upgrade will offer 12 times smaller sources with the new SBM. This reduction in source size will further increase the coherence length and thus increase the proportion of flux present as a fully coherent beam.

The simulations carried out by OASIS for a state-of-the-art optical system show that the monochromatic **coherent flux from a SBM at ESRF will be comparable to the best current beamline worldwide**, i.e. [cSAXS-X12SA](#) beamline on an undulator at SLS in Switzerland.

We therefore propose to develop the XANES-ptychography technique on FAME to address the chemical heterogeneity with a resolution of about 50 nm in heterogeneous samples such as catalysts, cements...

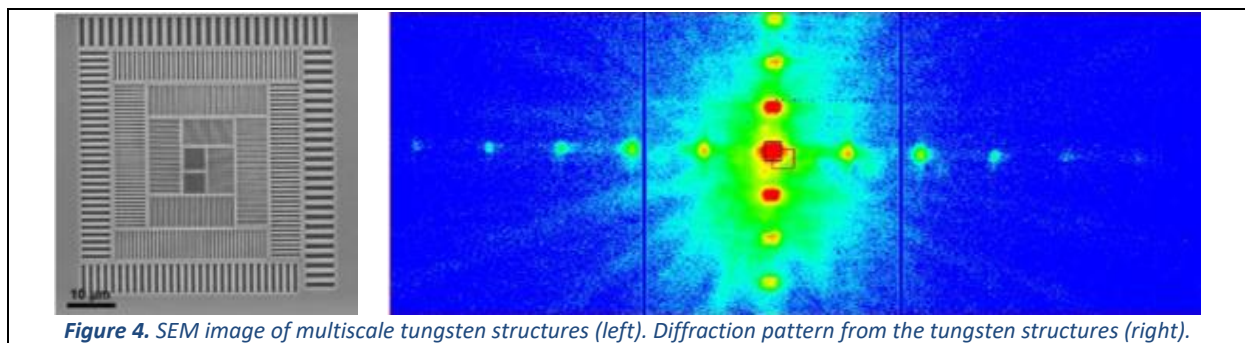


Figure 4. SEM image of multiscale tungsten structures (left). Diffraction pattern from the tungsten structures (right).

These new tools will make it possible to explore the effect of numerous experimental parameters on structural, physical and chemical quantities, to conduct experiments *in situ* or *operando*, on model systems from fundamental research as well as real systems of technological and industrial interest. Such experiments would deal with metrology for microelectronics and energy materials, mapping/imaging of complex and heterogeneous samples such as those of heritage, biology, health, environment and geosciences, chemical and structural analysis of all these materials etc.

The proposed project, with the improvement of instruments providing increased spatial resolution, reduction in acquisition time thanks to the gain in brightness and development of new methods of analysis such as spectral ptychography¹¹, will offer the scientific community the possibility of carrying out unprecedented experiments. Thus, the scientific quality and quantity resulting from the spectroscopy F-CRG platform will result in an important surge in publications, as has already been established on a smaller scale when creating new equipment.

6.4. Impact on the beamlines: new equipments

As FAME-UHD has been very recently built (2016-2017), the main investments will be made around FAME and the new experimental station, most of whose equipment is very old and dates from its construction (2000-2002). While the challenge for FAME is largely to build a new imaging station, its experimental station for the *in-situ* study of dilute elements will also be renovated. We plan to merge the two experimental cabins to accommodate the macro

¹¹ See the special issue on Ptychography state of the art in *J. Appl. Cryst.* <https://doi.org/10.1107/S1600576721002983>

EXAFS station and the imaging station. Two new mirror assemblies, M1 and M2, will be used to focus either on the macro station or on a secondary source at the end of the second optical cabin for the micro station.

All the elements of the experimental station will be replaced: an optical support table identical to that of FAME-UHD, and especially the 30-element hybrid detector and its electronics (on the beamline since 1993!). A mini cryostat similar to that of FAME-UHD with a sample exchanger will be integrated and will be interchangeable with the one used in FAME-UHD. The new layout is shown in figure 5.

Optical elements

To take full advantage of the unique and new ESRF-EBS source characteristics, the optical elements of the FAME beamline need to be adjusted with the appropriate shapes, polished with state-of-the-art roughness and slope errors, in order to guide the photons on the sample without any aberration. Such optimum optical elements will allow the primary focusing of the photons with as little distortion as possible, over a spot size as small as possible, with the best energy resolution or maximum of flux (monochromator purpose). In all cases, the quality of the optical devices must preserve the coherence of the photons in order to exploit fully the opportunities provided by the new sources.

Primary mirrors and associated benders (BM30-FAME). State-of-the-art values for large mirrors are around $<1 \text{ \AA}$ rugosity and $<0.5 \text{ \mu rad}$ slope error. While FAME-UHD mirrors have these characteristics, FAME mirrors are far from it. New mirrors with such characteristics will allow a gain of a factor 4 on the vertical spot size to reach a vertical size lower than 30 \mu m as compared to more than 100 \mu m currently available.

Micro-focusing optics (μ beam station on BM30-FAME). Inserting micro-focusing devices will allow to reduce the beam size on the sample down to $1 \times 1 \text{ \mu m}^2$. So-called KB achromatic focusing mirrors will be placed in experimental hutches in the vicinity of sample.

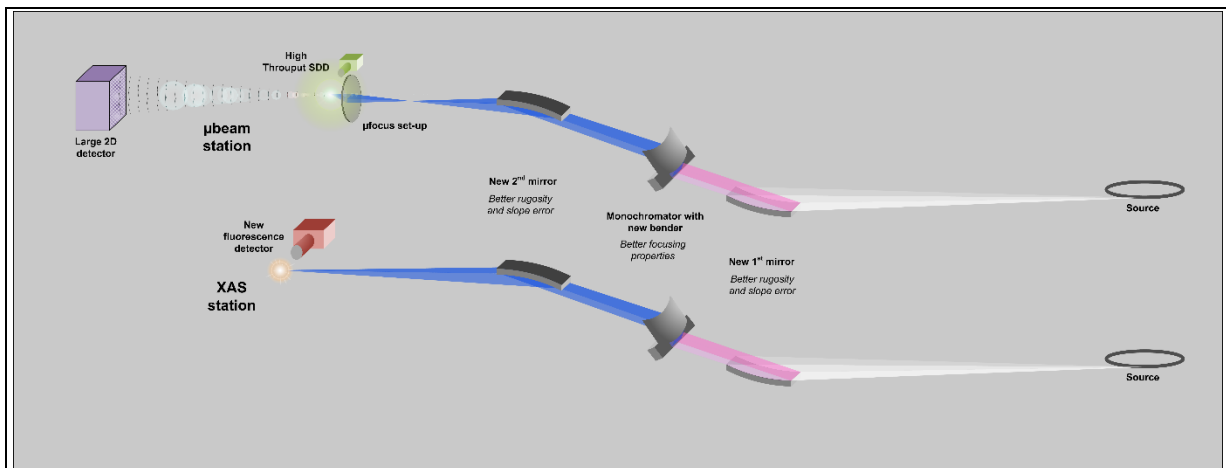


Figure 5. FAME sketch after its upgrade, in the standard and actual XAS configuration (bottom) and in the new μ beam configuration for ptychography or μ XAS (top)

Innovative monochromators: on both beamlines

To take full advantage of the reduced source size, it will be necessary to optimize the geometry of the 2nd crystal of the double-crystal monochromators, to reduce vibrations effects on the diffracting surface at the maximum and to limit thermal effects.

Perspectives

A silicon 2nd crystal with a new design will be installed on BM30-FAME and BM16-FAME-UHD. This new design made at Institut Néel proposes a materialization of the optimal theoretical design¹² which was not feasible until now, a design adjusted to the new source characteristics. Its purpose is to have an optimal energy resolution with focus possibilities almost free from distortions.

New Detectors

A single photon counting X-ray pixel detector is required to perform Ptychography imaging on FAME. The best resolution will be achieved by combining small pixel size with fast noise-free measurements. The [Lambda 250K](#) from X-Spectrum is for example well adapted to the purpose, with its 55µm pixel size on a 28x28mm² detection size and acquisitions with 1ms time gap between images.

Ultra high energy resolution on FAME-UHD. Collecting the maximum of the photons of interest with an energy bandwidth in the eV range is the aim of a Crystal Analyzer Spectrometer (CAS). Performances depend on the crystal *i) quality* (bandwidth and number of diffracted photons), *ii) nature* of the diffraction plane and *iii) quantity* (14 crystals, covered solid-angle). The aim is to fully equip the 14 crystal spectrometer on FAME UHD with 14 Si and Ge crystals for all the reflections of interest.

High energy resolution and high counting rate on macro EXAFS station on FAME. The new generation of multichannel Ge detectors for fluorescence measurement delivers an energy resolution close to the intrinsic resolution even at high counting rate. [Mirion-Canberra ones](#), with closely packed discrete elements, allows to detect up to 1 Mcts/s with an energy resolution < 200 eV, with a very good linearity and without any cross-talk between elements, when associated to the appropriate digital pulse processor electronics such as [XIA-FalconX](#).

Experimental devices

To be fully efficient such optical devices and detectors will need to be associated with sample or experimental devices with the same properties (motions sensitivity, dynamic positioning...) or optimize to preserve the samples from radiation damages due to the photons flux increase (sample cryo-cooling).

New optical tables. BM30-FAME beamline needs two new optical tables, for conventional XAS and ptychography measurements. State-of-the-art optical tables (such as the one on FAME-UHD) have a motorized positioning with a linear sensitivity equals to 100nm (or even better), holding the beam at a constant position on the sample even when changing slightly the monochromatic beam energy, especially with a micro-beam.

New instrumentation for ptychography station. The new ptychography station implemented on FAME would be positioned on the previously described high sensitivity optical table. The instrumentation required for the X-ray imaging measurements is composed of *i)* a high-precision sample positioning motor with long travel range for scanning the sample, *ii)* a rotation stage for the tomographic experiments, *iii)* an optical microscope, with objectives and a high-resolution camera CMOS for sample inspection and preparation before the X-ray experiments.

Infrastructure

The currently unused space on BM30-FAME will be used and modified to implement the new micro-XAS station and adapted to perform ptychography experiment, in particular the length between the sample and the detector which requires large tunable distances.

¹² Hazemann et al "Modelization by finite-elements of sagittal focusing" *Nuclear Instruments and methods B*, **97** (1995) 547-550 [https://doi.org/10.1016/0168-583X\(94\)00731-4](https://doi.org/10.1016/0168-583X(94)00731-4)

Data analysis

With the new experimental station for spectral imaging (Micro-XAS and Spectral Ptychography), a large amount of data will be processed on FAME in particular. It is expected to have to manage more than one Tera bytes per day. To be fully compatible with the ESRF (networking, IT manpower, data analysis unit, [FAIR data policy](#)...) which is committed to archive the raw data for 10 years and to share the data after a 3-year embargo, the F-CRG platform will adopt their infrastructure and data format choices. On each beamline, numerical hardware complying with the ESRF choice¹³ will be installed as close as possible to the detectors with a fast network link (Edge computing) in view of a better interoperability with ESRF services. These computers will allow using fast routines for online visualization (*e.g.* during ptychography acquisitions), handling the external computing power needed by the users ([PANOSC](#): software in packages called containers like dockers), developing Artificial Intelligence routines to align the beamline optical components (decision support tools), finding weak signals in large noisy data sets... As for the storage, a BeeGFS solution is foreseen to handle the detectors fast output.

6.5. Actual and future technics FAME & FAME-UHD

To conclude this perspectives part, an overview of the actual and future technics available at the spectroscopy F-CRGs is presented on Table 2.

Technique	Actual specificities	Improved specificities with MAGNIFIX
X-ray Absorption Spectroscopy	<ul style="list-style-type: none"> dilution level from 100% to 1ppm high spectral resolution (HERFD) <i>in situ</i> and <i>operando</i> measurements 	<ul style="list-style-type: none"> dilution level from 100% to 100ppb <i>focused beam (1 to 10 μm) to probe each inhomogeneity</i>
X-ray Emission Spectroscopy	<ul style="list-style-type: none"> large beam (200 μm to 1 mm) to integrate inhomogeneities high throughput time scale, up to 5' by spectrum 	<ul style="list-style-type: none"> improved throughput, x5 time scale, up to 30" by spectrum
X-ray imaging (Ptycho station)		<ul style="list-style-type: none"> 20 nm spatial resolution chemical sensitivity (XANES-ptychography) <i>in situ and operando measurements</i>

Table 2. Characterization techniques implemented on FAME & FAME-UHD and associated specificities, actual and with the MAGNIFIX project

¹³ IBM power 9 with 2 NVIDIA TESLA V100 GPU

7. Scientific results

This part of the BLRP report has been written by different users (or us for the in-house research activities) to represent the variety of topics investigated on FAME and FAME-UHD over the last years as well as their opinions and expectations on the beamlines. Some results presented below are the summary of a group or laboratory activity, while others are examples that illustrate selected points. The beamtime repartitions are shown on Figure 1 for the BLRP period.

Earth science still represents the main scientific activity of FAME, gathering geochemistry, hydrothermal fluids studies and mineralogy, a stable ratio of beamtime allocated to these scientific fields compare to previous BLRP period (55% from 2015 to 2021, 54% from 2010 to 2014). Unsurprisingly the ratio of beamtime for these thematics on FAME-UHD is in the same range, 52.5%.

Several laboratories are regular users since 2002: the 'Observatoire des Sciences de l'Univers de Grenoble' (OSUG, including ISTerre, the 'hydrothermal fluids' team of Institut Néel...), the 'Centre Européen de Recherche et d'Enseignement des Géosciences de l'Environnement' (CEREGE, Aix en Provence), the 'Institut de Minéralogie et de Physique des Milieux Condensés' (IMPMC, Paris), the 'Géosciences Environnement Toulouse' laboratory (GET, Toulouse), the 'Division of Mineralogy of the South Australian Museum' & CSIRO (Adelaïde and Melbourne)... Several contributions illustrate these scientific activities in the "Geochemistry and Environmental Sciences" and "Hydrothermal Fluids" fields. If the first point is the fruit of external users' activity, the second one is entirely the result either of in-house research or strong collaborations.

Following an introductive part by S. Bohic from INSERM, biochemistry activities on the beamlines (13% of the beamtime on FAME, 6% on FAME-UHD) will be illustrated by examples of experiments performed by CEA-Grenoble laboratories, different Italian labs and by a group gathering scientists from the beamlines, ISTerre, INSERM, Welsh and Swiss institutes.

The beamtime dedicated to chemistry (catalysis & electrochemistry) and material sciences represents 33% and 41% of the beamtime on FAME and FAME-UHD respectively. The context of these activities are well-explained by the three introductive parts, by IFP Energies Nouvelles, IRCELyon and Karlsruhe Institute of Technology, by King Abdullah University of Science and Technology Catalysis Center (with which a strong collaboration is under progress), and by I. Maurin from Neel Institute (and now a beamline staff).

Scientific Results

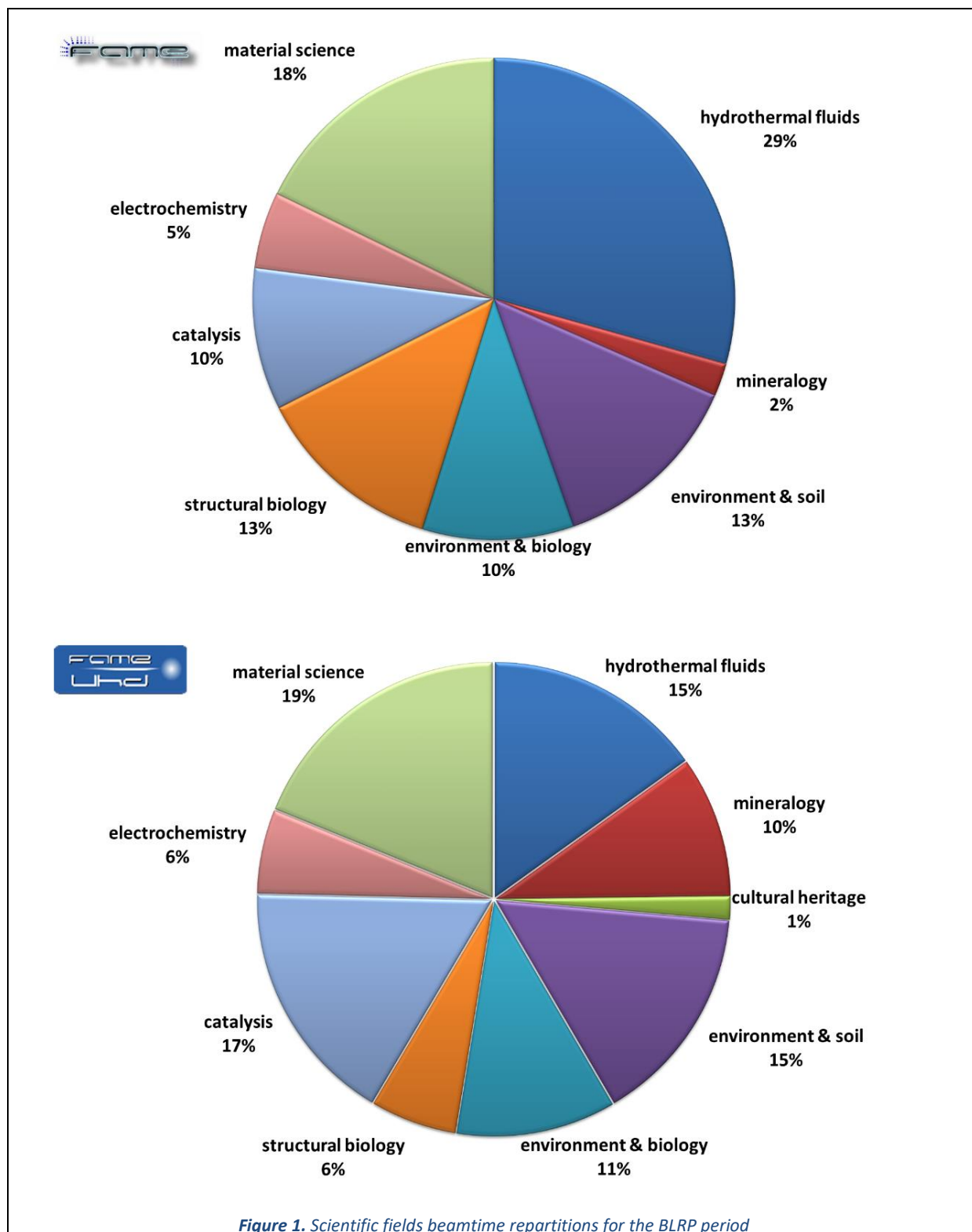


Figure 1. Scientific fields beamtime repartitions for the BLRP period

Geochemistry and Environmental Sciences**Fate of metallic contaminants in soil-plant systems**

Anthropogenic activities including mining, smelting, industrial and urban activities, agriculture and transport have strongly impact the cycling of trace element metals and metalloids, and generated strong local enrichments as well as diffuse contaminations. In addition, some areas face the problem of natural enrichments in some potentially toxic trace elements. In parallel, there is an increasing awareness of the toxicity of some metallic contaminants. For example, cadmium (Cd) is known as a non essential element, toxic as very low dose. The limit for Cd content in phosphate fertilizers has been decreased (60 mg/kg P₂O₅ starting from 2022)¹ to limit the building up of Cd content in agricultural soils. Likewise, to decrease human exposure to Cd through dietary intake, in 2019, the European Union decreased the limit for Cd content in chocolate products at 0.8 mg kg⁻¹ for chocolate containing more than 50% cacao (European Commission 2014). These new limits represent a threat for the producers of phosphate fertilizers and regions of cacao production with high Cd background, and trigger intense research on the geochemistry of cadmium. In parallel, there is an increased awareness that agricultural practices should be sustainable. In this perspective, the use of biosolids as soil amendments has many benefits, although it may inadvertently introduce contaminants into the soil. These contaminants include traditional metallic contaminants (Zn, Cu, Pb, Cd,...) and emerging contaminants such as pharmaceuticals and nanomaterials. A key factor for evaluating the risk associated to these practices, tracing the fate of these contaminants in soils, evaluating they mobility, availability and possible trophic transfer, is the speciation. The characteristics of FAME and FAME-UHD beamlines (sensitivity to trace elements, easy use of cryostats, bulk analysis) make them perfectly suitable for this purpose. In the past five years, studies have been conducted on these beamlines to elucidate the fate of silver nanoparticles contained in sewage sludge after application on agricultural soils and plant culture², and the interactions of silver nanoparticles with a model bacterial strain present in the rhizosphere of plants was studied³. Other studies focused on the fate of Cu and Zn in biosolids applied on soils^{4,5,6,7}. For these studies, metal concentrations are in the range of a few tens of mg/kg. A major challenge for future studies is to do EXAFS at lower concentrations (around 1 mg/kg), in order to study not only contaminated environments but also diffuse contaminations or background concentrations, such as, for example, soils and plants from cacao plantations. This is particularly important when studying bioaccumulation and fate in plants because the

¹ Marini, M., Caro, D. and Thomsen, M. "The new fertilizer regulation: A starting point for cadmium control in European arable soils?" *Sci. Total Environ.* **745** (2020) 140876. <https://doi.org/10.1016/j.scitotenv.2020.140876>

² Pradas del Real et al., "Fate of Ag-NPs in sewage sludge after application on agricultural soils", *Environ. Sci. Technol.* **50** (2016) 1759-1768 <http://dx.doi.org/10.1021/acs.est.5b04550>/ see highlight below

³ Eymard-Vernain et al., "Impact of a model soil microorganism and of its secretome on the fate of silver nanoparticles", *Environ. Sci. Technol.* **52** (2018) 71-78 <http://dx.doi.org/10.1021/acs.est.7b04071> / Id., "The poly-gamma-glutamate of *Bacillus subtilis* interacts specifically with silver nanoparticles", *Plos One* **13** (2018) e0197501 <https://doi.org/10.1371/journal.pone.0197501> / see highlight below

⁴ Hodomihou et al., "Zinc Speciation in Organic Waste Drives Its Fate in Amended Soils", *Environ. Sci. Technol.* **54** (2020) 12034-12041 <https://doi.org/10.1021/acs.est.0c02721>

⁵ Le Bars et al., "Drastic change in zinc speciation during anaerobic digestion and composting: instability of nano-sized zinc sulfide", *Environ. Sci. Technol.* **52** (2018) 12987-12996 <http://dx.doi.org/10.1021/acs.est.8b02697>

⁶ Formentini et al., "Radical change of Zn speciation in pig slurry amended soil: Key role of nano-sized sulfide particles", *Environmental Pollution* **222** (2017) 495-503 <http://dx.doi.org/10.1016/j.envpol.2016.11.056>

⁷ Tella et al., "Increased zinc and copper availability in organic waste amended soil potentially involving distinct release mechanisms", *Environmental Pollution* **212** (2016) 299-306 <http://dx.doi.org/10.1016/j.envpol.2016.01.077>

detoxification processes depend on the level of exposure. So far, most studies on plants dealt with hyperaccumulating plants^{8,9} or plants exposed to contaminated matrices^{10,11,12,13,14,15,16}. These studies provide key information on metal homeostasis and rhizospheric processes, which can be used to develop remediation processes and improve micronutrient acquisition by crop plants (biofortification). To go one step beyond, future studies should focus on the speciation of essential (*e.g.*, Zn, Cu) and non essential (*e.g.*, Hg, Cd, Pb) trace elements close to diffuse contaminations and background levels. The instrumental developments planned for fame and fame-uhd, particularly the replacement of the 30-element Ge detector on fame, and continuous scan on both beamlines, should make it possible to push back the limits.

In the last years, more and more studies performed on FAME and FAME UHD beamlines combined bulk analysis with spectromicroscopy performed on other beamlines^{2,3,8,9,17,18,19}. This combination of techniques has emerged as powerful tools to study the distribution and the speciation of metals in soils, plants and microorganisms. Concerning micro- and nano-focused techniques, coupling imaging and speciation on samples with limited preparation, and when possible in cryoconditions, are major advantages. The future implementation of microfocused techniques on FAME and FAME UHD will be an additional asset for the study of environmental and biological systems.

Géraldine Sarret, Institut des Sciences de la Terre, Grenoble

⁸ Huguet *et al.*, "Impact of *Arabidopsis halleri* growth on cadmium localization and speciation in highly contaminated dredged sediment", *Sci. Total Environ.* **536** (2015) 468-480 <http://dx.doi.org/10.1016/j.scitotenv.2015.07.026>

⁹ Isaure *et al.*, "Evidence of various mechanisms of Cd sequestration in the hyperaccumulator *Arabidopsis halleri*, the non accumulator *Arabidopsis lyrata* and their progenies by combined synchrotron-based techniques", *Journal of Experimental Botany* **66** (2015) 3201-3214 <http://dx.doi.org/10.1093/jxb/erv131>

¹⁰ Aucour *et al.*, "Zn speciation and stable isotope fractionation in a contaminated urban wetland soil- *Typha latifolia* system", *Environ. Sci. Technol.* **51** (2017) 8350-8358 <http://dx.doi.org/10.1021/acs.est.6b02734>

¹¹ Aucour *et al.*, "Dynamics of Zn in an urban wetland soil-plant system: Coupling isotopic and EXAFS approaches", *Geochim. Cosmochim. Acta* **160** (2015) 55-69 <http://dx.doi.org/10.1016/j.gca.2015.03.040>

¹² Chiarantini *et al.*, "Mercury speciation in *Pinus nigra* barks from Monte Amiata (Italy): An X-ray absorption spectroscopy study", *Environmental Pollution* **227** (2017) 83-88 <https://doi.org/10.1016/j.envpol.2017.04.038>

¹³ Schreck *et al.*, "Is *Tillandsia capillaris* an efficient bioindicator of atmospheric metal and metalloid deposition? Insights from five months of monitoring in an urban mining area", *Ecological Indicators* **67** (2016) 227-237 <http://dx.doi.org/10.1016/j.ecolind.2016.02.027>

¹⁴ Sayen *et al.*, "Enrofloxacin and copper plant uptake by *Phragmites australis* from a liquid digestate: Single versus combined application", *Sci. Total Environ.* **664** (2019) 188-202 <https://doi.org/10.1016/j.scitotenv.2019.01.134>

¹⁵ Mariet *et al.*, "Lead Highly Available in Soils Centuries after Metallurgical Activities", *Journal of Environmental Quality* **46** (2017) 1146-1157 <http://dx.doi.org/10.2134/jeq2016.12.0469>

¹⁶ Sarret *et al.*, "Extreme variability in As bioaccumulation factor in Lake Titicaca, Bolivia", *Scientific Reports* **9** (2019) 10626 <https://doi.org/10.1038/s41598-019-47183-8>

¹⁷ Isaure *et al.*, "Relationship between Hg speciation and Hg methylation/demethylation processes in the sulfate-reducing bacterium *Pseudodesulfovibrio hydrargyri*: evidences from HERFD XANES and nano-XRF", *Frontiers in microbiology* **11** (2020) 584715 <https://doi.org/10.3389/fmicb.2020.584715>

¹⁸ Veronesi *et al.*, "Visualization, quantification and coordination of Ag⁺ ions released from silver nanoparticles in hepatocytes", *Nanoscale* **8** (2016) 17012-17021 <http://dx.doi.org/10.1039/C6NR04381J>

¹⁹ Penen *et al.*, "Pools of cadmium in *Chlamydomonas reinhardtii* revealed by chemical imaging and XAS spectroscopy", *Metallomics* **9** (2017) 910-923 <http://dx.doi.org/10.1039/C7MT00029D>

Fate of silver nanoparticles in agricultural soils amended with sewage sludge

Waste water treatments plants are considered as major hubs controlling the release and fate of silver nanoparticles (Ag-NPs) in the environment. Sulfidation plays a major role in the reduction of the potential impact of these nanoparticles. This study confirms Ag₂S as the main species in polluted sludge and amended soils. However, thanks to a combination of techniques available at the ESRF, the presence of another secondary Ag-S species and mixed metallic sulfides have also been evidenced. Despite the extremely low solubility of Ag₂S, our results showed a possible interconversion between Ag₂S and Ag secondary species under the influence of soil components, microorganisms and plant exudates. Nanosized Ag₂S was present as heteroaggregates, Ag bound to thiol groups and/or amorphous Ag₂S and nanosized mixed metallic sulfides found in this study may have very different properties to pure, macrocrystalline, Ag₂S. A possible release of Ag due to the mobilisation of micronutrients by plants still needs to be evaluated. The high preferential association of Ag to the organic fraction of soils is another important insight of this work since a release of Ag is possible in the long term through organic matter turnover.

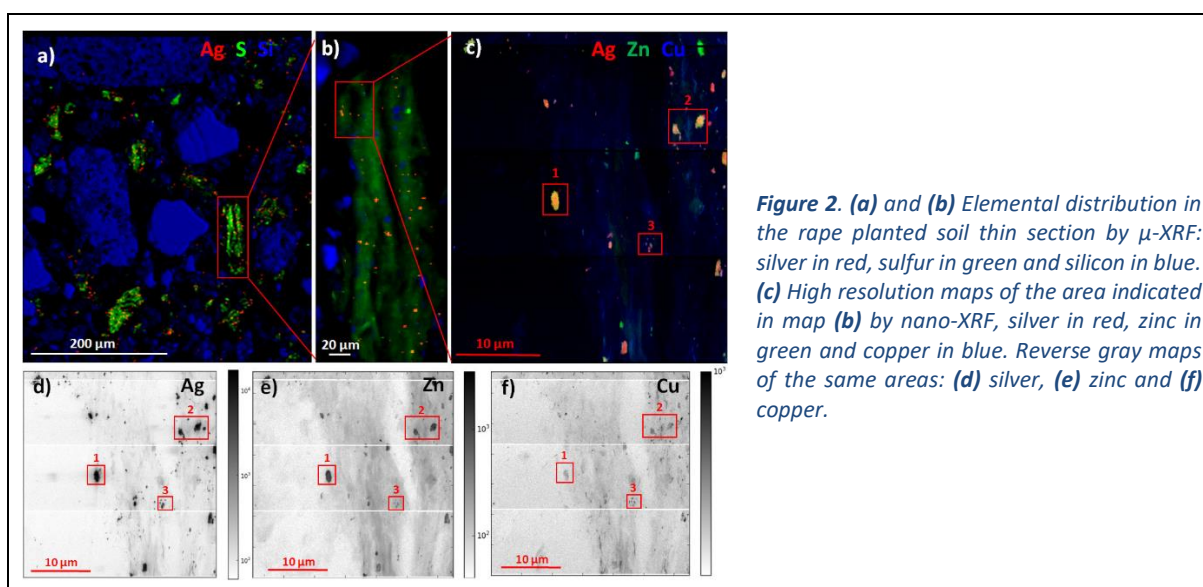


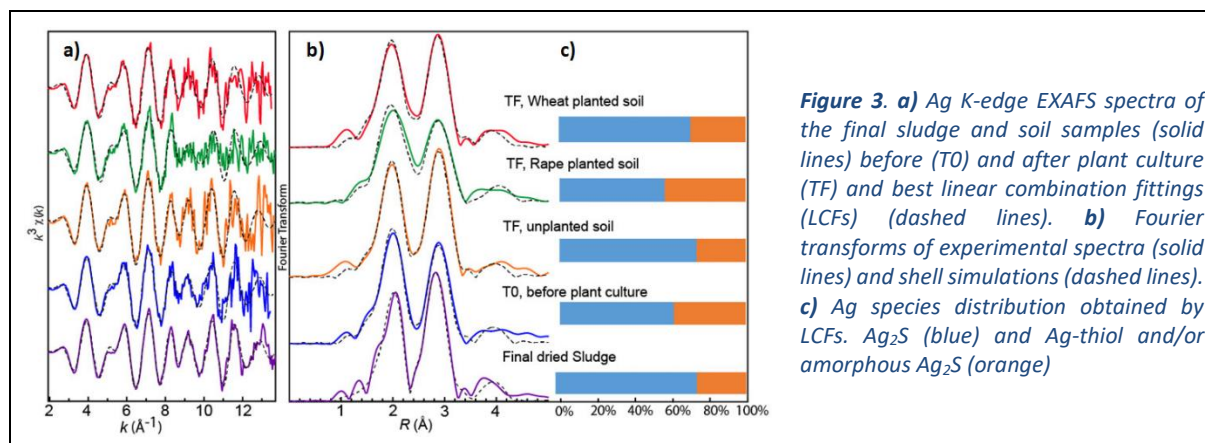
Figure 2. (a) and (b) Elemental distribution in the rape planted soil thin section by μ -XRF: silver in red, sulfur in green and silicon in blue. (c) High resolution maps of the area indicated in map (b) by nano-XRF, silver in red, zinc in green and copper in blue. Reverse gray maps of the same areas: (d) silver, (e) zinc and (f) copper.

Due to their antimicrobial activity, silver nanoparticles are used in many consumer products²⁰ from where they are easily leached and transported by sewer systems to waste-water treatment plants. In these plants, the treated water is separated from a solid phase (sewage sludge) where the pollutants, such as Ag-NPs, are retained. This sludge is rich in organic matter and nutrients and is often applied to agricultural soils as fertiliser. The aim of this work was to characterise the fate of Ag-NPs in a sludge-amended soil cultivated with crop species with agricultural interest to assess Ag-NPs impact on soil quality and crops production, and also to assess the risk of their transfer to the food chain. To this end, a polluted sludge was produced by spiking a pilot waste water treatment plant with Ag-NPs. The sludge was mixed with an agricultural soil and then rape and wheat were grown on the mixture.

Ag K-edge spectroscopy performed on FAME (Figure 3) confirmed that Ag₂S was the main species in the sludge and amended soil before and after plant culture. However, a second Ag-S species, organic and/or amorphous Ag-S, was also identified. The proportion of this secondary species varied slightly (24% to 36%) depending on the sample, suggesting a possible

²⁰ The project on emerging nanotechnologies: <http://www.nanotechproject.org/>

interconversion between Ag_2S and Ag secondary species under the influence of soil components, microorganisms and plant exudates.



Micro X-ray fluorescence analyses performed at ID21 (Figure 2) showed that Ag-containing particles were well distributed throughout the sludge and soil matrix and were located in spots with size ranging from ≤ 0.5 to 1–3 μm . Ag formed heteroaggregates and was preferentially associated with S-rich particles, including organic fragments, with very few spots of Ag associated with Si-rich minerals. These findings have environmental implications since, on one hand heteroaggregates of nanoparticles with soil components have been shown to be better transported than homoaggregates²¹ and on the other hand because the decomposition of organic matter may lead to the release of Ag-containing particles.

Nano-XRF performed at ID16B (Figure 2) also allowed us to detect nanosized Ag-containing particles, as well as diffuse and low Ag concentration in organic particles. This observation confirmed the formation of Ag bound to thiol groups of organic matter suggested by EXAFS. This analysis also evidenced the presence of mixed metallic sulfides with Zn and Cu. The solubility and availability of Ag in these sulfides is likely to be different, and possibly higher than in pure Ag_2S phase. Also, as Zn and Cu are micronutrients, their mobilisation by plants could lead to the release of the Ag associated with them.

Together, these results have shown a more complex picture for the fate of silver nanoparticles in soils than would have been expected for simple sulfidation.

Authors and principal publication:

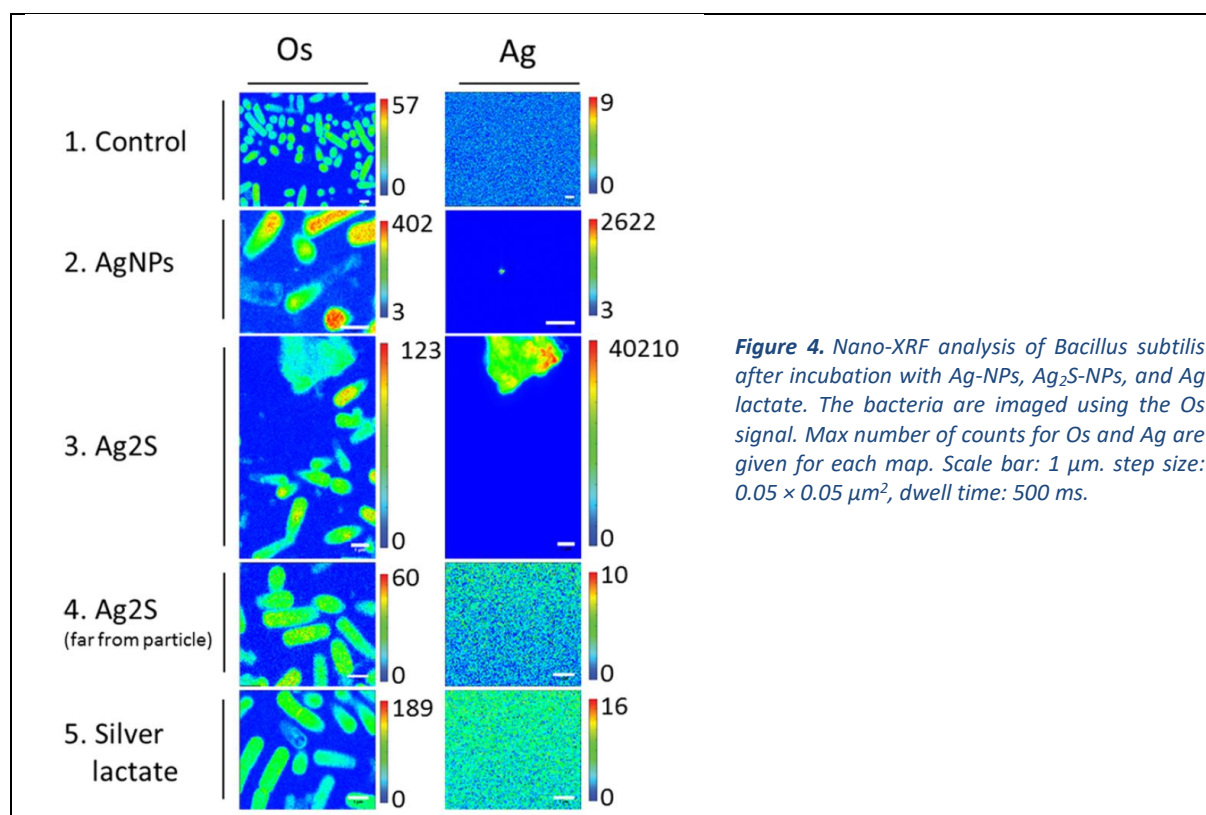
A.E. Pradas del Real,^{a,b} H. Castillo-Michel,^b R. Kaegi,^c B. Sinnet,^c V. Magnin,^a N. Findling,^a J. Villanova,^b M. Carrière,^d C. Santaella,^e A. Fernandez-Martinez,^a C. Levard,^f G. Sarret,^a *Environ. Sci. Technol.* **50**, 1759–1768 (2016)
^a ISTERre, Univ. Grenoble Alpes & CNRS, Grenoble (Fr.) | ^b ESRF | ^c EAWAG, Particle Laboratory, Dübendorf (Switz.) | ^d INAC-SCIB, Univ. Grenoble Alpes & CEA, Grenoble (Fr.) | ^e Lab Ecol Microb Rhizosphere & Environ Extrem, UMR 7265 CEA-CNRS-Aix Marseille Univ., CEA Cadarache (Fr.) | ^f CEREGE, Aix-Marseille Univ., CNRS & IRD, Aix en Provence (Fr.)

²¹ Hotze et al., *Journal of Environmental Quality* 39, 1909–1924 (2010) <https://doi.org/10.2134/jeq2009.0462>

Impact of a Model Soil Microorganism and of Its Secretome on the Fate of Silver Nanoparticles

Sulfidation is a key process for silver nanoparticles (Ag-NPs) released from consumer products in the environment. This study focuses on the impact of a model soil microorganism, *Bacillus subtilis*, on the fate of pristine and already sulfidized Ag-NPs. It is a good illustration of all the studies performed since several years on FAME, FAME-UHD, in combination with other ESRF beamlines such as ID21 and ID16b, in the framework of nano-ecotoxicology. This research topic aims at understanding the fate, physico-chemical transformations upon aging, exposure, and impacts of nanoparticles and nano-composite on organisms, and also to develop a safer-by-design approach of nanomaterials.²²

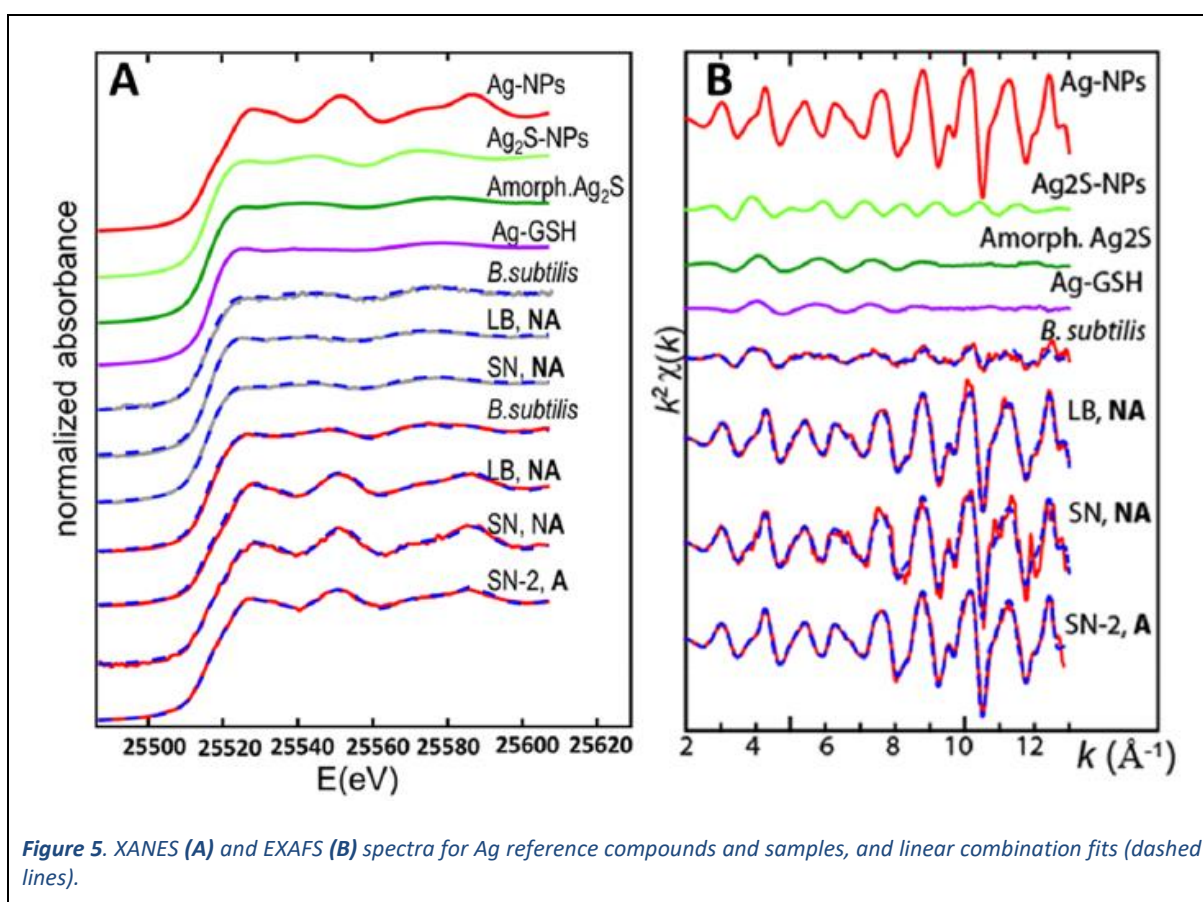
The purpose of this particular study was to evaluate the effect of bacterial activity on the chemical transformation of Ag-NPs. We were particularly interested in the secretome, composed of all the molecules excreted by the bacteria. Ag-NPs were incubated with the initial growth medium, the isolated secretome, and the living bacteria in their growth medium, at a sub-toxic dose. They were characterized for their size and morphology, agglomeration state, structure, and Ag speciation before and after incubation. No Ag internalization or sorption on the cell wall was detected by nanoXRF (Figure 4) and TEM-EDX. A partial sulfidation, leading to an Ag–Ag₂S core–shell structure, was observed in the presence of the secretome (Figure 5). The sulfidation was favoured near the crystal dislocations, and the rate limiting step was the oxidation of Ag⁰. The sulfidation was complete in the presence of the living bacteria and followed an indirect pathway. Both crystalline Ag₂S and amorphous Ag₂S and/or Ag-thiol were identified. At the opposite, the bacteria had no impact on silver sulfide (Ag₂S) NPs.



²² Several laboratories, regular users of FAME and FAME-UHD, are part of the LabEx SERENADE, Safe(r) Ecodesign Research and Education applied to NANomaterial DEVELOPMENT (<http://www.labex-serenade.org/>): CEREGE (Aix-en-Provence), ISTerre (Grenoble), LCBM (BIG, Grenoble), LITEN (Grenoble), LAN (Grenoble).

This study shows that the bacterial activity may have a major impact on the fate of Ag-NPs, by enhancing their sulfidation. The results suggest that the bacterial activity favours the first step of the reaction, which is the oxidation of Ag^0 . Concerning the second step, the sulfidation itself, thiol-containing proteins and peptides are the most likely source of reduced S. These results suggest that microorganisms may participate to the sulfidation of Ag-NPs in aerobic systems in the environment, such as unsaturated soils, and thus affect the bioavailability of Ag. On the contrary, *B. subtilis* does not modify the speciation of Ag_2S -NPs.

The development of safer-by-design nanoparticles is a growing research topic. In the case of Ag-NPs, a decrease of the release of Ag from products (which can reach large amounts, for example for textiles) while keeping the antibacterial properties, should be targeted. Partly sulfidized Ag-NPs, with an Ag– Ag_2S core–shell structure, such as those produced in this study, might be a material to test in this perspective. The secretome of *Bacillus subtilis* may have some potential for the green synthesis of these nanocomposites.



Authors and principal publication:

Eymard-Vernain E.^{1,2}, Lelong C.², Pradas del Real A.^{1,3}, Soulas R.⁴, Bureau S.¹, Tardillo Suarez V.,⁵ Gallet B.⁶, Proux O.⁷, Castillo-Michel H.³, Sarret G.¹, *Environmental Science & Technology* **52** (2018) 71-78

¹ ISTERre (UMR 5275 CNRS / Univ. Grenoble Alpes) / ² BIG (FR 3425 CEA / CNRS / Univ. Grenoble Alpes) / ³ ID21, ESRF / ⁴ LITEN (CEA-Grenoble) / ⁵ ID16b, ESRF / ⁶ IBS (UMR 5075 CNRS / CEA / Univ. Grenoble Alpes) / ⁷ OSUG (UMS 832 CNRS / Univ. Grenoble Alpes)

Safer by design of nanomaterials

Developing safe(r) nanomaterials (ENMs) has become a major concern in all the industry sectors using these advanced materials. To investigate the safe(r)-by-design (SbD) development of ENMs, one approach is to cover multiple technology readiness levels and lifecycle stages, and to combined with hazard and end-of life assessments.²³ In this regard, research activities were centered these past years around environmental and human exposure reduction, ENMs biocompliance, and risk assessment. Among all the interdisciplinary information needed for this SbD, it is necessary to thoroughly determine the (bio)distribution and (bio)transformation of ENMs in environmental matrices following relevant exposure scenario. However, adhering to environmentally relevance implicitly represents a technical challenge since it requires to explore the localization and the speciation of a target chemical element at low doses (ng.L⁻¹- mg.L⁻¹) in complex matrices.

The recent and significant improvements of X-ray imaging (2D and 3D) and X-Ray Absorption Spectroscopy techniques in term of detection limit and resolution (spectroscopic²⁴ and spatial) helped us to determine unambiguously and with greater precision the speciation and distribution of the probed metal composing ENMs in mammals, invertebrates, microorganisms, plants, soils, sediments... Recently, the FAME and FAME-UHD beamlines were used to decipher the phytoavailability and *in planta* speciation of CeO₂ nanomaterials based on their surface properties,²⁵ the *ex vivo* detection and location of CeO₂ nanomaterials in the lung of mice following intra-tracheal instillation,²⁶ or also the shape-dependent behavior and fate of Ag nanomaterials within freshwater ecosystems under realistic exposure scenarios, i.e. mid-term exposure to chronic low-level additions of Ag.²⁷ To go deeper into the mechanisms of interactions between these advanced materials and biota, chemical imaging at high energy and spatial resolution (<100 nm), but also getting access to the 3D speciation ((x,y,z) as well as (x, y, time)) would be a breakthrough and an added value in the fields of environmental and biogeochemistry sciences. With the FAME upgrade, its new spectroptychography station and high-throughput detector, the FAME-UHD development, its new crystal analyzers, research activities in this scientific field will benefit from a completely adapted platform.

Mélanie Auffan, Centre de Recherche et d'Enseignement de Géosciences de l'Environnement, Aix-en-Provence

²³ Rose et al. "The SERENADE project; a step forward in the safe by design process of nanomaterials: The benefits of a diverse and interdisciplinary approach" *Nano Today* **37** (2021): 101065. <https://doi.org/10.1016/j.nantod.2020.101065>.

²⁴ See highlight below p.58 / Proux et al. "High-Energy Resolution Fluorescence Detected X-Ray Absorption Spectroscopy: A Powerful New Structural Tool in Environmental Biogeochemistry Sciences" *Journal of Environmental Quality* **46** (2017) 1146-57. <https://doi.org/10.2134/jeq2017.01.0023>.

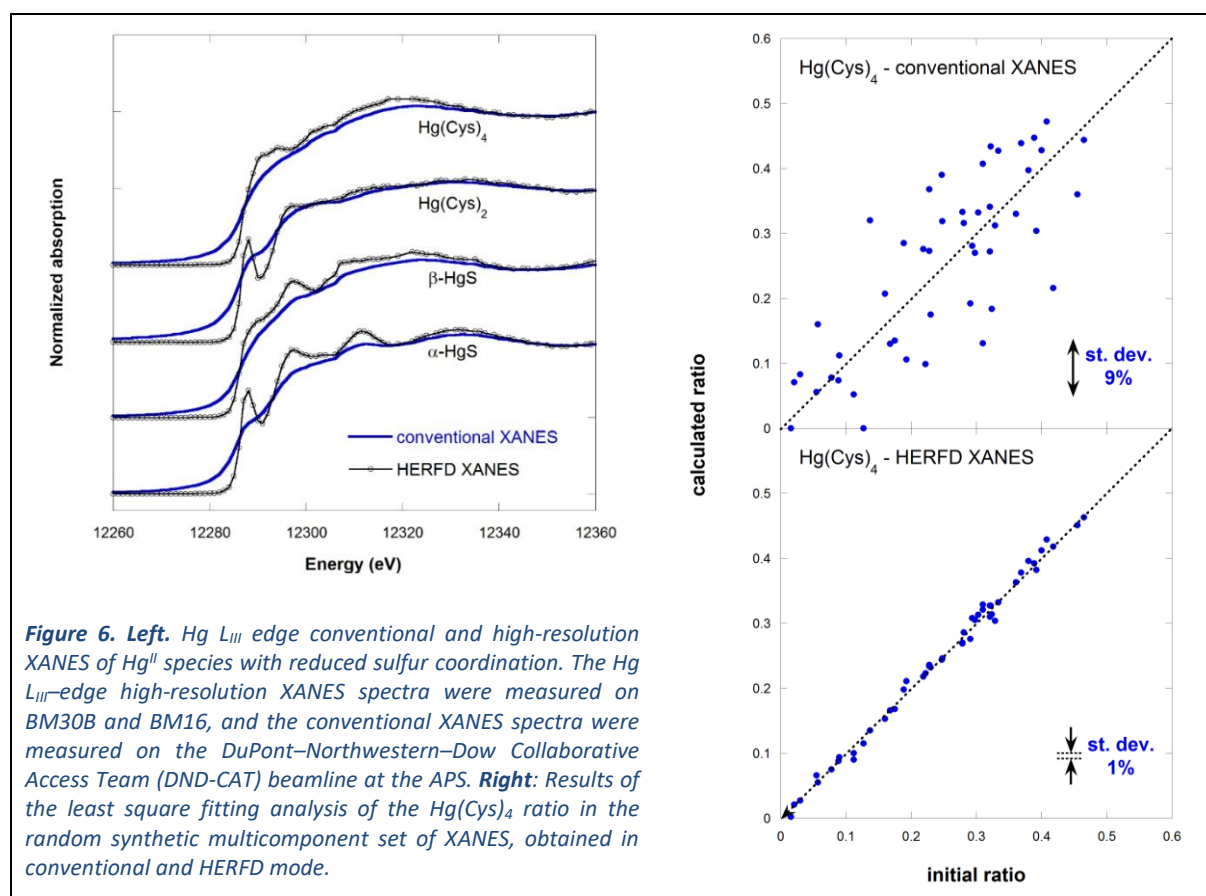
²⁵ See highlight below p.59 / Layet et al. "Evidence that Soil Properties and Organic Coating Drive the Phytoavailability of Cerium Oxide Nanoparticles" *Environmental Science & Technology* **51** (2017) 9756-64. <https://doi.org/10.1021/acs.est.7b02397>.

²⁶ See highlight below p.60 / Chaurand et al., "Multi-scale X-ray computed tomography to detect and localize metal-based nanomaterials in lung tissues of in vivo exposed mice", *Scientific reports* **8** (2018): 4408 <https://doi.org/10.1038/s41598-018-21862-4>

²⁷ Auffan et al. "The shape and speciation of Ag nanoparticles drive their impacts on organisms in a lotic ecosystem", *Environmental Science-Nano*, **7** (2020) 3167-3177 <https://doi.org/10.1039/D0EN00442A>

High-Energy Resolution Fluorescence Detected X-Ray Absorption Spectroscopy: A Powerful New Structural Tool in Environmental Biogeochemistry Sciences.

The study of the speciation of highly diluted elements by X-ray absorption spectroscopy (XAS) is extremely challenging, especially in environmental biogeochemistry sciences. Here we present an innovative synchrotron spectroscopy technique: high-energy resolution fluorescence detected XAS (HERFD-XAS). With this approach, measurement of the XAS signal in fluorescence mode using a crystal analyzer spectrometer with a ~ 1 -eV energy bandwidth helps to overcome restrictions on sample concentrations that can be typically measured with a solid-state detector. The positive impact of this technique in terms of detection limit is illustrated with measurement of Hg species in natural environments. The sharp and well-marked features of the HERFD-X-ray absorption near-edge structure spectra obtained enable us to determine unambiguously and with greater precision the speciation of the probed elements (Figure 6). This is a major technological advance, with strong benefits for the study of highly diluted elements using XAS. It also opens new possibilities to explore the speciation of a target chemical element at natural concentration levels, which is critical in the fields of environmental and biogeochemistry sciences.



Authors and principal publication:

Proux O.^(a), Lahera E.^(a), Del Net W.^(a), Kieffer I.^(a), Rovezzi M.^(a), Testemale D.^(b), Irar M., Thomas S.^(b,c,d), Aguilar-Tapia A.^(b), Bazarkina E. F.^(b,e), Prat A.^(b), Tella M.^(f), Auffan M.^(g), Rose J.^(g), Hazemann J.-L.^(b), *Journal of Environmental Quality* **46** (2017) 1146-1157

^(a) OSUG, UMS 832 CNRS, Univ. Grenoble Alpes. ^(b) Inst. Néel, UPR 2940 CNRS, Univ. Grenoble Alpes. ^(c) Dep. of Civil and Environmental Engineering, Northwestern Univ., Evanston, USA. ^(d) LCBM, UMR 5249 CNRS, CEA, Univ. Grenoble Alpes. ^(e) Inst. of Geology of Ore Deposits, Mineralogy, Petrography and Geochemistry, RAS, Moscow ^(f) CIRAD, Montpellier. ^(g) CEREGE, UMR 7330 CNRS, Aix-Marseille Univ., IRD, Coll. de France, Aix en Provence.

Evidence that soil properties and organic coating drive the phytoavailability of cerium oxide nanoparticles

The ISO-standardized RHIZOtest is used here for the first time to decipher how plant species, soil properties, physical-chemical properties of the nanoparticles (NPs) and their transformation regulate their phytoavailability. Two plants, tomato and fescue, were exposed to two soils with contrasted properties: a sandy soil poor in organic matter and a clay soil rich in organic matter, both contaminated with 1, 15, and 50 mg.kg⁻¹ of dissolved Ce₂(SO₄)₃, bare and citrate-coated CeO₂ NPs. All the results demonstrate that two antagonistic soil properties controlled Ce uptake. The clay fraction enhanced the retention of the CeO₂ NPs and hence reduced Ce uptake, whereas the organic matter content enhanced it. The chemical stability modelled for CeO₂ NPs was experimentally confirmed by XANES of fescue roots exposed in sandy (Figure 7 left) and clay soils (Figure 7 right) for eight days. XANES at the Ce L₃-edge is sensitive to the oxidation state of Ce with one absorption edge for Ce^{III} species (e.g. Ce^{III}-acetate) and two absorption edges for Ce^{IV} (e.g. initially bare and coated CeO₂ NPs). In the present study, XANES spectra of fescue roots exposed to CeO₂ NPs superimposed on the spectra of initially bare and coated CeO₂ NPs indicated that, in our experimental conditions, the atomic structure of the CeO₂ NPs was not significantly affected. All our attempts to include the contribution of Ce^{III} in the fits did not improve the fit residues. Moreover, in the soil poor in organic matter, the organic citrate coating significantly enhanced the phytoavailability of Ce by forming smaller aggregates thereby facilitating the transport of nanoparticles to the roots. By getting rid of the dissimilarities between the root systems of the different plants and normalizing the surfaces exposed to nanoparticles, the RHIZOtest demonstrated that the species of plant did not drive the phytoavailability, and provided evidence for soil-plant transfers at concentrations lower than those usually cited in the literature and closer to predicted environmental concentrations.

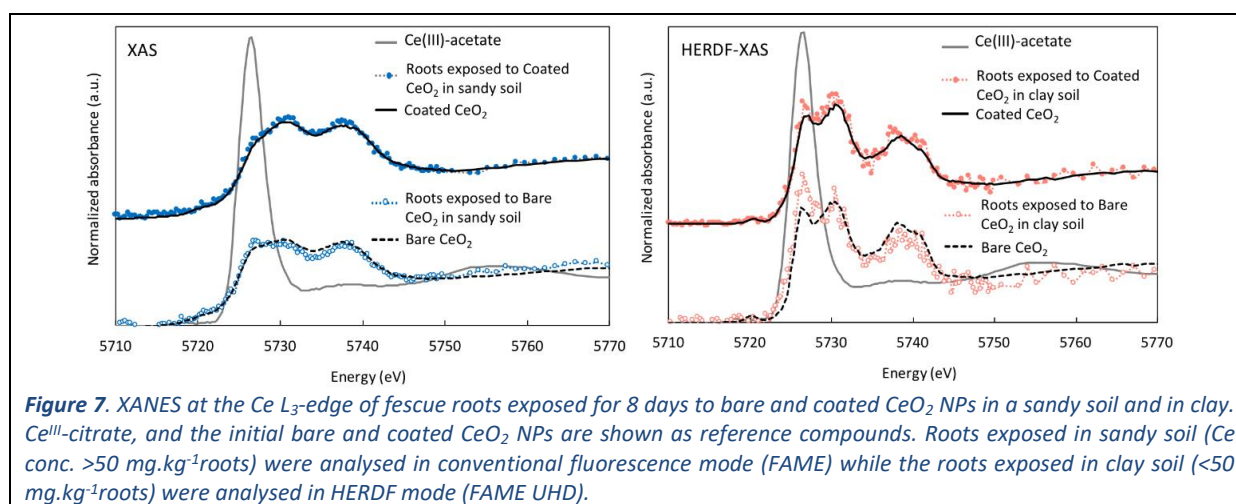


Figure 7. XANES at the Ce L₃-edge of fescue roots exposed for 8 days to bare and coated CeO₂ NPs in a sandy soil and in clay. Ce^{III}-citrate, and the initial bare and coated CeO₂ NPs are shown as reference compounds. Roots exposed in sandy soil (Ce conc. >50 mg.kg⁻¹roots) were analysed in conventional fluorescence mode (FAME) while the roots exposed in clay soil (<50 mg.kg⁻¹roots) were analysed in HERDF mode (FAME UHD).

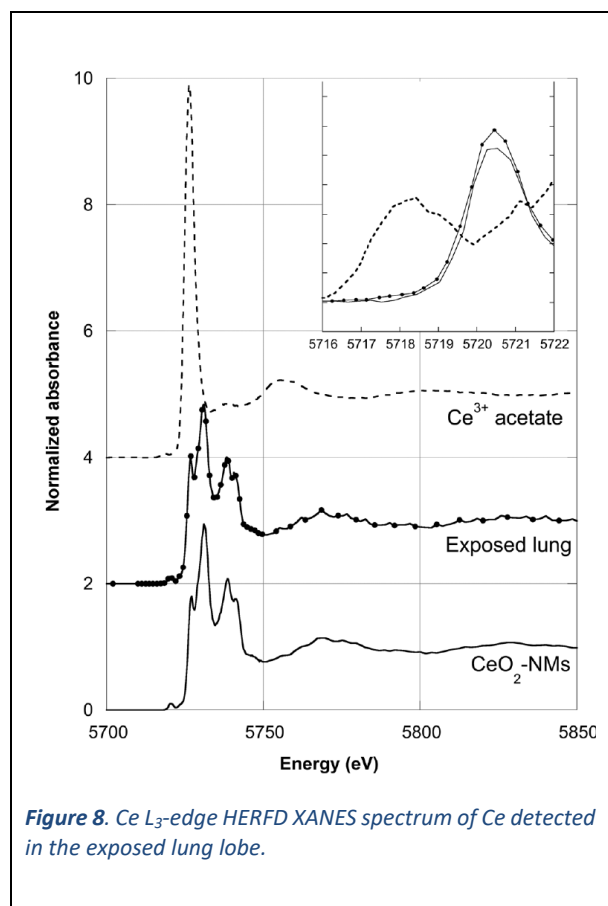
Authors and principal publication:

Layet C.^{1,2}, Auffan M.^{1,2}, Santaella C.^{2,3}, Chevassus-Rosset C.⁴, Montes M.⁴, Ortet P.³, Barakat M.³, Collin B.^{1,2}, Legros S.⁵, Bravin M.⁶, Angeletti B.¹, Kieffer I.⁷, Proux O.⁷, Hazemann J.-L.⁸, Doelsch E.⁴, *Environmental Science & Technology* **51** (2017) 9756–9764

⁽¹⁾ CEREGE, Aix-Marseille Univ. - CNRS - IRD, Aix en Provence. ⁽²⁾ iCEINT, CNRS - Duke Univ. ⁽³⁾ Lab. of Microbial Ecology of the Rhizosphere and Extreme Environments, Aix-Marseille Univ. – CEA - CNRS, UMR 7265 BIAM, St-Paul-lez-Durance. ⁽⁴⁾ CIRAD, UPR Recyclage et risque, Montpellier. ⁽⁵⁾ CIRAD, UPR Recyclage et risque, Dakar. ⁽⁶⁾ CIRAD, UPR Recyclage et risque, Saint-Denis, Réunion. ⁽⁷⁾ OSUG, UMS 832 CNRS - Univ. Grenoble Alpes, F-Grenoble / ⁽⁸⁾ Inst. Néel, UPR 2940 CNRS - Univ. Grenoble Alpes, Grenoble

Multi-scale X-ray computed tomography to detect and localize metal-based nanomaterials in lung tissues of *in vivo* exposed mice

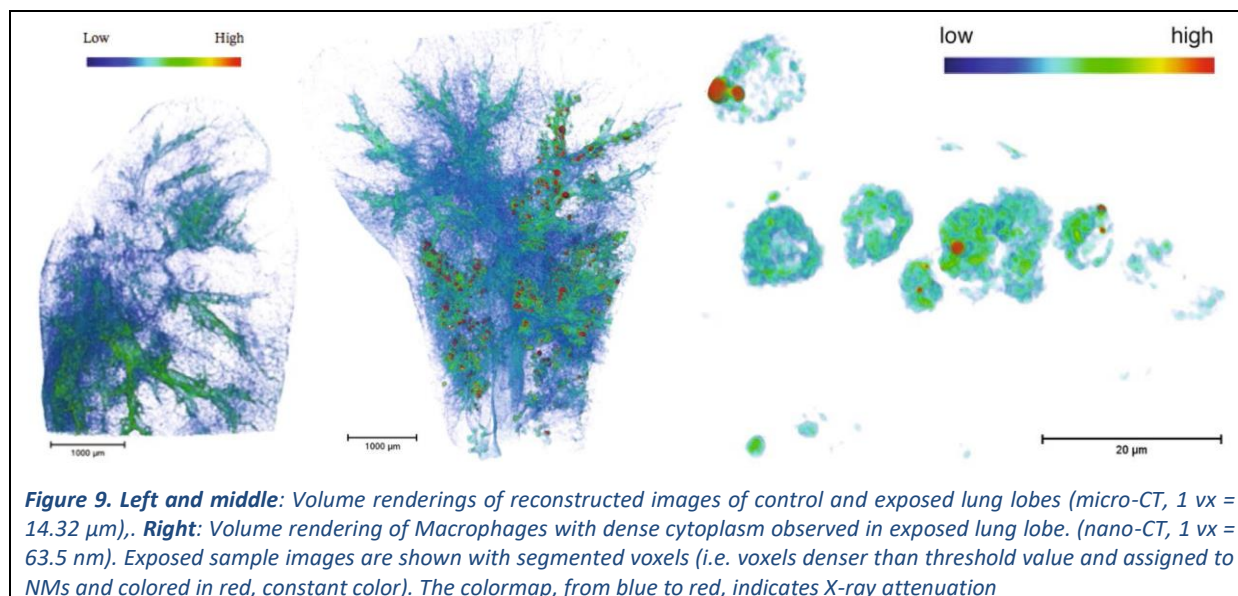
In this methodological study, we demonstrated the relevance of 3D imaging performed at various scales for the *ex vivo* detection and location of cerium oxide nanomaterials (CeO₂-NMs) in mouse lung, combined with a vast variety of techniques among them High-Energy Resolution Fluorescence Detection X-ray Absorption Near Edge Spectroscopy (HERFD-XANES).



Mice were exposed by intra-tracheal instillation to a single dose of 50 µg CeO₂-NMs. One week after administration, Ce in exposed lung was quantified at 450 µg of Ce/g. Chemical analysis suggests the presence of Ce in lung tissue. But as initial CeO₂-NMs can be subjected to biotransformation (*e.g.* partial reductive dissolution of Ce⁴⁺ to Ce³⁺) when reaching biological media, *in-situ* Ce speciation analyses were required. HERFD-XANES spectrum of exposed lung was compared to initial CeO₂-NMs spectrum (Figure 8). Both spectra exhibited the same structures, confirming unambiguously the presence of non-transformed CeO₂-NMs in exposed lung tissue. X-ray micro-computed tomography (micro-CT) with a voxel size from 14 µm to 1 µm was combined with X-ray nano-computed tomography with a voxel size of 63 nm (nano-CT) and performed at the lab-scale on the same non-modified sample.

As micro and nano-CT provides no direct chemical and speciation information, detection and location of NMs in 3D images were obtained following a multi-steps data analysis procedure: (i) histogram normalization; (ii) comparison of exposed and control sample and (iii) denser voxels thresholding.

Micro-CT results revealed that the 3D distribution of CeO₂-NMs in the lung lobe, following intra-tracheal instillation, was non-uniform (Figure 9, middle). Large NMs accumulation regions were detected in the conducting and respiratory airway as well as in the alveolar parenchyma of exposed mice. Nano-CT images allows to go further. The circular structures observed (Figure 9, right) can be attributed to macrophages with dense cytoplasm. Indeed, shape and size of these objects are similar to macrophages observed by histology in Ce-rich region of exposed sample. Even if histological observations are generally performed on multiple samples and field of view (FOV) for a better representativeness, it could become tricky to find metal-rich or NMs-rich regions in a whole lung lobe or organ. Combining histological observation with multi-scale 3D is then an interesting approach as 3D imaging have a larger FOV, is non-destructive and does not exhibit artefacts induced by sample slicing.



This original methodological approach was developed following a worst-case scenario of exposure, *i.e.* high dose of exposure with administration via intra-tracheal instillation. Results highlighted both the non-uniform distribution of CeO₂-NMs within the entire lung lobe (using large FOV micro-CT) and the detection of CeO₂-NMs down to the individual cell scale, *e.g.* macrophage scale (using nano-CT). In the future, this methodology requires to be tested with more realistic exposure conditions (dose, route and timing of NMs administration). It also requires to be supplemented by a more statistical approach, based on analyses of various lobes in order to provide complementary information on NMs distribution at the lung scale. After such a validation, it could be applied in nanotoxicological studies and will represent a significant advance to precisely describe the metal-based NMs exposure related to toxicity results. This will help identifying the toxicity mechanisms following metal-based NMs exposure.

Authors and principal publication:

P. Chaurand^{1,2}, W. Liu^{1,2}, D. Borschneck^{1,2}, C. Levard,^{1,2} M. Auffan^{1,2}, E. Paul³, B. Collin^{1,2}, I. Kieffer⁴, S. Lanone³, J. Rose^{1,2}, J. Perrin¹, *Scientific Reports* **8** (2018) 4408

¹ Aix Marseille Univ, CNRS, IRD, INRA, Coll France, CEREGE, Aix-en-Provence, France / ² International Consortium for the Environmental Implications of Nanotechnology, CNRS–Duke University, Aix en Provence, France / ³ INSERM, Equipe 04, U955, & Univ. Paris Est Creteil, IMRB, Creteil, France / ⁴ OSUG (UMS 832 CNRS / Univ. Grenoble Alpes)

Hydrothermal Fluids

Research on hydrothermal fluids has always been central to the in-house scientific activity of FAME (and now FAME and FAME-UHD), mainly in the field of metal speciation in geological fluids. It is based on the autoclave equipment developed internally with the Néel Institute (X'Press technological group) which makes the FAME installation unique to conduct such *in situ* studies (see more details in the technical part of this document). Along with the autoclave, robust methods have also been established to determine both metal solubility (transmission and fluorescence measurements) and speciation (EXAFS and XANES analysis) in challenging experimental conditions. Consequently a solid user base, whose research topics are related to hydrothermal fluids, has progressively grown over the last 20 years into a strong collaborative and international network of research groups at the forefront of their scientific domain, mainly earth sciences but also material chemistry more recently : we mention here G. Pokrovski, GET Toulouse ; J. Brugger, Monash University Australia ; M. Louvel, Münster University, Germany ; G. Dantelle, Néel Insitute. The complex experiments that they plan at FAME beamlines drive the constant improvement of our hydrothermal equipment and methods which benefit to the whole user community.

In the following pages G. Pokrovski's introductive text and the detailed scientific highlights are good examples of ongoing hydrothermal research conducted at FAME beamlines, and also demonstrate what are the actual and future challenges. To complement them and evaluate the impact of the research on geological fluids conducted on our beamlines we show Figure 10 which is a graphical summary of all the metals investigated in the last 15 years.

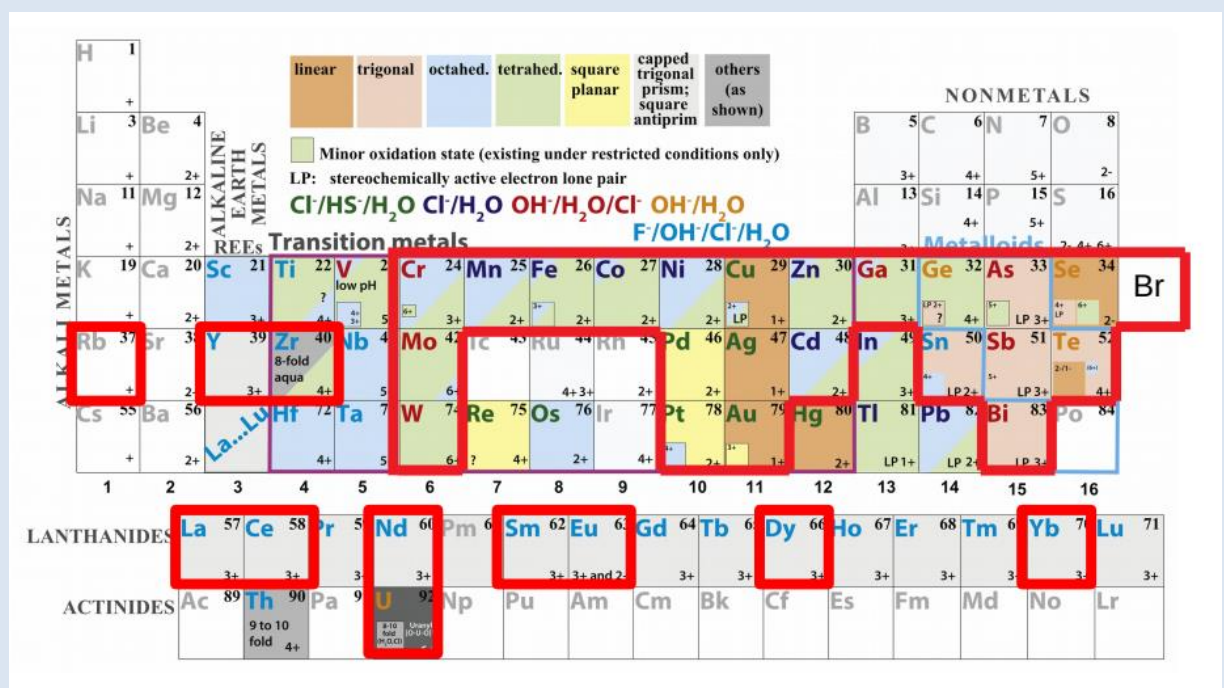


Figure 10. Periodic table adapted from Brugger at al. 2016²⁸ reference to highlight the metallic elements that were studied by XAS at FAME and FAME-UHD beamlines in the last 15 years, making use of our autoclave installation.

²⁸ Brugger J., Liu W., Etschmann B., Mei Y., Sherman D. M., Testemale D., "A review of the coordination chemistry of hydrothermal systems, or do coordination changes make ore deposits?", *Chemical Geology* **447** (2016) 219-253 <http://dx.doi.org/10.1016/j.chemgeo.2016.10.021>

Similarly, a recent study was published by B. von der Heyden in *Ore Geology Reviews*²⁹ which (sic) “seeks to critically review and highlight the power and affordances of synchrotron X-ray techniques specifically to the fields of fundamental- and applied ore geology”. In this work, the author compiled a database of the ore related studies which made use of synchrotron techniques. From this database it appears that from year 2005 the most used beamline in that scientific field is FAME.

Finally, as an introduction to the following highlights, the situation of hydrothermal research at FAME beamlines can be summarized and put into context of the future scientific, methodological and technical trends, with the following points :

- *Scientific topics* : After years of focus on 3d metals and metalloids, the trend is now on studies of Rare Earth Elements and rare/critical metals because of their economic importance, but also thanks to the technical possibility to now conduct measurements at their typical low concentrations. Furthermore, our autoclaves start to be used in other fields than Earth sciences : several studies in material science (hydrothermal chemistry) have been conducted in recent years.
- *Methods* : in addition to the « classical » EXAFS analysis, *ab initio* XANES calculations combined with Molecular Dynamics (MD) simulations are now almost *de facto* integrated to all studies, and bring very useful information about the molecular structure of dissolved metals.
- *Sample environment* : the autoclave equipment is now fully integrated on the FAME-UHD spectrometer, which opens new scientific opportunities. In parallel, we’ve been constantly maintaining and improving the autoclave technology to fulfill more challenging experimental conditions.
- *Néel Institute* : our autoclaves are installed on several laboratories installations at Néel Institute for complementary techniques (hydrothermal synthesis, Raman spectrometry, density measurements, etc.).

Denis Testemale & Jean-Louis Hazemann, Institut Néel & FAME/FAME-UHD beamlines

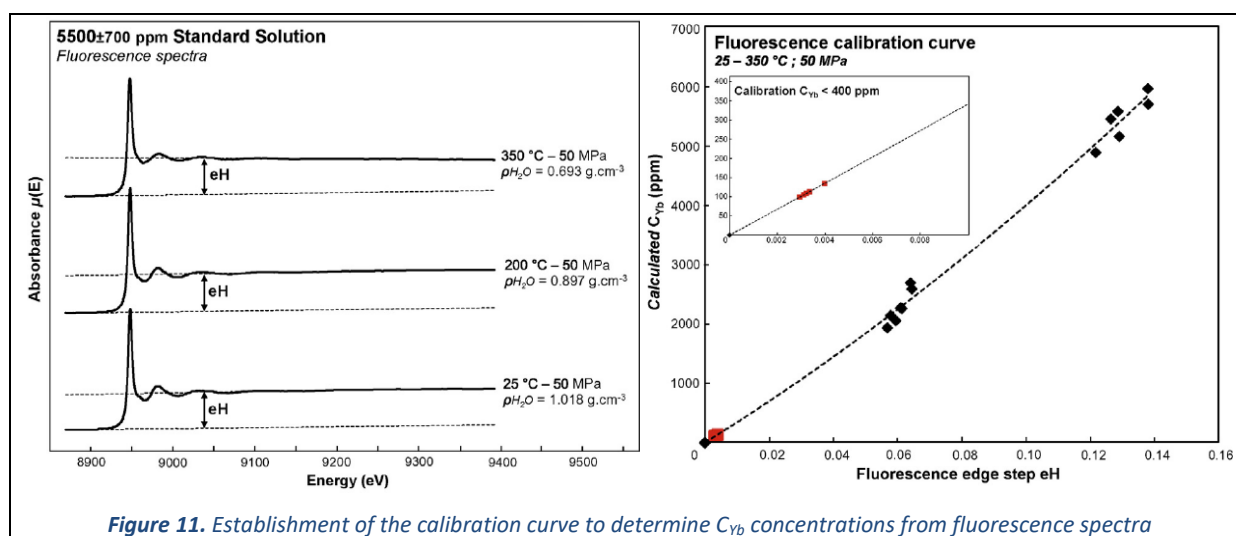
²⁹ Bjorn P. von der Heyden. “Shedding light on ore deposits: A review of synchrotron X-ray radiation use in ore geology research”. *Ore Geology Reviews*, **117** (2020) 103328. <https://doi.org/10.1016/j.oregeorev.2020.103328>

FAME Hydrothermal controls on the genesis of rare earth elements deposits

The growing industrial demand for rare earth elements (REE), especially in the green energy and advanced communications sectors nowadays requires efficient and sustainable mining operations. This can only occur with an improved understanding of the factors controlling the emplacement and grade of REE enrichments in various geological settings.

It is becoming recognized that deposits associated with magmatic intrusions may only reach significant ore grades thanks to hydrothermal remobilization and reconcentration of the REE by high temperature fluids of magmatic origin. Yet, the effect of combined magmatic and hydrothermal processes on REE concentrations, and especially on LREE/HREE preferential enrichment is not well understood. For that reason, an important step to improve the current understanding of rare metals deposits is to identify the effects of cooling, decompression and interaction with host rocks on the composition of the hydrothermal fluids and on the mobilization, transport and precipitation of REE. In this context, we performed *in situ* experiments with the objective to study the solubility and speciation of REE in aqueous fluids involving F, Cl, P, Si or Na up to 600 °C and 1000 bar.

The first set of *in situ* XAS measurements have been conducted at FAME beamline at 500 bar to determine simultaneously the solubility of Yb compounds and Yb speciation from 200 to 350-400°C in fluids containing Cl, F and P ligands. Yb concentrations were monitored down to tens of ppm from the height of the fluorescence absorption edge (Figure 11 Figure 12) while XANES and EXAFS analyses were used to refine the aqueous speciation of Yb in the high temperature fluids (Figure 13).



The fluorescence measurements suggests (Figure 12) that Yb solubility is retrograde above 200 °C and that only 10 to 100 ppm Yb could be dissolved in acidic fluids ($\text{pH} < 2$) containing no ligands at 350-400°C, most probably as $\text{Yb}[(\text{H}_2\text{O})_{7,8}]^{3+}$ species. However, the solubility of $\text{Yb}_2\text{Si}_2\text{O}_7$ is much higher in the wt% range up to 350°C in 0.75m HCl. The EXAFS analysis suggests that the formation of chloro-aqua complexes with Yb surrounded by ~ 5 O and 1-2 Cl, is responsible for this enhanced solubility. Yet, the EXAFS analysis limits the onset of chlorination to these particular conditions and suggests that Yb^{3+} aqua ion is the dominant specie in acidic fluids over the entire P-T-X range investigated.

Increasing pH and adding phosphorus trigger the precipitation of Yb solid compounds from 200 to 400 °C. Indeed, the XANES spectra collected upon dissolution of Yb_2O_3 in 0.18m H_3PO_4

Scientific Results

from 200 to 350°C differ from that of the Yb^{3+} aqua ion in HCl solution but bear significant resemblance to the YbPO_4 crystalline standard (Figure 13). Hence buffering of acid orthomagmatic fluids and leaching of P from host rocks could be major mechanisms in the development of (H)REE enrichments in magmatic-hydrothermal systems.

The present experiments constitute the first *in situ* investigation of REE speciation and solubility in aqueous fluids at the high temperature-low pressure conditions that prevail during the late stage evolution of magmatic-hydrothermal rare metal deposits. Yb solubility significantly decreases with increasing temperature, pH and in the presence of phosphorus. Thus significant (H)REE precipitation is expected around 300–400 °C due to the interaction of acidic magmatic fluids with host rocks. While the precipitation of xenotime may be limited by the availability of phosphorus from the host rock, pH buffering should systematically trigger the precipitation of REE ores minerals. These results are the first of our ongoing study of REE hydrothermal speciation and will complement the existing database to improve the modeling of the hydrothermal transport and precipitation of REE in magmatic-hydrothermal environments.

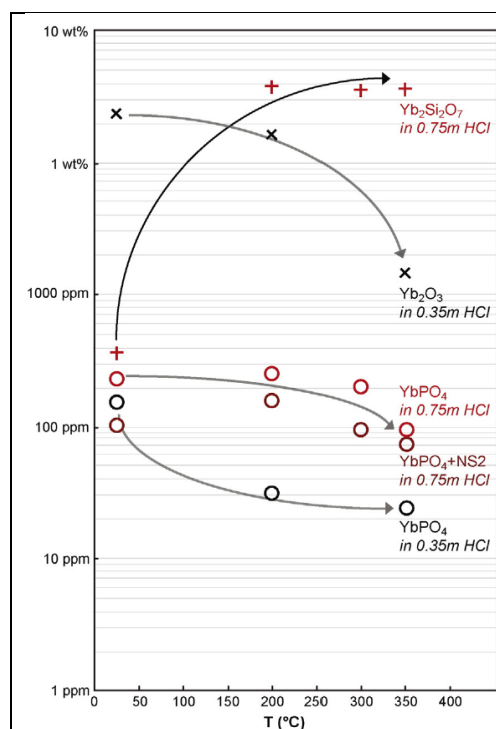


Figure 12. The effect of temperature and fluid composition on Yb_2O_3 , $\text{Yb}_2\text{Si}_2\text{O}_7$ and YbPO_4 (xenotime) solubilities at 50MPa. The arrows underline the solubility trend with increasing temperature for each composition

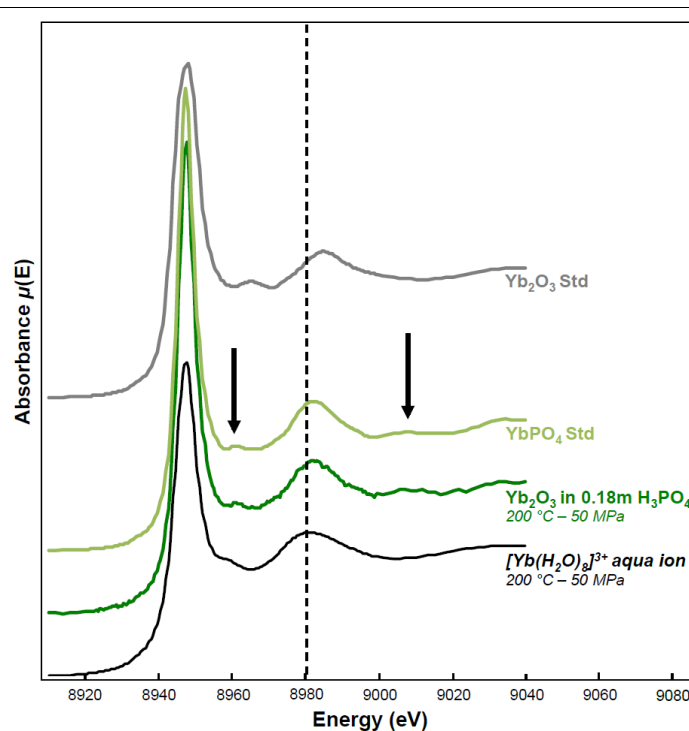


Figure 13. Comparison between the XANES spectrum of Yb_2O_3 in H_3PO_4 solution (dark green) and those of the Yb^{3+} aqua ion and Yb_2O_3 and YbPO_4 crystalline standards. The black arrows underline similarities with the YbPO_4 standard.

Authors and principal publication:

M. Louvel^a, A. Bordage^b, D. Testemale^c, L. Zhoua,^d, J. Mavrogenes^a, *Chemical Geology* **417**, 228-237 (2015)
^a Research School of Earth Sciences, Australian National University, Canberra, Australia | ^b ICMMO, Univ. Paris-Sud 11, UMR CNRS 8182, Orsay, France | ^c Inst. Neel, Univ. Grenoble Alpes, UPR CNRS 2940, Grenoble, France | ^d Key Laboratory of High-temperature and High-pressure Study of the Earth's Interior, Institute of Geochemistry, Chinese Academy of Sciences, Guiyang, China

Effect of sulfur on the aqueous and gaseous transport of Cu in porphyry and epithermal systems

Together, porphyry and high-sulfidation epithermal deposits supply about 75% of the world's Cu and 20% of the world's Au resources. These metal enrichments originate from the exsolution of a volatile-rich phase from crystallizing andesitic to rhyolitic magmas. Thus, the establishment of such porphyry and epithermal systems mainly depends on the composition and density of the volatile-rich phase that escapes the crystallizing magmatic intrusion and travels through the host rocks. This density of this fluid phase can be liquid-like ($0.3\text{--}0.6\text{ g}\cdot\text{cm}^{-3}$) or gas-like ($\rho < 0.3\text{ g}\cdot\text{cm}^{-3}$) or mixed with associated brine + vapour. The details of the processes leading to the precipitation of the sulfide-dominated Cu- and Au-rich ores in associated porphyry and epithermal environments are still widely discussed.

In order to constrain the compositional, pH and $f\text{O}_2$ controls on both the high- and low-density transport of Cu at porphyry to epithermal conditions, specially designed experiments were performed and competing roles of Cl and S species on Cu solubility were tested. In situ X-ray absorption spectroscopy (XAS) with the FAME autoclave³⁰ was employed to simultaneously investigate the solubility and speciation of Cu vs P and T . In parallel, *in situ* Raman spectroscopy and thermodynamic calculations have been used to assess the speciation of S in such fluids to help discriminate potential Cu-S complexes.

In S-free HCl solutions, Cu metal solubility is about 10 times higher in high-density versus low density fluids. During the transition from high- to low-density, Cu speciation evolves from CuCl_2^- complexes to $\text{CuCl}(\text{H}_2\text{O})$ or $\text{CuCl}(\text{HCl})$, depending on HCl concentrations. In sulfur-only solutions Cu solubility is extremely low. The addition of S to Cl-bearing fluids results in a drop of Cu solubility in both high- and low-density fluids. In high-density fluids, solubility drops from weight percent levels (in Cl-only solutions) to hundreds of ppm (containing sulfur). In such a case, Cu speciation is then similar to Cu speciation in pure 0.15 m HCl, with Cu surrounded by 2.1 ± 0.8 Cl atoms. Thus it is the formation of CuCl_2^- and not Cu-S complexes that enable to retain hundreds of ppm in the Cl+S bearing high-density fluids. In low-density fluids, Cu concentrations similarly drop, from hundreds of ppm to below 100 ppm. XANES spectra are characteristic of Cu_2S solid, suggesting precipitation of Cu_2S in the high T fluids or on the wall of the sample cell (Figure 14).

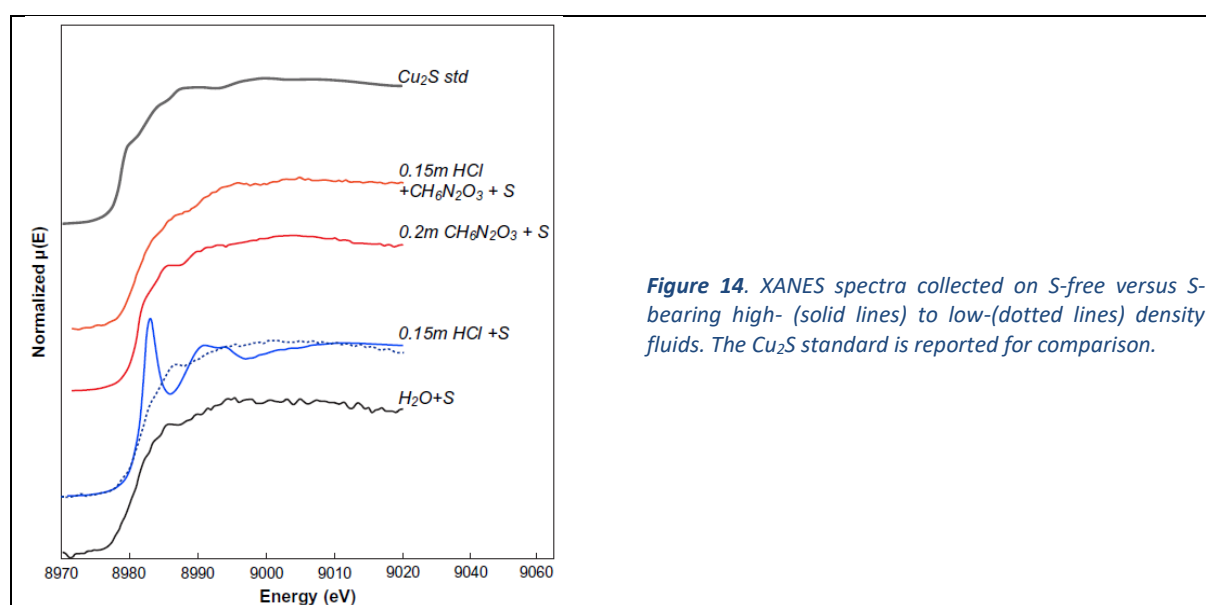


Figure 14. XANES spectra collected on S-free versus S-bearing high- (solid lines) to low- (dotted lines) density fluids. The Cu_2S standard is reported for comparison.

³⁰ D. Testemale, R. Argoud, O. Geaymond, J.-L. Hazemann, Rev. Sci. Instrum. **76**, 043905-043909 (2005)

Scientific Results

It hence appears that the presence of S of different oxidation state (S^{2-} , S^{4+} and S^{6+} , as shown by *in situ* Raman measurements conducted in the autoclave, see Figure 15) limits transport of Cu and may even trigger Cu precipitation at porphyry to epithermal conditions. These observations support recent hypothesis that proposed that the injection of H_2S gas from deeper magmatic source could trigger Cu precipitation in the porphyry system. Furthermore, it has not been demonstrated that the presence of the S_3^- ion increase Cu solubility in fluids in contrast to that of Au. Thus, if present in such environments, S_3^- ion could fractionate Cu from Au in porphyry-epithermal environments.

Overall our spectroscopic study supports recent scenarios that underline the critical role of S speciation in the formation of porphyry and epithermal deposits. New efforts should be dedicated to conduct *in situ* XAS measurements at temperature above 600 °C and study the potential role of Cu chlorides in solution with oxidized S or alkaline complexation (as (Na,K)CuClS neutral complexes) in the early extraction of Cu from magmatic intrusions. Combined with high energy resolution fluorescence techniques (on FAME-UHD) that enable better resolved XANES spectra (in particular for Cu-Cl-S complexes that have feature-less spectra) in dilute fluids, such experimental techniques should enable refinement of the nature and geometry of the complexes forming in high T S-rich fluids.

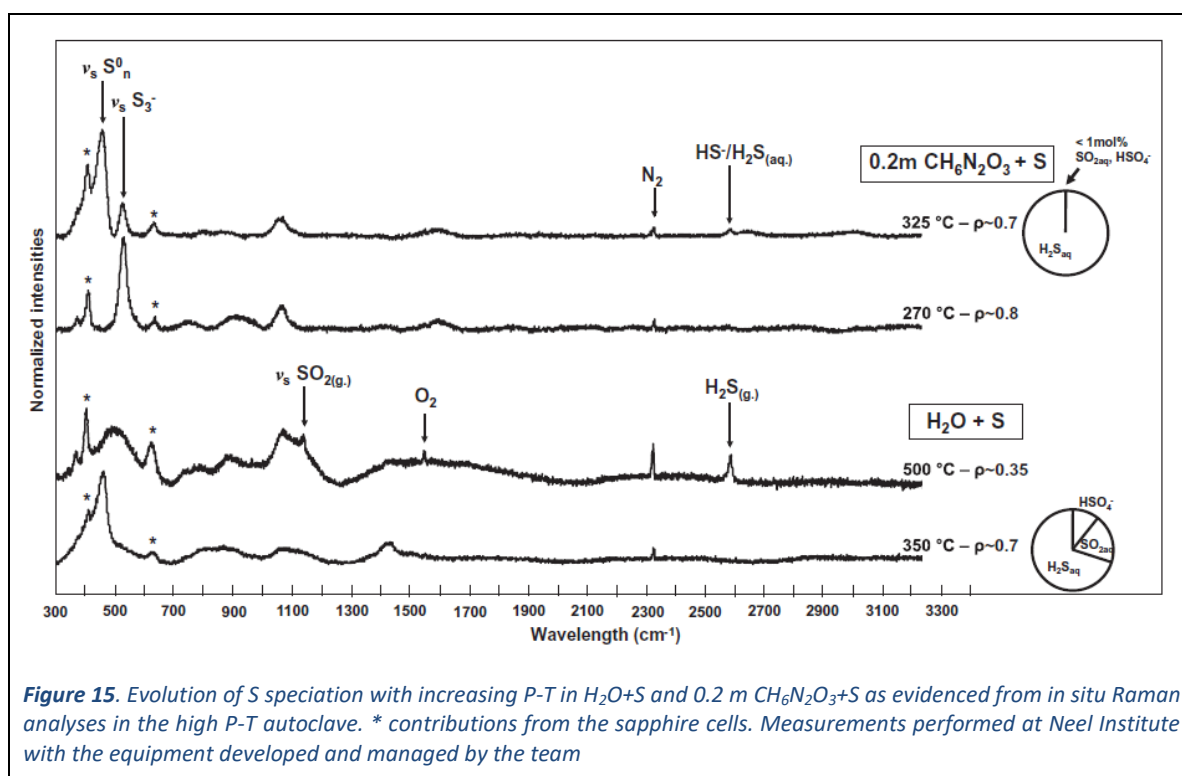


Figure 15. Evolution of S speciation with increasing P-T in H_2O+S and $0.2\text{ m }CH_6N_2O_3+S$ as evidenced from *in situ* Raman analyses in the high P-T autoclave. * contributions from the sapphire cells. Measurements performed at Neel Institute with the equipment developed and managed by the team

Authors and principal publication:

M. Louvel^a, A. Bordage^b, B. Tripoli^c, D. Testemale^d, J.-L. Hazemann^d, J. Mavrogenes^e, *Chemical Geology* **466**, 500-511 (2017).

^a School of Earth Sciences, Bristol University, United Kingdom / ^b ICMO - UMR 8182 – Univ. Paris-Sud 11, Orsay / ^c Earth & Planetary Science, University of California, Berkeley, USA / ^d Institut NEEL CNRS/UGA UPR2940, Grenoble / ^e Research School of Earth Sciences, Canberra, Australia.

Sulfur-bearing complexes of zinc and cadmium in hydrothermal fluids

Zinc and cadmium are chalcophile elements, *i.e.* they have a low affinity for oxygen and prefer to bind with reduced sulfur (*i.e.* sulfides) and are typically concentrated in hydrothermal sulfide ores. They are common in many types of hydrothermal ore deposits from porphyry to epithermal. These ores are formed by hot (100-600°C) aqueous solutions, in which sulfur is ubiquitous. At such conditions, sulfur can be an important complexing ligand, competitive with other ligands, *e.g.* chloride. Numerous studies were devoted to Zn and Cd chloride complexes, but, to date, comparatively little attention has been paid to the identity, structure and stability of S-bearing complexes.³¹ The goal of this study is to characterise these species by *in situ* X-ray absorption spectroscopy at high temperature and pressure (T-P), measuring both solubility and the local atomic environments of dissolved metal. These data are essential to quantify the role of sulfur in Zn and Cd transport and precipitation in natural geological hydrothermal systems.

Experiments were carried out in a glassy carbon cell placed in autoclave equipped with T-P regulations,³⁰ allowing both transmission and fluorescence acquisitions at controlled T-P. For solubility experiments, ZnS_(s) (sphalerite) and CdS_(s) (greenockite) monocrystals were placed at the bottom of the cell. The cell position was optimized such that the solid phases were out of the beam path through the solution (Figure 16, left).

Solubility of both sphalerite and greenockite attain up to 10⁻³ mol per kg of fluid values at high sulfur concentrations (3 mol of S per kg of fluid). With increasing sulfur concentration, ZnS and CdS solubility increases. The experimental fluorescence XANES spectra of Cd and Zn complexes in S-rich and S-free hydrothermal solutions at high T-P obtained in this study are presented in Figure 16, right. Comparative analysis of XANES spectra of metal solids with known structure and containing O, Cl or S at ambient T-P demonstrates that the XANES signature of Zn and Cd S-bearing solutions is typical of tetrahedral structures (reduction of the amplitude of the white line and shift of its position to lower energies). Further XANES calculations are in progress to derive more detailed structural information.

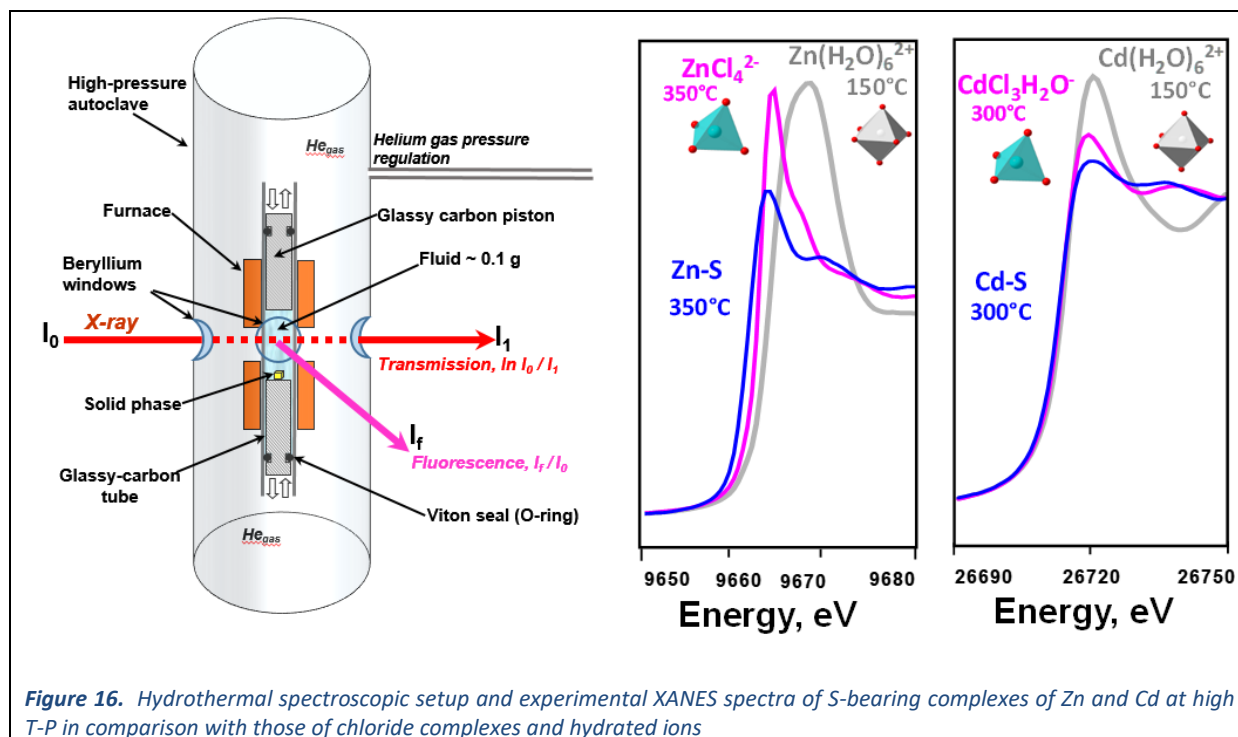
EXAFS modelling confirms these observations. In S-rich solutions at 300-350°C, both Zn and Cd are surrounded by 3.5±0.5 S atoms at 2.33±0.01Å (for Zn) and at 2.50±0.01Å (for Cd). These distances are longer than those measured in hydrated ions (2.07±0.02Å for Zn-O, 2.29±0.02Å for Cd-O) and chloride complexes (2.27±0.03Å for Zn-Cl, 2.44±0.03Å for Cd-Cl).

The interpretation of XAS data and the development of a final speciation model are not trivial. The main difficulty is the poorly known sulfur chemistry at high T-P and high S concentration. Above 200°C, thiosulfate becomes unstable and decomposes to SO₄²⁻, H₂S⁰_(aq)/HS⁻ and other intermediate-valence S species such as S₃⁻.³² In our studied solutions, no O atoms were detected in the S-bearing observed complexes. Thus, sulfate is not bounded to Zn or Cd. Due to the fact that hydrogensulfide HS⁻ and trisulfur S₃⁻ are the major reduced S species in such solution at 350°C, the question is open to assign these species to hydrosulfide complexes such as trigonal Me(HS)₃⁻, tetrahedral Me(HS)₄²⁻ or Me(HS)₃(H₂O)⁻ or more disordered Me(HS)₂S₃⁻. Comparison with results obtained in polysulfide-free solutions (NaHS-H₂S-H₂O) does not allow yet to separate these species, XANES in both types of solutions being very similar.

³¹ N.N. Akinfiev, B.R. Tagirov, *Geochem. Int.* **52**, 214-232 (2014) / B.R. Tagirov, T.M. Seward, *Chem. Geol.* **269**, 301-311 (2010)

³² G.S. Pokrovski, J. Dubessy, *Earth Planet. Sci. Lett.* **411**, 298-309 (2015)

Scientific Results



In conclusion, we have found that in S-rich fluids speciation of both Cd and Zn is dominated by S-bearing complexes. Solubility of sphalerite and greenockite increases with S concentration and attains 10^{-3} molality level at 3 mol of S per kg of fluid. These species may be predominant in natural hydrothermal systems at high S-concentrations and thus should be taken into account in the geochemical models. We are now working on better description of these new complexes using theoretical XANES calculations, solubility and thermodynamic analysis.

Authors and principal publication:

E.F. Bazarkina^{1,2}, O. Proux³, E. Lahera³, W. Del Net³, J.-L. Hazemann¹ In situ X-ray absorption spectroscopy study of Zn and Cd transport by S-rich fluids. *16th Intern. Symp. on Water-Rock Interaction* (July 21-26, 2019, Tomsk, Russia)

¹Institut Néel, UPR 2940 CNRS - Université Grenoble Alpes, F-38000 Grenoble, France / ²IGEM RAS, 119017 Moscow, Russia / ³OSUG (OSUG), UMS 832 CNRS, Université Grenoble Alpes, F-38041 Grenoble, France

Although water represents only a tiny fraction of the terrestrial lithosphere (~1%), hydrothermal fluids are indispensable to the formation of economic metal concentrations in the crust. This is because it is impossible to imagine a process without a fluid phase which would allow extracting metals present in low concentrations from a large volume of rock or magma, massively transporting them through the crust, and precipitating them in a much focused fashion at the right place in the right moment to form an economically exploitable mineral resource. In this complex process that yields enrichment factors typically from 100 to 100,000 for metals compared to their abundance in common rocks, the fundamental thing to know is the solubility of ore minerals and the speciation of metals and major volatile elements such as sulfur, carbon or halogens.

In situ synchrotron X-ray absorption spectroscopy and laboratory Raman spectroscopy are the methods of choice to obtain identity, molecular structure and concentration of metal complexes and their S-C-Cl-F ligands in the fluid at elevated temperatures and pressures. These methods benefit from a high-pressure high-temperature spectroscopic cells designed and setup at FAME and FAME-UHD beamlines³³. Combined with more routine ex-situ solubility experiments in hydrothermal reactors (*e.g.*, at the GET laboratory) and molecular and thermodynamic modelling, these approaches have enabled in the last decade unprecedented advances in our understanding of the speciation and transport of noble and base (Au, Cu, Ni, Co) and critical (*e.g.*, REE, PGE) metals by geological fluids. These new data enabled the establishment of predictive models of the solubility of the metal-bearing minerals thereby enabling quantitative predictions of hydrothermal fluid evolution and metal transport, distribution, and deposition. These advances primarily concern the impact of sulfur on the transport of chalcophile metals (*i.e.* sulfur-loving, Au, Cu, Zn, Cd, PGE). The results reveal, in particular, the key role of the trisulfur radical ion which was recently discovered and quantified by our teams³⁴, as one of the major carriers of those metals in S-rich hydrothermal fluids across the lithosphere (*cf.* examples below).

However, many trace elements precipitating from the ore-bearing fluids do not form their own pure mineral phases but rather get incorporated into major sulfide, oxide or silicate minerals. Despite significant advances in microanalytical techniques in Geosciences over the past 20 years allowing the bulk concentration and distribution of such elements to be quantified from microscopic to mineral-deposit scale, their exact structural and redox state, the link with major elements, and the mechanisms of their uptake and release by the host mineral remain poorly known. Such knowledge is required, in particular, for the use of trace element signatures for tracing metal sources for ore deposits, reconstructing fluid evolution and metal precipitation, and for more efficient metal georesources exploration and ore processing. *In situ* high-resolution synchrotron X-ray absorption spectroscopy recently developed at FAME-UHD, combined with physical-chemical and molecular modeling, is the most direct method to provide information about a trace element redox state, chemical bonding, and coordination at the atomic scale. For example, our recent concerted study carried out in the framework of a large ANR program Radicals³⁵ revealed the atomic state of gold in arsenian pyrite and arsenopyrite, which are the major concentrators of “invisible” gold and other chalcophile trace elements in the Earth’s crust (see below).

Future advances of *in-situ* HR-XAS spectroscopy and associated techniques under development at FAME and FAME-UHD (XES, Ptichography), coupled with laboratory

³³ Testemale et al., *Rev. Sci. Instrum.* **76** (2005) 043905. See also the corresponding part in §4

³⁴ G.S. Pokrovski & L.S. Dubrovinsky, *Science* **331** (2011) 1052-1054 ; G.S. Pokrovski & J. Dubessy, *EPSL*. 411 (2015) 298-309

³⁵ Gathering GET, Institut Néel/FAME & FAME-UHD, ENS, IMPG and CRPG

experiments and physical-chemical and molecular modelling, will allow systematic quantification of many valuable critical metals hidden in major minerals, thereby enabling a better understanding of trace element geochemical cycles and improving resource assessment, exploration and recovery.

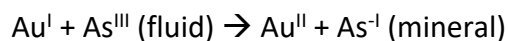
Gleb Pokrovski, Géosciences Environnement Toulouse

An arsenic-driven mineral pump for gold in hydrothermal systems

Pyrite, arsenopyrite and löllingite are the key minerals in hydrothermal systems capable of concentrating gold by up to 10^6 times its mean crustal and mantle abundance, which is only about 1 ng/g. A large part of gold hosted by these minerals is “invisible” or “refractory” (*i.e.* optically undetectable) occurring both as metal nanoparticles (Au^0) and chemically bound Au, the latter being often the dominant gold state. The contents of this ‘hidden’ gold are ubiquitously correlated with those of As in pyrite on the (sub)micron scale - a 40-year old observation that has still remained unexplained. The redox and structural state of chemically bound Au and its link with As may be controlling factors of a deposit’s economic potential, determine the type and cost of Au recovery from ore and, more generally, affect the gold distribution at the Earth crust scale. Despite significant advances in micro/nanoanalytical techniques over the past 20 years, the fundamental causes of the Au-As relationship and processes that could drive gold, the most chemically inert metal of the Periodic Table, to such levels of enrichment in a host mineral yet remain enigmatic.

To elucidate fundamental factors controlling the nature of invisible Au in arsenian pyrite and Fe sulfarsenides and the role played by As in Au intake, we used HERFD-XAS at FAME then FAME-UHD beamlines - the most direct method to provide information about a trace element redox state, chemical bonding, and coordination at the atomic scale. The XANES and EXAFS spectra were acquired on a set of thoroughly characterized Au-bearing pyrite and arsenopyrite samples from major metamorphic and sedimentary-hosted gold deposits and their synthetic analogues prepared in controlled laboratory experiments. The spectroscopic data were interpreted using ab-initio quantum chemistry simulations of Au structural position and molecular environment (Figure 18), and Au partition coefficient data between the fluid and mineral were assessed using thermodynamic modelling.

Our data show that Au enters As-enriched Fe crystallographic sites of the three minerals in a formal oxidation state of Au^{II} , forming $[\text{AuAs}_n\text{S}_{6-n}]$ units, whereas in As-poor pyrite Au is dominantly chemisorbed as $[\text{Au}^{\text{I}}\text{S}_2]$ moieties in much lower concentrations (Figure 17). Thus, arsenic exerts a universal control on gold incorporation in iron sulfides and sulfarsenides via coupled Au-As redox reactions, between $\text{Au}^{\text{I}}/\text{As}^{\text{III}}$ in the hydrothermal fluid, which are represented by $\text{Au}^{\text{I}}\text{-HS-S}_3^-$ type of complexes (Pokrovski et al., 2015) and $\text{As}^{\text{III}}(\text{OH})_3$ ^{36,37} and $\text{Au}^{\text{II}}/\text{As}^{\text{I}}$ in these As-bearing minerals:

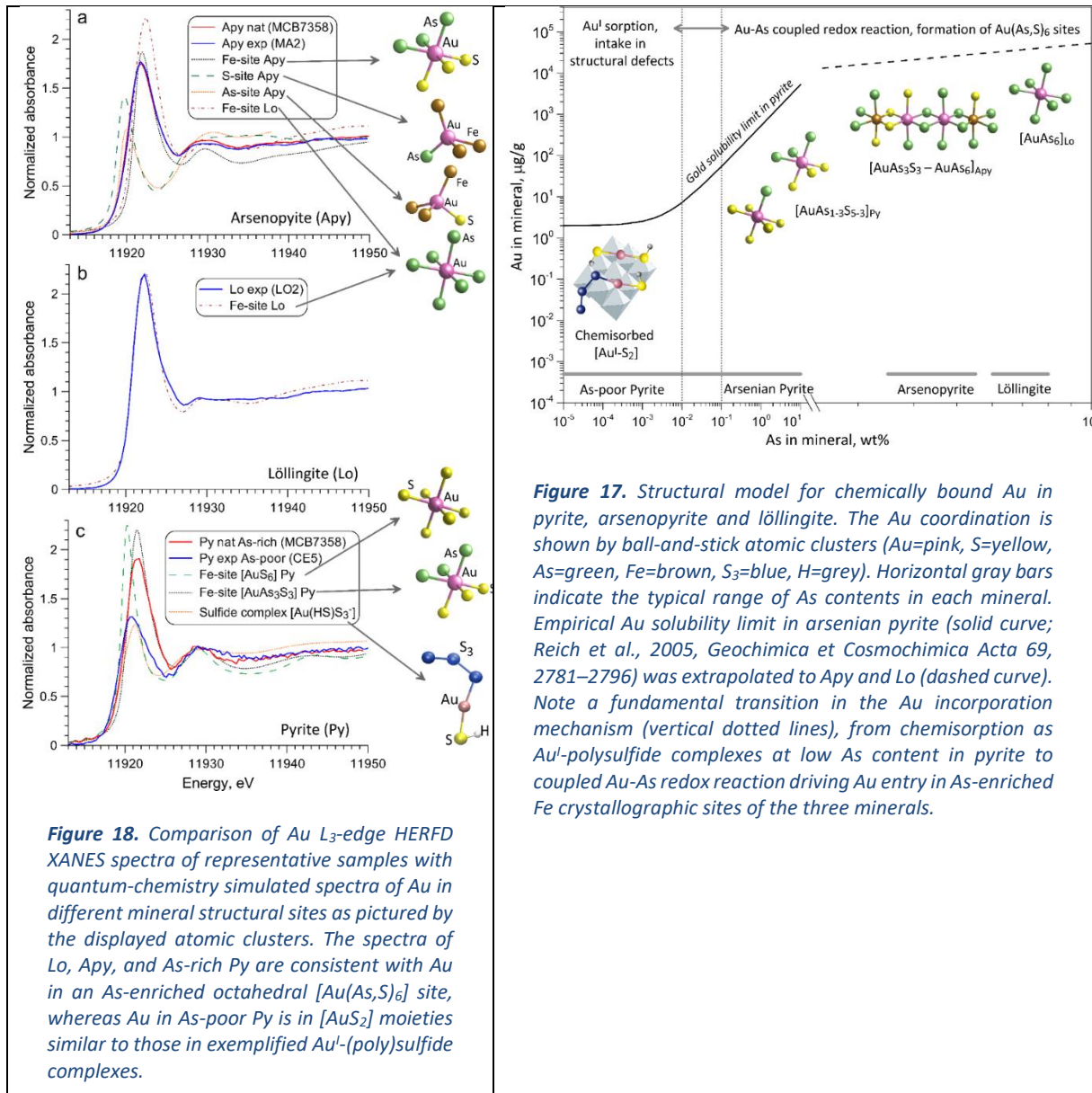


These reactions account for the observed variations in invisible gold contents in the minerals from different deposit types and enable quantitative prediction of Au uptake and release by these gold “mineral pumps” in hydrothermal systems. The results of this integrated study thus help in resolving one of the oldest enigmas in Geochemistry and Ore Deposit Geology about the ubiquitous Au-As associations in hydrothermal ore minerals. Furthermore, these new findings open perspectives for improving resource assessment, exploration and recovery for

³⁶ Testemale D., Pokrovski G.S., Hazemann J.-L., *European Journal of Mineralogy* **23** (2011) 379-390

³⁷ Perfetti et al., *Geochimica et Cosmochimica Acta* **72** (2008) 713-731

gold and other valuable trace elements “hidden” in arsenian pyrite - the most abundant iron sulfide mineral on Earth.



Authors and principal publications:

Pokrovski G.S.¹, Escoda C.¹, Blanchard M.¹, Testemale D.², Kokh M.A.³, Gouy S.¹, Boiron M.-C.³, de Parseval F.¹, Aigouy T.¹, Menjot L.¹, de Parseval P.¹, Beziat D.¹, Salvi S.¹, Proux O.⁴, Rovezzi M.⁴, Hazemann J.-L.², Pöttgen R.⁵, Doert T.⁶, Kouzmanov K.⁷ An arsenic-driven pump for invisible gold in hydrothermal systems. *Geochemical Perspective Letters* (under moderate revision at 03/2021).

Pokrovski G.S.¹, Kokh M.A.³, Proux O.⁴, Hazemann J.-L.², Bazarkina E.F.², Testemale D.², Escoda C.¹, Boiron M.-C.³, Blanchard M.¹, Aigouy T.¹, Gouy S.¹, de Parseval P.¹, Thibaut M.¹ The nature and partitioning of invisible gold in the pyrite-fluid system. *Ore Geology Reviews* **109** (2019) 545-563

¹ Géosciences Environnement Toulouse (GET), UMR 5563 CNRS, IRD, Observatoire Midi-Pyrénées, Univ. Toulouse, France | ² Univ. Grenoble Alpes, CNRS, Institut Néel, Grenoble, France | ³ GeoRessources, Univ. Lorraine, CNRS, Vandœuvre-lès-Nancy, France | ⁴ Univ. Grenoble Alpes, CNRS, IRD, Irstea, Météo France, OSUG, FAME, Grenoble, France | ⁵ Univ. Geneva, Department of Earth Sciences, Geneva, Switzerland | ⁶ Institut für Anorganische und Analytische Chemie, Universität Münster, Germany | ⁷ Technische Universität Dresden, Faculty of Chemistry and Food Chemistry, Dresden, Germany

Resolving the enigma of gold deposit formation using XAS

To better understand how gold economic resources form on Earth, *in situ* X-ray absorption spectroscopy (XAS) and solubility measurements were combined with molecular dynamics and thermodynamic simulations to show that the trisulfur radical ion S_3^- strongly binds gold in aqueous solution and enables very efficient extraction, transport, and precipitation of the metal by hydrothermal fluids, explaining many enigmatic features of gold deposits.

Gold economic resources on Earth result from an exceptional concentration phenomenon yielding metal contents in ore of thousand to million times higher than those in common rocks. This process is thought to be controlled by aqueous fluids enriched in salt, sulfur and CO_2 , which flow through the Earth's crust, extract the metal from rocks or magmas and transport and precipitate it in the right place at the right moment. Yet, the factors responsible for this transfer remain enigmatic in the face of the extraordinary chemical inertness of gold and the weak capacities of the major fluid components, chloride (Cl^-), hydrogen sulfide (H_2S/HS^-) and sulfate (SO_4^{2-}), to solubilise this noble metal. In particular, all gold and sulfur speciation models ignore sulfur radical ions (S_3^-) recently shown to be stable in aqueous fluid phase at elevated temperature (from 200 to 700°C) and pressure (to GPa)^{38,39}.

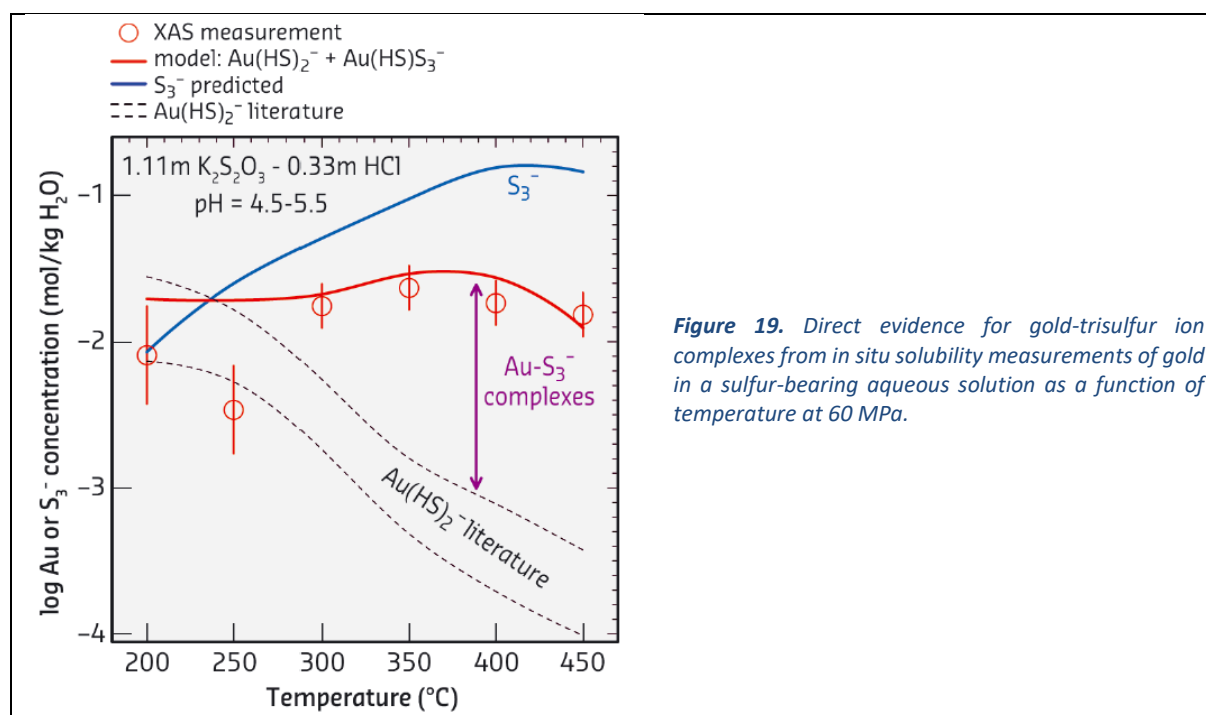


Figure 19. Direct evidence for gold-trisulfur ion complexes from *in situ* solubility measurements of gold in a sulfur-bearing aqueous solution as a function of temperature at 60 MPa.

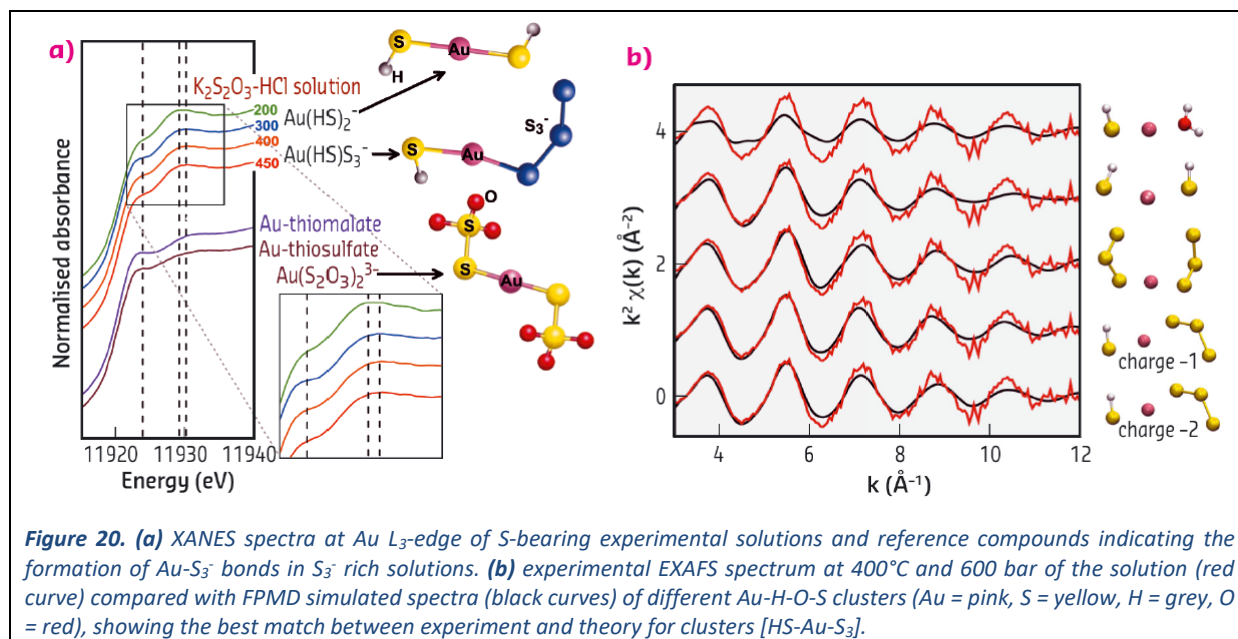
To quantify the effect of the radical ions on Au behaviour in hydrothermal fluids, we combined *in situ* XAS and solubility measurements with first-principles molecular dynamics (FPMD) and thermodynamic modelling of Au structure and speciation in aqueous solutions saturated with gold metal and containing hydrogen sulfide, sulfate and S_3^- . These experimental solutions are representative of fluids that formed major types of gold deposits in the crust (temperatures to 500°C, pressures to 200 MPa equivalent to ~7 km depth, sulfur contents to 3 wt%, and NaCl-KCl salt contents to 20 wt%).

XAS experiments were carried out at FAME beamline using a unique spectroscopic cell that enables simultaneous measurement of both total metal concentration in the fluid and its local

³⁸ G.S. Pokrovski and L.S. Dubrovinsky, *Science* **331**, 1052-1054 (2011)

³⁹ G.S. Pokrovski and J. Dubessy, *Earth Planet. Sci. Lett.* **411**, 298-309 (2015).

atomic structure.⁴⁰ We found that the presence of S_3^- in the fluid yields Au solubility enhancement by a factor of 10 to 100 compared to the traditional Au chloride and sulfide complexes such as $Au(HS)_2^-$ and $AuCl_2^-$ (Figure 19). XAS spectra, aided by FPMD simulations, indicate that S_3^- binds Au by forming complexes of the type $Au(HS)S_3^-$ (Figure 20). These data, complemented by Au solubility measurements using a flexible cell hydrothermal reactor, were analyzed with a thermodynamic model that allowed the stability of the new Au-trisulfur ion species to be constrained across a wide range of geological conditions, from deep subduction-zone magmas to thermal springs at the surface.



Applying this model to natural fluids shows that sulfur radical ions, even though less abundant than sulfide or chloride, are capable of extracting large amounts of gold from magmas or rocks at depth and transporting the metal in high concentrations through the Earth's crust. When these hot fluids rise to the surface, cool down or encounter a rock of different composition (e.g., carbonate or organic-rich), the sulfur radicals break down and deposit the metal in veins and cavities. As such, the discovery of soluble and mobile Au- S_3^- complexes helps explain the enigma of gold deposit formation and offers new possibilities for resource prospecting. Furthermore, such complexes may find applications in ore processing and hydrothermal synthesis of Au-based nanomaterials. This study shows that old gold known from Antiquity has yet to reveal all its secrets.

Authors and principal publication:

G.S. Pokrovski^a, M.A. Kokh^a, D. Guillaume^a, A.Y. Borisova^a, P. Gisquet^a, J.-L. Hazemann^b, E. Lahera^c, W. Del Net^c, O. Proux^c, D. Testemale^b, V. Haigis^{d,e}, R. Jonchère^{d,e}, A.P. Seitsonen^d, G. Ferlat^e, R. Vuilleumier^d, A.M. Saitta^e, M.-C. Boiron^f, J. Dubessy^f, Sulfur radical species form gold deposits on Earth, *PNAS* **112**, 13484-13489 (2015)

^a Groupe Métallogénie Expérimentale, Géosciences Environnement Toulouse, Observatoire Midi-Pyrénées, Univ. de Toulouse, CNRS, IRD, Toulouse | ^b CNRS, Univ. Grenoble Alpes, Institut NEEL, Grenoble | ^c OSUG, CNRS - Univ. Grenoble Alpes, Saint Martin d'Hères | ^d École Normale Supérieure, PSL Research Univ., Département de Chimie, Sorbonne Univ., UPMC, Univ. Paris 06, CNRS, UMR 8640 Pasteur, Paris | ^e Sorbonne Univ., UPMC, Univ. Paris 06 and CNRS, Institut de Minéralogie, de Physique des Matériaux et de Cosmochimie, Paris | ^f Univ. de Lorraine, CNRS, CREGU, GeoRessources, Vandoeuvre lès Nancy

⁴⁰ D. Testemale et al., *Rev. Sci. Instrum.* **76**, 043905-043909 (2005).

Biochemistry

Metal ions play an important role in several biological processes that have both structural and functional importance. The functioning of an organism depends on the properties on many length scales and hierarchical levels. The synchrotron spectroscopy techniques contribute to elucidate the distribution, concentration and chemical state of elements inside tissues and cells. This contribution is not only highly challenging but represents important objectives of modern analytical chemistry and an essential step towards the precise understanding of some cellular pathophysiological or toxicological processes. At the biological level, a great number of trafficking pathways, intracellular transport and compartmentalization can be probed and characteristic molecular signatures can be found. Imbalance in the amount of metals in the body and exposure to toxic metals are associated with severe health problems. They are linked to several abnormalities, including cardiovascular diseases, metabolic disorders and neurodegenerative disorders (Alzheimer's disease, Parkinson's disease, and Huntington's disease and others)^{41,42}. The latter highlighted the well-established association between aberrant protein deposition in neurodegenerative disorders, and disrupted metabolism of metals. Still, it is not clear yet to which extent metal-protein interactions are a contributing factor in disease pathogenesis their studies being a difficult analytical challenge. The toxicity of metals and pathways involved in metal imbalances are now considered to be highly active areas of biomedical research. Further, the chemical speciation and imaging of targeting of metal-based drugs or medical imaging contrast agents is a necessary step to improve their efficiency. Also, the recent development of nanotechnologies for nanomedicine or for industrial and engineering purposes, raising concerns about their unintentional health and environmental impact, urges the need for efficient analytical tools able to characterize their bio-distribution bio-transformation and interaction with living systems. Among the analytical methods available to probe the chemical composition of biological systems, and to determine their chemical speciation, X-ray Absorption Spectroscopy (XAS), provides specific and unique information on the local structure of the absorbing elements (oxidation state, and sensitive to the types and numbers of coordinated ligand atoms and metalligand distances) in situ, with high resolution and almost without sample preparation prone to modify the chemical species. The characteristics of FAME and FAME-UHD beamlines can answer these analytical challenges and particularly the possibility to tackle speciation close-to-native biological state, at very low concentration that is highly relevant for the biological mechanism that involve metals, highly relevant to pharmacological concentration (μM - nM range) when organo-metallic drugs are concerned and for toxicology where toxic metals implicated (Hg, As, Cr, Ni, Ag...) have deleterious biological effects well below mg/Kg concentration. The past five years have demonstrated the increasing interest of the biological – biomedical field towards the high-quality of information provided by FAME and FAME-UHD in the above-mentioned domain and well-illustrated by the relevant highlights below. This bring to an even more exciting future taking advantage of the upgrade program and development made at FAME and FAME-UHD. Key steps will be in tackling EXAFS analysis at very low concentration i.e well below mg/Kg level of analyte. We expect that new detector capabilities will bring the capabilities of FAME and FAME-UHD to an even higher level of analytical capability. Further, nearly all users in the above-mentioned domains required to do high-resolution imaging and speciation (bulk or

⁴¹ Ferreira, C.R.; Gahl,W.A. Disorders of metal metabolism. *Transl. Sci. Rare Dis.* **2017**, *2*, 101–139

⁴² Barnham, K.J.; Bush, A.I. Biological metals and metal-targeting compounds in major neurodegenerative diseases. *Chem. Soc. Rev.* **2014**, *43*, 6727–6749

micro). This critical to better understand all the mechanism behind metal's role in biology and as a holy grail the speciation at organelle levels. The sensitivity to highly-diluted elements, the use of cryogenic strategies/workflow to preserve at best the chemical integrity of the hydrated biological samples and the capabilities to perform in the future micro-imaging and possibly higher resolution speciation through XANES ptychography will clearly bring this research facility and group at the world leading forefront of chemical analysis for the highly active research domain of metals in biology and biomedicine.

Sylvain Bohic, INSERM UA7, Synchrotron Radiation for Biomedicine (STROBE), Grenoble

Sub-ppm level high energy resolution fluorescence detected X-ray absorption spectroscopy of selenium in articular cartilage

The speciation of highly-diluted elements by X-ray absorption spectroscopy (XAS) in a diverse range of materials is extremely challenging, especially in biological matrices such as articular cartilage. Here we present the development of a synchrotron spectroscopy analysis, namely high energy resolution fluorescence detected (HERFD) XAS using an array of crystal analyzers (CAS), which demonstrated selenium speciation down to 400 ppb ($\mu\text{g}/\text{kg}$) within articular cartilage. This is a major advance in the speciation of highly-diluted elements through XAS and opens new possibilities to study the metabolic role of selenium and other elements in biological samples. We applied this highly performant method of Se speciation determination to an *in vitro* model of articular cartilage maturation, with the aim to understand the selenium role in articular cartilage physiology, and in particular, the relationship between osteoarthritis and Se deficiency. Through a meta-analysis of studies covering five types of Se supplementation for treatment of Kashin-Beck disease, it was demonstrated that Se-supplemented treatments was beneficial in repairing metaphyseal lesions.⁴³ The ability to identify and quantify speciation of highly diluted element, i.e. much below ppm level, is of key importance to advance understanding of Se bio-transformation and incorporation in cartilage matrix.

The narrow energy resolution of the CAS allows selection of only the photons with the appropriate energy, with almost no background. Even if the signal of interest is very small, which is the case when the probed element is highly diluted, the low background allows spectra with a good signal-to-background ratio to be obtained. Selenium concentration for cartilage cultured in standard serum-free medium (ITS) was in the range 400-500 ppb, HERFD-XAS measurements allow then the Se speciation.

Identification of the major Se species present in cartilage were performed by a least-squares fitting process of linear combinations (LCF) of edge spectra from a series of inorganic and organoselenium reference compounds measured in the same experimental conditions. The LCF analysis of the HERFD-XAS spectra indicate that a major contributing species is in the form of a thioselenide compound such as selenodiglutathione (R-S-Se-S-R). It is the major metabolite of selenite in mammalian tissues. Selenite and reduced glutathione spontaneously react to form R-S-Se-S-R, and reduced glutathione concentrations are known to be high in nearly all tissues. The Se HERFD-XAS spectra of ITS treated cartilage explants and those treated both with ITS and growth factors ("FT-treated") were found similar. Despite a highly accelerated maturational response for the later, the LCF analysis of the HERFD-XAS spectra

⁴³ D. Xie, Y. Liao, J. Yue, C. Zhang, Y. Wang, C. Deng, L. Chen, *BMJ open*, 2018, **8**, e017883

Scientific Results

indicate that in both case alkyl selenide (R-Se-R) is the main contributing Se compounds (Selenocysteine-like and glutathione peroxidase type of compounds) of the ITS and ITS FT-treated cartilage explants.

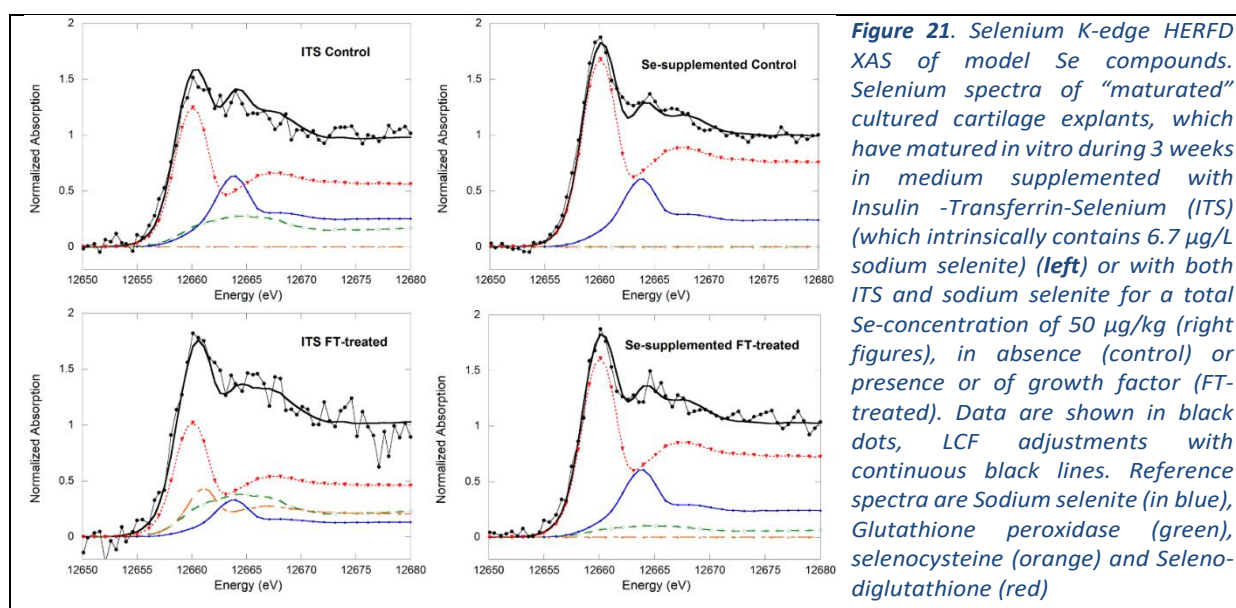


Figure 21. Selenium K-edge HERFD XAS of model Se compounds. Selenium spectra of “matured” cultured cartilage explants, which have matured in vitro during 3 weeks in medium supplemented with Insulin -Transferrin-Selenium (ITS) (which intrinsically contains 6.7 $\mu\text{g/L}$ sodium selenite) (left) or with both ITS and sodium selenite for a total Se-concentration of 50 $\mu\text{g/kg}$ (right figures), in absence (control) or presence of growth factor (FT-treated). Data are shown in black dots, LCF adjustments with continuous black lines. Reference spectra are Sodium selenite (in blue), Glutathione peroxidase (green), selenocysteine (orange) and Selenodiglutathione (red)

This result indicate that we are able to detect in these cartilage explants chemical forms of Se typical of selenoproteins that are also of key interest for cellular metabolism.⁴⁴ Actually, the importance of monitoring Sec levels is highlighted by studies showing that deleting the Sec tRNA gene produced KBD-like phenotypes in mice. In humans the genetic polymorphisms in the glutathione peroxidase-1 gene has been reported to be associated to higher risk of developing KBD.

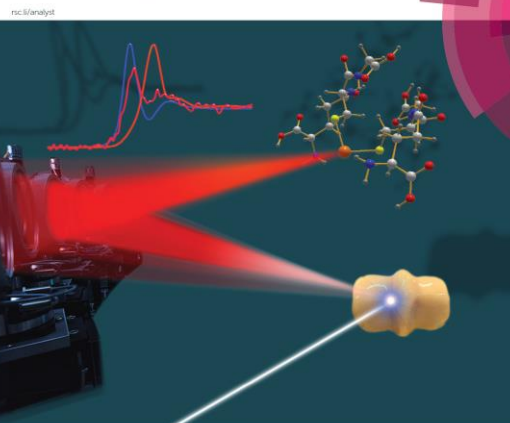
Authors and principal publication:

C. Bissardon^(a,d), O. Proux^(b), L.H.E. Winkel^(c), E. Suess^(c), S. Bureau^(d), R. S. Conlan^(e), L. W. Francis^(e), I. L. Khan^(e), L. Charlet^(d), J.-L. Hazemann^(f), S. Bohic^(a), *Analyst* **144** (2019) 3488-3493

^(a) Université Grenoble Alpes, EA 7442 INSERM, ESRF, Grenoble / ^(b) OSUG, UMS 832 CNRS, Univ. Grenoble Alpes, Grenoble / ^(c) Institute of Biogeochemistry and Pollutant Dynamics, ETH Zurich, Switzerland; and Eawag, Swiss Federal Institute of Aquatic Science and Technology, Dübendorf, Switzerland / ^(d) ISTERre, UMR 5275 CNRS, Univ. Grenoble Alpes, Grenoble / ^(e) Centre of Nanohealth, Swansea Univ. Medical School, Swansea, UK / ^(f) Institut Néel UPR 2940 CNRS, Univ. Grenoble Alpes, Grenoble

Volume 144 | Number 11 | 07 June 2019 | Pages 3453–3692

Analyst

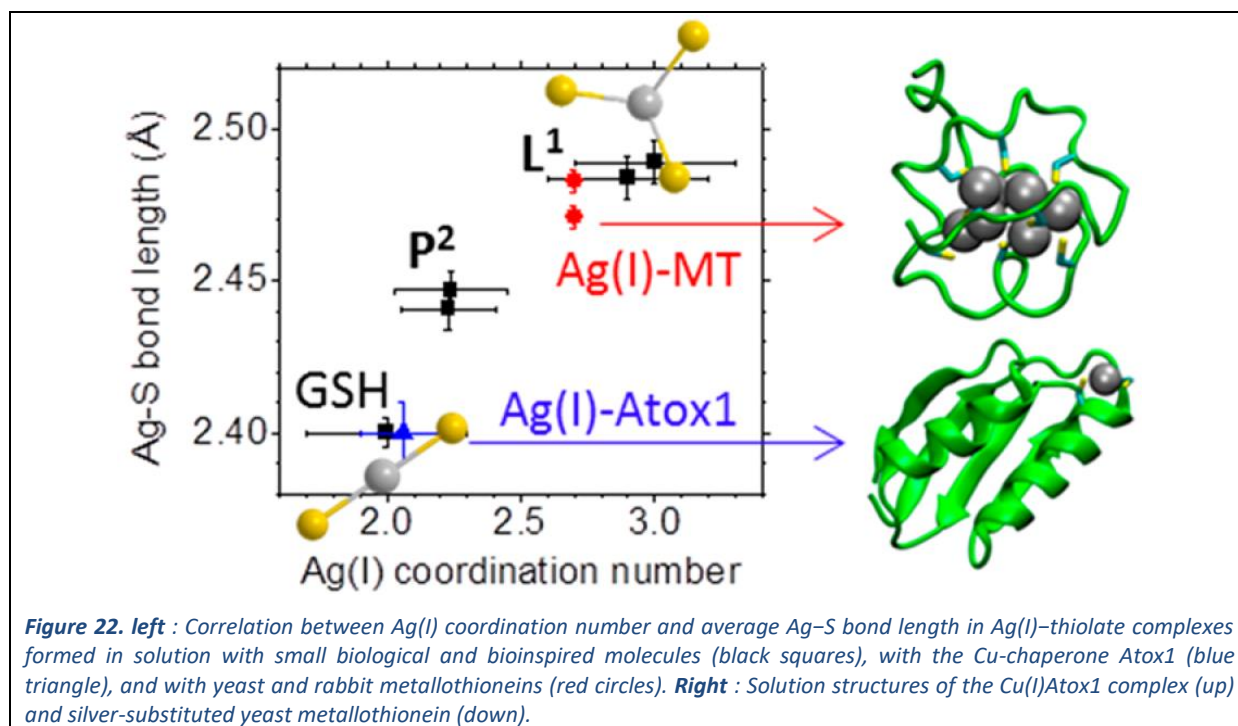


ROYAL SOCIETY OF CHEMISTRY Celebrating 175th 2019
COMMUNICATION
S. Bohic et al.
Sub-pptm-level high-energy resolution fluorescence detected K-edge absorption spectroscopy of selenium in articular cartilage

⁴⁴ S. J. Fairweather-Tait, Y. Bao, M. R. Broadley, R. Collings, D. Ford, et al., *Antioxid. Redox Signal.* **2011**, *14*, 1337-1383

Investigation of silver(I) coordination in copper(I) biological binding sites

Silver(I) is an unphysiological ion that, as the physiological copper(I) ion, shows high binding affinity for thiolate ligands; its toxicity has been proposed to be due to its capability to replace Cu(I) in the thiolate binding sites of proteins involved in copper homeostasis. Nevertheless, the nature of the Ag(I)–thiolate complexes formed within cells is poorly understood, and the details of Ag(I) coordination in such complexes in physiologically relevant conditions are mostly unknown. By making use of X-ray absorption spectroscopy, we characterized the Ag(I) binding sites in proteins related to copper homeostasis, such as the chaperone Atox1 and metallothioneins (MTs), as well as in bioinspired thiolate Cu(I) chelators mimicking these proteins, in solution and at physiological pH. Different Ag(I) coordination environments were revealed: the Ag–S bond length (Figure 22) was found to correlate to the Ag(I) coordination number, with characteristic values of 2.40 and 2.49 Å in AgS₂ and AgS₃ sites, respectively, comparable to the values reported for crystalline Ag(I)–thiolate compounds. The bioinspired Cu(I) chelator L1 is proven to promote the unusual trigonal AgS₃ coordination and, therefore, can serve as a reference compound for this environment. In the Cu(I)-chaperone Atox1, Ag(I) binds in digonal coordination to the two Cys residues of the Cu(I) binding loop, with the AgS₂ characteristic bond length of 2.40 ± 0.01 Å. In the multinuclear Ag(I) clusters of rabbit and yeast metallothionein, the average Ag–S bond lengths are 2.48 ± 0.01 Å and 2.47 ± 0.01 Å, respectively, both indicative of the predominance of trigonal AgS₃ sites. This work lends insight into the coordination chemistry of silver in its most probable intracellular targets and might help in elucidating the mechanistic aspects of Ag(I) toxicity.



Authors and principal publication:

G. Veronesi,^a T. Gallon,^{a,c} A. Deniaud,^a B. Boff,^c C. Gateau,^c C. Lebrun,^c C. Vidaud,^d F. Rollin-Genetet,^d M. Carrière,^c I. Kieffer,^e E. Mintz,^a P. Delangle,^c I. Michaud-Soret,^a XAS investigation of silver(I) coordination in copper(I) biological binding sites, *Inorganic Chemistry* **54** (2015)11688–11696

^a LCBM, UMR 5249 CNRS - CEA - UGA, Grenoble | ^b ESRF, Grenoble | ^c INAC-SCIB, University Grenoble Alpes & CEA, Grenoble | ^d CEA/DSV/iBEB/SBTN, Bagnols sur Cèze | ^e OSUG, UMS 832 CNRS - UGA, Grenoble, France

How prions are generated by a copper switch

The conversion of the prion protein into a misfolded isoform in the brain causes prion diseases, a group of transmissible neurodegenerative disorders affecting humans and animals. The structural events underlying this conversion have escaped detailed characterisation due to the insoluble nature of prions. By using XAS at beamline BM30B, a team of Italian scientists have identified a novel copper-mediated mechanism that acts as a switch that turns the normal protein into its pathological alter ego.

Prions are misfolded proteins that cause a group of incurable neurodegenerative diseases, including spongiform encephalopathies, such as mad cow diseases and Creutzfeldt-Jakob disease in human. Prions are unique infective agents —unlike viruses, bacteria, fungi and other parasites, prions do not contain either DNA or RNA. They can propagate their pathological effects like “wildfire” by infecting the normal proteins (termed PrPC) causing them to acquire the wrong conformation and convert into further disease-causing agents called prions or PrPSc. Despite the importance for pathogenesis, the mechanism of prion formation has escaped detailed characterisation due to the insoluble nature of prions. PrPC interacts with copper through octarepeat and non-octarepeat binding sites. Copper coordination to the non-octarepeat (non-OR) region has garnered interest due to the possibility that this interaction may impact prion conversion.

We have identified a new mechanism underlying the pathological transformation of prion proteins: it all depends on a metal, copper, and its bond with the protein. We used EXAFS spectroscopy, cell-biology and molecular dynamic simulations to investigate how copper coordination in the fifth copper binding site may influence prion conversion.

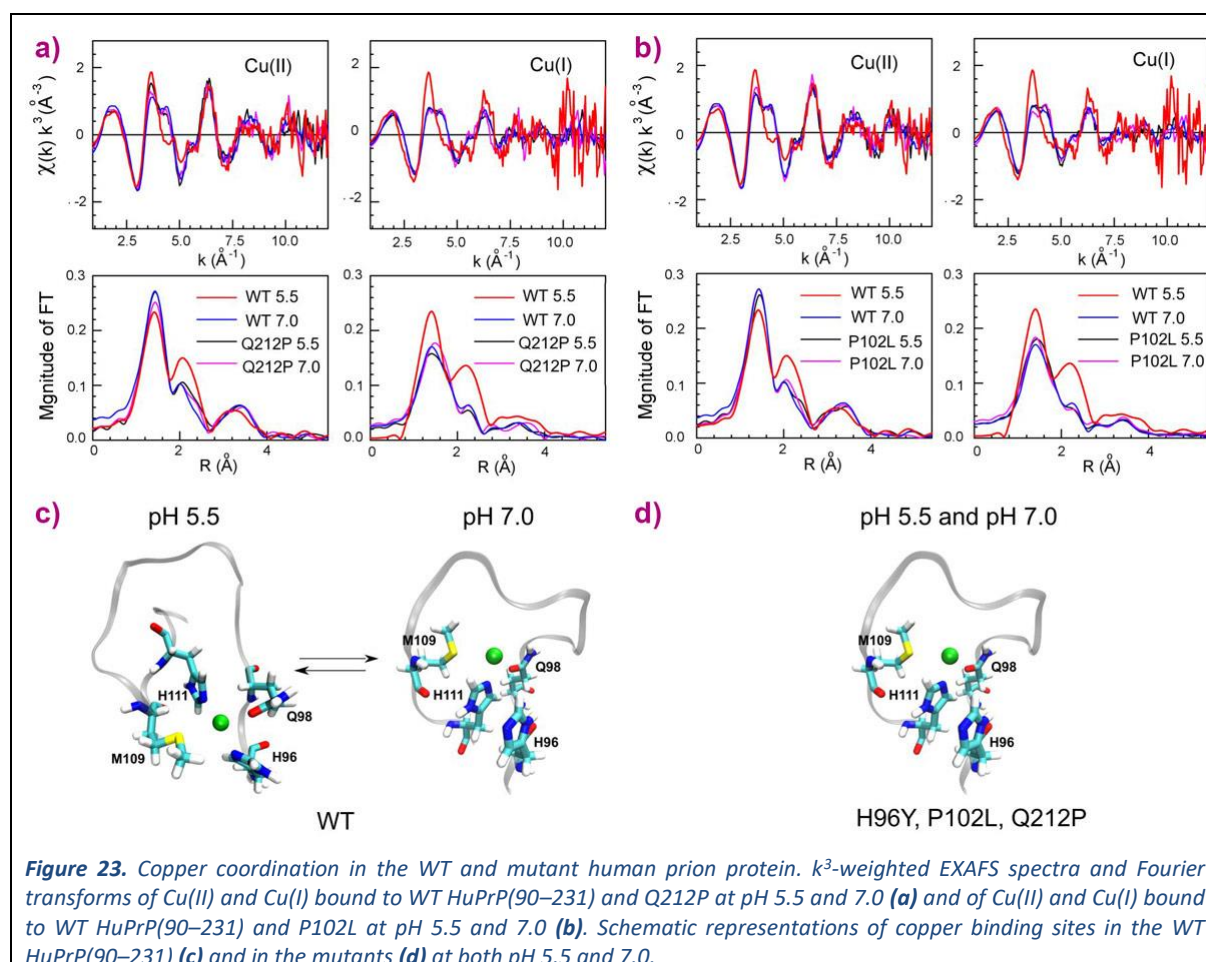
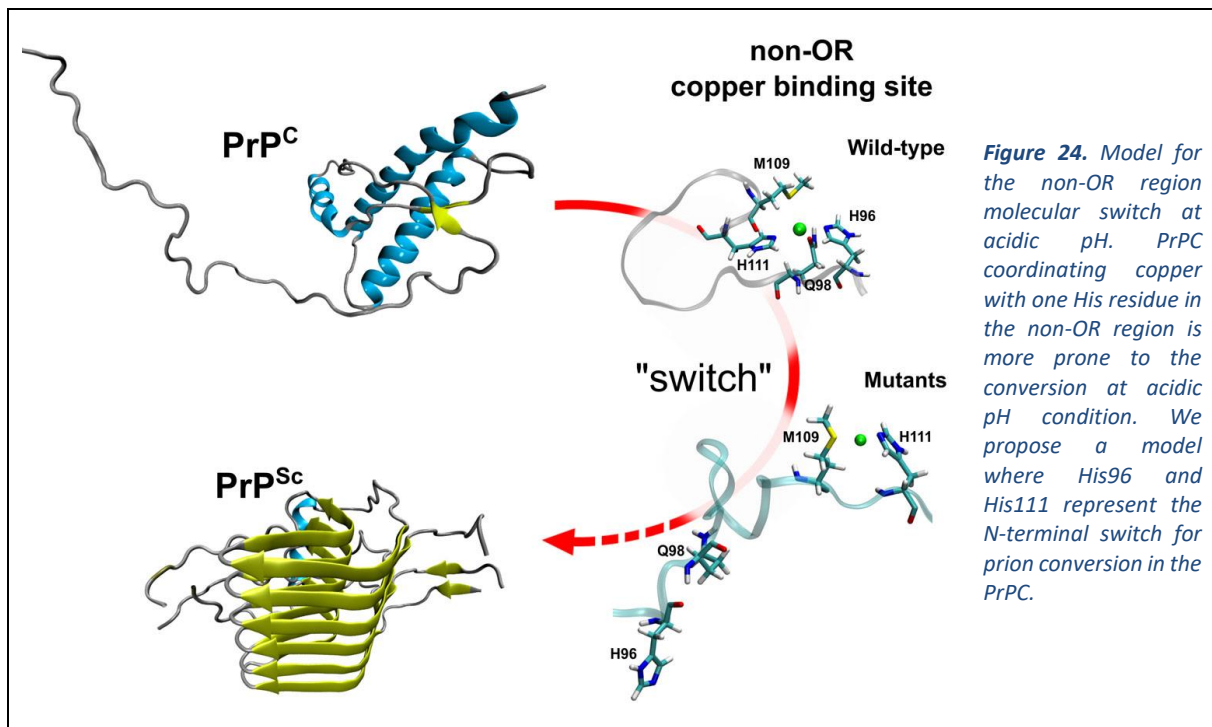


Figure 23. Copper coordination in the WT and mutant human prion protein. k^3 -weighted EXAFS spectra and Fourier transforms of Cu(II) and Cu(I) bound to WT HuPrP(90–231) and Q212P at pH 5.5 and 7.0 (a) and of Cu(II) and Cu(I) bound to WT HuPrP(90–231) and P102L at pH 5.5 and 7.0 (b). Schematic representations of copper binding sites in the WT HuPrP(90–231) (c) and in the mutants (d) at both pH 5.5 and 7.0.

Using X-ray absorption spectra collected at beamline FAME, we determined the copper coordination in the wild type (WT) human prion protein (HuPrP) and in different pathological mutants at both pH 7.0 and pH 5.5. We found that mutations (H96Y, P102L and Q212P) and pH changes cause a dramatic modification on both Cu(II) and Cu(I) coordination in the non-OR region. In the WT HuPrP Cu(II) and Cu(I) are anchored to His96 and His111 only at pH 5.5, while at pH 7.0 copper at both oxidative states is coordinated by His111. Conversely, in the mutants copper is bound only to H111 independently of the pH (Figure 23).

The observed structural differences in the copper coordination among WT and pathological mutants at pH 5.5 may have relevant physiological effects since this alteration in the copper binding site might trigger PrPC to PrPSc conversion. To understand the physiological implications of EXAFS data, we performed in vitro and cell-based assays. Intriguingly, the removal of one single copper ligand (H96) promoted prion conversion and generation of infectious prion material in neuronal cells.

These findings suggest a pivotal role for non-OR region as a critical molecular switch for prion conversion. We therefore argue that copper bound to the non-OR region may stabilise this segment when coordinated by His96 and His111, preventing misfolding events through transient short and long range interaction contacts between the 90–127 residues and the C-terminal structured domain. This study highlights the importance of the non-OR region for prion conversion and suggests a model in which PrPC coordinating copper with one His may be more prone to the conversion in acidic conditions (Figure 24).



Authors and principal publication:

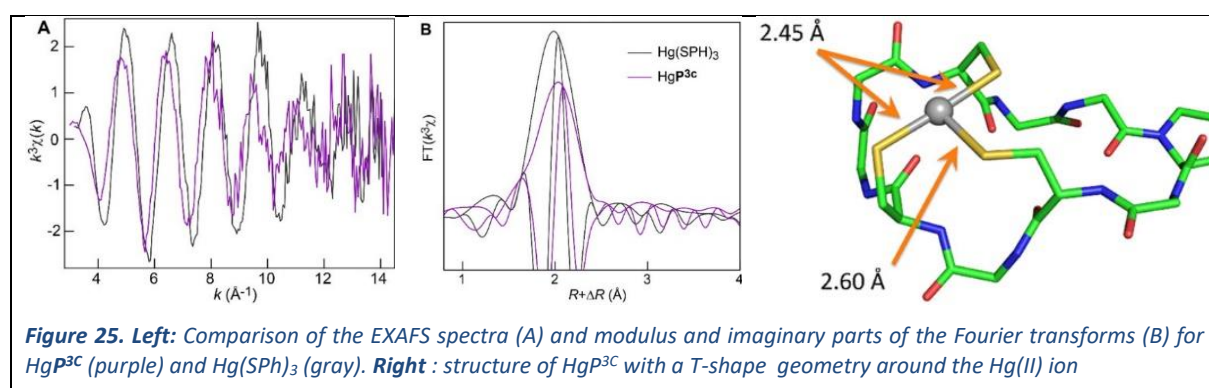
G. Giachin^{a,b}, P.T. Mai^b, T.H. Tran^b, G. Salzano^b, F. Benetti^b, V. Migliorati^c, A. Arcovito^d, S.D. Longa^e, G. Mancini^{f,g}, P. D'Angelo^c, G. Legname^{b,h}, *Sci Rep.* **5**, 15253 (2015);

^a ESRF | ^b Department of Neuroscience, Scuola Internazionale Superiore di Studi Avanzati (SISSA), Trieste (Italy) | ^c Department of Chemistry, Sapienza Univ. of Rome (Italy) | ^d Istituto di Biochimica e Biochimica Clinica, Univ. Cattolica del Sacro Cuore, Rome (Italy) | ^e Department of Medicine, Public Health, Life and Environmental Science, Univ. of L'Aquila, Coppito Aquila (Italy) | ^f Scuola Normale Superiore, Pisa (Italy) | ^g Istituto Nazionale di Fisica Nucleare (INFN) sezione di Pisa (Italy) | ^h ELETTRA - Sincrotrone Trieste S.C.p.A (Italy)

Mercury trithiolate binding (HgS_3) to a de novo designed cyclic decapeptide with three preoriented cysteine side chains

Mercury(II) is an unphysiological soft ion with high binding affinity for thiolate ligands. Its toxicity lies in the interactions with low molecular weight thiols including glutathione and cysteine-containing proteins that disrupt the thiol balance and alter vital functions. However, mercury can also be detoxified via interactions with Hg^{II} -responsive regulatory proteins such as MerR, which coordinates Hg^{II} with three cysteine residues in a trigonal planar fashion (HgS_3 coordination). The model peptide $\text{P}^{3\text{C}}$ was designed to promote the orientation of three cysteine side chains for metal chelation in MS_3 coordination environments, taking as a starting point the $\text{P}^{2\text{C}}$ peptide developed as a model of d^{10} metal transporters. The cyclic peptide $\text{P}^{3\text{C}}$ having an open and solvent-accessible structure would be considered as a predisposed peptide for metal coordination in MS_3 arrangements, meaning that the placement of ligands allows an appropriate layer to complex a metal

$\text{P}^{3\text{C}}$ is forming a mononuclear Hg^{II} complex with absorption properties characterizing the HgS_3 coordination. This coordination is of particular interest for Hg^{II} , since the coordination site of Hg^{II} in MerR, a bacterial metalloregulatory protein, has been demonstrated to involve three cysteine in a trigonal mode, which is thought to be responsible for the high sensitivity and selectivity of this sensor for Hg^{II} . Hg L_{III}-edge EXAFS confirms that the three sulfur atoms are mostly in a T-shape environment around Hg^{II} with two short distances at 2.45 Å and one longer distance at 2.60 Å (Figure 25). This dissymmetry is in accordance with the rectangular shape of the cyclodecapeptide scaffold that makes the cysteine moieties nonequivalent for Hg^{II} coordination. The Hg–S distances obtained from EXAFS were implemented in the refinement of the solution NMR structure of $\text{HgP}^{3\text{C}}$, derived on ^1H – ^1H distances measured on the ROESY spectrum of the complex. The peptide adopts an elongated structure with all three cysteines oriented on the same side of the cycle. The structure of $\text{HgP}^{3\text{C}}$ is very similar to that of $\text{HgP}^{2\text{C}}$, its two-cysteine analogue. One major asset of preorganized or highly predisposed peptides such as de novo designed three-stranded coiled coils is that they form unique mononuclear Hg^{II} complexes in a protected hydrophobic pocket, that do not evolve into polymetallic species in excess of metal. By contrast, the cyclic peptide $\text{P}^{3\text{C}}$ described here has a significantly more open structure with a lower degree of predisposition that makes possible the evolution of the $\text{HgP}^{3\text{C}}$ complex into 2-coordinated mercury polymetallic species such as $\text{Hg}_3(\text{P}^{3\text{C}})_2$.



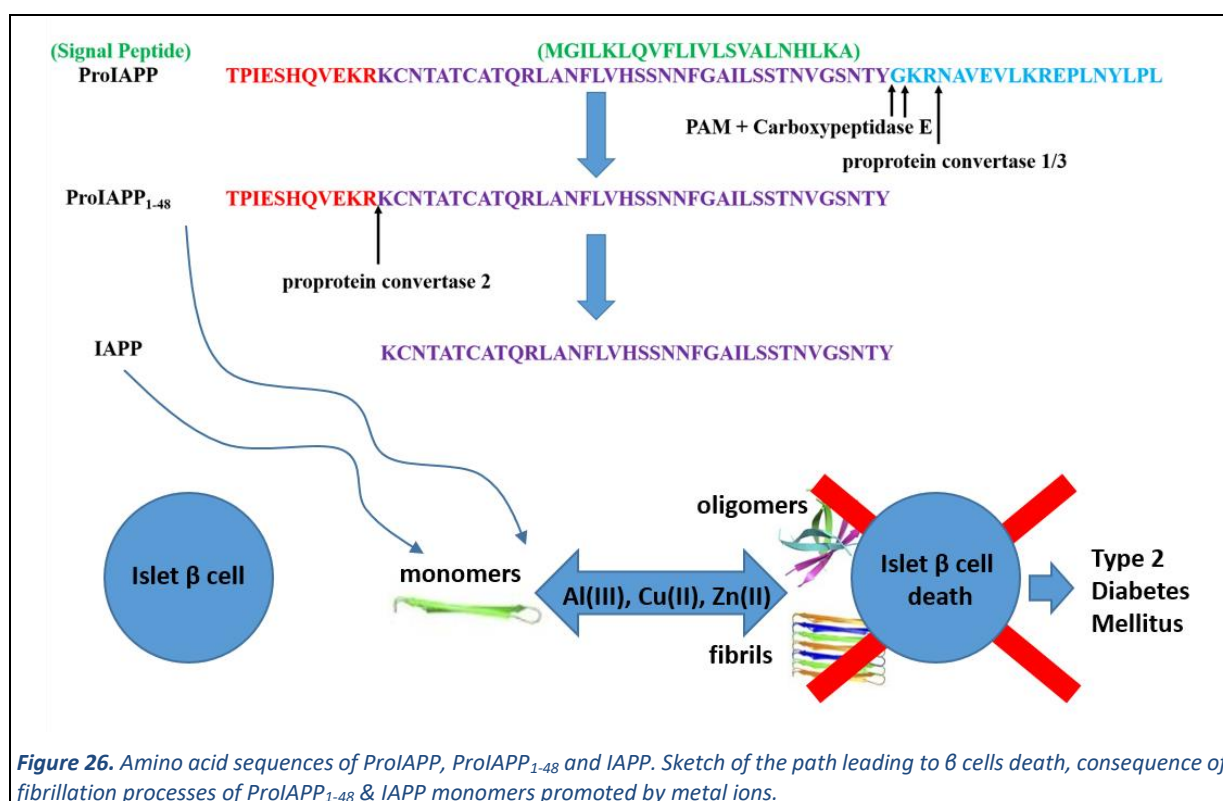
Authors and principal publication:

Sénèque O.^{1,3}, Rousselot-Pailley P.¹, Pujol A.¹, Boturyn D.², Crouzy S.³, Proux O.⁴, Manceau A.⁵, Lebrun C.¹, Delangle P.¹, *Inorganic Chemistry* **57** (2018) 2705–2713

¹ INAC-SyMMES, CEA, CNRS, Univ. Grenoble Alpes | ² DCM UMR 5250, CNRS, Univ. Grenoble Alpes | ³ LCBM UMR 5249, CNRS - CEA, Univ. Grenoble Alpes | ⁴ BM30B, Grenoble | ⁵ ISTERre, CNRS - Univ. Grenoble Alpes

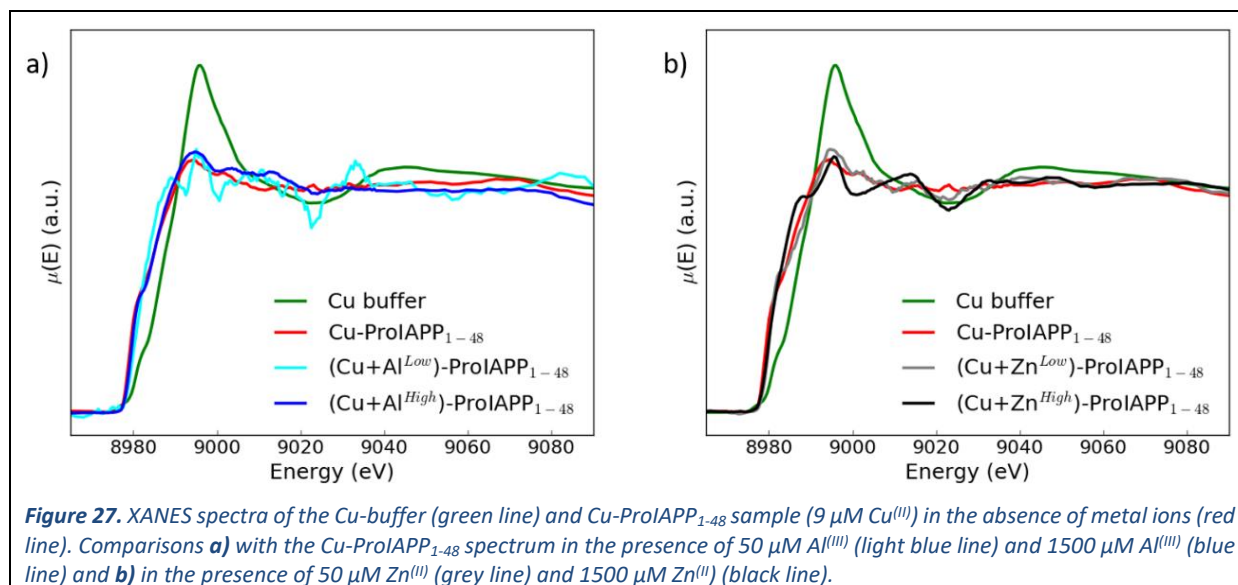
XAS measurements of Cu-ProIAPP complexes at physiological micromolar concentrations

The amyloidogenic islet amyloid polypeptide (IAPP) and the associated pro-peptide ProIAPP₁₋₄₈ are involved in cell death in type 2 diabetes mellitus. It has been observed that interactions of this peptide with metal ions have an impact on the cytotoxicity of the peptides as well as on their deposition in the form of amyloid fibrils. It remains equivocal as to whether Al^(III), Fe^(III) and Zn^(II) promote amyloid (β sheet) formation while it is clear that Cu^(II) prevents IAPP from assembling into β -sheet structures Cu^(II) seems to inhibit amyloid fibril formation, thus suggesting that Cu homeostasis imbalance may be involved in the pathogenesis of type 2 diabetes mellitus. ProIAPP₁₋₄₈ forms amyloid less readily than IAPP and while there are few data on its interactions with metals it is also the case that Cu^(II) prevents ProIAPP₁₋₄₈ from forming β -sheets structures more prone to amyloidogenesis. A sketch of the process leading to the formation of ProIAPP₁₋₄₈ and IAPP and of their effect on islet β cells is depicted in *Figure 26*.



Our data (*Figure 27*) show that XAS measurements at micromolar concentrations are feasible and confirm that ProIAPP₁₋₄₈-Cu^(II) binding at near-physiological conditions (9 μ M) can be detected. We are well aware that the quality of the collected spectra does not allow any speculation about the structural differences of the possible different Cu^(II) coordination modes induced by the presence of Al^(III) or Zn^(II). Nevertheless, we think that the results we obtained are relevant in two respects.

Though yet at a qualitative level, the existence of differences in the XANES spectral features induced by the presence of the Zn^(II) or Al^(III) in the Cu^(II)-ProIAPP₁₋₄₈ binding mode sample is clearly established. These differences appear to be dependent from the added ion concentration.



Experiments of the kind we have been able to perform at the FAME-UHD beamline demonstrate the general feasibility of XAS measurements on samples where the absorbing atom is present at micromolar concentration. This last fact is of special methodological relevance as it shows that it is possible to perform XAS measurements on very diluted metal-peptide complexes in physiological conditions, when raising metal ions concentration to improve the signal-to-noise ratio is not possible, as this would dramatically alter their physiological coordination mode.

Authors and principal publication:

E. De Santis^{1,2}, E. Shardlow³, F. Stellato², O. Proux⁴, G. Rossi^{1,2,5}, C. Exley³, S. Morante^{1,2}, *Condens. Matter* **4** (2019) 13

¹ Dipartimento di Fisica, Università di Roma "Tor Vergata" / ² INFN, Sezione di Roma 2 / ³ The Birchall Centre, Lennard-Jones Laboratories, Keele University / ⁴ OSUG (UMS 832 CNRS / Univ. Grenoble Alpes) / ⁵ Centro Fermi – Museo Storico della Fisica e Centro Studi e Ricerche "Enrico Fermi", Roma

Catalysis & material energy

Catalysis and mostly heterogeneous catalysis is always an active topic in Synchrotron Radiation facilities. Many types of *in situ* cells are now available on FAME and FAME-UHD beamlines for characterizations under either activation or reaction conditions. Both beamlines offers the possibility to detect in fluorescence mode or HERFD active phases under *in situ* or operando conditions. This is of great interest for the characterization of low loadings (below 1wt% of noble metals for instance) which corresponds to those employed in environmental catalysis, petrochemistry or as promoters of other catalytic systems.

Thus, **IFPEN** research topics related to XAS on BM16-FAME-UHD during the period 2015-2020 concerned mainly catalysis and the activation of supported nanoclusters of Pt under H₂ for naphta reforming applications. From a methodological point of view, the analysis by EXAFS was a key step as it allowed to assess the general characteristics of the catalyst at the macroscopic scale and to validate the chemical descriptors determined from complementary localized observations techniques and DFT simulations. The unique configuration of the FAME-UHD beamline with the development of the operando reactor made available to the scientists has proved to be a real asset in achieving these objectives.

KIT and IRCELYON have been involved in the characterization of Pt/CeO₂ catalysts for CO and alkanes oxidation under soft conditions. KIT investigated the dynamic properties of Pt/CeO₂ during reducing/oxidizing cycles is a way to improve significantly the oxidation properties at low temperature. XAS permits to characterize the oxidation and reduced states of these catalysts during activation cycles and catalysis, as well as the impact of the presence of Pt nanoparticles (<2 nm) on the reducibility of CeO₂. Thus, The HERFD-XANES spectra of the Pt-SS catalyst in the reaction mixture (1,000 ppm CO, 10% O₂ in He) recorded in the temperature range 50–400 °C showed pronounced changes in the white line position and intensity (Figure 28). Multivariate analysis reveals four different Pt states (isolated Pt⁴⁺, Pt²⁺ and Pt^{δ+} with adsorbed CO and Pt_x^{δ+} clusters and the dynamic of transformation during reaction.

Christelle Legens, IFP Energies Nouvelles, Lyon

Christophe Geantet, Institut de Recherches sur la Catalyse et l'Environnement de Lyon

Jan-Dierk Grunwaldt, Karlsruhe Institute of Technology

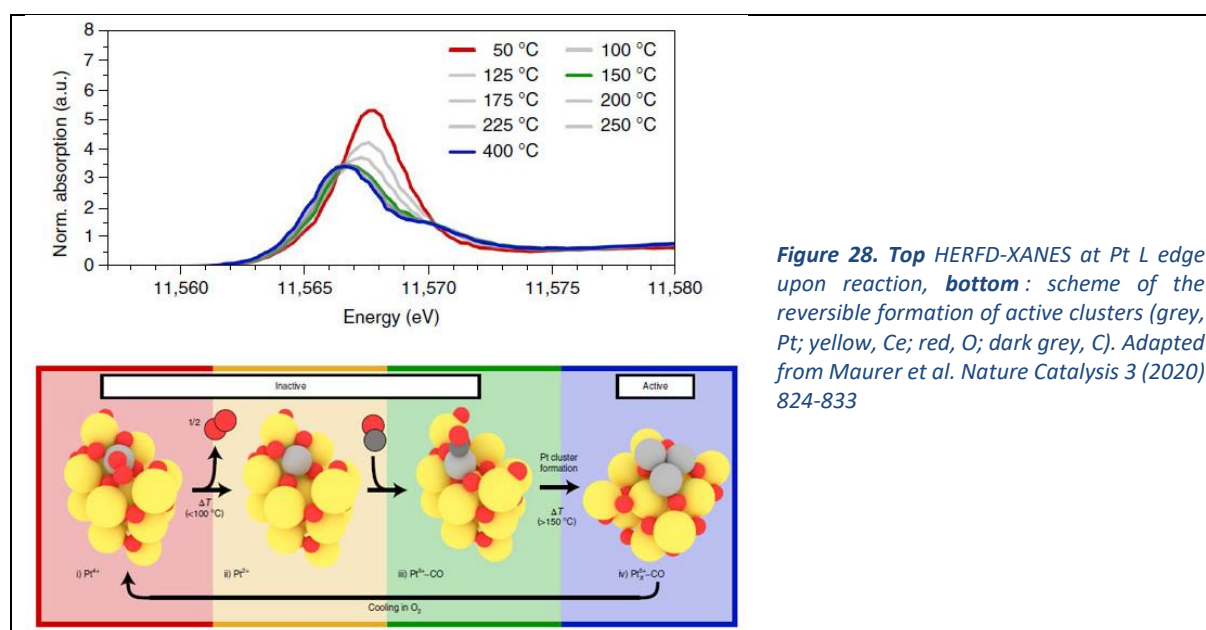


Figure 28. Top HERFD-XANES at Pt L edge upon reaction, **bottom**: scheme of the reversible formation of active clusters (grey, Pt; yellow, Ce; red, O; dark grey, C). Adapted from Maurer et al. *Nature Catalysis* 3 (2020) 824-833

Platinum nanoparticles living on the edge

A unique combination of high resolution electron microscopy, electron tomography, *in situ* X-ray absorption spectroscopy and density functional theory (DFT) calculations applied to the study of Pt/ γ -Al₂O₃ catalysts provides new insight into the formation and the evolution of Pt nanoparticles in terms of size, location and interaction with the support. The association of these tools for the study of a catalytic system by considering a global conceptualization of the main findings is unprecedented. Applied in a quantitative way, this multi-scale methodology highlights the preferential localization of Pt NPs on the edges of alumina crystallites which seem to be thermodynamically as favourable as the crystallite surfaces.

Platinum supported on chlorinated γ -Al₂O₃ is a typical catalyst used in the naphtha reforming process. This bifunctional catalyst contains simultaneously metallic (Pt) and acidic sites (Brønsted hydroxyls boosted by chlorine). It is generally accepted that the mean distance between the two types of sites is one of the main parameters controlling the selectivity of the catalyst and which consequently requires a fine analysis and subsequent optimization. In this context, our work was principally focused on the quantitative assessment of the localization of Pt on the support by using advanced electron microscopy techniques, EXAFS spectroscopy at the Pt L₃ edge and theoretical calculations and modelling.

The studied systems contain small amounts of Pt (between 0.3 and 1 wt %) and were studied as-prepared (in an oxidized state) and after activation under H₂ (in the metallic phase) according to a well-defined IFPEN protocol. The electron microscopy analysis in the high resolution and 3D modes were performed at IPCMS, the XAS spectra were acquired at the FAME-UHD beamline and the quantum simulations at DFT level were undertaken at IFPEN. For the XAS analysis of the reduced catalysts, a dedicated *operando* reactor⁴⁵ was used on the ESRF beamline allowing *in situ* re-reduction prior to the acquisition procedure.

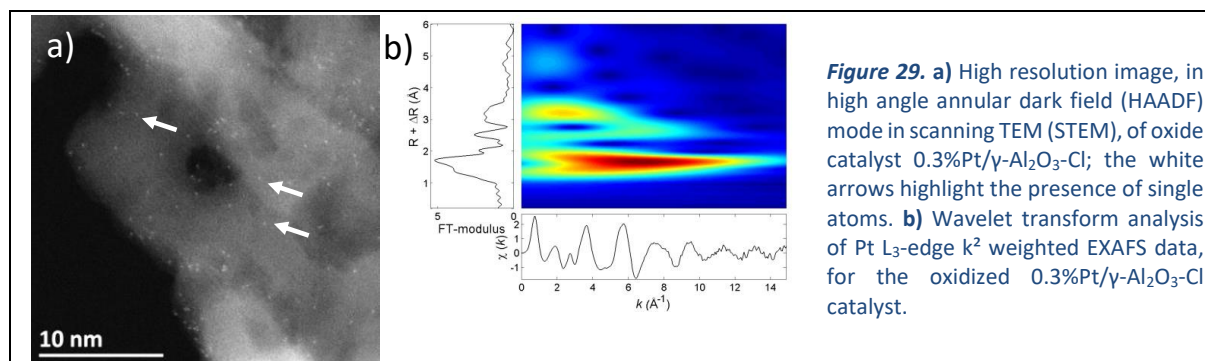


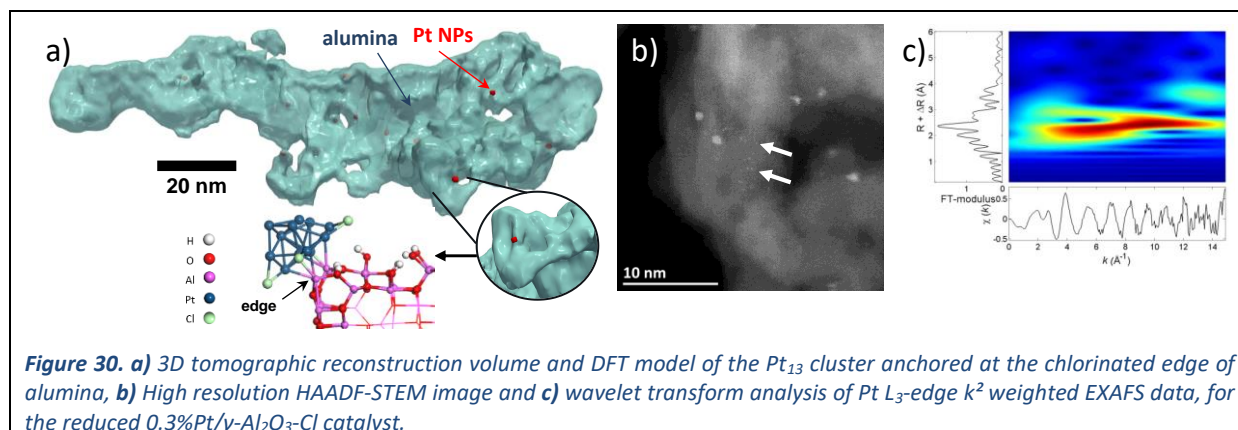
Figure 29. a) High resolution image, in high angle annular dark field (HAADF) mode in scanning TEM (STEM), of oxide catalyst 0.3%Pt/ γ -Al₂O₃-Cl; the white arrows highlight the presence of single atoms. b) Wavelet transform analysis of Pt L₃-edge k² weighted EXAFS data, for the oxidized 0.3%Pt/ γ -Al₂O₃-Cl catalyst.

In the case of the oxidized samples (Figure 29), the Pt-based phase was found to be mostly in single atom oxide complex, the formation of clusters being noticeable only at high Pt loading. The analysis of the EXAFS data confirms the very localized electron microscopy findings for all the analysed specimens: excepting the oxygen and chlorine neighbour atoms, no significant contribution of Pt neighbours can be deduced.

In contrast, for the reduced samples (Figure 30) the Pt phase forms well-defined nanoparticles with an average size of about 0.9 nm. It is worth noting that the increase of the Pt loading induces a proportional rise of the number of nanoparticles and not of their general size. These electron microscopy findings were confirmed by the quantitative XAS analysis in which an average Pt-Pt coordination number of 3 was obtained for both low and high loadings. Another feature is the occurrence of a single-atom population which can be directly visualized on the

⁴⁵ A. Aguilar-Tapia *et al*, Rev. Sci. Instrum. **89**, 35109_1-35109_8 (2018)

high resolution images, the strong anchoring of such Pt species to the support being one of the factors responsible of the low k-signal in the XAS spectra.



3D analyses by electron tomography in the high angle annular dark field mode were performed on the reduced catalysts and showed that at least 70% of nanoparticles are located on the edges of the support crystallites or on edge-like features. Interestingly, our previous work established the first DFT model of alumina edge⁴⁶, which combined with NMR, showed that hydroxyls located at edges are preferentially exchanged with chlorine. A synergistic effect based on the stabilization of the Pt phase at these sites, due to the presence of chlorine, may explain the preferential location of the particles as illustrated by the DFT model of the Pt₁₃ cluster on the chlorinated edge (insets of Figure 30a). This DFT model is also compatible with EXAFS. From a quantitative point of view, the average distances between Pt nanoparticles in the analysed specimens were also properly quantified by using a customized geometrical analysis⁴⁷ of the 3D reconstructions; a direct comparison of the as-obtained values (9 and 16 nm for the lowest and highest loadings, respectively) shows that the interparticular distance can be finely tuned by varying the Pt metal loading.

This in-depth multi-selective study realized on industrially relevant catalysts consisting of Pt-based phase supported on chlorinated γ-alumina showed for the first time that the Pt particles are located mostly on the edges of the crystallites and are uniformly distributed through the support aggregate. The role of chlorine to stabilize the Pt close to the edges as suggested by DFT models can be at the origin of the catalytic performance observed for these catalytic systems. From a methodological point of view, the analysis by EXAFS was a key step as it allows to assess the general characteristics of the catalyst at the macroscopic scale and to validate the chemical descriptors determined from the very localized TEM observations and DFT simulations. The unique set-up of the FAME-UHD beamline with the *operando* reactor could be used in future works in order to investigate, for instance, the genesis of the Pt NPs during the activation step under H₂.

Authors and principal publication:

A.T.F. Batista^a, W. Baazib^b, A.-L. Taleb^a, J. Chaniot^{a,c}, M. Moreaud^{a,d}, C. Legens^a, A. Aguilar-Tapia^e, O. Proux^f, J.-L. Hazemann^e, F. Diehl^g, C. Chizallet^a, A.-S. Gay^a, O. Ersen^b, P. Raybaud^a, *ACS Catalysis* **10**, 4193–4204 (2020)

^(a) IFP Energies nouvelles, Solaize (France) | ^(b) Inst. de Physique et Chimie des Matériaux de Strasbourg, CNRS – Univ. de Strasbourg (Fr.) | ^(c) Lab. H. Curien, CNRS - Univ. J. Monnet de Saint-Etienne (Fr.) | ^(d) Centre for Mathematical Morphology, MINES ParisTech, Fontainebleau (Fr.) | ^(e) Inst. Néel, CNRS – Univ. Grenoble Alpes (Fr.) | ^(f) OSUG, CNRS – Univ. Grenoble Alpes (Fr.)

⁴⁶ A. T. F. Batista *et al*, *J. Catal.* **378**, 140-143 (2019)

⁴⁷ J. Chaniot *et al*, *Image Anal. Stereol.* **38**, 25–41 (2019)

Tracking the evolution of Pt single site on CeO₂ by HERFD-XANES

Platinum single sites show excellent atom economy, but their role in the oxidation of pollutants (e.g. CO, CH₄) is strongly discussed. Using advanced *operando* infrared/hard X-ray techniques, we were able to localize these sites, show that they are very dynamic and form small clusters/particles that are more active.

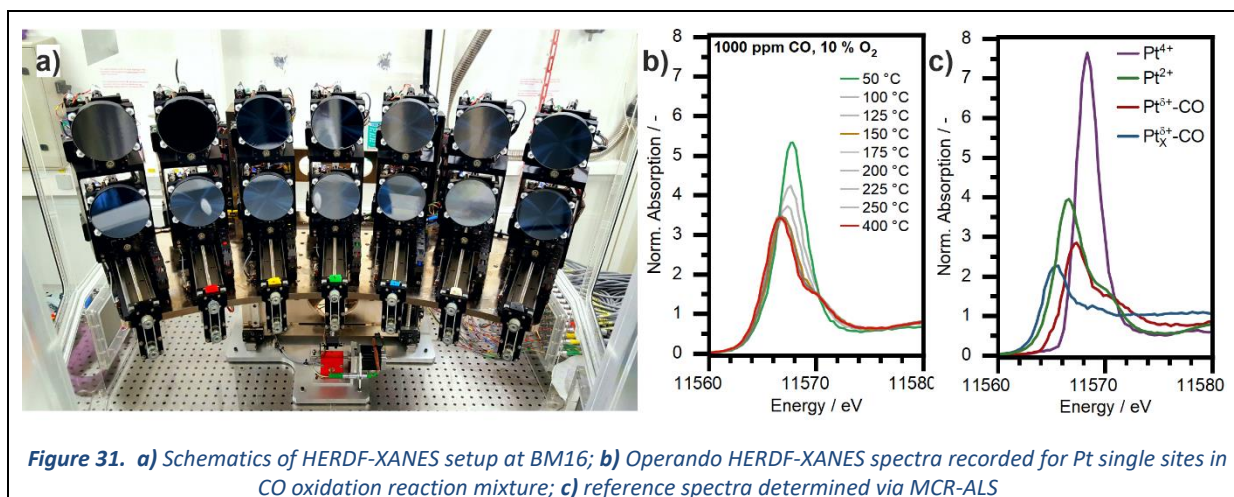
In heterogeneous catalysis, for example in emission control, the interaction of the support with the active noble metal can have a huge impact on the catalytic activity. In the case of platinum dispersed on ceria, the strong synergy between the two components can lead to the fine distribution – possibly down to atomically dispersed species – of Pt on the surface of the oxide under strongly oxidizing conditions. These single atom catalysts are of high interest since each individual noble metal atom is accessible and thus potentially an active site. This high atom efficiency would lead optimal noble metal usage. However, their real performance and the structure of these sites during the catalytic reaction (in particular stability, electronic state and fate) is still unclear.

In order to find the way in this intricate maze, a systematic and elaborate *operando* multitechnique approach is decisive. In our study, the nature of atomically dispersed platinum supported on ceria, the dynamic changes occurring during oxidation reactions and the impact on the activity of such catalytic systems was investigated via complementary *operando* X-ray absorption spectroscopy (XAS), X-ray photoelectron spectroscopy (XPS) and *in situ* infrared (IR) spectroscopy combined with DFT calculations.

In particular, due to the complexity of the diluted system and to better appreciate subtle changes as a result of the dynamic behaviour of the Pt species under catalytic conditions, high-energy-resolution fluorescence detected X-ray absorption near edge structure (HERFD-XANES) spectroscopy experiments at the Pt L_{III} edge were performed at the BM16/FAME-UHD beamline at the European Synchrotron Radiation Facility. HERFD-XANES allows for a unique increase in the resolution of Pt L_{III} edge spectra⁴⁸. Together with an appropriate the photon flux (maximum brilliance without beam-inducing effects on samples), this constellation offered optimal conditions for the investigation of the sensitive system. Thanks to these aspects, we could follow the changes on the white line induced by the presence of adsorbates, ranging from clear increase in intensities to fainter shifts in position, these latter not appreciable by conventional XANES.

Whereas high CO conversion was reached already below 100°C for nanoparticles, in the case of single sites there is no appreciable CO conversion below 200°C, despite a 100 % dispersion of Pt atoms on the CeO₂ surface. The HERFD-XANES spectra recorded at BM16 in the reaction mixture (1000 ppm CO, 10% O₂ in He, temperature range 50–400 °C) showed pronounced changes in both the white line position and intensity (Figure 31). Up to 150°C the peak intensity experiences a steep decrease (an effect not noticeable in conventional XAS), while at higher temperature, as the activity sets in, the white line undergoes a shift towards lower energies. The intermediate structural states in the spectroscopic data were interpreted and quantified using the references obtained by a multivariate curve resolution alternating least squares (MCR-ALS) algorithm. Four reference states were identified and confirmed also on the basis of complementary XPS, *in situ* UVH-FTIR studies and FDMNES calculations: Pt⁴⁺, Pt²⁺, reduced Pt^{δ+} interacting with CO and a cluster-like species, Pt_x^{δ+}-CO.

⁴⁸ O. Proux, E. Lahera, W. Del Net, I. Kieffer, M. Rovezzi, D. Testemale, et al., *J. Environ. Qual.* **2017**, 46, 1146.



Thanks to these findings, substantiated also by DFT calculation, it was possible to describe in detail the relationship between the variations in the structure of Pt single sites on ceria and the corresponding effect on catalytic activity. During its formation at elevated temperature, single Pt²⁺ species bind to square-planar hollow sites in, e.g., {110} facets of ceria. Particularly we found a noble-metal induced restructuring of the ceria surface usually known for adsorbates. These Pt²⁺-CeO₂ structures are very stable and explain the poor performance of Pt single sites in CO, C₃H₆ or CH₄ oxidation. Only when the cluster-like Pt_x^{δ+}-CO species becomes predominant in the HERFD-XANES spectra the catalytic activity becomes relevant. These species, most likely containing only a few Pt atoms, are formed only at high temperatures (> 200 °C) in lean conditions, and are thus essential for CO oxidation (Figure 32). The stabilization of these highly dispersed reduced clusters or improving the dynamics of single sites on less interacting facets could be promising approaches to efficiently use the noble metal and maintain a high activity, a research endeavour presently studied by a whole team of researchers at KIT, Germany.

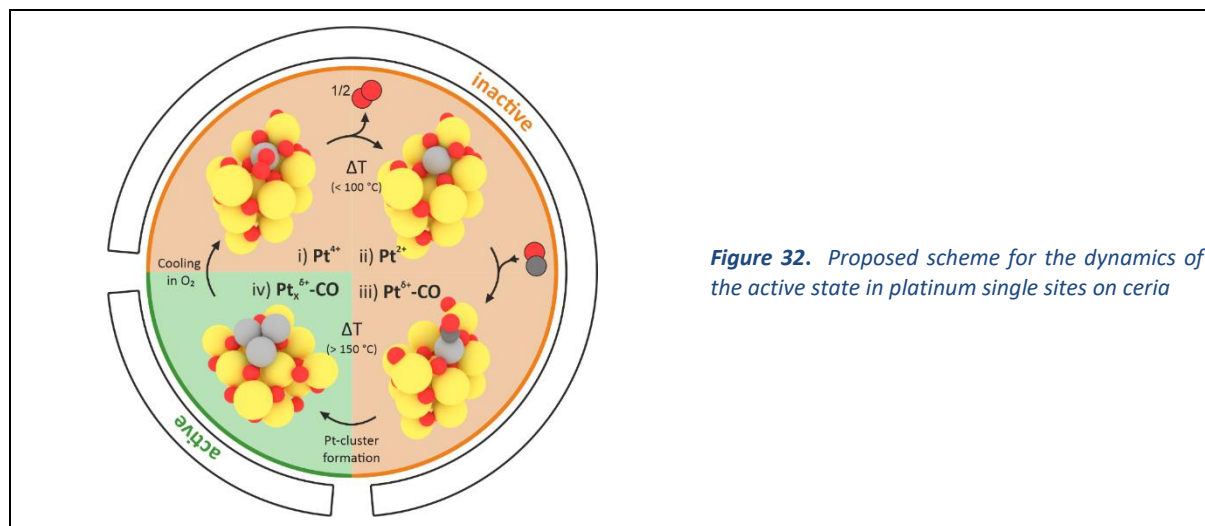


Figure 32. Proposed scheme for the dynamics of the active state in platinum single sites on ceria

Authors and principal publication:

F. Maurer^(a), J. Jelic^(b), J. Wang^(c), A. Gänzler^(a), P. Dolcet^(a), C. Wöll^(b), Y. Wang^(b), F. Studt^(a,b), M. Casapu^(a) & J.-D. Grunwaldt^(a,b), *Nat. Catal.* **2020**, 3, 824.

^(a) Institute for Chemical Technology and Polymer Chemistry (ITCP), Karlsruhe Institute of Technology (KIT), Karlsruhe, Germany | ^(b) Institute of Catalysis Research and Technology (IKFT), Karlsruhe Institute of Technology (KIT), Eggenstein-Leopoldshafen, Germany | ^(c) Institute for Functional Interfaces (IFG), Karlsruhe Institute of Technology (KIT), Eggenstein-Leopoldshafen, Germany

In the field of SR and more especially XAS, heterogeneous catalysis is a highly demanding domain. As a player in the field of catalysis science, KAUST need advanced characterization tools to pinpoint the nature of the active sites during chemical reaction in order to design further new improved catalysts. Techniques based on the use of synchrotron radiation are an essential part of those investigations (XRD, PDF, XAS, XES, HERFD-XANES). The French installations of the European synchrotron, the proximity and the direct link with scientists specializing in experimental techniques allow KAUST scientists to carry out in-depth studies necessary for effective innovation. Since 2014, the KAUST catalysis center is conducting research in partnership with the Neel Institute through the design of two custom operando reactors able to reach a temperature of 1000 °C and a pressure of 100 bars. Thanks to those unique tools and the possibilities offered by the CRG beamlines in Grenoble, the structure of our catalysts are studied elegantly under relevant operating conditions.

The new upcoming fourth generation synchrotron source (EBS @ ESRF) will provide a beam with outstanding features that will open new scientific challenges. In addition to these *in-operando* characterizations, the KAUST catalysis center has interests in the development of the spectral ptychography technique on FAME beamline. X-ray coherent diffraction imaging will exploit the coherent properties of the new X-ray beam in order to obtain high-resolution structural and chemical images with the capability of resolving the absorption edge. This has tremendous application to enable the structural and textural characterization of real technical catalyst used in industrial processes.

*Samy Ould-Chikh, King Abdullah University of Science and Technology,
Catalysis Center, Saoud Arabia*

Operando XAS observation of Mo transforming to its active phase for converting methane to aromatics

Methane can be converted to benzene and naphthalene at temperatures above 600 °C. Molybdenum (Mo) supported on a zeolite is the most active catalyst to date but it is not well understood, how it is able to activate methane and why the performance of Mo is superior over other metals. The reaction is thermodynamically limited with benzene yields of 7.8 – 21.5 at.% between 650 and 800 °C. In addition, much improvement is still needed as the catalyst suffers from fast deactivation due to deposition of carbonaceous species. A better understanding of the reaction pathway and structural information on the active Mo phase aides the improvement of the catalytic system. However, a fast blackening of the catalyst due to the deposition of carbonaceous deposits, means that many spectroscopic techniques, like IR or UV Vis cannot be used to characterize the active site of this catalyst. A major reason why XAS spectroscopy has become a critically useful probe of the catalysts' structure is that it is element-specific, applicable to a broad range of elemental concentrations (from tens of ppm to wt.%), and can be used at reactive atmospheres and high temperature. Operando characterization of molybdenum species up to 800 °C still poses challenges for the design of an operando cell. The present study was performed in a plug-flow reactor developed by the Neel institute in collaboration with the King Abudullah University of Science and Technology (KAUST)^{49,50}. The setup allows to flow, or pulse methane to a catalyst bed heated to reaction temperature while analyzing the products on a mass-spectrometer (MS) and simultaneously

⁴⁹ B. AlSabban *et al.*, *Applied Catalysis B: Environmental*, **213**, 177-189 (2017).

⁵⁰ A. Aguilar-Tapia *et al.*, *Review of Scientific Instruments*, **89**, 035109 (2018)

Scientific Results

measuring XAS either in transmission or fluorescence detection mode (Figure 33). Mo is usually found in its oxidic phase on the as-synthesized catalyst and transforms progressively to an (oxy-)carbide upon contact with methane at 700 °C. Benzene production is only observed after the transformation of Mo to its active phase is complete. During this activation, carbonaceous deposits in the form of large immobile aromatic compounds deposit simultaneously.

A CO-treatment is proposed to produce the active phase of Mo prior to the reaction with methane. The advantage of this approach is that it can create the active site without the formation of carbonaceous deposits, which are responsible for the deactivation of the catalyst. For the as-synthesized catalyst, XANES shows a strong pre-edge feature at 20008 eV attributable to a 1s–4d quadrupole/dipole transition, characteristic for distorted Mo oxide. During CO-treatment, clear changes in the pre-edge peak were detected, accompanied by a total shift of the rising absorption edge of about 4.2 eV (Figure 33). At the same time CO consumption and CO₂ evolution are observed on the MS indicating the oxygen removal, while some carbon is left behind as carbidic carbon. The changes in the pre-edge feature and the rising edge during CO-treatment are similar to what is observed when pulsing methane to the catalyst before benzene is formed. When methane reacts with the CO-treated sample, benzene forms with no delay, confirming that an active catalyst equivalent to the one forming under methane is produced with the CO-treatment. ¹³C NMR measurements on the samples activated in CO confirm the absence of any carbonaceous deposits other than carbidic carbon. Additional mass spectrometry studies with isotopically labeled CO and CH₄ have demonstrated how dynamic the carbon within the active Mo (oxy-) carbide is since it can be transferred into the final products of the reaction.

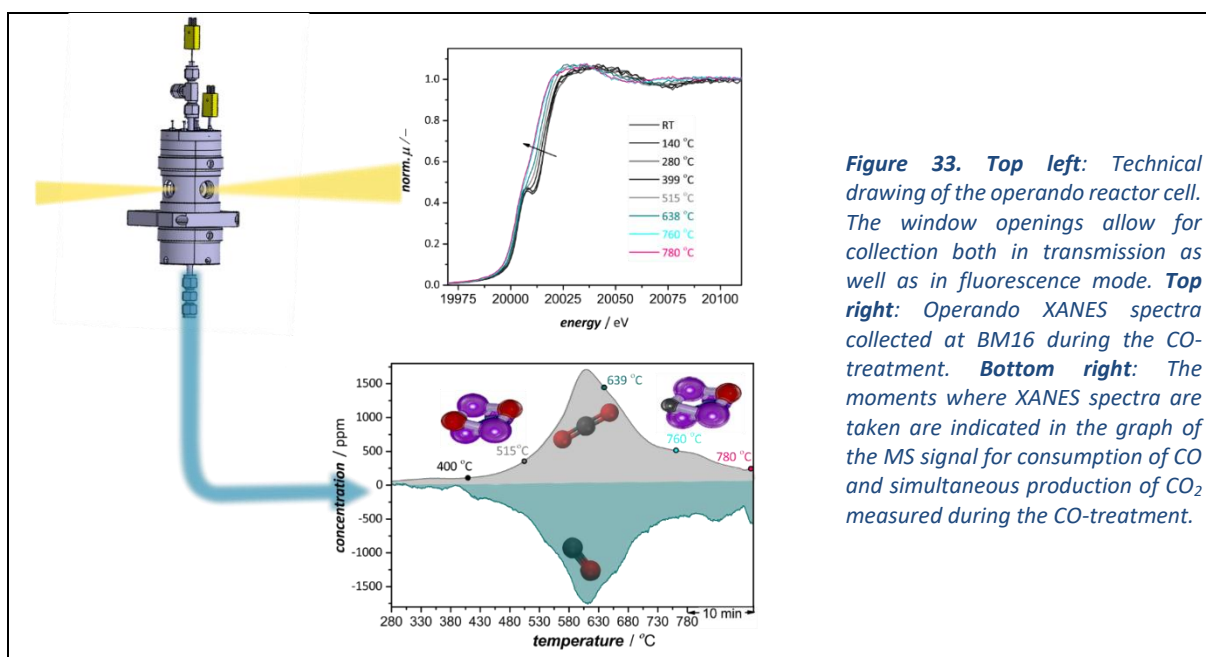


Figure 33. *Top left:* Technical drawing of the operando reactor cell. The window openings allow for collection both in transmission as well as in fluorescence mode. **Top right:** Operando XANES spectra collected at BM16 during the CO-treatment. **Bottom right:** The moments where XANES spectra are taken are indicated in the graph of the MS signal for consumption of CO and simultaneous production of CO₂ measured during the CO-treatment.

Authors and principal publication:

I. Vollmer¹, B. van der Linden¹, S. Ould-Chikh², A. Aguilar-Tapia³, I. Yarulina^{1,2}, E. Abou-Hamad², Y.G. Sneider⁴, A.I. Olivos Suarez¹, J.-L. Hazemann³, F. Kapteijn¹, J. Gascon^{1,2}, *Chemical Science*, **9** (2018) 4801-4807.

¹ Delft University of Technology, Delft (The Netherlands) / ² King Abdullah University of Science and Technology, Thuwal (Saudi Arabia) / ³ Inst. Néel, Grenoble (France) / ⁴ Sapienza Università, Rome (Italy)

In-operando elucidation of bimetallic CoNi nanoparticles during high-temperature CH₄/CO₂ reaction

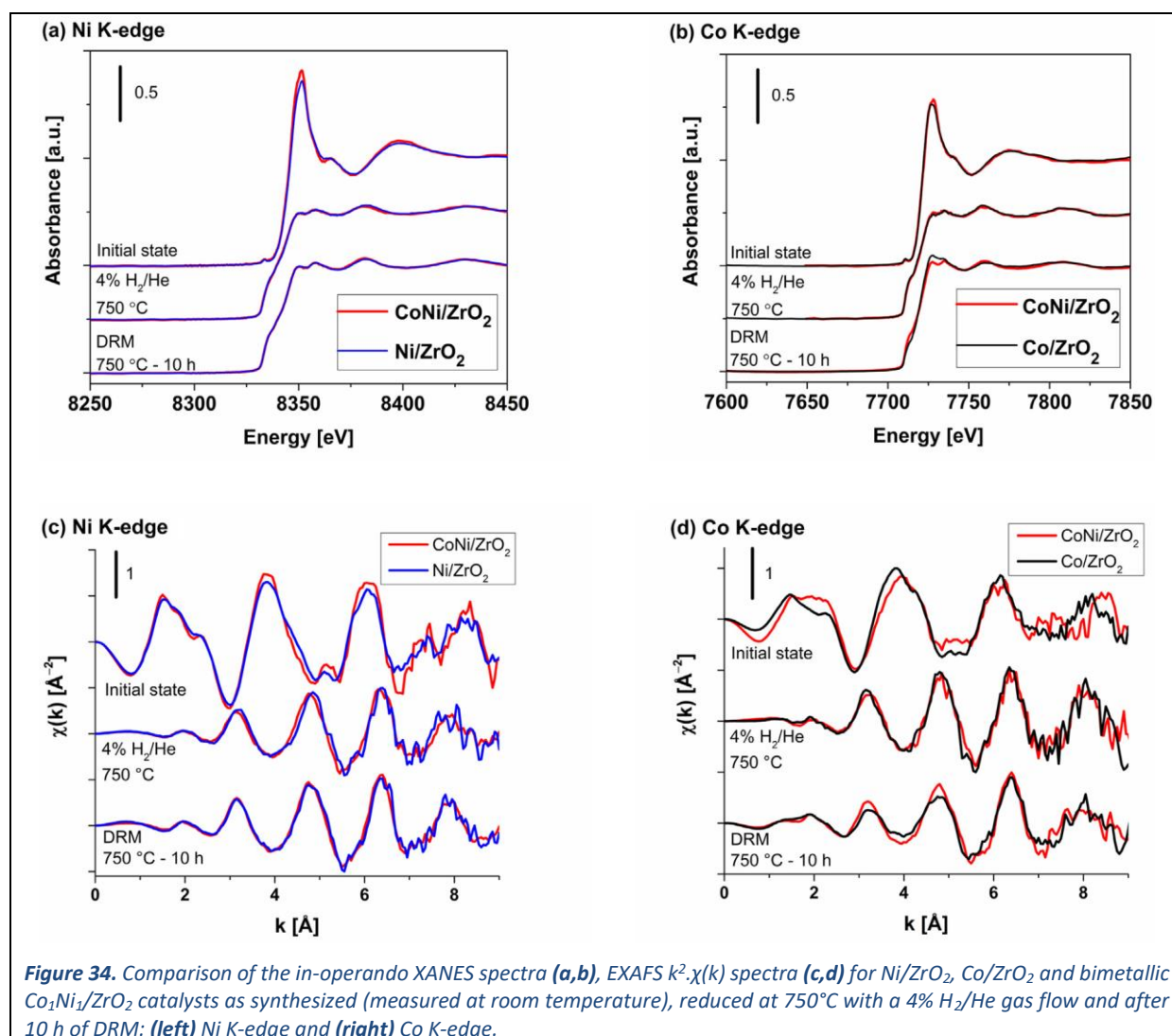
Dry reforming of methane (DRM) proceeds via CH₄ decomposition to leave surface carbon species, followed by their removal with CO₂-derived species. Reactivity tuning for stoichiometric CH₄/CO₂ reactants was attempted by alloying the non-noble metals Co and Ni, which have high affinity with CO₂ and high activity for CH₄ decomposition, respectively. This study was focused on providing evidence of the capturing surface coverage of the reactive intermediates and the associated structural changes of the metals during DRM at high temperature using *operando* X-ray absorption spectroscopy (XAS). On the Co catalysts, the first-order effects with respect to CH₄ pressure and negative-order effects with respect to CO₂ pressure on the DRM rate are consistent with the competitive adsorption of the surface oxygen species on the same sites as the CH₄ decomposition reaction. The Ni surface provides comparatively higher rates of CH₄ decomposition and the resultant DRM than the Co catalyst but leaves some deposited carbon on the catalyst surface. In contrast, the bimetallic CoNi catalyst exhibits reactivity towards the DRM but with kinetic orders resembling Co catalyst, producing negligible carbon deposition by balancing CH₄ and CO₂ activation.

In-operando XAS was used to investigate the structural differences among the bimetallic CoNi catalyst and its monometallic counterparts before DRM measurements. The XANES spectra for the Co and Ni K-edge, as shown in Figure 34 are similar for all catalysts after synthesis. The systematic occurrence of a weak peak in the pre-edge region due to the 1 s → 3d quadrupolar transitions and the intense white line are characteristic of an oxidized state of Co and Ni, both sitting in octahedral environments^{51,52}. This is further confirmed by examining the EXAFS spectra and their corresponding Fourier transforms, which display two scattering paths that are easily attributed to an oxygen and a metal shell (a Ni and/or Co atom). After treatment of the catalysts with a 4% H₂/He gas flow, all XANES spectra measured at 750 °C depicted an increase in the pre-edge peak intensity and the disappearance of the white line previously observed for the starting materials. Comparison of the XANES and EXAFS spectra taken at 750 °C with the reference spectra supports the formation of metallic NPs in all catalysts. A comparison of the final states of the Co and Ni atoms for all catalysts after DRM reaction conditions during 10h is shown in Figure 34. After 10 h of reaction, the total amount of metallic Co noticeably decreased for Co (74%) and slightly decreased for the CoNi catalyst (85%). This finding suggest that the bulk of the Co NPs was progressively oxidized in Co during the course of the reaction, while further oxidation in the CoNi catalyst remained minor. Moreover, no substantial oxidation of Ni atoms and no formation of Ni carbide was detected in the Ni and CoNi catalysts when examining the spectra recorded at the Ni K-edge.

Both kinetic data and *operando* XAS showed that the pure Co resulted in richer oxygen coverage (negative order in CO₂), while pure Ni maintained a reduced state and clean surface at the steady state (zero order in CO₂). The XAS results provided further evidence of the oxidation of pure Co during DRM, which progressively occurred from the surface to the bulk with time. The Ni catalyst experienced carbon deposition, while the bimetallic CoNi catalyst showed negligible amount of deposited carbon, likely due to balancing the oxidative (CO₂, H₂O) and reductive (CH₄, CO, H₂) species reactions on the catalyst surface.

⁵¹ F. de Groot, G. Vankó, P. Glatzel, *J. Phys. Condens. Matter* **21** (2009) 104207.

⁵² Cabaret et al., *Phys. Chem. Chem. Phys.* **12** (2010) 5619–5633.



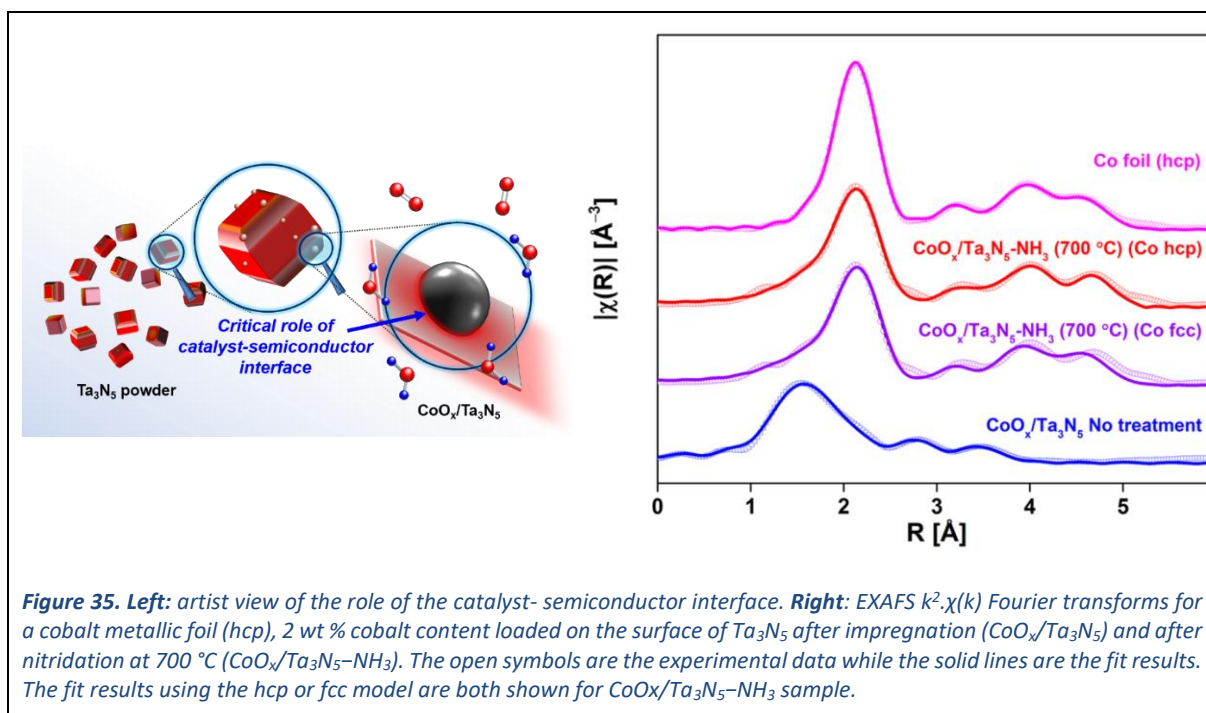
Authors and principal publication:

B. AlSabban^a, L. Falivene^a, S. M. Kozlov^a, A. Aguilar-Tapia^a, S. Ould-Chikh^a, J.-L. Hazemann^b, L. Cavallo^a, J.-M. Basset^a, K. Takanabe^a, *Applied Catalysis B: Environmental* **213** (2017) 177–189

^a King Abdullah University of Science and Technology, KAUST Catalysis Center and Physical Sciences and Engineering Division, Thuwal, Saudi Arabia. ^b Institut Néel, UPR 2940 CNRS, Grenoble

Establishing efficient cobalt-based catalytic sites for oxygen evolution on a Ta_3N_5 photocatalyst

In a photocatalytic suspension system with a powder semiconductor, the interface between the photocatalyst semiconductor and catalyst should be constructed to minimize resistance for charge transfer of excited carriers. This study demonstrates an in-depth understanding of pretreatment effects on the photocatalytic O_2 evolution reaction (OER) activity of visible-light-responsive Ta_3N_5 decorated with CoO_x nanoparticles. The CoO_x/Ta_3N_5 sample was synthesized by impregnation followed by sequential heat treatments under NH_3 flow and air flow at various temperatures. Various characterization techniques, including X-ray absorption spectroscopy (XAS) on FAME, were used to clarify the state and role of cobalt. No improvement in photocatalytic activity for OER over the bare Ta_3N_5 was observed for the as-impregnated CoO_x/Ta_3N_5 , likely because of insufficient contact between CoO_x and Ta_3N_5 . When the sample was treated in NH_3 at high temperature, a substantial improvement in the photocatalytic activity was observed. After NH_3 treatment at 700 °C, the Co^0 - CoO_x core-shell agglomerated cobalt structure was identified by XAS and scanning transmission electron microscopy. No metallic cobalt species was evident after the photocatalytic OER, indicating that the metallic cobalt itself is not essential for the reaction. Accordingly, mild oxidation (200 °C) of the NH_3 -treated CoO_x/Ta_3N_5 sample enhanced photocatalytic OER activity. Oxidation at higher temperatures drastically eliminated the photocatalytic activity, most likely because of unfavorable Ta_3N_5 oxidation. These results suggest that the intimate contact between cobalt species and Ta_3N_5 facilitated at high temperature is beneficial to enhancing hole transport and that the cobalt oxide provides electrocatalytic sites for OER.



Authors and principal publication:

E. Nurlaela,^a S. Ould-Chikh,^a I. Llorens,^b J.-L. Hazemann,^c K. Takanabe,^a Establishing efficient cobalt-based catalytic sites for oxygen evolution on a Ta_3N_5 photocatalyst, *Chemistry of Materials* **27**, 5685-5695 (2015)

^a Division of Physical Sciences and Engineering, KAUST Catalysis Center (KCC), King Abdullah University of Science and Technology, Saudi Arabia | ^b Institut de Recherches sur la Catalyse et l'Environnement de Lyon, CNRS-Univ. Lyon 1, France | ^c Institut Néel, CNRS, Grenoble, France

Catalyst structure identified in an operating PEM fuel cell

The structure of the palladium catalyst for hydrogen oxidation in proton exchange membrane (PEM) fuel cells has been revealed. Palladium is among the most active catalysts for the hydrogen oxidation reaction (HOR) and is thus a potential candidate for replacing platinum in fuel cell catalysis. Contrary to current views the results, obtained by applying X-ray spectroscopy under operating conditions, indicate the existence of a hydride phase throughout the operating range. Research performed in collaboration with the Technical Electrochemistry research group of Prof. Dr Hubert Gasteiger at the Technical University of Munich (Department of Chemistry), and the group of Dr Moniek Tromp of the University of Amsterdam.

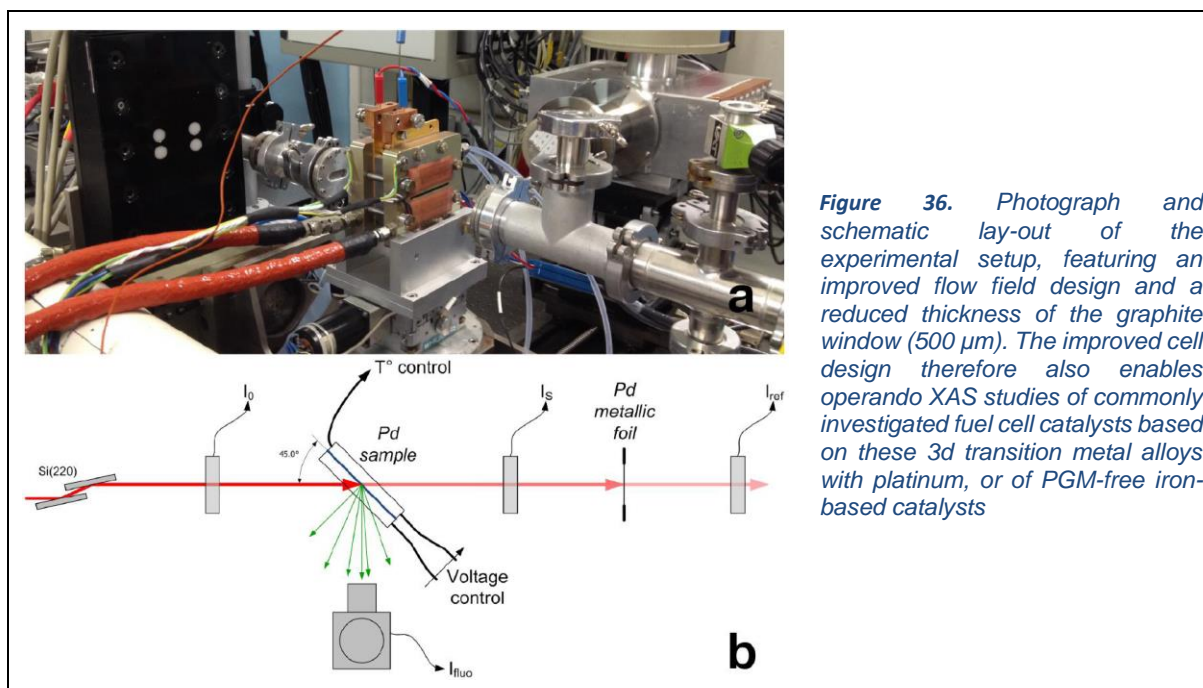


Figure 36. Photograph and schematic lay-out of the experimental setup, featuring an improved flow field design and a reduced thickness of the graphite window (500 μm). The improved cell design therefore also enables operando XAS studies of commonly investigated fuel cell catalysts based on these 3d transition metal alloys with platinum, or of PGM-free iron-based catalysts

Investigating palladium. In proton exchange membrane fuel cells (PEMFC) electrons are generated by means of the electrochemical oxidation of hydrogen, thus producing the electrical power to drive an electric car or provide electricity for industry or households. The best currently known electro-catalysts for this electron-generating oxidation reaction are the so-called platinum-group metals, with platinum itself as the most active catalyst. Palladium provides an interesting alternative for platinum since it is only slightly less active but more widely available and less expensive. However, in practice the activity of palladium decreases at high anodic potentials. This has until now been explained by a change in its catalytic properties, mainly hydride decomposition in the bulk of the material and oxide formation at the surface. These explanations are disputable, however, since they are based on laboratory experiments at room temperature. Typical operating conditions of a low temperature PEMFC involve temperatures up to 80 $^{\circ}\text{C}$. Both for a fundamental understanding of the performance and for the development of non-Pt based catalysts it is important to characterize the catalyst under real reaction conditions.

Improved experimental set-up. The current Amsterdam/Munich research cooperation bridges the gap between electrochemical studies in liquid electrolytes at room temperature and real operating fuel cells at 80 $^{\circ}\text{C}$. The researchers present electrochemical isotherms for the absorption of hydrogen into a Pd catalyst as a function of applied potential, temperature, and reaction atmosphere. They were obtained with a new, improved X-ray absorption

spectroscopy (XAS) electrochemical fuel cell, allowing the investigation of PEMFC electrodes during operation (operando spectroscopy). The research was performed at the BM30B/FAME beamline of the European Synchrotron Radiation Facility in Grenoble.

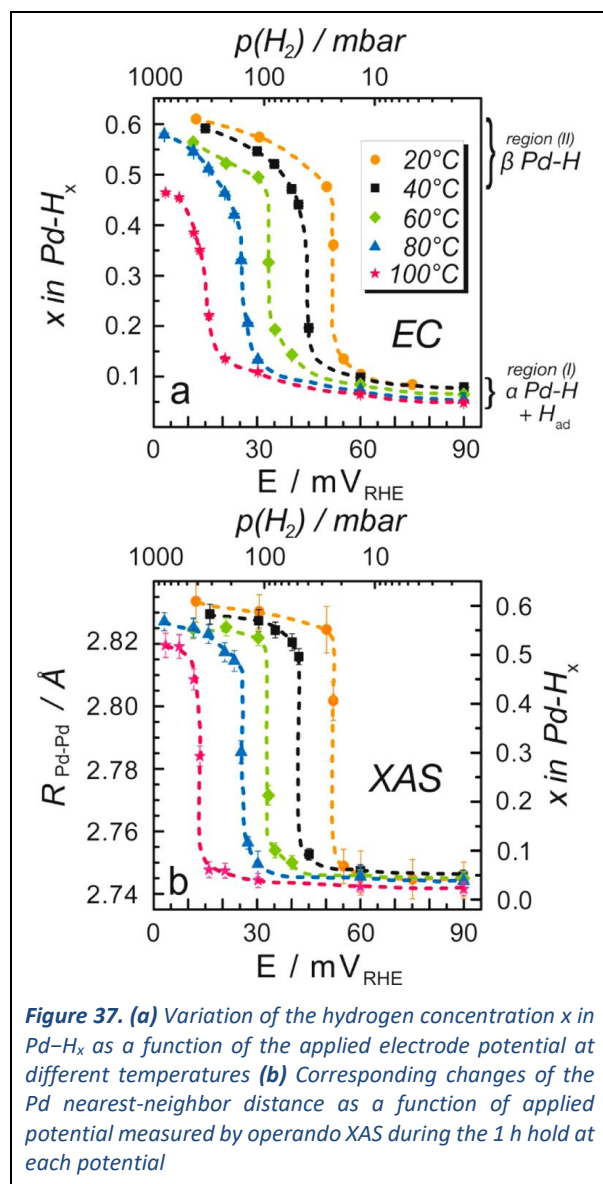


Figure 37. (a) Variation of the hydrogen concentration x in Pd-H_x as a function of the applied electrode potential at different temperatures **(b)** Corresponding changes of the Pd nearest-neighbor distance as a function of applied potential measured by operando XAS during the 1 h hold at each potential

Hydride phase maintained. The operando spectroscopic characterization during hydrogen oxidation unequivocally demonstrates that the hydride phase is maintained under practical operating conditions of a fuel cell anode, even at high anodic potentials. The transition from a hydride to a metallic state, previously observed in electrochemical cells based on a liquid electrolyte, does not occur. The researchers argue that the reaction environment of operating PEMFC's is so much unlike that in room-temperature liquid electrolytes cells that the chemical state of the Pd catalyst is completely different. One important feature explaining this is the orders of magnitude higher mass-transport rates in PEMFC's.

The recent findings highlight the necessity of characterizing the properties of electro-catalysts under realistic operating conditions. Furthermore the researchers argue that in fact for all electro-catalytic reactions in which the reactant is supplied in a gaseous form - not just for the hydrogen oxidation in a fuel cell - it is of utmost importance to maintain appropriate mass transfer regimes when establishing structure-activity relationships

Authors and principal publication:

A. Siebel^a, Y. Gorlin^a, J. Durst^b, O. Proux^c, F. Hasché^a, M. Tromp^d, H. A. Gasteiger^a, *ACS Catalysis* **6** (2016) 7326–7334

^a Chair of Technical Electrochemistry, Department of Chemistry and Catalysis Research Center, Technical University of Munich (Germ.) | ^b Energy & Environment Division, Paul Scherrer Institut, (Switz.) | ^c BM30B/FAME beamline, (Fr.) | ^d Van't Hoff Institute for Molecular Sciences, University of Amsterdam, (Netherlands)

Unravelling redox processes of Li_7MnN_4 upon electrochemical Li extraction–insertion using *operando* XAS

Lithium batteries are used in a wide range of applications, from small scale on-board electronics to electric vehicles. However, improvements are necessary to fulfil the requirements for high capacity and/or power applications. In this context Li_7MnN_4 displayed an interesting specific capacity, with an excellent cycle life. These interesting performances can be explained by the excellent reversibility and the limited volume variation induced by redox processes. A reversible three-phase mechanism was evidenced from X-ray Diffraction experiment (XRD) in good agreement with the electrochemical behaviour: two successive biphasic domains during the oxidation followed by one single phase at the end of the charge process. However, XRD does not give information on a possible amorphous contribution to the oxidation state variation of the redox centre, *i.e.* Mn ions, implied in the reaction.

To shed light on this issue, *operando* X-ray Absorption Spectroscopy experiments were performed upon electrochemical delithiation of Li_7MnN_4 , allowing the avoidance of contamination possibly induced by *ex situ* preparations. In addition, the collection of a large enough data set, possible with the *operando* collection mode, permits a fine analysis using various chemometric tools (PCA and MCR-ALS).

In this work, we clearly demonstrate the implication of the three highest oxidation states of manganese (*i.e.* Mn^{5+} , Mn^{6+} and Mn^{7+}) in the redox processes, which is remarkable in such a low potential range (0.9–1.7 V vs. Li^+/Li). The chemometric analysis presented here might have been facilitated by the presence of intense pre-edge peaks (inset on Figure 38, right). Indeed, the energy and the intensity of this $1s \rightarrow 3d + 4p$ transition, only allowed in a tetrahedral local environment, are very sensitive to the oxidation state. Indeed, the first voltage plateau (Figure 38, left) at 1.18 V vs. Li^+/Li , which indicates the oxidation of Li_7MnN_4 through a biphasic process into $\text{Li}_{6.1}\text{MnN}_4$, is attributed to the oxidation of Mn^{5+} ($3d^2$) ions in Mn^{6+} ($3d^1$). The second voltage plateau at 1.20 V vs. Li^+/Li , where $\text{Li}_{6.1}\text{MnN}_4$ is oxidised in $\text{Li}_{5.7}\text{MnN}_4$ again through a biphasic process, leads to the oxidation of roughly 50% of Mn^{6+} in Mn^{7+} . Then, the increase of potential recorded for $1.35 < 1.7$ in $\text{Li}_{7-x}\text{MnN}_4$, in line with the observed solid-solution like evolution of the structure, accounts for the additional 20% oxidation of Mn^{6+} in Mn^{7+} . In addition, the excellent reversibility of the Li_7MnN_4 structural response, which has already been demonstrated on a long-range scale, is also fully established on the local scale.

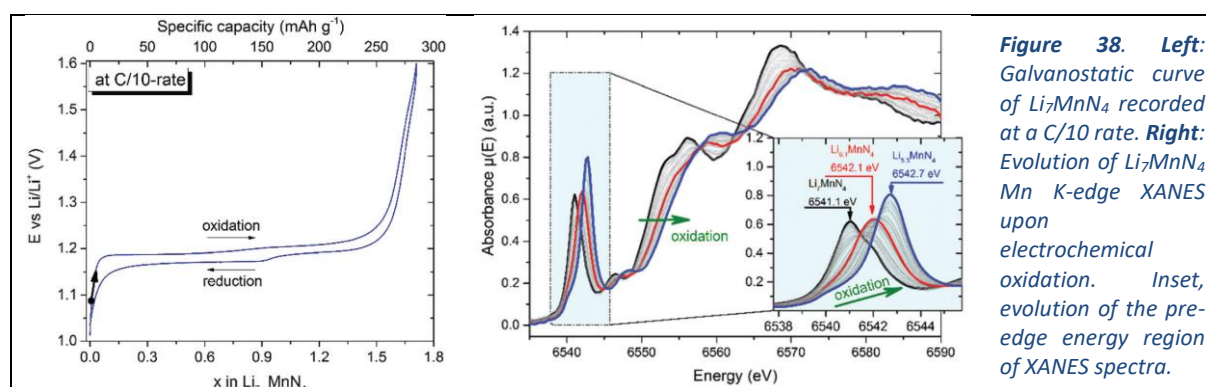


Figure 38. Left: Galvanostatic curve of Li_7MnN_4 recorded at a C/10 rate. Right: Evolution of Li_7MnN_4 Mn K-edge XANES upon electrochemical oxidation. Inset, evolution of the pre-edge energy region of XANES spectra.

Authors and principal publication:

Muller-Bouvet D.^a, Emery N., Tassali N.^a, Panabière E.^a, Bach S.^{a,b}, Crosnier O.^{c,d}, Brousse T.^{c,d}, Cénac-Morthe C.^e, Michalowicz A.^a, Pereira-Ramos J. P.^a, *Physical Chemistry Chemical Physics* **19** (2017) 27204–27211

^a Institut de Chimie et des Matériaux Paris Est, UMR 7182 CNRS / UPEC, Thiais / ^b Université d'Evry Val d'Essonne, Dép. Chimie / ^c IMN, UMR6502, Nantes / ^d RS2E, FR3459 CNRS / ^e CNES, Toulouse

An innovative method to study volatile fission products speciation in nuclear fuels under severe accident conditions

The objective of the project is to determine Fission Products (FP) behavior in conditions representative of a Severe Accident (SA) of a nuclear pressurized water reactor. This will help improving the actual understanding of their release mechanisms and confirming or not the assumptions on which some codes for SA scenario predictions are based. Within this frame, several XAS experiments have been performed on SIMFUEL samples composed of a UO_2 matrix doped with 12 oxides as FP surrogates after thermal treatments. However, post-test analyses do not allow the observation of potential intermediate compounds formed at high temperature which is of particular importance to understand volatile FP speciation. The goal of this experiment was to demonstrate the feasibility of an *in situ* XAS experiment at high temperature under controlled atmosphere on such samples. The sample (14 Bq activity) was maintained on a W-Re wire and heated by Joule effect up to 700°C . The atmosphere was set inside the furnace by pumping or adding O_2 to a gas mixture (He or He + 4% H_2). The sample temperature was monitored thanks to a thermocouple and a pyrometer.

Ba speciation was studied at two different oxygen potential conditions at room temperature in the sample as fabricated (T_0), 400°C and 700°C . Thermodynamic calculations indicate that Ba would be present in the samples as BaZrO_3 in reducing conditions whereas BaMoO_4 predominates above $-300 \text{ kJ.molO}_2^{-1}$. To avoid interferences with the signal of other elements present in the sample, High Energy Resolution Fluorescence Detection XANES have been performed at Ba L_3 edge (5.247 keV). The Crystal Analyzer Spectrometer was equipped with Ge(400) crystals, the diffracted signal was recorded with a SDD detector.

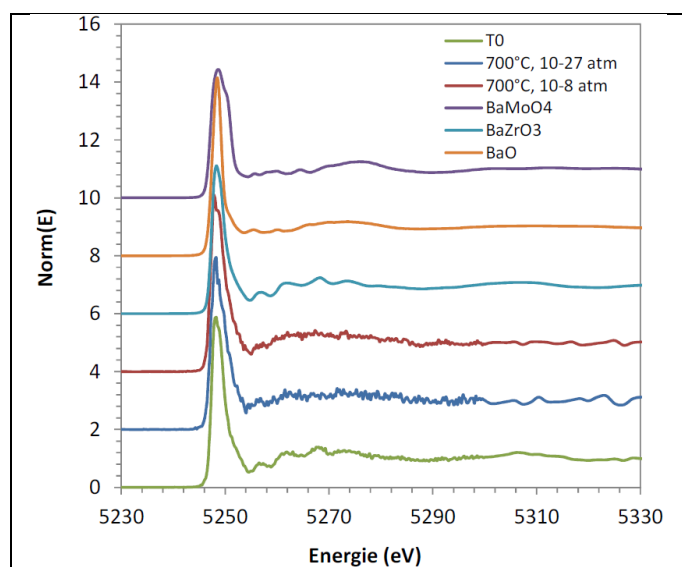


Figure 39. High Energy Resolution Fluorescence Detection XANES spectra collected at Ba L_3 edge on sample P9C2 at room temperature and as fabricated (T_0), at 400°C and 700°C under different atmospheres, along with several reference samples

The XANES spectra obtained for the sample in its initial state at room temperature and in the two probed atmospheres are shown on Figure 39. Edge energy of each spectrum are similar confirming that Ba is in oxidation state +II as expected for an alkaline earth element. At first glance, no evolution of Ba speciation is visible between both samples. The shape of the T_0 spectrum is very close to BaZrO_3 spectrum as already observed. The spectra recorded at 700°C are broadened and flattened (due to thermal agitation) but still look similar to BaZrO_3 spectrum. In conclusion, the feasibility of an in-temperature XAS experiment on SIMFUEL samples has been demonstrated.

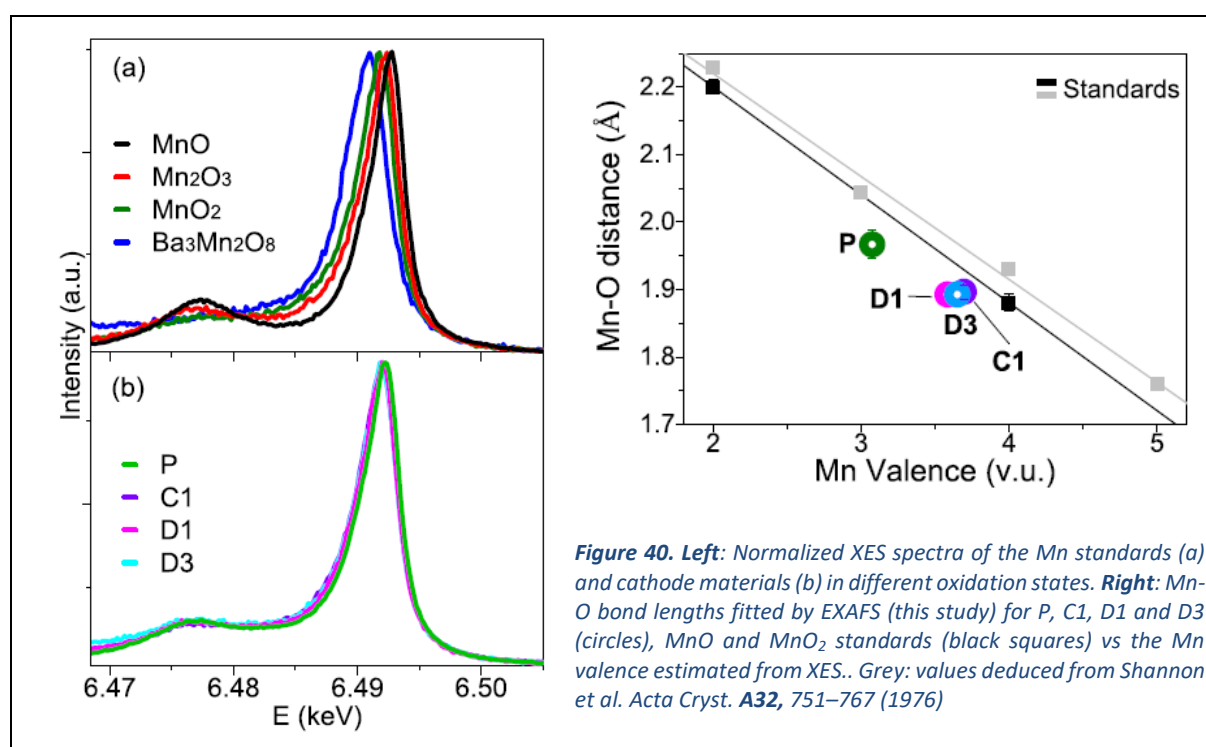
Authors and principal publication:

C. Le Gall^a, M. Colonna^b, J.-L. Hazemann^c, O. Proux^c, C. Riglet Martial^a, J. L chelle^a, F. Audubert^a, Y. Pontillon^a, 8th European Review Meeting on Severe Accident Research Warsaw, Poland, 16-18 May 2017.

^a CEA, DEN/DEC, Cadarache St Paul-lez-Durance, France / ^b EC, JRC Institute for Transuranium Elements, Karlsruhe, Germany / ^c OSUG, CNRS – UGA, Grenoble, France

Operando X-ray Absorption Spectroscopy and Emission $K\beta_{1,3}$ study of the manganese redox activity in high-capacity $\text{Li}_4\text{Mn}_2\text{O}_5$ cathode

In years to come, Lithium Ion Batteries (LIBs) will play a key role in the transition from fossil fuels into renewable power sources. Their energy density is determined by the capacity of the electrodes to store Li^+ cations and the discharge potential of the cell. Since current anode materials offer superior storage capacities to that of cathode, the latter is limiting the performance of LIBs and many researchers are exploring ways to improve their capacity. A new class of positive electrode materials has recently emerged utilizing the solid-state redox reactions of oxide anions along with that of transition metal cations. The electrochemical performance of nanostructured $\text{Li}_4\text{Mn}_2\text{O}_5$ (pristine composite) displaying an outstanding charge capacity was recently reported. Interestingly, the removal of Li in $\text{Li}_4\text{Mn}_2\text{O}_5$ is apparently found to take place beyond the oxidation limit of +4 for Mn. To characterize the nature of this extra capacity, we have approached the study of the redox chemistry and local structure of Mn in $\text{Li}_4\text{Mn}_2\text{O}_5$ via a combination of X-ray absorption and emission spectroscopies.



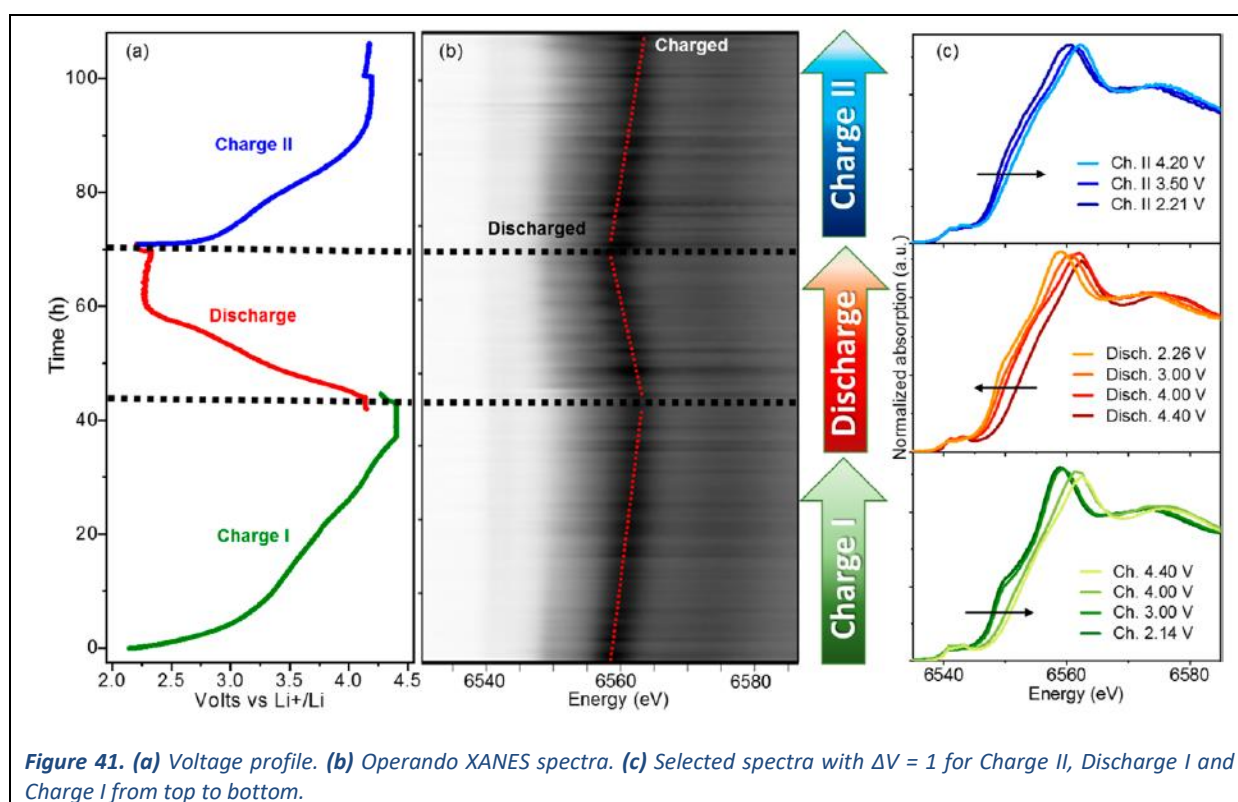
Starting from initial nanostructured $\text{Li}_4\text{Mn}_2\text{O}_5$ (P on Figure 40), 3 three new samples were prepared, by stopping the battery at the desired potential: at the end of the first charge (C1), at the end of the 1st and 3rd discharge (D1 and D3, respectively). X-ray Emission Spectroscopy around the $K\beta_{1,3}$ transition (main peak in Figure 40, left) was used as a gauge of the oxidation state (OS). The OS of the cathode materials were obtained by interpolation of the $K\beta_{1,3}$ transition position between the same transition for the MnO and MnO₂ standards (Figure 40, right). An increase of the Mn OS from +3 to $\sim +3.7$ between P and C1 is observed. Beyond C1, there is not a noticeable change in the OS of manganese for D1, nor for D3. Only the $\text{Mn}^{3+}/\text{Mn}^{4+}$ redox pair is active during the charge.

An electrochemical cell was employed to study the composite (P) in operando during a full charge-discharge cycle and a second charge over the course of >100 h. Figure 41 reveals a typical solid solution behaviour, where the concentration of lithium continuously changes

Scientific Results

across a single phase. A broadening of the XANES features as a function of the lapsed time is shown in Figure 41.c. Notice the difference between the broader shoulder of the reduced compositions at the fully discharged state of 2.2 V during the 2nd charge with that of the discharge cycle at the same potential, where the same shoulder feature is more clearly resolved. This observation indicates an increase of the structural disorder in the cathode material upon cycling. The structural amorphization accompanying battery cycling has been often associated to a fading of the capacity after extended cycling. However, in the present study, the same capacity value was retained between the Discharge I and Charge II cycles and no loss of performance could be detected.

Our results unequivocally rule out the participation of the Mn⁴⁺/Mn⁵⁺ redox couple and indicate the participation of oxygen in the electrochemistry. After the 1st charge, the battery cycles reversibly between charged and discharged states, Li⁺ exchange being compensated by anionic redox.



Authors and principal publication:

M. Diaz-Lopez¹, Y. Joly¹, M. Freire², C. Colin¹, O. Proux³, V. Pralong², P. Bordet¹, *J. Phys. Chem. C* **122** (2018) 29586–29597

¹ Inst. Néel (UPR 2940 CNRS, Grenoble) / ² CRISMAT (UMR 6508 CNRS / Univ. Caen / ENSI Caen) / ³ OSUG (UMS 832 CNRS / Univ. Grenoble Alpes)

Material science

A major challenge in materials science is the search for advanced materials with properties that satisfy the demands of continuously evolving technologies and whose manufacturing fulfills sustainability criteria. Several approaches of *material by design* have been proposed in the recent years such as high-throughput methods to rapidly explore large sections of composition space,⁵³ or predictive methods based on DFT or machine learning.⁵⁴ However, phase stability assessed from DFT calculations mostly relies on enthalpies of formation and neglect entropy terms that were recently shown to dominate the energy landscape even at relatively low temperatures in intermetallics or ionic compounds.⁵⁵ This new paradigm with the entropy as an additional “chemical” lever has already led to a variety of metal alloys, oxide, nitride, boride or disilicide compounds characterized by an intrinsic chemical disorder, and showing unexpected properties such as colossal dielectric constant or superionic Li⁺ conduction with potential applications in energy-saving technologies.⁵⁶ This example illustrates the fact there is still a large room for experimental approaches to expand the library of functional materials specifically in the case of molecular solids where properties are governed by low-energy intermolecular interactions that favor polymorphism, in systems with extensive defect densities or in mesoscale hybrid architectures where a large number of elements prohibit the use of computational approaches. Except for recent trials to account for disordered materials using computational techniques,⁵⁷ the largest efforts engaged over the last 10-15 years correspond to the development of increasingly complex synthesis routes such as combinatorial screening, artificial layering, strain engineering, etc. In this context, XAS and XES provide unique tools to (i) study ill-defined, heterogeneous or nanoscale materials due to their element and site-selectivity, (ii) determine the symmetry and valence state of trace dopants, (iii) have an *in situ* control of the growth process itself under specific conditions such as elevated temperature or pressure, vacuum or reactive gas environments.

The ongoing development of sample environments at the FAME and FAME-UHD beamlines (from very low temperature with liquid helium cryostats, up to high temperatures with HP/HT autoclaves), complemented with the possible integration of users’ equipments on the spectrometers, makes them perfectly suited to study a large variety of systems in particular phase-change or X-chrome materials involving valence tautomeric⁵⁸ or spin^{59,60} transitions controllable by different external stimuli (temperature, pressure or laser irradiation). These materials are currently studied by the teams of D. Luneau (Lab. des Multimatériaux et Interfaces, Lyon), A. Bordage (Institut de Chimie Moléculaire et des Matériaux, Orsay) and I. Maurin (Institut Néel, Grenoble) in collaboration with the FAME and FAME-UHD staff. *In situ* XAS-XES studies allow to directly quantify the charge transfer or spin state change, map diagrams of phase transformation and provide key information on the correlations between the electronic and short-range structural changes responsible for the energy barrier that give rise to molecular bistability. Some of these compounds exhibit large and reversible strains under visible light irradiation that were recently exploited to generate motion range from μm-

⁵³ Wang *et al.*, *Calphad* **28** (2004) 79; Curtarolo *et al.*, *Comput. Mater. Sci.* **58** (2012) 218.

⁵⁴ Hill *et al.*, *MRS Bull.* **41** (2016) 399; Schmidt *et al.*, *npj Computational Materials* **5** (2019) 83.

⁵⁵ Cantor *et al.*, *Mater. Sci. Eng. A* **375** (2004) 213; Rost *et al.*, *Nat. Commun.* **6** (2015) 8485.

⁵⁶ Bérardan *et al.*, *J. Mater. Chem. A* **4** (2016); Bérardan *et al.*, *Phys. Status Solidi RRL* **10** (2016) 328 ; Sarkar *et al.*, *Adv. Mater.* **31** (2019) 1806236.

⁵⁷ Chen *et al.*, *Nat. Comput. Sci.* **1** (2021) 46.

⁵⁸ See highlight below p.104/ Lannes *et al.*, *JACS* **138** (2016) 16493–16501 <http://dx.doi.org/10.1021/jacs.6b10544>

⁵⁹ Bordage *et al.*, *Physical Chemistry Chemical Physics* **17** (2015) 17260-17265 <http://dx.doi.org/10.1039/C5CP02591E>

⁶⁰ See highlight below p.105/ Adam *et al.*, *Nanoscale* **10** (2018) 16030-16039 <http://dx.doi.org/10.1039/C8NR03597K>

scale MEM devices to cm-scale “artificial muscles”.⁶¹ Their coupling to a strain-sensitive compound within a multi-layer or a core-shell structure has also been proposed to design new thermoelectrics or control magnetization switching using light.⁶² XAS actually combines several advantages for a deep understanding of heterostructures coupling ferroelastic and ferro(i)-magnetic properties (see highlight): (i) optimization of the coupling by screening different growth parameters and their influence on strain propagation (relative fraction of the two compounds,⁶³ adaptive lattice matching across the interface,⁶⁰ interface roughness, etc), (ii) assess the possibility of local symmetry breaking close to the interface from HERFD-XANES and its impact on magnetic anisotropy, (iii) kinetics investigations for structures in which deformations are triggered by an external field such as light irradiation. Even in the absence of films of uniform thickness, the dispersion of powder samples in an appropriate matrix allows for an easy matching between the absorption length of the x-rays and the penetration depth of the laser,⁶⁰ with a time resolution that will be improved in the future with the development of continuous scans both at FAME and FAME-UHD or the use of energy dispersion coupled to the CAS spectrometer (for sub-sec resolution). The implementation of microfocused and imaging techniques, in particular spectral ptychography at the FAME workstation, will open new avenues with the possibility of speciation in 3D during photo-induced phase transitions to address questions as the role of interfaces on nucleation and growth processes in mesoscale (few hundreds of nm) particles, identify domains walls and their mode of evolution. Up to now such studies were restricted to crystals of several μm using conventional microscopy techniques with a unique example of domain visualization in a single nanoparticle using 4D TEM.⁶⁴

In the field of nanoscale materials where properties are governed by structuration or surface /interface engineering, there are insistent needs to develop *in situ* tools to monitor nanocrystallization processes in liquid or harsh environment, including elevated temperature and pressure. Nanophosphors constitute a case study where HT-HP conditions control phase stability, cristallinity and doping. G. Dantelle (Institut Néel), in collaboration with the FAME and FAME-UHD staff, studies the synthesis of nanoparticles of YAG:Ce.⁶⁵ These particles provide an interesting alternative to the currently used micron-sized phosphors in white LED technologies in order to better control light propagation (optimization of absorption and enhanced light extraction) and ultimately increase the external quantum efficiency (EQE) of the device, if high luminescent properties are retained in the nanocrystals. The control of the oxidation state of the emitting ions (optically active Ce^{3+}) is of prime importance to obtain highly efficient optical properties. The HT-HP cells initially developed for researches on geological fluids have been successfully transposed to study widely-spread and industry-relevant solvothermal syntheses, and screen the reaction conditions (P, T, solvent, etc) which prevent $\text{Ce}^{3+} \rightarrow \text{Ce}^{4+}$ oxidation while leading to size-controlled well-crystallized YAG:Ce nanophosphors.^{65,66} A major advantage of these cell designs is that they combine relatively large reaction volumes allowing for *post-mortem* TEM analyses and transportable HT-HP regulation making the growth conditions directly comparable to lab experiments where the

⁶¹ Manrique-Juarez et al., *Adv. Funct. Mater.* **28** (2018) 1801970.

⁶² Chen et al., *J. Mater. Chem. C* **3** (2015) 945 ; see Cain et al. « Stimulus Induced Strain in Spin Transition Heterostructures » for a perspective article in *J. Appl. Phys.: Special Topic on Spin Transition Materials: Molecular and Solid-State* (2021).

⁶³ Presle et al., *J. Phys. Chem. C* **118** (2014) 13186, Felts et al., *J. Phys. Chem. C* **120** (2016) 5420.

⁶⁴ Van der Veen et al., *Nat. Chem.* **5** (2013) 395.

⁶⁵ See highlight below p.102 / Dantelle et al., *RSC Advances* **8** (2018) 26857 <http://dx.doi.org/10.1039/C8RA05914D>

⁶⁶ Cantarano et al., *J. Mater. Chem. C* **8** (2020) 9382 <https://doi.org/10.1039/D0TC02347G>

nanocrystal growth can be monitored by complementary photoluminescence, Raman spectroscopy or DLS measurements.

Isabelle Maurin & Géraldine Dantelle, Institut Néel, Grenoble

In situ characterization of cerium oxydation in YAG:Ce nanocrystals

Lighting accounts for about 20% of the global building electricity consumption. White LEDs (wLEDs) use 75% less energy and last 25 times longer than incandescent bulbs, allowing drastic energy savings evaluated at 40% at the horizon 2040. The structure of commercialized wLED (Figure 42.a) combines a blue LED (typically InGaN, $\lambda_{em} \approx 450$ nm) with a micron-sized luminescent powder, called phosphor, encapsulated into an epoxy resin. The commonly-used phosphor material is $Y_3Al_5O_{12}$ doped Ce^{3+} , labeled YAG:Ce, presenting a high internal luminescence quantum yield (iQY > 85%), a perfect photostability and good, though not perfect, optical properties ($\lambda_{exc} = 450$ nm, $\lambda_{em} = 550$ nm).⁶⁷ Commercially available wLEDs present two main drawbacks related to micron-size phosphors: (1) blue and yellow light beams can be backscattered towards the chip, and (2) phosphors are not easily coupled with semi-conducting nanostructures. Consequently, the external quantum efficiency (EQE) of a wLED is limited to $\approx 70\%$. These limitations could be overcome by using nanophosphors: backscattering would be avoided and extraction could be controlled independently. Furthermore, nanophosphors would enable better coupling with semi-conducting nanostructures. Hence nanophosphors could replace efficiently micron-sized phosphors as long as they present equivalent optical properties in terms of photostability and iQY.

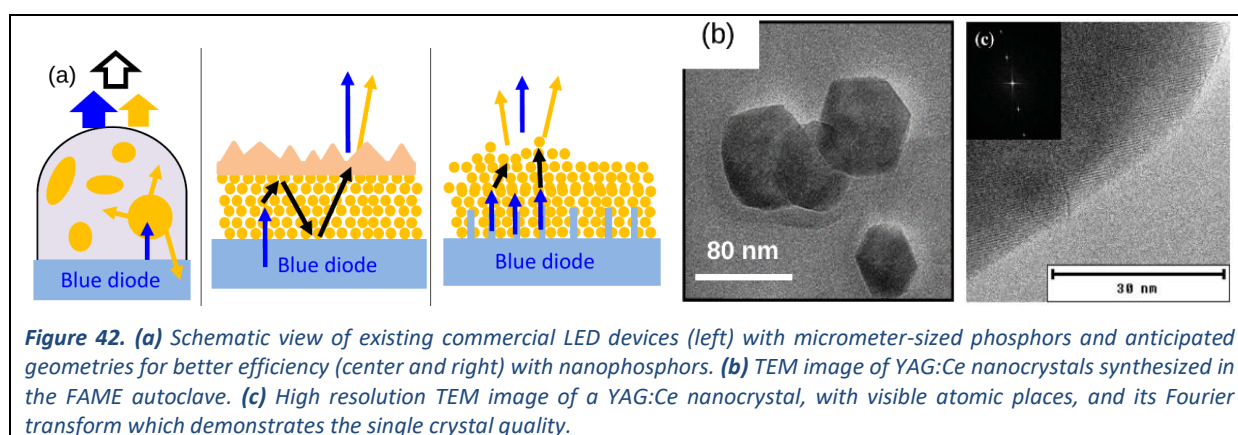


Figure 42. (a) Schematic view of existing commercial LED devices (left) with micrometer-sized phosphors and anticipated geometries for better efficiency (center and right) with nanophosphors. (b) TEM image of YAG:Ce nanocrystals synthesized in the FAME autoclave. (c) High resolution TEM image of a YAG:Ce nanocrystal, with visible atomic places, and its Fourier transform which demonstrates the single crystal quality.

There are mainly two types of envisioned nanophosphors: QDots and garnet-type nanoparticles, mainly YAG:Ce. The objective of this project is to explore the current most advanced route for the synthesis of YAG:Ce nanoparticles, the solvothermal method, which leads to stable colloidal solutions with particle size varying between 30 and 200 nm. The idea is to optimize this method with two goals, namely to produce nanophosphors 1) with high crystallinity to reach a high EQE and 2) with a good photostability (associated with a low Ce^{3+} oxidation) in order to maintain this efficiency over time.

The high pressure (P) and high temperature (T) setup developed over the years at Néel Institut and FAME beamlines⁶⁸ was used in this project. The independent control of P and T enabled to pinpoint the best experimental conditions (P , T , precursor concentration, time) to obtain

⁶⁷ George et al., *Chemistry of Materials* 25(20) 3979-3995 (2013).

⁶⁸ Testemale et al., *Rev. Sci. Instr.* 76, 043905 (2005). / Louvel et al., *J. Mol. Liq.* 205, 54-60 (2015).

the largest monocrystalline nanoparticles (Figure 42 b and c). This synthesis stage was conducted in the lab, and took advantage of the large sample volume (~1ml) available with this setup, which ultimately allowed for easy characterization of the products.

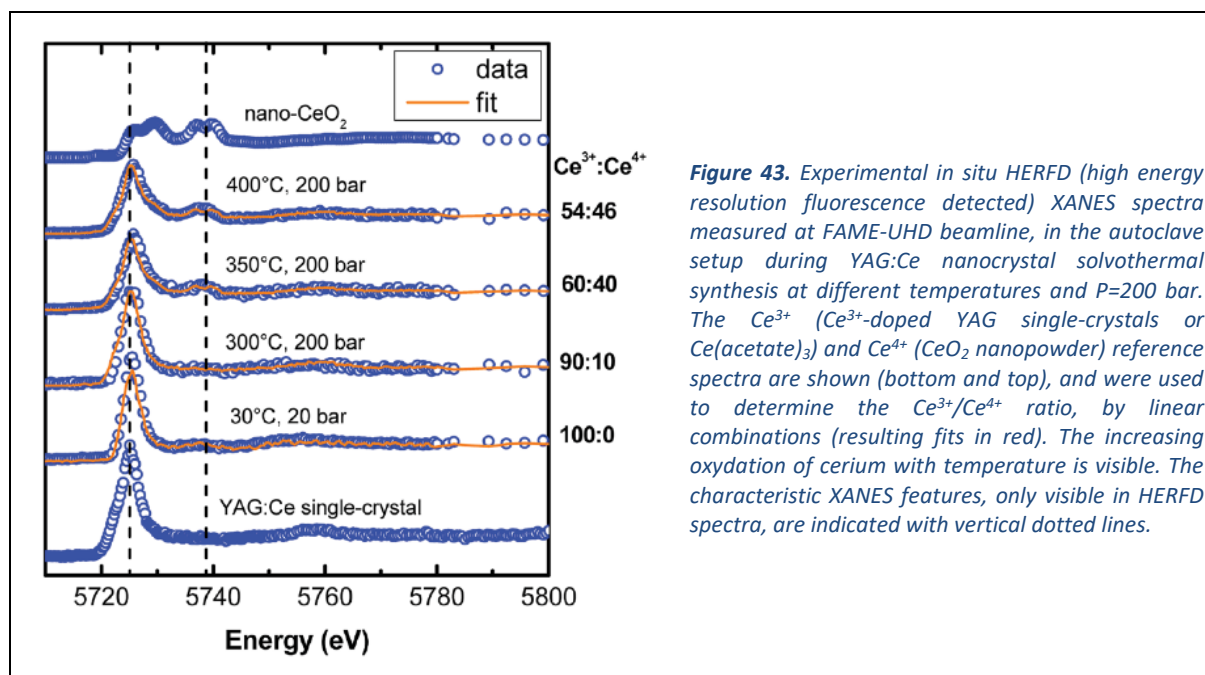


Figure 43. Experimental *in situ* HERFD (high energy resolution fluorescence detected) XANES spectra measured at FAME-UHD beamline, in the autoclave setup during YAG:Ce nanocrystal solvothermal synthesis at different temperatures and $P=200$ bar. The Ce^{3+} (Ce^{3+} -doped YAG single-crystals or $Ce(acetate)_3$) and Ce^{4+} (CeO_2 nanopowder) reference spectra are shown (bottom and top), and were used to determine the Ce^{3+}/Ce^{4+} ratio, by linear combinations (resulting fits in red). The increasing oxidation of cerium with temperature is visible. The characteristic XANES features, only visible in HERFD spectra, are indicated with vertical dotted lines.

The iQY of the 100 nm YAG:Ce nanocrystals was measured to be ~40%. This value is significantly higher than most of the values reported for as-made YAG:Ce nanophosphors (~20%), but still remains about twice lower than in bulk YAG:Ce (80%). One of the reasons which could explain this difference of optical efficiency between YAG nanocrystals and bulk is the potential presence of Ce^{4+} ions that behave as luminescence quenchers through energy transfer from Ce^{3+} to Ce^{4+} . This oxidation could occur during the solvothermal synthesis: we conducted then *in situ* HERFD-XANES measurements during the solvothermal process. Figure 43 shows one set of the spectra as a function of the synthesis T , as well as their corresponding fits based on the linear combination of standards for Ce^{3+} and Ce^{4+} . It can be seen that below 300°C (synthesis T) cerium remains in its 3+ redox state, but for higher T the proportion of Ce^{4+} raises. This oxidation is likely solvent-related (presence of dissolved oxygen, and dehydration with release of water at high T): for this reason, the investigation of other solvents is part of the current ongoing research.

Two FAME/FAME-UHD beamlines tools were essential to the successful outcome of this study.

- 1) The *HP/HT* setup available both at the Néel institute and at the beamlines, allowing very precise fine-tuning of the experimental conditions in the lab and crucial *in situ* measurements,
- 2) To detect the small XANES features that differ between Ce redox states is only possible using HERFD possibilities offered by the FAME-UHD spectrometer. Its sensitivity made also possible the estimation of Ce relative concentrations down to a few 100 ppm.

Authors and principal publication:

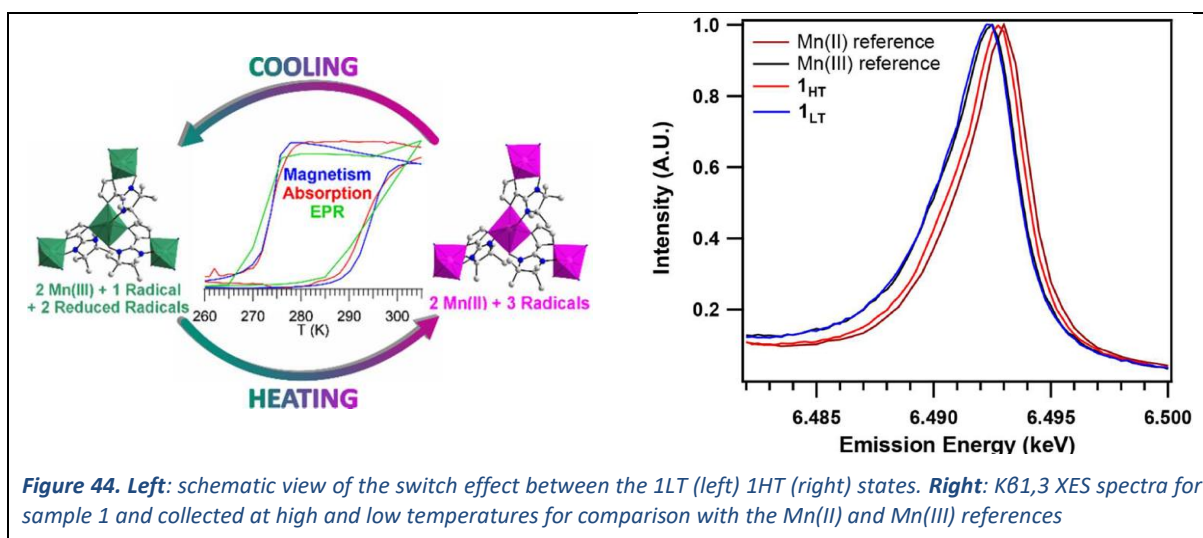
G. Dantelle¹, D. Testemale¹, E. Homeyer¹, A. Cantarano¹, S. Kodjikian¹, C. Dujardin², J.-L. Hazemann¹, A. Ibanez¹, *RSC Advances* 8, 26857–26870 (2018).

¹ Inst. Néel (UPR 2940 CNRS / UGA / INPG, Grenoble) / Inst. Lumière Matière (UMR 5306 CNRS / UCB, Lyon)

This project was funded by the ANR, *Nano-PhosforLED* project.

Magnetic switchability in new molecular materials

The manganese-nitronyl-nitroxide two-dimensional coordination polymer undergoes an unusual hysteretic thermo-induced valence tautomeric transition near room temperature, during which the manganese(II) ions are oxidized to manganese(III) and two of the three deprotonated radicals (NITIm⁻) are reduced to their diamagnetic aminoxy form. Upon cooling, the high temperature species $\{[\text{Mn}^{\text{II}}_2(\text{NITIm})_3]\text{ClO}_4\}_n$ (1_{HT}) turns into the low-temperature species $\{[\text{Mn}^{\text{III}}_2(\text{NIT}_{\text{Red}})_2(\text{NITIm})]\text{ClO}_4\}_n$ (1_{LT}) around 274 K, while on heating the process is reversed at about 287 K (Figure 44). This valence tautomeric phenomenon is supported by temperature dependent magnetic susceptibility measurements, differential scanning calorimetry, crystal structure determination, UV-vis absorption, X-ray absorption, emission (XES) and electron paramagnetic resonance spectroscopies in the solid state.



To the best of our knowledge, this is the first metal-nitroxide radical system to exhibit bistability based on valence tautomerism. Moreover, this is associated with a 20 K hysteresis at room temperature. This opens novel perspectives for the so-called metal-radical approach. Indeed, beyond the interest of nitronyl-nitroxide radicals as spin-carriers bridging ligands, this result shows that their redox activity can give rise in some cases to metal-radical electron transfer. This may be an additional advantage in the context of multifunctional materials, especially in the search for switchable magnets. The compound reported here is based on a layered 2D metal-radical coordination polymer. It is noteworthy that the $[\text{Mn}_2(\text{NITIm})_3]^+$ layers are cationic with the intercalated perchlorate anions in between, to afford a layered 3D chiral structure. From this point of view, it is a multifunctional material that gathers many interesting functionalities such as room temperature bistability, ferrimagnetic behaviour, and chirality. The synthesis is general and may be extended to the related imidazole type substituted nitronyl-nitroxide radical, while almost any type of anions can be intercalated. This allows a great versatility to tune the temperature of the transition or implement the multifunctionality, and accordingly, work is in progress in the group.

Authors and principal publication:

A. Lannes,^a Y. Suffren,^b J. B. Tommasino,^a R. Chiriac,^a F. Toche,^a L. Khrouz,^c F. Molton,^d C. Duboc,^d I. Kieffer,^{e,f} J.-L. Hazemann,^{e,g} C. Reber,^h A. Hauser,^b D. Luneau,^a *JACS* **138** (2016) 16493–16501

^a Lab. des Multimatériaux et Interfaces, UMR CNRS Univ. Claude Bernard Lyon, Villeurbanne | ^b Dép. de Chimie Physique, Univ. de Genève (Switz.) | ^c Lab. de Chimie, UMR CNRS, Univ. C. Bernard Lyon, ENS de Lyon | ^d DCM (UMR 5250), CNRS -Univ. Grenoble Alpes | ^e BM30B, ESRF, Grenoble | ^f OSUG, CNRS UMS 832, Saint Martin d'Hères | ^g Institut Néel, CNRS UPR 2940, Grenoble | ^h Dép. de Chimie, Univ. de Montréal (Canada)

Strain engineering of photo-induced phase transformations in Prussian blue analogue heterostructures

Heterostructures based on Prussian blue analogues (PBA) combining photo- and magnetostriction have shown a large potential for the development of light-induced magnetization switching.^{69,70} However, studies related to the microscopic parameters which control the transfer of the mechanical stresses across the interface and their propagation in the magnetic material are still scarce.^{70,71} This coupling strength was recently controlled by strain engineering in heteroepitaxial PBA core-shell heterostructures involving a same $\text{Rb}_{0.5}\text{Co}[\text{Fe}(\text{CN})_6]_{0.8}\cdot z\text{H}_2\text{O}$ photostrictive core (RbCoFe) and isostructural shells with a similar thickness and a variable mismatch with the core lattice (RbCoFe@KNiCr and RbCoFe@KNiFe). The shell deformation and the quantification of the light-induced electron transfer at the origin of photo-striction were investigated by combined *in situ* and in real time synchrotron x-ray powder diffraction (XRPD) and x-ray absorption near edge spectroscopy (XANES) under illumination (Figure 45, left).

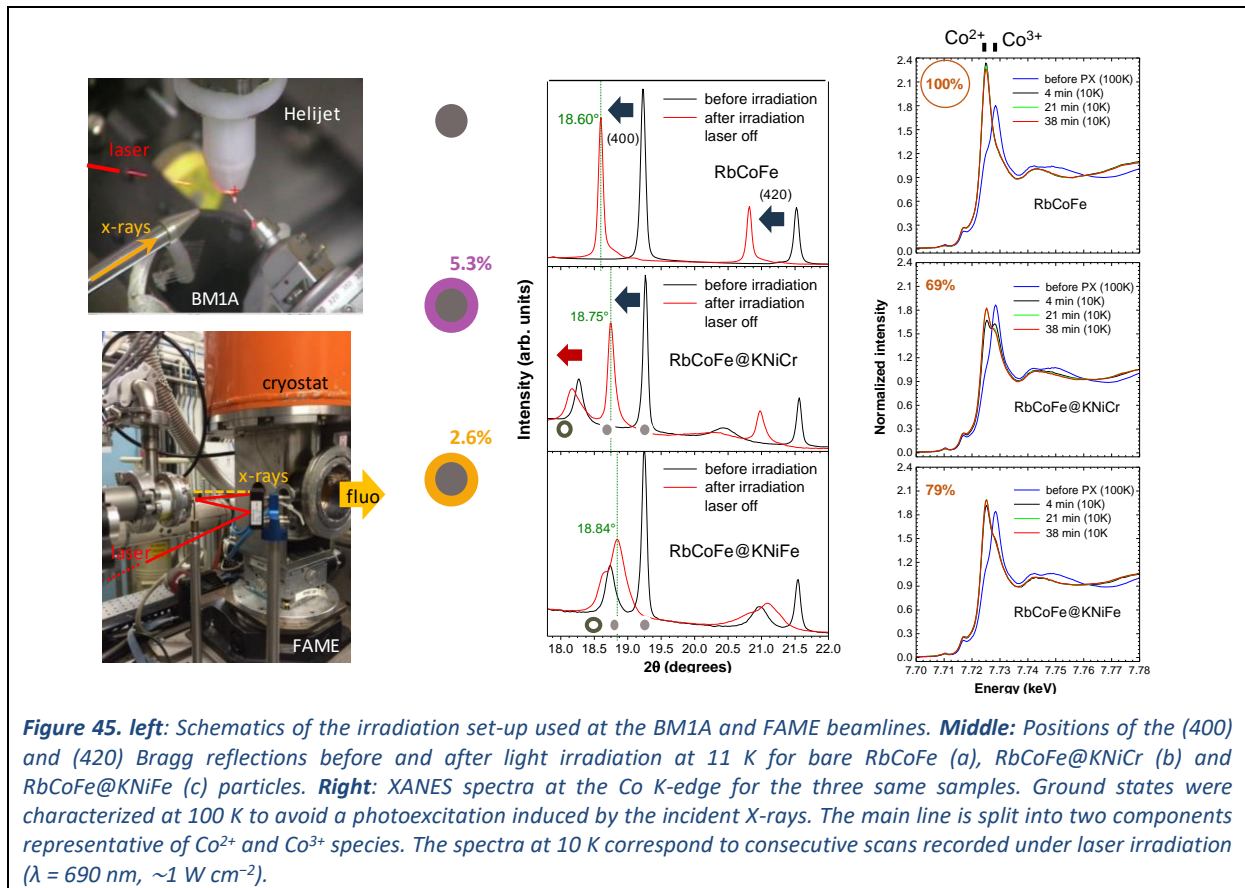
XRPD experiments show that rather large strains, up to +0.9%, are developed within the shells in response to the tensile stresses associated with the expansion of the core lattice. However, this deformation is driven by a reduced core dilatation in the case of RbCoFe@KNiFe with respect to RbCoFe@KNiCr (see Figure 45, middle). The strong asymmetry of the (400) KNiCr diffraction peak after light irradiation indicates the coexistence of crystallographic directions in tension, in compression or unchanged. This complex strain field may have multiple origins: a gradient of deformations along the normal to the interface for thick shells, the existence of biaxial rather than hydrostatic stresses, a specific response of the corners in faceted particles or the transformation of the core itself that may involve preferential nucleation of large α -parameter domains at vertices. The kinetics of these structural phase transformations are also informative on the strength of the mechanical coupling. The decrease of the intensity of the (400) Bragg peak, corresponding to the RbCoFe lattice before light exposure, suggests that a steady state is reached in about 40 to 50 min in the case of the KNiCr shell. The transformation rate is strongly increased for KNiFe (5 min). This result is supported by the time-dependent XANES spectra, for which the depth probed by the X-rays is comparable to the penetration of the laser beam. The XANES features displayed in Figure 45, right suggest no symmetry change around the Co ions after illumination for the three samples. Their evolution under continuous irradiation shows that the electron transfer rate is rather fast and all electronic changes occur within the first 4 min for RbCoFe and RbCoFe@KNiFe particles. In contrast, this transfer is slowed down in the case of RbCoFe@KNiCr and takes place over more than 20 min, in good agreement with the XRPD data.

This work showed that a tailored photo-response in terms of strain amplitude and kinetics requires a trade-off between the quality of the interface (*i.e.*, small mismatch between the core and shell lattices) and the difference of rigidity between the two compounds that is increased at large misfits. A shell rigidity comparable to that of the core actually increases the mechanical counteraction of the shell and strongly limits the core dilatation.

⁶⁹ Pajerowski *et al.*, *J. Amer. Chem. Soc.* **132**, 4058 (2010).

⁷⁰ Pajerowski *et al.*, *Chem. Mater.* **23**, 3045 (2011).

⁷¹ Risset *et al.*, *J. Amer. Chem. Soc.* **136**, 15660 (2014).



Authors and principal publication:

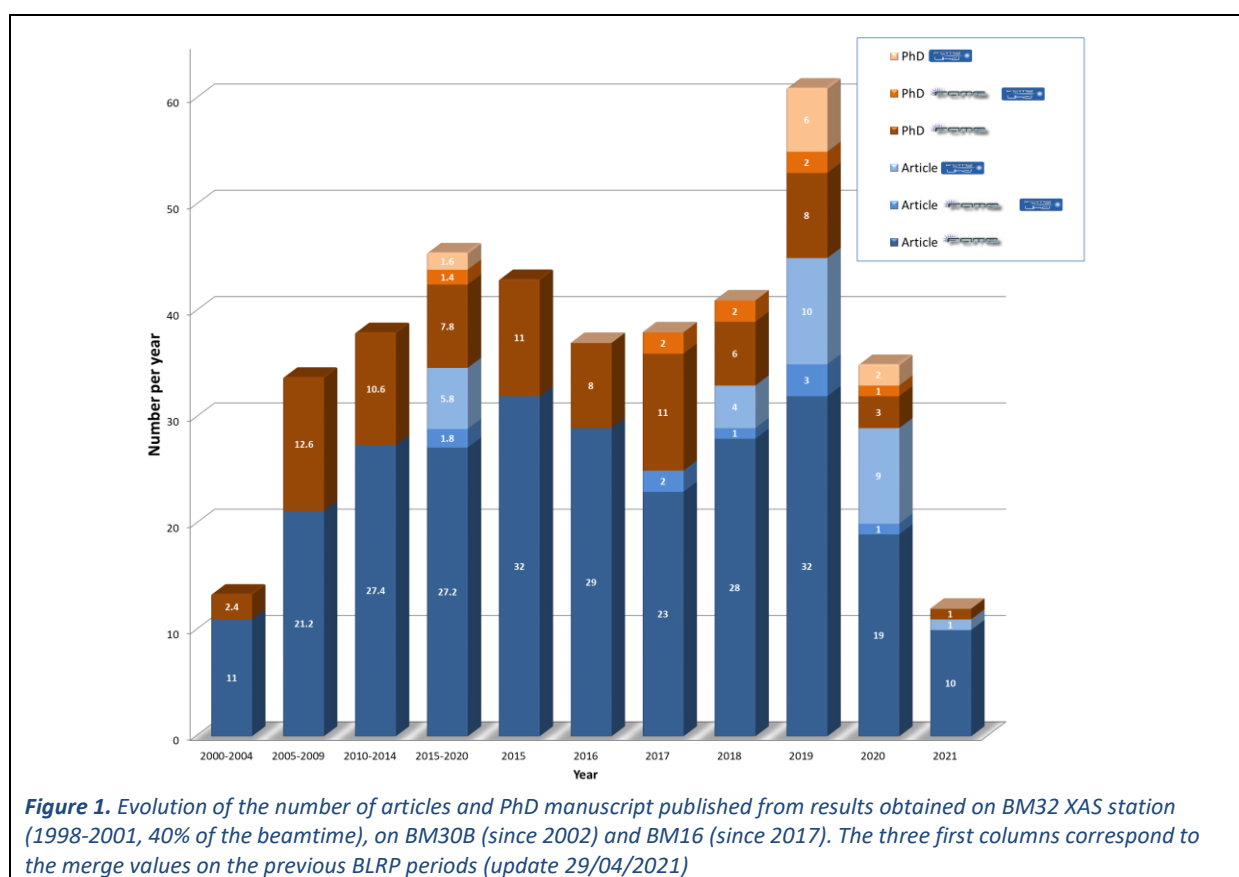
Adam A.,¹ Poggi M.,¹ Larquet E.,¹ Cortes R.,¹ Martinelli L.,¹ Coulon P.-E.,² Lahera E.,³ Proux O.,³ Chernyshov D.,⁴ Boukheddaden K.,⁵ Gacoin T.,¹ Maurin I.,¹ *Nanoscale* **10** (2018) 16030-16039.

¹ CNRS/INP - LPMC (UMR 7643 CNRS / Ecole Polytechnique) / ² Laboratoire des Solides Irradiés, Ecole polytechnique, CNRS, CEA, Univ. Paris-Saclay, / ³ BM30B/FAME beamline, ESRF / ⁴ BM31/SNBL beamline, ESRF / ⁵ Groupe d'Etude de la Matière Condensée, CNRS, Univ. de Versailles St-Quentin, Univ. Paris-Saclay

8. Scientific production 2015-2021

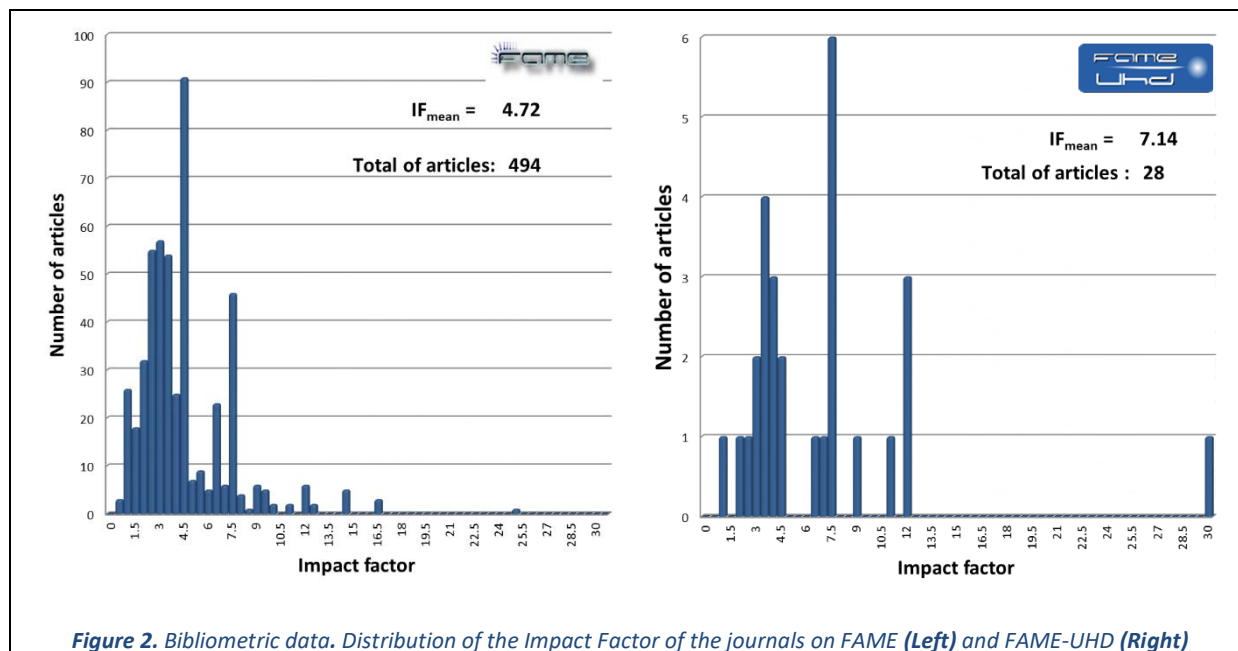
This chapter gathers the list of publications published during the BLRP period. The complete list of the publications can be found on the ESRF website on the corresponding [FAME-Biblio](#) and [FAME-UHD-Biblio](#) webpages. Moreover, bibliometric information about these articles can be obtained on the Publons pages of both beamlines.^{1,2} Finally, to better distinguish on the list the contributions of each instrument, thus performed using FAME-UHD are marked with the corresponding logo.

Evolution of the number of publications is shown on Figure 1. Since 1998, we contributed to 527 publications, 202 on the BLRP period. The number of publications is now around 27 per year on FAME. On FAME-UHD the mean number of publications is around 10 on the two last complete years. The mean impact factor is around 4.7 on FAME, 7.2 on FAME-UHD (Figure 2).

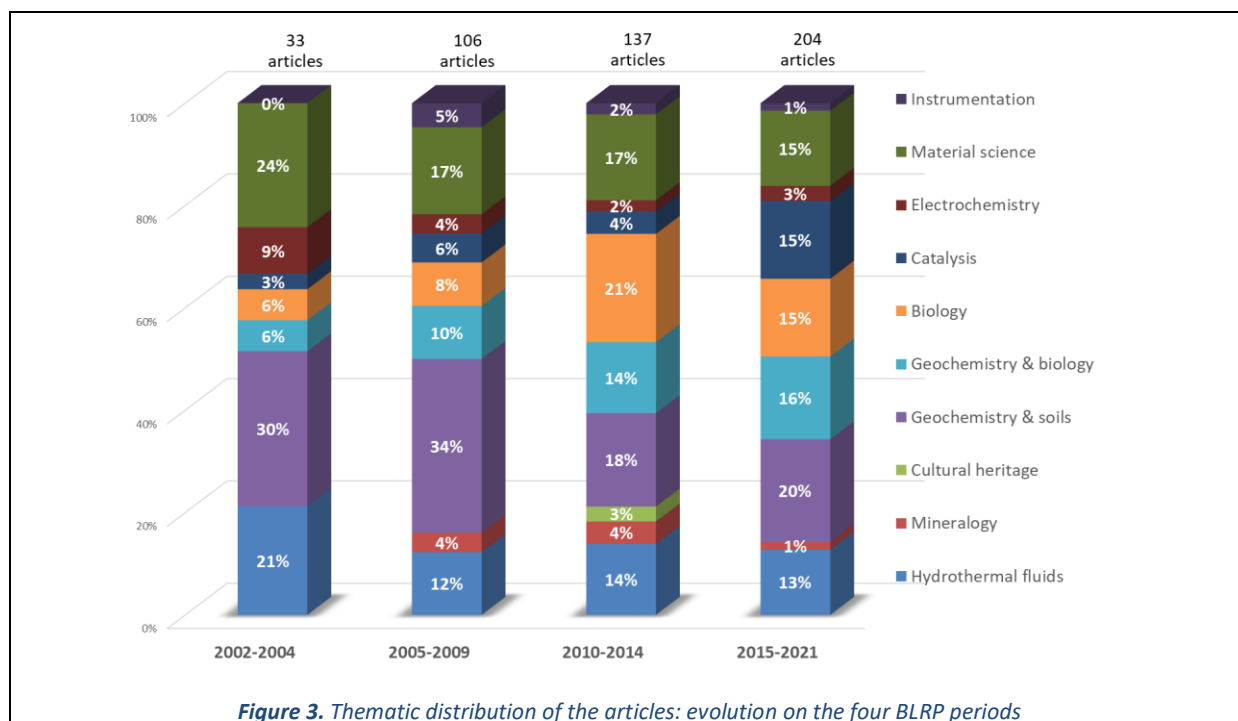


¹ <https://publons.com/researcher/2712027/beamline-fame-bm30/>

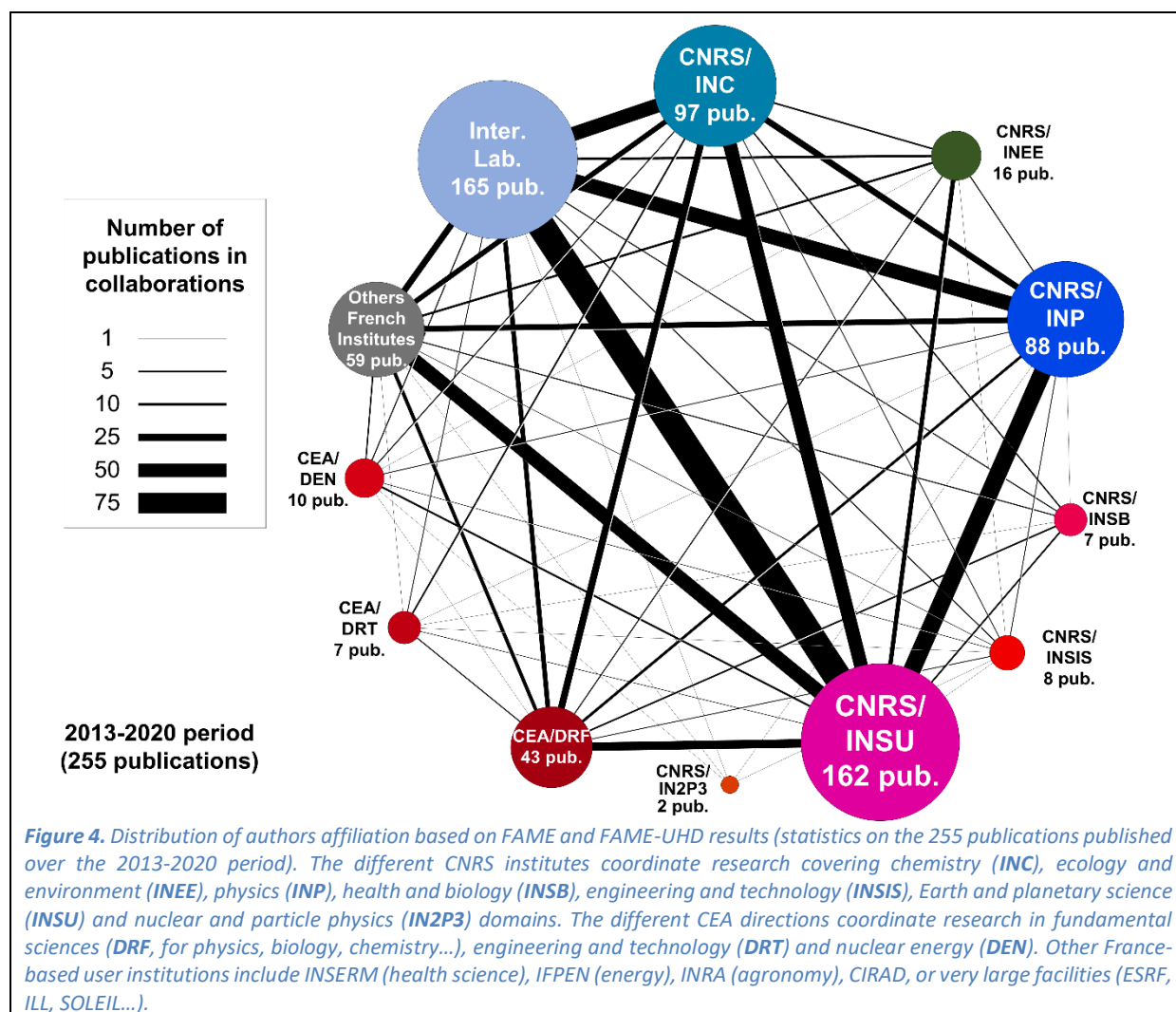
² <https://publons.com/researcher/1947069/beamline-fame-uhd-bm16/>



The variety of scientific thematics seen on the beamtime allocation is of course found in the publication thematics distribution (Figure 3), even if the ratio publication per experiment depends on the fields. In Earth science for example it needs sometimes 2 experiments for 1 publication.



Finally, we gathered on Figure 4 the number of publications as a function of the authors' affiliation, showing firstly the distribution of the scientific thematic, but secondly and more interestingly the collaborations inter-institutes. FAME and FAME-UHD platform is really an interdisciplinary place for scientists.










Articles

- 2021-1** Bobyk L., Tarantini A., Beal D., Veronesi G., Kieffer I., Motellier S., Valsami-Jones E., Lynch I., Jouneau P.-H., Pernet-Gallay K., Aude-Garcia C., Sauvaigo S., Douki T., Rabilloud T., Carriere M., "Toxicity and chemical transformation of silver nanoparticles in A549 lung cells: dose-rate-dependent genotoxic impact", *Environmental Science: Nano* (2021) <https://doi.org/10.1039/D0EN00533A>
- 2021-2** Borisova A. Y., Zagrtednov N. R., Toplis M. J., Bohrsen W. A., Nedelec A., *et al.*, "Hydrated Peridotite – Basaltic Melt Interaction Part I: Planetary Felsic Crust Formation at Shallow Depth", *Frontiers in Earth Science* **8** (2020) 84 <https://www.frontiersin.org/articles/10.3389/feart.2021.640464>
- 2021-3** Ciria M., Proietti M. G., Corredor E. C., Arnaud J. I., "Strain and dislocation blocking in Ni/Cu superlattices", *Surfaces and Interfaces* **23** (2021) 100929 <https://doi.org/10.1016/j.surfin.2021.100929>
- 2021-4** Courtois P., Rorat A., Lemiere S., Levard C., Chaurand P., Grobelak A., Lors C., Vandembulcke F., "Accumulation, speciation and localization of silver nanoparticles in the earthworm *Eisenia fetida*",





Environmental Science and Pollution Research **28** (2021) 3756–3765 <https://doi.org/10.1007/s11356-020-08548-z>

- 2021-5** Courtois P., Rorat A., Lemiere S., Guyoneaud R., Attard E., Longepierre M., Rigal F., Levard C., Chaurand P., Grosser A., Grobelak A., Kacprzak M., Lors C., Richaume A., Vandenbulcke F., “Medium-term effects of Ag supplied directly or via sewage sludge to an agricultural soil on *Eisenia fetida* earthworm and soil microbial communities”, *Chemosphere* **269** (2021) 128761 <https://doi.org/10.1016/j.chemosphere.2020.128761>
- 2021-6** Esmieu C., Balderrama-Martínez-Sotomayor R., Conte-Daban A., Iranzo O., Hureau C., “Unexpected trends in copper removal from Aβ peptide: when less ligand is better and Zn helps”, *Inorganic Chemistry* (2021) <https://doi.org/10.1021/acs.inorgchem.0c03407>
- 2021-7** Formentini T. A., Basile-Doelsch I., Legros S., Borschneck D., Venzon J. S., Pinheiro A., Fernandes C. V. S., Mallmann F. J. K., da Veiga M., Doelsch E., “Redistribution of Zn towards light-density fractions and potentially mobile phases in a long-term manure-amended clayey soil”, *Geoderma* **394** (2021) 115044 <https://doi.org/10.1016/j.geoderma.2021.115044>
- 2021-8** Hell J., Vespa P., Cabodi I., Citti O., Fournet-Fayard F., Fouletier J., Steil M. C. “Blistering phenomenon of molten glass in contact with zirconia-based refractories”, *Journal of the European Ceramic Society* (2021) <https://doi.org/10.1016/j.jeurceramsoc.2021.03.063>
- 2021-9** La Penna G., Machetti F., Proux O., Rossi G., Stellato F., Morante S., “Cu(II)-glycerol-N-ethylmorpholine complex stability revealed by X-ray spectroscopy”, *Journal of Physical Chemistry C* **125** (2021) 1483–1492 <https://dx.doi.org/10.1021/acs.jpcc.0c08676>
- 2021-10** Pokrovski G. S., Escoda C., Blanchard M., Testemale D., Hazemann J.-L., Gouy S., Kokh M. A., Boiron M.-C., de Parseval F., Aigouy T., Menjot L., de Parseval P., Proux O., Rovezzi M., Beziat D., Salvi S., Kouzmanov K., Pöttgen R., Doert T., “An arsenic-driven pump for invisible gold in hydrothermal systems”, *Geochem. Perspect. Lett.* **17** (2021) 39-44 <https://dx.doi.org/10.7185/geochemlet.2112>
-  **2021-11** Sanles Sobrido M., Bernard E., Angeletti B., Malard V., George I., Chaurand P., Uboldi C., Orsière T., Dine S., Vrel D., Rousseau B., Dinescu G., Soulas R., Herlin N., Proux O., Grisolia C., Rose J., “Oxidative transformation of tungsten (W) nanoparticles potentially released in aqueous and biological media in case of Tokamak (nuclear fusion) Lost of Vacuum Accident (LOVA)”, *Compte Rendus Géosciences* **352** (2021) 539-558 <https://doi.org/10.5802/crgeos.41>
- 2020-1** Al Abdulghani A. J., Park J.-H., Kozlov S. M., Kang D.-C., AlSabban B., Pedireddy S., Aguilar-Tapia A., Ould-Chikh S., Hazemann J.-L., Basset J.-M., Cavallo L., Takanabe K., “Methane Dry Reforming on Supported Cobalt Nanoparticles Promoted by Boron”, *Journal of Catalysis* **392** (2020) 126-134 <https://doi.org/10.1016/j.jcat.2020.09.015>
- 2020-2** Auffan M., Santaella C., Brousset L., Tella M., Morel E., Ortet P., Barakat M., Chaneac C., Issartel J., Angeletti B., Levard C., Hazemann J.-L., Wiesner M., Rose J., Thiéry A., Bottero J.-Y., “The shape and speciation of Ag nanoparticles drive their impacts on organisms in a lotic ecosystem”, *Environmental Science: Nano* **7** (2020) 3167-3177 <https://doi.org/10.1039/D0EN00442A>
- 2020-3** Auxemery A., Philippot G., Suchomel M. R., Testemale D., Aymonier C., “Stabilization of tetragonal zirconia nanocrystallites using an original supercritical-based synthesis route”, *Chemistry of Materials* **32** (2020) 8169-8181 <https://doi.org/10.1021/acs.chemmater.0c01550>
- 2020-4** Biquard X., Villora E. G., Shimamura K., Lorenz K., “XANES/EXAFS study of the Lu and Y incorporation in the single crystal Tb₃Sc₂Al₃O₁₂ Faraday rotator”, *Journal of Applied Physics* **127**, (2020) 115106 <https://doi.org/10.1063/1.5145188>
- 2020-5** Borisova A. Y., Zagrtzenov N. R., Toplis M. J., Ceuleneer G., Safonov O. L. G., Pokrovski G. S., Jochum K. P., Stoll B., Weis U., Shcheka S., Bychkov A. Y., “Hydrated peridotite – basaltic melt interaction Part II: Fast assimilation of serpentinized mantle by basaltic magma”, *Frontiers in Earth Science* **8** (2020) 84 <https://dx.doi.org/10.3389/feart.2020.00084>
- 2020-6** Bueno C. F., Ramos A., Bailly A., Mossang E., Scalvi L. V. A., “X-ray absorption spectroscopy and Eu³⁺ -emission characteristics in GaAs/SnO₂ heterostructure”, *SN Applied Sciences* **2** (2020) 1579 <https://doi.org/10.1007/s42452-020-03344-3> 




- 2020-7** Cantarano A., Testemale D., de Sousa Nobre S., Potdevin A., Bruyère R., Barbara A., Hazemann J.-L., Ibanez A., Dantelle G., “Twofold advantage of gas bubbling for the advanced solvothermal preparation of efficient YAG:Ce nanophosphors”, *J. Mater. Chem. C* **8** (2020) 9382-9390 <https://doi.org/10.1039/D0TC02347G> 
- 2020-8** Diaz-Lopez M., Chater P.A., Bordet P., Freire M., Jordy C., Lebedev O. I., Pralong V., “Li₂O:Li–Mn–O disordered rock-salt nanocomposites as cathode prelithiation additives for high-energy density Li-ion batteries”, *Advanced Energy Materials* **10** (2020) 1902788 <http://dx.doi.org/10.1002/aenm.201902788>
- 2020-9** Dupraz *et al.*, “The ThomX ICS source”, *Physics Open* **5** (2020) 100051 <https://doi.org/10.1016/j.physo.2020.100051>
- 2020-10** Fialho-Batista Ana T.; Baaziz W., Taleb A.-L., Chaniot J., Moreaud M., Legens C., Aguilar-Tapia A., Proux O., Hazemann J.-L., Diehl F., Chizallet C., Gay A.-S., Ersen O., Raybaud P., “Atomic scale insight into the formation, size and location of platinum nanoparticles supported on γ -alumina”, *ACS Catalysis* **10** (2020) 4193-4204 <https://doi.org/10.1021/acscatal.0c00042> 
- 2020-11** Filimonova O. N., Tagirov B. R., Trigub A. L., Nickolsky M. S., Rovezzi M., Belogub E. V., Reukov V. L., Vikentyev I. V., “The state of Au and As in pyrite studied by X-ray absorption spectroscopy of natural minerals and synthetic phases” *Ore Geology Reviews* **121** (2020) 103475 <https://doi.org/10.1016/j.oregeorev.2020.103475> 
- 2020-12** Finck N., “Iron speciation in Opalinus clay minerals”, *Applied Clay Science* **193** (2020) 105679 <https://doi.org/10.1016/j.clay.2020.105679>
- 2020-13** Guan Q., Mei Y., Etschmann B., Testemale D., Louvel M., Brugger J., “Yttrium complexation and hydration in chloride-rich hydrothermal fluids: a combined *ab initio* molecular dynamics and *in situ* X-ray absorption spectroscopy study” *Geochimica et Cosmochimica Acta* **281** (2020) 168-189 <https://doi.org/10.1016/j.gca.2020.04.015>
- 2020-14** Hodomihou N. R., Feder F., Legros S., Formentini T. A., Lombi E., Doelsch E., “Zinc Speciation in Organic Waste Drives Its Fate in Amended Soils”, *Environmental Science and Technology* **54** (2020) 12034-12041 <https://doi.org/10.1021/acs.est.0c02721>
- 2020-15** Isaure M.-P., Albertelli M., Kieffer I., Tucoulou R., Petrel M., Gontier E., Tessier E., Monperrus M., Goñi-Urriza M., “Relationship between Hg speciation and Hg methylation/demethylation processes in the sulfate-reducing bacterium *Pseudodesulfovibrio hydrargyri*: evidences from HERFD XANES and nano-XRF”, *Frontiers in microbiology* **11** (2020) 584715 <https://doi.org/10.3389/fmicb.2020.584715> 
- 2020-16** Le Gall C., Audubert F., Léchelle J., Pontillon Y., Hazemann J.-L., “Contribution to the study of fission products release from nuclear fuels in severe accident conditions: effect of the pO₂ on Cs, Mo and Ba speciation”, *Eur. J. Phys. N* **6** (2020) 2 <https://doi.org/10.1051/epjn/2019058> 
- 2020-17** Liu W., Etschmann B.E., Mei Y., Guan Q., Testemale D., Brugger J., “The role of sulfur in molybdenum transport in hydrothermal fluids: insight from *in situ* synchrotron XAS experiments and molecular dynamics simulations”, *Geochimica et Cosmochimica Acta* **290** (2020) 162-179 <https://doi.org/10.1016/j.gca.2020.08.003>
- 2020-18** Louvel M., Cadoux A., Brooker R., Proux O., Hazemann J.-L., “New insights on Br speciation in volcanic glasses and structural controls on halogens degassing”, *American Mineralogist* **105** (2020) 795-802 <https://dx.doi.org/10.2138/am-2020-7273> 
- 2020-19** Maurer, F., Jelic, J., Wang, J. Gänzler A., Dolcet P., Wöll C., Wang Y., Studt F., Casapu M., Grunwaldt J.-D., “Tracking the formation, fate and consequence for catalytic activity of Pt single sites on CeO₂”, *Nature Catalysis* **3** (2020) 824-833 <https://doi.org/10.1038/s41929-020-00508-7> 
- 2020-20** Paleo C., Dupuis V., Wilhelm F., Rogalev A., Proux O., Boisron O., Kieffer I., Epicier T., Bugnet M., Le Roy D., “Interplay between local structure and magnetic properties of graded exchange-coupled Co@FePt nanocomposite films”, *Physical Review B* **102** (2020) 224409 <https://doi.org/10.1103/PhysRevB.102.224409>

- 2020-21** Patriarca M., Daier V., Camí G., Rivière E., Hureau C., Signorella S., "Preparation, characterization and activity of CuZn and Cu₂ superoxide dismutase mimics encapsulated in mesoporous silica", *Journal of Inorganic Biochemistry* **207** (2020) 111050 <https://doi.org/10.1016/j.jinorgbio.2020.111050>
- 2020-22** Piccolo L., Afanasiev P., Len T., Dessal C., Morfin F., Rousset J.-L., Aouine M., Bourgain F., Aguilar-Tapia A., Proux O., Soler L., Llorca J., "Operando X-ray absorption spectroscopy investigation of photocatalytic hydrogen evolution over ultradispersed Pt/TiO₂ catalysts", *ACS Catalysis* **10** (2020) 12696–12705 <https://doi.org/10.1021/acscatal.0c03464>
- 2020-23** Pustovarenko A., Dikhtiarenko A., Bavykina A., Gevers L. E., Ramirez A., Russkikh A., Telalovic S., Aguilar A., Hazemann J.-L., Ould-Chikh S., Gascon J., "Metal organic framework derived synthesis of cobalt indium catalysts for the hydrogenation of CO₂ to methanol", *ACS Catalysis* **10** (2020) 5064–5076 <https://doi.org/10.1021/acscatal.0c00449>
- 2020-24** Salzano G., Brennich M., Mancini G., Tran T. H., Legname G., D'Angelo P., Giachin G., "Deciphering copper coordination in the mammalian prion protein amyloidogenic domain", *Biophysical Journal* **118** (2020) 676-687 <https://doi.org/10.1016/j.bpj.2019.12.025>
- 2020-25** Stetten L., Lefebvre P., Le Pape P., Mangeret A., Blanchart P., Merrot P., Brest J., Julien A., Bargar J.R., Cazala C., Morin G., "Experimental redox transformations of uranium phosphate minerals and mononuclear species in a contaminated wetland", *Journal of Hazardous Materials* **384** (2020) 121362 <https://doi.org/10.1016/j.jhazmat.2019.121362>
- 2020-26** Sutton S.R., Lanzirotti A., Newville M., Dyar M.D., Delaney J. "Oxybarometry and valence quantification based on microscale X-ray absorption fine structure (XAFS) spectroscopy of multivalent elements", *Chem. Geol.* **531** (2020) 119305 <http://dx.doi.org/10.1016/j.chemgeo.2019.119305>
- 2020-27** Thomas S.A., Mishra B., Myneni S.C.B., "Cellular mercury coordination environment, and not cell surface ligands, influence bacterial methylmercury production", *Environmental Science and Technology* **54** (2020) 3960-3968 <https://doi.org/10.1021/acs.est.9b05915>
- 2020-28** Vehmas T., Montoya V., Cruz Alonso M., Vašiček R., Rastrick E., Gaboreau S., Večerník P., Leivo M., Holt E., Fink N., Mouheb N. A. Svoboda J., Read D., Červinka R., Vasconcelos R., Corkhill C., "Characterization of Cebama –Low-pH Reference Concrete and assessment of its alteration with representative waters in Radioactive Waste Repositories", *Applied Geochemistry* **121** (2020) 104703 <https://doi.org/10.1016/j.apgeochem.2020.104703>
- 2020-29** Zhang K., Cha J. H., Jeon S. Y., Kirlikovali K. O., Ostadhassan M., Rasouli V., Farha O Jang H. W., Varma R. J., Shokouhimehr M., "Pd modified prussian blue frameworks: Multiple electron transfer pathways for improving catalytic activity toward hydrogenation of nitroaromatics", *Molecular Catalysis* **492** (2020) 110967 <https://doi.org/10.1016/j.mcat.2020.110967>
- 2019-1** Afanasiev P., Lorentz C. "Oxidation of nanodispersed MoS₂ in ambient air: the products and the mechanistic steps", *J. Phys. Chem. C* **123** (2019) 7486–7494 <https://doi.org/10.1021/acs.jpcc.9b01682>
- 2019-2** Alfano M., Veronesi G., Musiani F., Zambelli B., Signor L., Proux O., Rovezzi M., Ciurli S., Cavazza C., "A solvent-exposed cysteine forms a peculiar Ni(II)-binding site in the metallochaperone CooT from *Rhodospirillum rubrum*", *Chemistry - A European Journal* **25** (2019) 15351-15360 <http://dx.doi.org/10.1002/chem.201903492>
- 2019-3** Aljuhani M. A., Zhang Z., Barman S., El Eter M., Failvene L., Ould-Chikh S., Guan E., Abou-Hamad E., Emwas A.-H., Pelletier J. D. A., Gates B. C., Cavallo L., Basset J.-M., "Mechanistic Study of Hydroamination of Alkyne through Tantalum-Based Silica-Supported Surface Species", *ACS Catalysis* **9** (2019) 8719-87254 <https://doi.org/10.1021/acscatal.9b02184>
- 2019-4** Ardiccioni C., Arcovito A., Della Longa S., van der Linden P., Bourgeois D., Weik M., Celeste Montemiglio L., Savino C., Avella G., Exertier C., Carpentier P., Prangé T., Brunori M., Colloc'h N., Vallone B., "Ligand pathways in neuroglobin revealed by low-temperature photodissociation and docking experiments", *IUCrJ* **6** (2019) 832-842 <https://doi.org/10.1107/S2052252519008157>

- 2019-5** Atrián-Blasco E., Cerrada E., Faller P., Laguna M., Hureau C., "Role of PTA in the prevention of Cu(amyloid- β) induced ROS formation and amyloid- β oligomerisation in the presence of Zn", *Metalomics* **11** (2019) 1154-1161 <http://dx.doi.org/10.1039/C9MT00011A>
- 2019-6** Bau J. A., Haspel H., Ould-Chikh S., Aguilar-Tapia A., Hazemann J.-L., Idriss H., Takanahe K., "On the reconstruction of NiMo electrocatalysts by operando spectroscopy", *Journal of Materials Chemistry A* **7** (2019) 1531-1535 <http://dx.doi.org/10.1039/C9TA04494A>
- 2019-7** Bavykina A., Yarulina I., Al Abdulghani A. J., Gevers L. E., Hedhili M. N., Miao X.-H., Ramirez A., Pustovarenko A., Dikhtiarenko A., Cadiou A., Aguilar Tapia A., Hazemann J.-L., Kozlov S. M., Ould-Chikh S., Cavallo L., Gascon J., "Turning a methanation Co catalyst into an In-Co methanol producer", *ACS Catalysis* **9** (2019) 6910-6918 <https://doi.org/10.1021/acscatal.9b01638>
- 2019-8** Bernard E., Jambon F., Georges I., Sanles Sobrido M., Rose J., Herlin-Boime N., Miserque F., Beaunier P., Vrel D., Dine S., Hodille E., Chêne J., Garcia-Argote S., Pieters G., Peillon S., Gensdarmes F., Dinescu G., Acsente T., Uboldi C., Orsiere T., Malard V., Rousseau B., Delaporte P., Grisolia C., "Design of model tokamak particles for future toxicity studies: Morphology and physical characterization", *Fusion Eng. Des.* **145** (2019) 60-65 <https://doi.org/10.1016/j.fusengdes.2019.05.037>
- 2019-9** Bissardon C., Proux O., Bureau S., Suess E., Winkel L. H. E., Conlan R. S., Francis L. W., Kahn I. L., Charlet L., Hazemann J.-L., Bohic S., "Sub-ppm high energy resolution fluorescence detected X-ray absorption spectroscopy of selenium in articular cartilage", *Analyst* **144** (2019) 3488-3493 <https://dx.doi.org/10.1039/C9AN00207C>
- 2019-10** Crede L.-S., Liu W., Evans K. A., Rempel K. U., Testemale D., Brugger J., "Crude oil as ore fluids: An experimental in-situ XAS study of gold partitioning between brine and organic fluid from 25 to 250°C", *Geochim. Cosmochim. Acta* **224** (2019) 352-365 <https://doi.org/10.1016/j.gca.2018.10.007>
- 2019-11** Dalzon B., Guidetti M., Testemale D., Reymond S., Proux O., Vollaire J., Collin-Faure V., Testard I., Fenel D., Schoehn G., Arnaud J., Carrière M., Josserand V., Rabilloud T., Aude-Garcia C., "Utility of macrophages in an antitumor strategy based on the vectorization of iron oxide nanoparticles", *Nanoscale* **11** (2019) 9341-9352 <http://dx.doi.org/10.1039/c8nr03364a>
- 2019-12** Dantelle G., Boulon G., Guyot Y., Testemale D., Guzik M., Kurosawa S., Kamada K., Yoshikawa A., "Research of efficient fast scintillators. Evidence and XANES characterization of Ce⁴⁺ in Ce³⁺, Mg²⁺-co-doped Gd₃Al₂Ga₃O₁₂ garnet crystals", *Physica Status Solidi B* (2019) <https://doi.org/10.1002/pssb.201900510>
- 2019-13** De Santis E., Shardlow E., Stellato F., Proux O., Rossi G., Exley C., Morante S., "XAS measurements of Cu-ProIAPP complexes at physiological concentrations", *Condensed Matter* **4** (2019) 13 <http://dx.doi.org/10.3390/condmat4010013>
- 2019-14** Domergue J., Pécaut J., Proux O., Lebrun C., Gateau C., Le Goff A., Maldivi P., Duboc C., Delangle P., "A Ni-SOD mimic with a S3O coordination sphere based on a tripodal cysteine-rich ligand: pH tuning of the SOD activity", *Inorganic Chemistry* **58** (2019) 12775-12785 <https://doi.org/10.1021/acs.inorgchem.9b01686>
- 2019-15** Dupuis V., Khadra G., Montejano-Carrizales J. M., Tournus F., Aguilera-Granja F., Tamion A., "Mass-Selected FeCo Clusters Embedded in Carbon Matrix as Benchmark Nano-Catalysts", *ACS Appl. Nano Mater.* **5** (2019) 2864-2872 <http://dx.doi.org/10.1021/acsanm.9b00313>
- 2019-16** Faye Nd D., Biquard X., Nogales E., Felizardo M., Peres M., Redondo-Cubero A., Auzelle T., Daudin B., Tizei L. H. G., Kociak M., Ruterana P., Moeller W., Mendez B., Alves E., Lorenz K., "Incorporation of Europium Into GaN Nanowires by Ion Implantation", *J. Phys. Chem. C* **123** (2019) 11874-11887 <http://dx.doi.org/10.1021/acs.jpcc.8b12014>
- 2019-17** Finck N., Schlegel M. L., Dardenne K., Adam C., Kraft S., Bauer A., Robert J.-L., "Structural iron in smectites with different charge locations", *Physical and Chemistry of Minerals* **46** (2019) 639-661 <https://doi.org/10.1007/s00269-019-01028-y>
- 2019-18** Garenne A., Beck P., Montes-Hernandez G., Bonal L., Quirico E., Proux O., Hazemann J.-L., "The iron record of asteroidal processes in carbonaceous chondrites", *Meteoritics & Planetary Science* **54** (2019) 2652-2665 <http://dx.doi.org/10.1111/maps.13377>

- 2019-19** Gelly R., Fekiacova Z., Guihou A., Doelsch E., Deschamps P., Keller C., "Lead, zinc, and copper redistributions in soils along a deposition gradient from emissions of a Pb-Ag smelter decommissioned 100 years ago", *Science of The Total Environment* **665** (2019) 502-512 <https://doi.org/10.1016/j.scitotenv.2019.02.092>
- 2019-20** Hajji S., Montes-Hernandez G., Sarret G., Tordo A., Morin G., Ona-Nguema G., Bureau S., Turki T., Mzoughi N., "Arsenite and chromate sequestration onto ferrihydrite, siderite and goethite nanostructured minerals: Isotherms from flow-through reactor experiments and XAS measurements", *J. Haz. Mat.* **362** (2019) 358-367 <https://doi.org/10.1016/j.jhazmat.2018.09.031>
- 2019-21** Ingrao N.J., Hammouda T., Boyet M., Gaborieau M., Moine B.N., Vlastelic I., Bouhifd M.A., Devidal J.-L., Mathon O., Testemale D., Hazemann J.-L., Proux O., "Rare Earth elements partitioning between sulphides and melt: Evidence for Yb²⁺ and Sm²⁺ in EH chondrites", *Geochimica et Cosmochimica Acta* **265** (2019) 182-197 <https://doi.org/10.1016/j.gca.2019.08.036> 
- 2019-22** Jeantelot G., Qureshi M., Harb M., Ould-Chikh S., Anjum D. H., Abou-Hamad E., Aguilar Tapia A., Hazemann J.-L., Takanabe K., Basset J.-M., "TiO₂-supported Pt single atoms by surface organometallic chemistry for photocatalytic hydrogen evolution", *Phys. Chem. Chem. Phys.* **21** (2019) 24429-24440 <https://doi.org/10.1039/C9CP04470A> 
- 2019-23** Kavčič A., Mikuš K., Debeljak M., Teun van Elteren J., Arčon I., Kodre A., Kump P., Germanos Karydas A., Migliori A., Czyzycki M., Vogel-Mikuš K., "Localization, ligand environment, bioavailability and toxicity of mercury in *Boletus spp.* and *Scutiger pes-caprae* mushrooms", *Ecotoxicology and Environmental Safety* **184** (2019) 109623 <https://doi.org/10.1016/j.ecoenv.2019.109623>
- 2019-24** Layet C., Santaella C., Auffan M., Chevassus-Rosset C., Montes M., Levard C., Ortet P., Barakat M., Doelsch E., "Phytoavailability of silver at predicted environmental concentrations: does the initial ionic or nanoparticulate form matter?", *Environmental Science: Nano* **6** (2019) 127-135 <http://dx.doi.org/10.1039/C8EN00644J>
- 2019-25** Lozano A., Fernandez-Martinez A., Ayora C., Di Tommaso D., Poulain A., Rovezzi M., Marini C., "Solid and aqueous speciation of yttrium in passive remediation systems of acid mine drainage", *Environ. Sci. Technol.* **53** (2019) 11153-11161 <https://doi.org/10.1021/acs.est.9b01795>
- 2019-26** Merrot P., Juillot F., Noël V., Lefebvre P., Brest J., Menguy N., Guigner J.-M., Blondeau M., Viollier E., Fernandez J.-M., Moreton B., Barga J., Morin G., "Nickel and iron partitioning between clay minerals, Fe-oxides and Fe-sulfides in lagoon sediments from New Caledonia", *Science of The Total Environment* **689** (2019) 1212-1227 <https://doi.org/10.1016/j.scitotenv.2019.06.274>
- 2019-27** Patriarca M., Daier V., Camí G., Pellegrini N., Rivièrè E., Hureau C., Signorella S., "Biomimetic Cu, Zn and Cu₂ complexes inserted in mesoporous silica as catalysts for superoxide dismutation", *Micropor. Mesopor. Mat.* **279** (2019) 133-141 <https://doi.org/10.1016/j.micromeso.2018.12.027>
- 2019-28** Pokrovski G.S., Kokh M.A., Proux O., Hazemann J.-L., Bazarkina E., Testemale D., Escoda C., Boiron M.-C., Blanchard M., Aigouy T., Gouy S., de Parseval P., Thibaut M., "The nature and partitioning of invisible gold in the pyrite-fluid system", *Ore Geology Reviews* **109** (2019) 545-563 <https://doi.org/10.1016/j.oregeorev.2019.04.024>
- 2019-29** Qureshi Z. S., Garcia-Esparza A. T., Jeantelot G., Ould-Chikh S., Aguilar-Tapia A., Hazemann J.-L., Basset J.-M., Loffreda D., Le Bahers T., Takanabe K., "Catalytic consequences of ultrafine Pt clusters supported on SrTiO₃ for photocatalytic overall water splitting", *Journal of Catalysis* **109** (2019) 545-563 <https://doi.org/10.1016/j.jcat.2019.06.045> 
- 2019-30** Ramirez A., Ould-Chikh S., Gevers L., Dutta Chowdhury A., Abou Hamad E., Aguilar-Tapia A., Hazemann J.-L., Wehbe N., Al Abdulghani A., Kozlov S., Cavallo L., Gascon J., "Tandem conversion of CO₂ to valuable hydrocarbons in highly concentrated potassium iron catalysts", *ChemCatChem* **11** (2019) 2879-2886 <http://dx.doi.org/10.1002/cctc.201900762> 
- 2019-31** Resende J., Chaix-Pluchery O., Rovezzi M., Malier Y., Renevier H., Duy Nguyen N., Deschanvres J.-L., Jiménez C., "Resilience of cuprous oxide under oxidizing thermal treatments via magnesium doping", *J. Phys. Chem. C* **123** (2019) 8663-8670 <http://dx.doi.org/10.1021/acs.jpcc.9b00408>

- 2019-32** Sarret G., Guédron S., Acha D., Bureau S., Arnaud-Godet F., Tisserand D., Goni-Urriza M., Gassie C., Duwig C., Proux O., Aucour A.-M., "Extreme variability in As bioaccumulation factor in Lake Titicaca, Bolivia", *Scientific Reports* **9** (2019) 10626 <https://doi.org/10.1038/s41598-019-47183-8>
- 2019-33** Sayen S., Rocha C., Silva C., Vulliet E., Guillon E., Almeida M. R., "Enrofloxacin and copper plant uptake by *Phragmites australis* from a liquid digestate: Single versus combined application", *Science of The Total Environment* **664** (2019) 188-202 <https://doi.org/10.1016/j.scitotenv.2019.01.134>
- 2019-34** Stellato F., Chiaraluce R., Consalvi V., De Santis E., La Penna G., Proux O., Rossi G., Morante S., "Dealing with Cu reduction in X-ray Absorption Spectroscopy experiments", *Metallomics* **11** (2019) 1401-1410 <https://doi.org/10.1039/C9MT00110G>
- 2019-35** Sun X., Wang R., Ould-Chikh S., Osadchii D., Li G., Aguilar-Tapia A., Hazemann J.-L., Kapteijn F., Gascon J., "Structure-activity relationships in metal organic framework derived mesoporous nitrogen-doped carbon containing atomically dispersed iron sites for CO₂ electrochemical reduction", *Journal of Catalysis* **378** (2019) 320-330 <https://doi.org/10.1016/j.jcat.2019.09.013>
- 2019-36** Tarantini A., Wegner K.-D., Dussert F., Sarret G., Beal D., Mattera L., Lincheneau C., Proux O., Boutry D., Moriscot C., Gallet B., Jouneau P.-H., Reiss P., Carrière M., "Physicochemical alterations and toxicity of InP alloyed quantum dots aged in environmental conditions: a safer by design evaluation", *NanoImpact* **14** (2019) 100168 <https://doi.org/10.1016/j.impact.2019.100168>
- 2019-37** Thomas S.A., Mishra B., Myneni S.C.B., "High Energy Resolution (HR)-XANES Spectroscopy Reveals Zn Ligation in Whole Cell Bacteria", *Journal of Physical Chemistry Letters* **10** (2019) 2585-2592 <http://dx.doi.org/10.1021/acs.jpcllett.9b01186>
- 2019-38** Thomas S.A., Catty P., Hazemann J.-L., Michaud-Soret I., Gaillard J.-F., "The role of cysteine and sulfide in the interplay between microbial Hg(II) uptake and sulfur metabolism", *Metallomics* **11** (2019) 1219-1229 <http://dx.doi.org/10.1039/C9MT00077A>
- 2019-39** Vollmer I., Kosinov N., Szécsényi A., Li G., Yarulina I., AbouHamad E., Gurinov A., Ould-Chikh S., Aguilar-Tapia A., Hazemann J.-L., Pidko E., Hensen E., Kapteijn F., Gascon J., "A site-sensitive quasi-in situ strategy to characterize Mo/HZSM-5 during activation", *Journal of Catalysis* **370** (2019) 321-331 <https://doi.org/10.1016/j.jcat.2019.01.013>
- 2019-40** Vollmer I., Ould-Chikh S., Aguilar-Tapia A., Li G., Pidko E., Hazemann J.-L., Kapteijn F., Gascon J., "Activity descriptors derived from comparison of Mo and Fe as active metal for methane conversion to aromatics", *Journal of the American Chemical Society* **141** (2019) 18814-18824 <https://doi.org/10.1021/jacs.9b09710>
- 2019-41** Werghi B., Bendjeriou-Sedjerari A., Jedidi A., Morlanes N., Abou-Hamad E., Bhatte K., Guan E., Ma T., Aguilar-Tapia A., Ould-Chikh S., Cavallo L., Gates B. C., Basset J.-M., "Tungsten catalyst incorporating a well-defined tetracoordinated aluminum surface ligand for selective metathesis of propane, [(≡Si-O-Si≡)(≡Si-O-)2Al-O-W(≡CtBu) (H)2]", *ChemCatChem* **11** (2019) 614-620 <https://doi.org/10.1002/cctc.201801779>
- 2019-42** Xing Y., Etschmann B.E., Liu W., Mei Y., Shvarov Y., Testemale D., Tomkins A., Brugger J., "The role of fluorine in hydrothermal mobilization and transportation of Fe, U and REE and the formation of IOCG deposits", *Chem. Geol.* **504** (2019) 158-176 <https://doi.org/10.1016/j.chemgeo.2018.11.008>
- 2019-43** Tamrat W. Z., Rose J., Grauby O., Doelsch E., Levard C., Chaurand P., Basile-Doelsch I., "Soil organo-mineral associations formed by co-precipitation of Fe, Si and Al in presence of organic ligands", *Geochim. Cosmochim. Acta* **260** (2019) 15-28 <https://doi.org/10.1016/j.gca.2019.05.043>
- 2019-44** Zeyen N., Benzerara K., Menguy N., Brest J., Templeton A. S., Webb S. M., Gérard E., Moreira D., López-García P., Tavera R., Morin G., "Fe-bearing phases in modern lacustrine microbialites from Mexico", *Geochim. Cosmochim. Acta* **253** (2019) 201-230 <https://doi.org/10.1016/j.gca.2019.03.021>
- 2019-45** Zhang K., Lee T. H., Bubach B., Ostadhassan M., Jang H. W., Choi J.-W., Shokouhimehr M., "Layered metal-organic framework based on tetracyanonickelate as a cathode material for in situ Li-ion storage", *RSC Advances* **37** (2019) 21363-21370 <https://doi.org/10.1039/C9RA03975A>
- 2018-1** Adam A., Poggi M., Larquet E., Cortes R., Martinelli L., Coulon P.-E., Lahera E., Proux O., Chernyshov D., Boukheddaden K., Gacoin T., Maurin I., "Strain engineering of photo-induced phase

- transformations in Prussian blue analogue heterostructures”, *Nanoscale* **10** (2018) 16030-16039 <http://dx.doi.org/10.1039/C8NR03597K>
- 2018-2** Aguilar-Tapia A., Ould-Chikh S., Lahera E., Prat A., Delnet W., Proux O., Kieffer I., Basset J.-M., Takanahe K., Hazemann J.-L., “A new high temperature reactor for *operando* XAS: application for the dry reforming of methane over Ni/ZrO₂ catalyst” *Review of Scientific Instruments* **89** (2018) 035109 <https://doi.org/10.1063/1.4998929>
- 2018-3** Al-Shareef R., Harb M., Saih Y., Ould-Chikh S., Roldan M. A., Anjum D. H., Guyonnet E., Candy J.-P., Jan D.-Y., Abdo S. F., Aguilar-Tapia A., Proux O., Hazemann J.-L., Basset J.-M., “Understanding of the structure activity relationship of PtPd bimetallic catalysts prepared by Surface organometallic chemistry and ion exchange during the reaction of iso-butane with hydrogen” *Journal of Catalysis* **363** (2018) 34-51 <https://doi.org/10.1016/j.jcat.2018.04.009>
- 2018-4** Aliès B., Borghesani V., Noël S., Sayen S., Guillon E., Testemale D., Faller P., Hureau C., “Mutation of histidine 13 to arginine but also of arginine 5 to glycine are responsible for the different coordination sites of Zn(II) to human and murine peptides”, *Chemistry – A European Journal* **24** (2018) 14233-14241 <http://dx.doi.org/10.1002/chem.201802759>
- 2018-5** Aljuhani M. A., Barman S., Abou-Hamad E., Gurinov A., Ould-Chikh S., Guan E., Jedidi A., Cavallo L., Gates B. C., Pelletier J. D. A., Basset J.-M., “Imine metathesis catalyzed by a silica-supported hafnium imido complex”, *ACS Catalysis* **8** (2018) 9440-9446 <http://dx.doi.org/10.1021/acscatal.8b01395>
- 2018-6** Bonnot C. A., Gélabert A., Louvat P., Morin G., Proux O., Benedetti M. F., “Trace metals dynamics under contrasted land uses: contribution of statistical, isotopic and EXAFS approaches”, *Environmental Science and Pollution Research* **25** (2018) 23383–23403 <http://dx.doi.org/10.1007/s11356-016-6901-0>
- 2018-7** Chaurand P., Liu W., Borschneck D., Levard C., Auffan M., Paul E., Collin B., Kieffer I., Lanone S., Rose J., Perrin J., “Multi-scale X-ray computed tomography to detect and localize metal-based nanomaterials in lung tissues of in vivo exposed mice” *Scientific Reports* **8** (2018) 4408 <http://dx.doi.org/10.1038/s41598-018-21862-4> 
- 2018-8** Ciria M., Proietti M. G., Corredor E. C., Coffey D., Begué A., de la Fuente C., Arnaudas J. I., Ibarra A., “Crystal structure and local ordering in epitaxial Fe_{100-x}Ga_x/MgO(001) films”, *Journal of Alloys and Compounds* **767** (2018) 905-914 <https://doi.org/10.1016/j.jallcom.2018.07.120>
- 2018-9** Conte-Daban A., Beyler M., Tripiet R., Hureau C., “Kinetic is crucial when targeting copper ions to fight Alzheimer's disease: an illustration with azamacrocyclic ligands”, *Chemistry – A European Journal* **24** (2018) 8447 – 8452 <http://dx.doi.org/10.1002/chem.201801520>
- 2018-10** Dantelle G., Testemale D., Homeyer E., Cantarano A., Kodjikian S., Dujardin C., Hazemann J.-L., Ibanez A., “A new solvothermal method for the synthesis of size-controlled YAG:Ce single-nanocrystals”, *RSC Advances* **8** (2018) 26857-26870 <http://dx.doi.org/10.1039/C8RA05914D> 
- 2018-11** Diaz-Lopez M., Freire M., Joly Y., Colin C. V., Fischer H. E., Blanc N., Boudet N., Pralong V., Bordet P., “Local structure and lithium diffusion pathways in Li₄Mn₂O₅ high capacity cathode probed by total scattering and XANES”, *Chemistry of Materials* **30** (2018) 3060-3070 <http://dx.doi.org/10.1021/acs.chemmater.8b00827>
- 2018-12** Diaz-Lopez M., Joly Y., Freire M., Colin C., Proux O., Pralong V., Bordet P., “Operando X-ray Absorption Spectroscopy and emission K $\beta_{1,3}$ study of the manganese redox activity in Li₄Mn₂O₅ high capacity cathode”, *Journal of Physical Chemistry C* **122** (2018) 29586–29597 <http://dx.doi.org/10.1021/acs.jpcc.8b09397> 
- 2018-13** Dupuis V., Hillion A., Robert A., Loiselet O., Khadra G., Capiod P., Albin C., Boisron O., Le Roy D., Bardotti L., Tournus F., Tamion A., “Bottom-up strategies for the assembling of magnetic systems using nanoclusters”, *J. Nanoparticle Res.* **20** (2018) 128 <https://doi.org/10.1007/s11051-018-4189-3>
- 2018-14** Etschmann B.E., Mei Y., Liu W., Shermann D., Testemale D., Müller H., Rae N., Kappen P., Brugger J., “The role of Pb(II) complexes in hydrothermal mass transfer: An X-ray absorption spectroscopic study”, *Chemical Geology* **502** (2018) 88-106 <https://doi.org/10.1016/j.chemgeo.2018.10.022>

- 2018-15** Eymard-Vernain E., Lelong C., Pradas del Real A., Soulas R. Bureau S., Tardillo Suarez V., Gallet B., Proux O., Castillo-Michel H., Sarret G., "Impact of a model soil microorganism and of its secretome on the fate of silver nanoparticles", *Environ. Sci. Technol.* **52** (2018) 71-78 <http://dx.doi.org/10.1021/acs.est.7b04071>
- 2018-16** Eymard-Vernain E., Coute Y., Adrait A., Rabilloud T., Sarret G., Lelong C., "The poly-gamma-glutamate of *Bacillus subtilis* interacts specifically with silver nanoparticles", *Plos One* **13** (2018) e0197501 <https://doi.org/10.1371/journal.pone.0197501>
- 2018-17** Garad H., Usmani S., Barral D., David P., Cagnon L., Testemale D., Mannix D., Fettar F., Proux O., Rosa A., Mathon O., Paskarelli S., "Influence of the pore diameter in Cu/Co/Cu antidotes: XANES study", *Phys. Rev. Mat.* **2** (2018) 066001 <https://doi.org/10.1103/PhysRevMaterials.2.066001>
- 2018-18** Le Bars M., Legros S., Levard C., Chaurand P., Tella M., Rovezzi M., Browne P., Rose J., Doelsch E., "Drastic change in zinc speciation during anaerobic digestion and composting: instability of nano-sized zinc sulfide", *Environ. Sci. Technol.* **52** (2018) 12987–12996 <http://dx.doi.org/10.1021/acs.est.8b02697>
- 2018-19** Maity N., Barman S., Minenkov Y., Ould-Chikh S., Abou-Hamad E., Tao Ma, S. Qureshi Z. S., Cavallo L., D'Elia V., Gates B. C., Basset J.-M., "A Silica-Supported Monoalkylated Tungsten Dioxo Complex Catalyst for Olefin Metathesis", *ACS Catalysis* **8** (2018) 2715–2729 <http://dx.doi.org/10.1021/acscatal.7b04304>
- 2018-20** Napporn T. W., Dubau L., Morais C., Camilo M. R., Durst J., Lima F. H. B., Maillard F., Kokoh K. B., "Tools and Electrochemical In Situ and On-Line Characterization Techniques for Nanomaterials", In: Kumar C. (eds) *In-situ Characterization Techniques for Nanomaterials*. Springer, Berlin, Heidelberg (2018) 383-439 https://doi.org/10.1007/978-3-662-56322-9_11
- 2018-21** Pensel A., Peulon S., "In situ XANES measurements during electrodeposition of thin film: Example of birnessite, a promising material for environmental applications", *Electrochimica Acta* **281** (2018) 738-745 <https://doi.org/10.1016/j.electacta.2018.06.001>
- 2018-22** Préaubert L., Tassistro V., Auffan M., Sari-Minodier I., Rose J., Courbiere B., Perrin J., "Very low concentration of cerium dioxide nanoparticles induce DNA damage, but no loss of vitality, in human spermatozoa", *Toxicol. in Vitro* **50** (2018) 236-241 <https://doi.org/10.1016/j.tiv.2018.03.013>
- 2018-23** Scholten L., Watenphul A., Beermann O., Testemale D., Ames D., Schmidt C., "Nickel and platinum in high-temperature H₂O+HCl fluids: implications for hydrothermal mobilization", *Geochimica et Cosmochimica Acta* **224** (2018) 187-199 <https://doi.org/10.1016/j.gca.2018.01.005>
- 2018-24** Scifo L., Chaurand P., Bossa N., Avellan A., Auffan M., Masion A., Angeletti B., Kieffer I., Labille J., Bottero J.-Y., Rose J., "Non-linear release dynamics for a CeO₂ nanomaterial embedded in a protective wood stain, due to matrix photo-degradation", *Environmental Pollution* **241** (2018) 182–193 <https://doi.org/10.1016/j.envpol.2018.05.045>
- 2018-25** Seder-Colomina M., Mangeret A., Stetten L., Merrot P., Diez O., Julien A., Barker E., Thouvenot A., Bargar J., Cazala C., Morin G., "Carbonate facilitated mobilization of uranium from lacustrine sediments under anoxic conditions", *Environ. Sci. Technol.* **52** (2018) 9615-9624 <http://dx.doi.org/10.1021/acs.est.8b01255>
- 2018-26** Sénèque O., Rousselot-Pailley P., Pujol A., Boturyn D., Crozy S., Proux O., Manceau A., Lebrun C., Delangle P., "Mercury trithiolate binding (HgS₃) to a de novo designed cyclic decapeptide with three pre-oriented cysteine side-chains", *Inorganic Chemistry* **57** (2018) 2705–2713 <http://dx.doi.org/10.1021/acs.inorgchem.7b03103>
- 2018-27** Stetten L., Mangeret A., Brest J., Seder-Colomina M., Le Pape P., Ikogou M., Zeyen N., Thouvenot A., Julien A., Alcalde, G., Reyss J.L., Bombléd B., Rabouille C., Olivi L., Proux O., Morin G., "Geochemical control on the reduction of U(VI) to mononuclear U(IV) species in a contaminated lake sediment", *Geochim. Cosmochim. Acta* **222** (2018) 171-186 <https://doi.org/10.1016/j.gca.2017.10.026>
- 2018-28** Stetten L., Blanchart P., Mangeret A., Lefebvre P., Le Pape P., Brest J., Merrot P., Julien A., Proux O., Webb S. M., Bargar J.R., Cazala C., Morin G., "Redox fluctuations and organic complexation govern uranium redistribution from U(IV)-phosphate minerals in a mining-polluted wetland soil,

- Brittany, France", *Environ. Sci. Technol.* **52** (2018) 13099–13109
<http://dx.doi.org/10.1021/acs.est.8b03031>
- 2018-29** Tamrat W. Z., Rose J., Grauby O., Doelsch E., Levard C., Chaurand P., Basile-doelsch I., "Composition and molecular scale structure of nanophases formed by precipitation of biotite weathering products", *Geochim. Cosmochim. Acta* **229** (2018) 53-64
<https://doi.org/10.1016/j.gca.2018.03.012>
- 2018-30** Velimirovic M., Auffan M., Carniato L., Micić Batka V., Schmid D., Wagner S., Borschneck D., Proux O., von der Kammer F., Hofmann T., "Effect of field site hydrogeochemical conditions on the corrosion of milled zerovalent iron particles and their dechlorination efficiency", *Science of The Total Environment* **618** (2018) 1619-1627 <https://doi.org/10.1016/j.scitotenv.2017.10.002>
- 2018-31** Viennet R., Roussel H., Rapenne L., Deschanvres J.-L., Renevier H., Jousseau V., Jalaguier E., Proietti M.G., "XAFS atomistic insight of the oxygen gettering in Ti/HfO₂ based OxRRAM", *Physical Review Materials* **2** (2018) 055002 <https://doi.org/10.1103/PhysRevMaterials.2.055002>
- 2018-32** Vollmer I., van der Linden B., Ould-Chikh S., Aguilar Tapia A., Yarulina I., Abou-Hamad E., Sneider Y. G., Olivos Suarez A., Hazemann J.-L., Kapteijn F., Gascon J., "On the dynamic nature of Mo sites for methane dehydroaromatization", *Chemical Science* **9** (2018) 4801-4807
<http://dx.doi.org/10.1039/C8SC01263F>
- 2018-33** Yoshida K., Yamaguchi T., "Structure Analysis of Electrolyte Solution with X-Rays and Neutrons under High Temperatures and High Pressures", *The Review of High Pressure Science and Technology* **28** (2018) 72-80 <https://doi.org/10.4131/jshpreview.28.72>
- 2017-1** Al Sabban B., Falivene L., Kozlov S. M., Aguilar-Tapia A., Ould-Chikh S., Hazemann J.-L., Cavallo L., Basset J.-M., Takanabe K., "In-operando elucidation of bimetallic CoNi nanoparticles during high-temperature CH₄/CO₂ reaction", *Applied Catalysis B* **213** (2017) 177-189
<http://dx.doi.org/doi:10.1016/j.apcatb.2017.04.076>
- 2017-2** Aucour A.-M., Bedell J.P., Queyron M., Thomé R., Lamboux A., Sarret G., "Zn speciation and stable isotope fractionation in a contaminated urban wetland soil- Typha latifolia system", *Environ. Sci. Technol.* **51** (2017) 8350–8358 <http://dx.doi.org/10.1021/acs.est.6b02734>
- 2017-3** Bonnet J., Cauzid J., Testemale D., Kieffer I., Proux O., Bailly L., André-Mayer A.-S., "Characterization of germanium speciation in sphalerite (ZnS) by X-ray absorption spectroscopy", *Minerals* **7** (2017) 79 <http://dx.doi.org/10.3390/min7050079>
- 2017-4** Cheignon C., Jones M., Atrian-Blasco E., Kieffer I., Faller P., Collin F., Hureau C., "Identification of key structural features of the elusive Cu-Aβ complex generating ROS in Alzheimer's Disease", *Chemical Science* **8** (2017) 5107-5118 <http://dx.doi.org/10.1039/C7SC00809K>
- 2017-5** Chiarantini L., Rimondi V., Bardelli F., Benvenuti M., Cosio C., Costagliola P., Di Benedetto F., Lattanzi P., Sarret G., "Mercury speciation in *Pinus nigra* barks from Monte Amiata (Italy): An X-ray absorption spectroscopy study", *Environmental Pollution* **227** (2017) 83-88
<https://doi.org/10.1016/j.envpol.2017.04.038>
- 2017-6** Conte-Daban A., Borghesani V., Sayen S., Guillon E., Journaux Y., Gontard G., Lisnard L., Hureau C., "Link between affinity and Cu(II) binding sites to amyloid-β peptides evaluated by a new water-soluble UV-Visible ratiometric dye with a moderate Cu(II) affinity", *Anal. Chem.* **89** (2017) 2155-2162
<http://dx.doi.org/10.1021/acs.analchem.6b04979>
- 2017-7** Conte-Daban A., Boff B., Candido A., Montes Aparicio C., Gateau C., Lebrun C., Cerchiaro G., Kieffer I., Sayen S., Guillon E., Delangle P., Hureau C., "A trishistidine pseudopeptide with ability to remove both Cu(I) and Cu(II) from the amyloid-β peptide and to stop the associated ROS formation", *Chemistry - A European Journal* **23** (2017) 17078-17088 <http://dx.doi.org/10.1002/chem.201703429>
- 2017-8** Dublet G., Juillot F., Brest J., Noel V., Fritsch E., Proux O., Olivi L., Ploquin F., Morin G., "Vertical changes of the Co and Mn speciation along a lateritic regolith developed on peridotites (New Caledonia)", *Geochim. Cosmochim. Acta* **217** (2017) 1-15 <https://doi.org/10.1016/j.gca.2017.07.010>
- 2017-9** Formentini T. A., Legros S., Scapulatempo Fernandes C. V., Pinheiro A., Le Bars M., Levard C., Kochem Mallmann F. J., da Veiga M., Doelsch E., "Radical change of Zn speciation in pig slurry amended

- soil: Key role of nano-sized sulfide particles”, *Environmental Pollution* **222** (2017) 495-503 <http://dx.doi.org/10.1016/j.envpol.2016.11.056>
- 2017-10** Garad H., Fettar F., Gay F., Joly Y., Auffret S., Rodmacq B., Dieny B., Ortega L., “Temperature variation of magnetic anisotropy in Pt/Co/AIO_x trilayers”, *Phys. Rev. Applied* **7** (2017) 034023 <https://doi.org/10.1103/PhysRevApplied.7.034023>
- 2017-11** Khadra G., Tamion A., Tournus F., Boisson O., Albinand C., Dupuis V., “Structure and magnetic properties of FeCo clusters: carbon environment and annealing effects”, *J. Phys. Chem. C* **121** (2017) 10713-10718 <http://dx.doi.org/10.1021/acs.jpcc.6b10715>
- 2017-12** Lamirand A.D., Grenier S., Ramos A.Y., De Santis M., Bailly A., Mossang E., Tonnerre J.M., Testemale D., Tolentino H.C.N., Jaouen N., Soares M.M., Jamet M., Proux O., “Growth and properties of CoO/Fe perpendicular exchange coupled ultra-thin films”, *Journal of Magnetism and Magnetic Materials* **443** (2017) 195-201 <https://doi.org/10.1016/j.jmmm.2017.07.079>
- 2017-13** Layet C., Auffan M., Santaella C., Chevassus-Rosset C., Montes M., Ortet P., Barakat M., Collin B., Legros S., Bravin M. N., Angeletti B., Kieffer I., Proux O., Hazeman J.-L., Doelsch E., “Evidence that soil properties and organic coating drive the phytoavailability of cerium oxide nanoparticles”, *Environ. Sci. Technol.* **51** (2017) 9756–9764 <http://dx.doi.org/10.1021/acs.est.7b02397>
- 2017-14** Liu W., Etschmann B., Migdisov A., Boukhalfa H., Testemale D., Müller H., Hazemann J.-L., Brugger J., “Revisiting the hydrothermal geochemistry of europium(II/III) in light of new in-situ XAS spectroscopy results”, *Chem. Geol.* **459** (2017) 61-74 <http://dx.doi.org/10.1016/j.chemgeo.2017.04.005>
- 2017-15** Louvel M., Mavrogenes J., Etschmann B., Brugger J., Hazemann J.-L., Testemale D., “Solubility and speciation of REE in high temperature fluids: insights from in situ XAS studies”, *Applied Earth Science - Transactions of the Institutions of Mining and Metallurgy: Section B* **126** (2017) 73 <http://dx.doi.org/10.1080/03717453.2017.1306271>
- 2017-16** Louvel M., Bordage A., Tripoli B., Testemale D., Hazemann J.-L., Mavrogenes J., “Effect of S on the aqueous and gaseous transport of Cu in porphyry and epithermal systems: Constraints from in situ XAS measurements up to 600 °C and 300 bars”, *Chemical Geology* **466** (2017) 500-511 <https://doi.org/10.1016/j.chemgeo.2017.06.039>
- 2017-17** Mariet A.-L., Sarret G., Bégeot C., Walter-Simonnet A.-V., Gimbert F., “Lead Highly Available in Soils Centuries after Metallurgical Activities”, *Journal of Environmental Quality* **46** (2017) 1146-1157 <http://dx.doi.org/10.2134/jeq2016.12.0469>
- 2017-18** Muller-Bouvet D., Emery N., Tassali N., Panabièrre E., Bach S., Crosnier O., Brousse T., Cénac-Morthe C., Michalowicz A., Pereira-Ramos J. P., “Unravelling redox processes of Li₇MnN₄ upon electrochemical Li extraction–insertion using operando XAS”, *Physical Chemistry Chemical Physics* **19** (2017) 27204-27211 <http://dx.doi.org/10.1039/C7CP05207C>
- 2017-19** Paris E., Sugimoto T., Wakita T., Barinov A., Terashima K., Kandyba V., Proux O., Kajitani J., Higashinaka R., Matsuda T. D., Aoki Y., Yokoya T., Mizokawa T., Saini N. L., “Electronic structure of self-doped layered Eu₃F₄Bi₂S₄ material revealed by x-ray absorption spectroscopy and photoelectron spectromicroscopy”, *Phys. Rev. B* **95** (2017) 035152 <http://dx.doi.org/10.1103/PhysRevB.95.035152>
- 2017-20** Paris E., Wakita T., Proux O., Yokoya T., Kudo K., Mitsuoka D., Kimura T., Nishimoto N., Ioka S., Nohara M., Mizokawa T., Saini N. L., “Distinct local structure of superconducting Ca₁₀M₄As₈(Fe₂As₂)₅ (M=Ir,Pt)”, *Phys. Rev. B* **96** (2017) 224507 <https://doi.org/10.1103/PhysRevB.96.224507>
- 2017-21** Penen F., Isaure M.-P., Dobritzsch D., Bertalan I., Castillo-Michel H., Proux O., Gontier E., Le Coustumer P., Schaumlöffel D., “Pools of cadmium in *Chlamydomonas reinhardtii* revealed by chemical imaging and XAS spectroscopy”, *Metallomics* **9** (2017) 910-923 <http://dx.doi.org/10.1039/C7MT00029D>
- 2017-22** Peres M., Lorenz K., Alves E., Nogales E., Méndez B., Biquard X., Daudin B., Vllora E.G., Shimamura K., “Doping β-Ga₂O₃ with europium: Influence of the implantation and annealing temperature”, *Journal of Physics D* **50** (2017) 325101 <https://dx.doi.org/10.1088/1361-6463/aa79dc>
- 2017-23** Proux O., Lahera E., Del Net W., Kieffer I., Rovezzi M., Testemale D., Irar M., Thomas S., Aguilar-Tapia A., Bazarkina E. F., Prat A., Tella M., Auffan M., Rose J., Hazemann J.-L., “High Energy

Resolution Fluorescence Detected X-ray Absorption Spectroscopy : a new powerful structural tool in environmental biogeochemistry sciences”, *Journal of Environmental Quality* **46** (2017) 1146-1157

<http://dx.doi.org/10.2134/jeq2017.01.0023>

- 2017-24** Qureshi Z. S., Hamieh A., Barman S., Maity N., Samantaray M. K., Ould-Chikh S., Abou-hamad E., Falivene L., D'Elia V., Rothenberger A., Llorens I., Hazemann J.-L., Basset J.-M., “SOMC-Designed Silica Supported Tungsten Oxo Imidazolin-2-iminato Methyl Precatalyst for Olefin Metathesis Reactions”, *Inorg. Chem.* **56** (2017) 861–871 <http://dx.doi.org/10.1021/acs.inorgchem.6b02424>
- 2017-25** Zhou L., Enakonda L. R., Harb M., Saih Y., Aguilar-Tapia A., Ould-Chikh S., Hazemann J.-L., Li J., Wei N., Gary D., Del-Gallo P., Basset J.-M., “Fe catalysts for methane decomposition to produce hydrogen and carbon nano materials”, *Applied Catalysis B: Environmental* **208** (2017) 44-59 <http://dx.doi.org/10.1016/j.apcatb.2017.02.052>
- 2016-1** Adra A., Morin G., Ona-Nguema G., Brest J., “Arsenate and Arsenite Adsorption onto Al-containing ferrihydrites. Implications for Arsenic Immobilization After Neutralization of Acid Mine Drainage”, *Applied Geochemistry* **64** (2016) 2-9 <http://dx.doi.org/10.1016/j.apgeochem.2015.09.015>
- 2016-2** Alies B., Conte-Daban A., Sayen S., Collin F., Kieffer I., Guillon E., Faller P., Hureau C., “Zinc(II) Binding Site to the Amyloid- β Peptide: Insights from Spectroscopic Studies with a Wide Series of Modified Peptides”, *Inorg. Chem.* **55** (2016) 10499-10509 <http://dx.doi.org/10.1021/acs.inorgchem.6b01733>
- 2016-3** Avenier P., Bazer-Bachi D., Bazer-Bachi F., Chizallet C., Deleau F., Diehl F., Gornay J., Lemaire É., Moizan-Basle V., Plais C., Raybaud P., Richard F., Lacombe S., “Catalytic Reforming: Methodology and Process Development for a Constant Optimisation and Performance Enhancement”, *Oil & Gas Science and Technology* **71** (2016) 41 <http://dx.doi.org/10.2516/ogst/2015040>
- 2016-4** Barman S., Maity N., Bhatte K., Ould-Chikh S., Dachwald O., Haessner C., Saih Y., Abou-Hamad E., Llorens I., Hazemann J.-L., Köhler K., D'Elia V., Basset J.-M., “Single-site VOx moieties generated on silica by surface organometal-lic chemistry: a way to enhance the catalytic activity in the oxidative dehydrogenation of propane”, *ACS Catalysis* **6** (2016) 5908–5921 <http://dx.doi.org/10.1021/acscatal.6b01263>
- 2016-5** Bélar J.F., Boudet N., Blanc N., Hosokawa S., “Resonant scattering in condensed matter, experiments that reveal short to long range atomic order”, *Zeitschrift für Physikalische Chemie* **230** (2016) 301-311 <https://doi.org/10.1515/zpch-2015-0699>
- 2016-6** Bourke J. D., Christopher T. Chantler C. T., Joly Y., “FDMX: extended X-ray absorption fine structure calculations using the finite difference method”, *Journal of Synchrotron Radiation* **23** (2016) 551–559 <http://dx.doi.org/10.1107/S1600577516001193>
- 2016-7** Brugger J., Liu W., Etschmann B., Mei Y., Sherman D. M., Testemale D., “A review of the coordination chemistry of hydrothermal systems, or do coordination changes make ore deposits?”, *Chemical Geology* **447** (2016) 219-253 <http://dx.doi.org/10.1016/j.chemgeo.2016.10.021>
- 2016-8** Bureau H., Auzende A.-L., Marocchi M., Raepsaet C., Munsch P., Testemale D., Mézouar M., Kubsy S., Carrière M., Ricolleau A., Fiquet G., “Modern and past volcanic degassing of iodine”, *Geochim. Cosmochim. Acta* **173** (2016) 114-125 <http://dx.doi.org/10.1016/j.gca.2015.10.017>
- 2016-9** Cheignon C., Faller P., Testemale D., Hureau C., Collin F., “Metal-catalyzed oxidation of A β and the resulting reorganization of the Cu binding sites promote ROS production”, *Metallomics* **8** (2016) 1081-1089 <http://dx.doi.org/10.1039/C6MT00150E>
- 2016-10** Conte-Daban A., Day A., Faller P., Hureau C., “How Zn can impede Cu detoxification by chelating agents in Alzheimer's Disease: a proof-of-concept study”, *Dalton Transactions* **45** (2016) 15671-15678 <https://doi.org/10.1039/C6DT02308H>
- 2016-11** Daier V.A., Rivière E., Mallet-Ladeira S., Moreno D. M., Hureau C., Signorella S.R., “Synthesis, characterization and activity of imidazolate-bridged and Schiff-base dinuclear complexes as models of Cu₂Zn-SOD. A comparative study”, *Journal of Inorganic Biochemistry* **163** (2016) 162-175 <http://dx.doi.org/10.1016/j.jinorgbio.2016.07.008>
- 2016-12** Etschmann B.E., Liu W., Pring A., Grundler P. V., Tooth B., Borg S., Testemale D., Brewe D., Brugger J., “The role of Te(IV) and Bi(III) chloride complexes in hydrothermal mass transfer: An X-ray





- absorption spectroscopic study”, *Chemical Geology* **425** (2016) 37-51
<http://dx.doi.org/10.1016/j.chemgeo.2016.01.015>
- 2016-13** Garaud M., Auffan M., Devin S., Felten V., Pagnout C., Pain-Devin S., Proux O., Rodius F., Sohm B., Giambérini L., “Long-term integrated assessment of ceria nanoparticle impacts on the freshwater bivalve *Dreissena polymorpha*: a mesocosm approach”, *Nanotoxicology* **10** (2016) 935-944
<http://dx.doi.org/10.3109/17435390.2016.1146363>
- 2016-14** Guigues S., Bravin M. N., Garnier C., Masion A., Chevassus-Rosset C., Cazevieuille P., Doelsch E., “Involvement of nitrogen functional groups in high-affinity copper binding in tomato and wheat root apoplasts: spectroscopic and thermodynamic evidence”, *Metallomics* **8** (2016) 366-376
<http://dx.doi.org/10.1039/c5mt00298b>
- 2016-15** He J., Bardelli F., Gehin A., Silvester E., Charlet L., “Novel chitosan goethite bionanocomposite beads for arsenic remediation”, *Water Research* **101** (2016) 1-9
<http://dx.doi.org/10.1016/j.watres.2016.05.032>
- 2016-16** Joly Y., Grenier S., “Theory of X-Ray Absorption Near Edge Structure”, *X-Ray Absorption and X-Ray Emission Spectroscopy: Theory and Applications*, Ed. Van Bokhoven J. A. and Lamberti C., Wiley & Sons (2016) 73-97 <http://dx.doi.org/10.1002/9781118844243.ch4>
- 2016-17** Lafay R., Montes-Hernandez G., Janots E., Muñoz M., Auzende A.L., Gehin A., Chiriac R., Proux O., “Experimental investigation of As, Sb and Cs behaviour during olivine serpentinization in hydrothermal alkaline systems”, *Geochim. Cosmochim. Acta* **179** (2016) 177-202
<http://dx.doi.org/10.1016/j.gca.2016.02.014>
- 2016-18** Lannes A., Suffren Y., Tommasino J. B., Chiriac R., Toche F., Khrouz L., Molton F., Duboc C., Kieffer I., Hazemann J.-L., Reber C., Hauser A., Luneau D., “Room temperature magnetic switchability assisted by hysteretic valence tautomerism in a layered two dimensional manganese-radical coordination framework”, *J. Am. Chem. Soc.* **138** (2016) 16493–16501
<http://dx.doi.org/10.1021/jacs.6b10544>
- 2016-19** Mei Y., Etschmann B.E., Liu W., Sherman D.M., Testemale D., Brugger J., “Speciation and thermodynamic properties of zinc in sulfur-rich hydrothermal fluids: insights from ab initio molecular dynamics simulations and X-ray absorption spectroscopy”, *Geochim. Cosmochim. Acta* **179** (2016) 32-52
<http://dx.doi.org/10.1016/j.gca.2016.01.031>
- 2016-20** Morin G., Mangeret A., Othmane G., Stetten L., Brest J., Ona-Nguema G., Bassot S., Courbet C., Barker E., Thouvenot A., Guillevic J., Mathon O., Proux O., Bargar J., “Monomeric U(IV)-phosphate complexes as major uranium species in contaminated lake sediments”, *Geochemical Perspectives Letters* **2** (2016) 95-105 <http://dx.doi.org/10.7185/geochemlet.1610>
- 2016-21** Muehe E. M., Morin G., Scheer L., Le Pape P., Esteve I., Daus B., Kappler A., “Arsenic(V) incorporation in vivianite during microbial reduction of arsenic(V)-bearing biogenic Fe(III) (oxyhydr)oxides”, *Environ. Sci. Technol.* **50** (2016) 2281-2291
<http://dx.doi.org/10.1021/acs.est.5b04625>
- 2016-22** Pradas del Real A. E., Castillo-Michel H. A., Kaegi R., Sinnet B., Magnin V., Findling N., Villanova J., Carrière M., Santaella C., Fernandez-Martinez A., Levard C., Sarret G., “Fate of Ag-NPs in sewage sludge after application on agricultural soils”, *Environ. Sci. Technol.* **50** (2016) 1759-1768
<http://dx.doi.org/10.1021/acs.est.5b04550>
- 2016-23** Schreck E., Sarret G., Oliva P., Calas A., Sobanska S., Guédron S., Barraza F., Point D., Huayta C., Couture R.-M., Prunier J., Henry M., Tisserand D., Goix S., Chincheros J., Uzu G., “Is *Tillandsia capillaris* an efficient bioindicator of atmospheric metal and metalloid deposition? Insights from five months of monitoring in an urban mining area”, *Ecological Indicators* **67** (2016) 227-237
<http://dx.doi.org/10.1016/j.ecolind.2016.02.027>
- 2016-24** Siebel A., Gorlin Y., Durst J., Proux O., Hasché F., Tromp M., Gasteiger H. A., “Identification of catalyst structure during hydrogenoxidation reaction in an operating PEM fuel cell”, *ACS Catalysis* **6** (2016) 7326–7334 <http://dx.doi.org/10.1021/acscatal.6b02157>
- 2016-25** Tella M., Bravin M. N., Thuriès L., Cazevieuille P., Chevassus-Rosset C., Collin B., Chaurand P., Legros S., Doelsch E., “Increased zinc and copper availability in organic waste amended soil potentially

- involving distinct release mechanisms”, *Environmental Pollution* **212** (2016) 299-306 <http://dx.doi.org/10.1016/j.envpol.2016.01.077>
- 2016-26** Testemale D., Prat A., Lahera E., Hazemann J.-L., “Novel high-pressure windows made of glass-like carbon for x-ray analysis”, *Review of Scientific Instrument* **87** (2016) 075115 <http://dx.doi.org/10.1063/1.4959110>
- 2016-27** Veronesi G., Deniaud A., Gallon T., Jouneau P.-H., Villanova J., Delangle P., Carrière M., Kieffer I., Charbonnier P., Mintz E., Michaud-Soret I., “Visualization, quantification and coordination of Ag⁺ ions released from silver nanoparticles in hepatocytes”, *Nanoscale* **8** (2016) 17012-17021 <http://dx.doi.org/10.1039/C6NR04381J>
- 2016-28** Volant A., Héry M., Desoeuvre A., Casiot C., Morin G., Bertin P.N., Bruneel O. “Spatial Distribution of Eukaryotic Communities Using High-Throughput Sequencing Along a Pollution Gradient in the Arsenic-Rich Creek Sediments of Carnoulès Mine, France”, *Microbial Ecology* **72** (2016) 608-620 <http://dx.doi.org/10.1007/s00248-016-0826-5>
- 2016-29** Wakita T., Paris E., Mizokawa T., Hacisalihoğlu M. Y., Terashima K., Okazaki H., Proux O., Kieffer I., Lahera E., Del Net W., Olivi L., Takano Y., Muraoka Y., Yokoya T., Saini N. L., “Determination of the local structure of CsBi_{4-x}Pb_xTe₆ (x = 0, 0.5) by X-ray absorption spectroscopy”, *Physical Chemistry Chemical Physics* **18** (2016) 25136-25142 <http://dx.doi.org/10.1039/C6CP04949D>
- 2015-1** Atrian Blasco E. L., Cerrada E., Conte-Daban A., Testemale D., Faller P., Laguna M., Hureau C., “Copper(I) targeting in the Alzheimer's disease context: a first example using the biocompatible PTA ligand”, *Metallomics* **7** (2015) 1229-1232 <http://dx.doi.org/10.1039/C5MT00077G>
- 2015-2** Aucour A.-M., Bedell J.-P., Queyron M., Magnin V., Testemale D., Sarret G., “Dynamics of Zn in an urban wetland soil-plant system: Coupling isotopic and EXAFS approaches”, *Geochim. Cosmochim. Acta* **160** (2015) 55-69 <http://dx.doi.org/10.1016/j.gca.2015.03.040>
- 2015-3** Beck P., Pommerol A., Zanda B., Remusat L., Lorand J.-P., Göpel C., Hewins R., Pont S., Lewin E., Quirico E., Schmitt B., Montes-Hernandez G., Garenne A., Bonal L., Proux O., Hazemann J.-L., Chevrier V.C.F., “A Noachian source region for the “Black Beauty” meteorite, and a source lithology for Mars surface hydrated dust?”, *Earth and Planetary Science Letters* **427** (2015) 104-111 <http://dx.doi.org/10.1016/j.epsl.2015.06.033>
- 2015-4** Bordage A., Trannoy V., Proux O., Vitoux H., Moulin R., Bleuzen A., “In Situ Site-Selective K-edge XAS: A Powerful Probe of the Transformation of Mixed-Valence Compounds”, *Physical Chemistry Chemical Physics* **17** (2015) 17260-17265 <http://dx.doi.org/10.1039/C5CP02591E>
- 2015-5** Bresson C., Spezia R., Solari P. L., Jankowski C. K., Den Auwer C., “XAS examination of glutathione cobalt complexes in solution”, *J. Inorg. Biochem.* **142** (2015) 126–131 <http://dx.doi.org/10.1016/j.jinorgbio.2014.10.006>
- 2015-6** Colomban C., Kudrik E. V., Tyurin D. V., Albrieux F., Nefedov S. E., Afanasiev P., Sorokin A. B., “Synthesis and characterization of μ -nitrido, μ -carbido and μ -oxo dimers of iron octapropylporphyrine”, *Dalton Transactions* **44** (2015) 2240-2251 <http://dx.doi.org/10.1039/c4dt03207a>
- 2015-7** De Santis E., Minicozzi V., Morante S., Proux O., Rossi G., Saxena S. S., Silva I. K., Stellato F., “Cu(II)-Zn(II) cross-modulation in amyloid-beta peptide binding: an X-ray Absorption Spectroscopy study”, *J. Phys. Chem. B* **119** (2015) 15813–15820 <http://dx.doi.org/10.1021/acs.jpcc.5b10264>
- 2015-8** Dupuis V., Khadra G., Blanc N., Hillion A., Tamion A., Tuillon-Combes J., Bardotti L., Tournus F., “Intrinsic magnetic properties of bimetallic nanoparticles elaborated by cluster beam deposition”, *Physical Chemistry Chemical Physics* **17** (2015) 27996-28004 <http://dx.doi.org/10.1039/C5CP00943J>
- 2015-9** Finck N., Schlegel M. L., Bauer A., “Structural iron in dioctahedral and trioctahedral smectites: a polarized XAS study”, *Physical and Chemistry of Minerals* **42** (2015) 847-859 <http://dx.doi.org/10.1007/s00269-015-0768-3>
- 2015-10** Giachin G., Mai P. T., Tran T.H., Salzano G., Benetti F., Migliorati V., Arcovito A., Della Longa S., Mancini G., D’Angelo P., Legname G., “The non-octarepeat copper binding site of the prion protein is a key regulator of prion conversion”, *Scientific Reports* **5** (2015) 15253 <http://dx.doi.org/10.1038/srep15253>

- 2015-11** Graouer-Bacart M., Sayen S., Guillon E., "Adsorption of enrofloxacin in presence of Zn(II) on a calcareous soil", *Ecotoxicology and Environmental Safety* **122** (2015) 470-476 <http://dx.doi.org/10.1016/j.ecoenv.2015.09.019>
- 2015-12** Guda A.A., Soldatov M.A., Soldatov A.V., "Group III–V and II–VI quantum dots and nanoparticles", X-Ray Absorption Spectroscopy of Semiconductors. *Springer Series in Optical Sciences* **190** (2015) 247-268 https://doi.org/10.1007/978-3-662-44362-0_12
- 2015-13** Huguët S., Isaure M.-P., Bert V., Laboudigue A., Proux O., Flank A.-M., Vantelon D., Sarret G., "Impact of *Arabidopsis halleri* growth on cadmium localization and speciation in highly contaminated dredged sediment", *Science of the Total Environment* **536** (2015) 468-480 <http://dx.doi.org/10.1016/j.scitotenv.2015.07.026>
- 2015-14** Isaure M.-P., Huguët S., Meyer C.L., Castillo-Michel H., Testemale D., Vantelon D., Saumitou Laprade P., Verbruggen N., "Evidence of various mechanisms of Cd sequestration in the hyperaccumulator *Arabidopsis halleri*, the non accumulator *Arabidopsis lyrata* and their progenies by combined synchrotron-based techniques", *Journal of Experimental Botany* **66** (2015) 3201-3214 <http://dx.doi.org/10.1093/jxb/erv131>
- 2015-15** Jacques A., Lebrun C., Casini A., Kieffer I., Proux O., Latour J.-M., Sénèque O., "Reactivity of Cys4 zinc finger domains with Au^{III} complexes: Insights into the formation of "gold fingers", *Inorganic Chemistry* **54** (2015) 4104–4113 <http://dx.doi.org/10.1021/acs.inorgchem.5b00360>
- 2015-16** La Penna G., Minicozzi V., Morante S., Rossi G.C., Stellato F., "A first-principle calculation of the XANES spectrum of Cu²⁺ in water", *J. Chem. Phys.* **143** (2015) 124508 <http://dx.doi.org/10.1063/1.4931808>
- 2015-17** Louvel M., Bordage A., Testemale D., Zhou L., Mavrogenes J., "Hydrothermal controls on the genesis of REE deposits: Insights from an in situ XAS study of Yb solubility and speciation in high temperature fluids (T < 400 °C)", *Chemical Geology* **417** (2015) 228-237 <http://dx.doi.org/10.1016/j.chemgeo.2015.10.011>
- 2015-18** Martin P. M., Vathonne E., Carlot G., Delorme R., Sabathier C., Freyss M., Garcia P., Bertolus M., Glatzel P., Proux O., "Behavior of fission gases in nuclear fuel: XAS characterization of Kr in UO₂", *J. Nucl. Mater.* **466** (2015) 379-392 <http://dx.doi.org/10.1016/j.jnucmat.2015.08.019>
- 2015-19** Mei Y., Sherman D. M., Liu W., Etschmann B., Testemale D., Brugger J., "Zinc complexation in chloride-rich hydrothermal fluids (25 to 600°C): a thermodynamic model derived from ab initio molecular dynamics", *Geochim. Cosmochim. Acta* **150** (2015) 265-284 <http://dx.doi.org/10.1016/j.gca.2014.09.023>
- 2015-20** Mei Y., Etschmann B., Liu W., Sherman D. M., Barnes S. J., Fiorentini M. L., Seward T. M., Testemale D., Brugger J., "Palladium complexation in chloride- and bisulfide-rich fluids: Insights from ab initio molecular dynamics simulations and X-ray absorption spectroscopy", *Geochim. Cosmochim. Acta* **161** (2015) 128-145 <http://dx.doi.org/10.1016/j.gca.2015.04.009>
- 2015-21** Nguyen T.S., Tayakout-Fayolle M., Lacroix M., Gotteland D., Aouine M., Afanasiev P., Geantet C., "Promotion effects with dispersed catalysts for residue slurry hydroconversion", *Fuel* **160** (2015) 50-56 <http://dx.doi.org/10.1016/j.fuel.2015.07.012>
- 2015-22** Nurlaela E., Ould-Chikh S., Llorens I., Hazemann J.-L., Takanahe K., "Establishing Efficient Cobalt-Based Catalytic Sites for Oxygen Evolution on a Ta₃N₅ Photocatalyst.", *Chemistry of Materials* **27** (2015) 5685–5694 <http://dx.doi.org/10.1021/acs.chemmater.5b02139>
- 2015-23** Picard A., Testemale D., Wagenknecht L., Hazael R., Daniel I., "Iron reduction by the deep-sea bacterium *Shewanella profunda* LT13a under subsurface pressure and temperature conditions", *Frontiers in Microbiology* **5** (2015) 796 <http://dx.doi.org/10.3389/fmicb.2014.00796>
- 2015-24** Pokrovski G.S., Kokh M.A., Guillaume D., Borisova A.Y., Gisquet P., Hazemann J.-L., Lahera E., Del Net W., Proux O., Testemale D., Haigis V., Jonchière R., Seitsonen A.P., Ferlat G., Vuilleumier R., Saitta A.M., Boiron M.-C., Dubessy J., "Important role for the trisulfur radical ion S₃⁻ in the formation of gold deposits on Earth", *Proceedings of the National Academy of Sciences* **112** (2015) 13484–13489 <http://dx.doi.org/10.1073/pnas.1506378112>


- 2015-25** Renard F., Putnis C.V., Montes-Hernandez G., Ruiz-Agudo E., Hovelmann J., Sarret G., “Interactions of arsenic with calcite surfaces revealed by in-situ nanoscale imaging”, *Geochim. Cosmochim. Acta* **159** (2015) 61-79 <http://dx.doi.org/10.1016/j.gca.2015.03.025>
- 2015-26** Revenant C., Benwadih M., Proux O., “Local structure around Zn and Ga in solution-processed In-Ga-Zn-O and implications for electronic properties”, *Physica Status Solidi - Rapid Research Letters* **9** (2015) 652–655 <http://dx.doi.org/10.1002/pssr.201510322>
- 2015-27** Rollin-Genetet F., Seidel C., Artells E., Auffan M., Thiery A., Vidaud C., “The redox reactivity of cerium oxide nanoparticles induces the formation of disulphide bridges in thiol-containing biomolecules”, *Chem. Res. Toxicol.* **28** (2015) 2304–2312 <http://dx.doi.org/10.1021/acs.chemrestox.5b00319>
- 2015-28** Tella M., Auffan M., Brousset L., Morel E., Proux O., Chanéac C., Angeletti B., Pailles C., Artells E., Santaella C., Rose J., Thiéry A., Bottero J-Y., “Chronic dosing of a simulated pond ecosystem in indoor aquatic mesocosms: Fate and Transport of CeO₂ nanoparticles”, *Environmental Science: Nano* **2** (2015) 653-663 <http://dx.doi.org/10.1039/C5EN00092K>
- 2015-29** Veronesi G., Aude-Garcia C., Kieffer I., Gallon T., Delangle P., Herlin N., Rabilloud T., Carrière M., “Exposure-dependent Ag⁺ release from silver nanoparticles and its complexation in AgS₂ sites in primary murine macrophages”, *Nanoscale* **7** (2015) 7323-7330 <http://dx.doi.org/10.1039/C5NR00353A>
- 2015-30** Veronesi G., Gallon T., Deniaud A., Boff B., Gateau C., Lebrun C., Vidaud C., Rollin-Genetet F., Carrière M., Kieffer I., Mintz E., Delangle P., Michaud-Soret I., “XAS investigation of silver(I) coordination in copper(I) biological binding sites”, *Inorganic Chemistry* **54** (2015) 11688–11696 <http://dx.doi.org/10.1021/acs.inorgchem.5b01658>
- 2015-31** Zhang N., Zeng D., Brugger J., Zhou Q., Ngothai Y., “Effect of solvent activity on solute association: the formation of aqueous Nickel(II) chloride complexes studied by UV-Vis and EXAFS spectroscopy”, *J. Solution Chem.* **44** (2015) 1320–1338 <http://dx.doi.org/10.1007/s10953-015-0334-0>
- 2015-32** Zhu H., Ould-Chikh S., Dong H., Llorens I., Saih Y., Anjum D. H., Hazemann J.-L., Basset J.-M., “VO_x/SiO₂ catalyst prepared by grafting VOCl₃ on silica for oxidative dehydrogenation of propane”, *ChemCatChem* **7** (2015) 3332–3339 <http://dx.doi.org/10.1002/cctc.201500607>









Highlights

- 2021-1** Daninos F., “Une soupe primitive reproduite en laboratoire”, *La Recherche* **564** (2021)
- 2021-2** Fialho-Batista Ana T.; Baaziz W., Taleb A.-L., Chaniot J., Moreaud M., Legens C., Aguilar-Tapia A., Proux O., Hazemann J.-L., Diehl F., Chizallet C., Gay A.-S., Ersen O., Raybaud P., “Atomic scale insight into the formation, size and location of platinum nanoparticles supported on γ -alumina”, *ESRF Highlights 2020* (2021) 
- 2021-3** Maurer, F., Jelic, J., Wang, J. Gänzler A., Dolcet P., Wöll C., Wang Y., Studt F., Casapu M., Grunwaldt J.-D., “Tracking the formation, fate and consequence for catalytic activity of Pt single sites on CeO₂”, *ESRF Highlights 2020* (2021) 
- 2020-1** Sun X., Wang R., Ould-Chikh S., Osadchii D., Li G., Aguilar-Tapia A., Hazemann J.-L., Kapteijn F., Gascon J., “Defining the iron active site for CO₂ electroreduction in mesoporous nitrogen-doped carbon”, *ESRF Highlights 2019* (2020) 124-125
- 2019-1** Petersen T., “Unraveling how nature arranges atoms in space”, *KAUST News* (2019),
- 2019-2** Vollmer I., van der Linden B., Ould-Chikh S., Aguilar-Tapia A., Yarulina I., et al., “Operando XAS observation of Mo transforming to its active phase for converting methane to aromatics”, *ESRF Highlights 2018* (2019)
- 2018-1** “News from the beamlines - The new 14-crystal high-resolution spectrometer on BM16 (FAME-UHD)”, *ESRF news* **79** (2018) 10 
- 2018-2** “Le spectromètre qui révèle la forme chimique d’éléments ultra-dilués”, *2017 – Une année avec le CNRS* (2018) 31 

- 2017-1** Chizallet C., "Apport du calcul ab initio en physico-chimie des surfaces catalytiques complexes", *L'Actualité chimique* **417** (2017) 34-39
- 2017-2** Veronesi G., Deniaud A., Gallon T., Jouneau P.-H., Villanova J., Delangle P., Carrière M., Kieffer I., Charbonnier P., Mintz E., Michaud-Soret I., "The intracellular dissolution of silver nanoparticles reveals the mechanism of their toxicity", *ESRF Highlights 2016* (2017) 42-43
- 2017-3** "FAME-UHD : un nouvel instrument national pour révéler la forme chimique et structurale d'éléments ultra dilués", *Actualités INSU*
- 2016-1** Giachin G., Mai P.T., Tran T.H., Salzano G., Benetti F., Migliorati V., Arcovito A., Della Longa S., Mancini G., D'Angelo P., Legname G., "The fifth copper binding site of the prion protein acts as molecular switch for prion conversion", *ESRF Highlights 2015* (2016) 112-113
- 2016-2** Pokrovski G.S., Kokh M.A., Guillaume D., Borisova A.Y., Gisquet P., Hazemann J.-L., Lahera E., Del Net W., Proux O., Testemale D., Haigis V., Jonchière R., Seitsonen A.P., Ferlat G., Vuilleumier R., Saitta A.M., Boiron M.-C., Dubessy J., "Resolving the enigma of gold deposit formation using XAS", *ESRF Highlights 2015* (2016) 86-87
- 2016-3** Pradas del Real A. E., Castillo-Michel H. A., Kaegi R., Sinnet B., Magnin V., Findling N., Villanova J., Carrière M., Santaella C., Fernandez-Martinez A., Levard C., Sarret G., "Fate of silver nanoparticles in agricultural soils amended with sewage sludge", *ESRF Spotlight on Science* (2016)
- 2016-4** "Prions generated by a copper switch", *ESRF news* **74** (2016) 7
- 2016-5** "ESRF user wins L'Oréal-UNESCO award", *ESRF news* **72** (2016) 6
- 2015-1** "La formation des gisements d'or enfin expliquée", *Actualités CNRS-INSU* (13/10/2015)
- 2015-2** Giachin G., Mai P.T., Tran T.H., Salzano G., Benetti F., Migliorati V., Arcovito A., Longa S.D., Mancini G., D'Angelo P., Legname G., "How prions are generated by a copper switch", *ESRF Spotlight on Science* (2015)

PhD thesis and french Habilitations à Diriger les Recherches

- 2021-1** Pustovarenko A., "Crystal Engineering of Metal-Organic Frameworks for Molecular Recognition", *PhD Delft University of Technology* (2021) <https://doi.org/10.4233/uuid:4384094a-a8ab-4ddc-87e1-078118280711>
- 2020-1** Cantarano A., "Nanocristaux de grenat pour l'éclairage blanc par LED et pour la nanothermométrie", *Thèse de doctorat de l'Univ. Grenoble Alpes* (2020) <https://www.theses.fr/s189973>
- 2020-2** Dussert F., "Vers des quantum dots moins toxiques, une approche "safer by design"", *Thèse de doctorat de l'Université Grenoble Alpes* (2020) <http://www.theses.fr/s185317>
- 2020-3** Molich U., "Improving Methods for X-ray Absorption Spectroscopy Studies of Metalloproteins", *Technical University of Denmark* (2020) <https://orbit.dtu.dk/en/publications/9c3b9771-fec1-4bf8-bf15-1cba5a4791b0>
- 2020-4** Testemale D., "Hydrothermal geochemistry: what can we learn with autoclaves and photons?", *Habilitation à Diriger des Recherches de l'Université Grenoble Alpes* (2020)
- 2020-5** Wang R., "Metal-organic Framework Mediated Electrode Engineering for Electrochemical CO₂ Reduction", *PhD Delft University of Technology* (2020), <https://doi.org/10.4233/uuid:7de36fae-025d-499a-a726-21657cffce6c> 
- 2020-6** Zhank K., "Metal-organic frameworks derived heterogeneous materials: Toward high-performance electrochemical applications of aluminum- and lithium-ion storage", *PhD Seoul National University*, <http://s-space.snu.ac.kr/handle/10371/167682>
- 2019-1** Aljuhani M. A., "Towards Supported Nitrogen Containing Fragments on Silica Surface for Catalytic Applications", *PhD King Abdullah University of Science and Technology, Physical Sciences and Engineering Division* (2019) <http://hdl.handle.net/10754/660092>
- 2019-2** Alfano M., "Etude de la biosynthèse de la monoxyde de carbone déshydrogénase, une enzyme-clé de la réaction du gaz à l'eau", *Thèse de doctorat de l'Univ. Grenoble Alpes* (2019) <http://www.theses.fr/s190862>

- 2019-3** Bueno C. de F., “Avaliação de propriedades ópticas e eletrônicas da heteroestrutura GaAs/SnO₂:Eu na forma de filmes finos”, *Tese (Doutorado) – Universidade Estadual Paulista. Faculdade de Ciências, Bauru* (2019) <http://hdl.handle.net/11449/182060> 
- 2019-4** De Santis E., “From molecules, to aggregates. A synergic experimental and computational approach”, *PhD Università di Roma Tor Vergata* (2019) http://www.infn.it/thesis/thesis_dettaglio.php?tid=13755 
- 2019-5** Domergue J., “Modulation de l’activité SOD par contrôle de la sphère de coordination du Ni^{II} dans des complexes bioinspirés”, *Thèse de doctorat de l’Univ. Grenoble Alpes* (2019) <http://www.theses.fr/s163014>
- 2019-6** Ferre G., “Etudes de cérites dopées pour le stockage des oxydes d’azote”, *Thèse de doctorat de l’Univ. de Lyon* (2019) <http://www.theses.fr/s144289> 
- 2019-7** Fialho Batista A. T., “Localisation et proximité des sites acides et métalliques sur les catalyseurs de reformage catalytique”, *Thèse de doctorat de Ecole Normale Supérieure de Lyon* (2019) <http://www.theses.fr/s169546> (2019) 
- 2019-8** Gelly R., “Potentiel des isotopes du Cu et du Zn comme traceurs de l’origine et des redistributions des métaux dans les sols”, *Thèse de doctorat de l’Univ. Aix-Marseille* (2019) <http://www.theses.fr/s152239>
- 2019-9** Ingrao N., “Metal volatility at high temperature: application to planetary accretion and volcanic degassing”, *Thèse de doctorat de l’Univ. Clermont-Auvergne* (2019) <http://www.theses.fr/s182074> 
- 2019-10** Jeantelot G., “Anatase Titanium Dioxide with Exposed {001} Facets as a Support for Molecular Catalysts: Surface Characterization and Application in Photocatalysis”, *PhD King Abdullah University of Science and Technology* (2019) <http://hdl.handle.net/10754/656858> 
- 2019-11** Le Bars M., “Devenir du zinc des produits résiduels organiques après méthanisation et recyclage agricole: rôle des nanoparticules de sulfure de zinc”, *Thèse de doctorat de l’Univ. Aix-Marseille* (2019) <http://www.theses.fr/s152247>
- 2019-12** Merrot P., “Géochimie, spéciation et mobilité des éléments traces métalliques (Fe, Ni, Cr et Mn) au sein des sédiments du lagon de Nouvelle-Calédonie”, *Thèse de doctorat de Sorbonne Univ.* (2019)
- 2019-13** Qureshi M., “Toward selective H₂ evolution from overall water splitting and the trifluoromethylation of heteroarenes via heterogeneous photocatalysis”, *PhD King Abdullah University of Science and Technology, Physical Sciences and Engineering Division* (2019) <http://hdl.handle.net/10754/656661>
- 2019-14** Terwey A., “Element-specific Characterization of Magnetocaloric La(Fe, Si)₁₃-based Compounds”, *PhD Duisburg-Essen Univ.* (2019) <https://doi.org/10.17185/duerpublico/70612>
- 2019-15** Vollmer I., “Towards activity descriptors for the methane dehydroaromatization catalyst Mo/HZSM-5”, *PhD Delft University of Technology* (2019) <https://doi.org/10.4233/uuid:96989fc0-eafb-40c2-a622-f9f1a71faa29> 
- 2018-1** Biquard X., “Fundamental research using synchrotron X-rays on key technological materials”, *Habilitation à Diriger des Recherches de l’Univ. Grenoble Alpes* (2018) <https://hal.archives-ouvertes.fr/tel-02002058/>
- 2018-2** Crede L.-S., “Gold transport in aqueous versus organic fluids: Experimental data and natural observations for describing ore-forming systems”, *PhD of Curtin University* (2018) <http://hdl.handle.net/20.500.11937/75248>
- 2018-3** Desmau M., “Rôle des biofilms bactériens sur le devenir des nanoparticules manufacturées dans les sols”, *Thèse de doctorat de l’Univ. Paris Sorbonne* (2018) <http://www.theses.fr/2018USPCC236>
- 2018-4** Isaure M.-P., “Biogéochimie des métaux dans l’environnement et interactions avec les organismes vivants : apport de l’imagerie et de la spectroscopie d’absorption X”, *Habilitation à Diriger des Recherches de l’Univ. de Pau et des Pays de l’Adour* (2018) 

- 2018-5** Le Gall C., "Contribution à l'étude du relâchement des produits de fission hors de combustibles nucléaires en situation d'accident grave: effet de la pO₂ sur la spéciation du Cs, Mo et Ba", *Thèse de doctorat de l'Univ. Grenoble Alpes* (2018) <https://www.theses.fr/2018GREAY053> 
- 2018-6** Nader S., "Structural studies on inhibition mechanisms, oligomerization and DNA binding of the transcription regulator Fur : from in silico simulations to in vitro biological assays. Quantitative Methods", *Thèse de doctorat de l'Univ. Grenoble Alpes* (2018) <https://tel.archives-ouvertes.fr/tel-02050234>
- 2018-7** Siebel A., "Operando X-ray Absorption Spectroscopy applied to batteries, fuel cells and electrolyzers", *PhD Technische Universität München* (2018) <http://mediatum.ub.tum.de/?id=1419686>
- 2018-8** Werghi B., "Catalysis by design: Well-Defined Aluminum tetra-coordinated Surface Ligand for Catalytic applications", *PhD King Abdullah University of Science and Technology, Physical Sciences and Engineering Division* (2018) <http://hdl.handle.net/10754/630158>
- 2017-1** Abbe J.-B., "Ingénierie de bactéries magnétotactiques pour la bioremédiation du cobalt", *Thèse de doctorat de l'Univ. Aix-Marseille* (2017) <http://www.theses.fr/2017AIXM0051>
- 2017-2** Adam A., "Etude du couplage élastique au sein d'hétérostructures cœur-coquille à base d'analogues du bleu de Prusse", *Thèse de doctorat de l'Ecole Polytechnique, Palaiseau* (2017) <http://www.theses.fr/2017SACLX076>
- 2017-3** Albertelli M., "Transformations du mercure à l'échelle cellulaire : cas de bactéries sulfato-réductrices", *Thèse de doctorat de l'Univ. de Pau* (2017) <http://www.theses.fr/2017PAUU3031>
- 2017-4** Chizallet C., "Complex heterogeneous catalysts in reactive environment : from density functional theory simulations to predictive kinetic models", *Habilitation à Diriger des Recherches de l'Univ. C. Bernard, Lyon* (2017)
- 2017-5** Collin C., "Structure et propriétés magnéto-électriques de nouveaux oxydes", *Habilitation à Diriger des Recherches de l'Univ. Grenoble Alpes* (2017) <https://hal.archives-ouvertes.fr/tel-01584374/>
- 2017-6** Conte-Daban A., "Nouvelles preuves de concept pour la chélothérapie dans le cadre de la maladie d'Alzheimer : études spectroscopiques des interactions entre les ions Cuivre et Zinc", *Thèse de doctorat de l'Univ. de Toulouse* (2017) <https://tel.archives-ouvertes.fr/tel-02013566>
- 2017-7** Eymard-Vernain E., " Etude des interactions entre trois types de nanoparticules métalliques et une bactérie du sol, Bacillus subtilis", *Thèse de doctorat de l'Univ. Grenoble Alpes, Grenoble* (2017) <http://www.theses.fr/2017GREAV065>
- 2017-8** Irar M., "Spectroscopie d'absorption des rayons X appliquée à l'étude des fluides hydrothermaux", *Thèse de doctorat de l'Univ. Grenoble Alpes, Grenoble* (2017) <http://www.theses.fr/2017GREAY060>
- 2017-9** Layet C., "Phytodisponibilité des nanomatériaux et impact sur le prélèvement d'éléments trace métalliques", *Thèse de doctorat de l'Univ. Aix-Marseille* (2017) <http://www.theses.fr/s184175> 
- 2017-10** Ma B., "Sorptions de Radionucléides dans des Barrières Cimentaires Renforcées", *Thèse de doctorat de l'Univ. Grenoble Alpes, Grenoble* (2017) <https://tel.archives-ouvertes.fr/tel-01961482>
- 2017-11** Paris E., "Understanding interlayer interaction in layered superconducting materials", *PhD University of Rome, Italy* (2017)
- 2017-12** Tamrat W. Z., "Séquestration des matières organiques des sols par les nanominéraux : approche expérimentale de la formation de complexes organo-minéraux à partir des produits d'altération de la biotite", *Thèse de doctorat de l'Univ. Aix-Marseille* (2017) <http://www.theses.fr/2017AIXM0624>
- 2017-13** Thomas S. A., "The Role of Chemical Speciation and Cell Physiology in Bacterial Mercury(II) Uptake: Insights from X-ray Absorption Spectroscopy", *PhD Northwestern University, Evanston, Illinois* (2017) 
- 2016-1** Al-Sabban B. E., "Development of Coke-tolerant Transition Metal Catalysts for Dry Reforming of Methane", *PhD King Abdullah University of Science and Technology, Physical Sciences and Engineering Division* (2016) <http://hdl.handle.net/10754/621976>
- 2016-2** Bissardon C., "Le Rôle du Sélénium dans le Métabolisme, la Croissance et la Maturation du Cartilage Articulaire", *Thèse de doctorat de l'Univ. Grenoble Alpes, Grenoble* (2016)
- 2016-3** Cheignon C., "Oxydation du peptide Amyloïde-Beta et conséquences dans l'étiologie de la maladie d'Alzheimer", *Thèse de doctorat de l'Univ. de Toulouse* (2016)

- 2016-4** Formentini T. A., "Macroscopic, microscopic and molecular scale interactions affecting Copper and Zinc transfer within a clayey hapludox soil subject to long-term pig slurry application", *PhD Federal University of Parana, Curitiba* (2016) <http://acervodigital.ufpr.br/handle/1884/43554>
- 2016-5** Mariet A.-L., "Contamination en éléments traces métalliques et changements de végétation liés aux activités minières dans le massif des Vosges : approche diachronique et synchronique des impacts environnementaux", *Thèse de doctorat de l'Université de Besançon* (2016) <http://theses.fr/2016BESA2077>
- 2016-6** Paris E., "Understanding interlayer interaction in layered superconducting materials", *PhD University "La Sapienza" of Rome* (2016)
- 2016-7** Tran T. H., "The non-octarepeat copper-binding site of the prion protein and its potential role in prion conversion", *PhD Scuola Internazionale Superiore Studi Avanzati* (2016) <http://hdl.handle.net/20.500.11767/4870>
- 2016-8** Vasilyev P., "The oxidation state of deeply subducted, altered oceanic crust: An experimental study and the evidence from natural samples", *PhD University "of The Australian National University* (2016) <https://doi.org/10.25911/5d78d5ba006b3>
- 2015-1** Andrei J., "Effets (sub)individuels et fonctionnels des nanoparticules manufacturées sur des Crustacés Gammaridae", *Thèse de doctorat de l'Univ. de Lorraine* (2015) <https://hal.univ-lorraine.fr/tel-01752274>
- 2015-2** Avellan A., "Relation entre structure, réactivité et interactions cellulaires de nanotubes inorganiques ; cas des imogolites", *Thèse de doctorat de l'Univ. Aix-Marseille* (2015) <http://www.theses.fr/2015AIXM4371>
- 2015-3** Bayle M., "Déchloration des objets archéologiques ferreux par le processus de stabilisation subcritique caractérisations physico-chimiques des systèmes transformés", *Thèse de doctorat de l'Univ. Pierre & Marie Curie* (2015) <https://tel.archives-ouvertes.fr/tel-01366638>
- 2015-4** Bonnot C., "L'origine des métaux et la dynamique du zinc dans le bassin de la Seine", *Thèse de doctorat de l'Univ. Paris Diderot* (2015)
- 2015-5** Garaud M., "Effets des nanoparticules manufacturées (nCeO₂ et nAg) sur la biologie du bivalve d'eau douce *Dreissena polymorpha*", *Thèse de doctorat de l'Univ. de Lorraine* (2015)
- 2015-6** Guigues S., "Caractérisation des interactions physico-chimiques entre le cuivre et les racines comme base de développement d'un modèle d'évaluation de la phytodisponibilité des éléments traces", *Thèse de doctorat de l'Univ. Aix-Marseille* (2015)
- 2015-7** Khadra G., "Magnetic and structural properties of size-selected FeCo nanoparticle assemblies", *Thèse de doctorat de l'Univ. Lyon 1* (2015) <https://tel.archives-ouvertes.fr/tel-01262653>
- 2015-8** Lofficial D., "Photosynthèse artificielle : élaboration de matériaux composites pour la valorisation de CO₂ par photocatalyse", *Thèse de doctorat de l'Univ. Lyon 1* (2015) <https://www.theses.fr/2015LYO10153>
- 2015-9** Nurlaela E., "Development of Ta₃N₅ as an Efficient Visible Light-responsive Photocatalyst for Water Oxidation", *PhD King Abdullah University of Science and Technology, Physical Sciences and Engineering Division* (2015) <http://hdl.handle.net/10754/582311>
- 2015-10** Penen F., "Imagerie cellulaire du stress métallique induit par le cadmium chez la micro-algue verte *Chlamydomonas reinhardtii* par techniques synchrotron μ XRF / XAS et nanoSIMS", *Thèse de doctorat de l'Univ. de Pau et des Pays de l'Adour* (2015) <http://www.theses.fr/2015PAUU3047>
- 2015-11** Tranoy V., "Vers l'élaboration de pistes magnétiques enregistrables : de la molécule au matériau", *Thèse de doctorat de l'Univ. Paris Sud* (2015) <https://tel.archives-ouvertes.fr/tel-01253610/>

9. List of selected publications

BM30

Geochemistry and Environmental Sciences

Pradas del Real A. E., Castillo-Michel H. A., Kaegi R., Sinnet B., Magnin V., Findling N., Villanova J., Carrière M., Santaella C., Fernandez-Martinez A., Levard C., Sarret G., "Fate of Ag-NPs in sewage sludge after application on agricultural soils", *Environ. Sci. Technol.* **50** (2016) 1759-1768 <http://dx.doi.org/10.1021/acs.est.5b04550>

Hydrothermal Fluids

Pokrovski G.S., Kokh M.A., Guillaume D., Borisova A.Y., Gisquet P., Hazemann J.-L., Lahera E., Del Net W., Proux O., Testemale D., Haigis V., Jonchière R., Seitsonen A.P., Ferlat G., Vuilleumier R., Saitta A.M., Boiron M.-C., Dubessy J., "Important role for the trisulfur radical ion S_3^- in the formation of gold deposits on Earth", *Proceedings of the National Academy of Sciences* **112** (2015) 13484–13489 <http://dx.doi.org/10.1073/pnas.1506378112>

Biochemistry

Alies B., Conte-Daban A., Sayen S., Collin F., Kieffer I., Guillon E., Faller P., Hureau C., "Zinc(II) Binding Site to the Amyloid- β Peptide: Insights from Spectroscopic Studies with a Wide Series of Modified Peptides", *Inorganic Chemistry* **55** (2016) 10499-10509 <http://dx.doi.org/10.1021/acs.inorgchem.6b01733>

Catalysis & material energy

Vollmer I., Ould-Chikh S., Aguilar-Tapia A., Li G., Pidko E., Hazemann J.-L., Kapteijn F., Gascon J., "Activity descriptors derived from comparison of Mo and Fe as active metal for methane conversion to aromatics", *Journal of the American Chemical Society* **141** (2019) 18814-18824 <https://doi.org/10.1021/jacs.9b09710>

Materials science

Adam A., Poggi M., Larquet E., Cortes R., Martinelli L., Coulon P.-E., Lahera E., Proux O., Chernyshov D., Boukheddaden K., Gacoin T., Maurin I., "Strain engineering of photo-induced phase transformations in Prussian blue analogue heterostructures", *Nanoscale* **10** (2018) 16030-16039 <http://dx.doi.org/10.1039/C8NR03597K>

BM16

Geochemistry and Environmental Sciences

Proux O., Lahera E., Del Net W., Kieffer I., Rovezzi M., Testemale D., Irar M., Thomas S., Aguilar-Tapia A., Bazarkina E. F., Prat A., Tella M., Auffan M., Rose J., Hazemann J.-L., "High Energy Resolution Fluorescence Detected X-ray Absorption Spectroscopy : a new powerful structural tool in environmental biogeochemistry sciences", *Journal of Environmental Quality* **46** (2017) 1146-1157 <http://dx.doi.org/10.2134/jeq2017.01.0023>

Hydrothermal Fluids

Louvel M., Cadoux A., Brooker R., Proux O., Hazemann J.-L., "New insights on Br speciation in volcanic glasses and structural controls on halogens degassing", *American Mineralogist* **105** (2020) 795-802 <https://dx.doi.org/10.2138/am-2020-7273>

Biochemistry

Bissardon C., Proux O., Bureau S., Suess E., Winkel L. H. E., Conlan R. S., Francis L. W., Kahn I. L., Charlet L., Hazemann J.-L., Bohic S., "Sub-ppm high energy resolution fluorescence detected X-ray absorption spectroscopy of selenium in articular cartilage", *Analyst* **144** (2019) 3488-3493 <https://dx.doi.org/10.1039/C9AN00207C>

Catalysis & material energy

Maurer, F., Jelic, J., Wang, J. Gänzler A., Dolcet P., Wöll C., Wang Y., Studt F., Casapu M., Grunwaldt J.-D., "Tracking the formation, fate and consequence for catalytic activity of Pt single sites on CeO₂", *Nature Catalysis* **3** (2020) 824-833 <https://doi.org/10.1038/s41929-020-00508-7>

Materials science

Dantelle G., Testemale D., Homeyer E., Cantarano A., Kodjikian S., Dujardin C., Hazemann J.-L., Ibanez A., "A new solvothermal method for the synthesis of size-controlled YAG:Ce single-nanocrystals", *RSC Advances* **8** (2018) 26857-26870 <http://dx.doi.org/10.1039/C8RA05914D>